Constructing Simplicial Surfaces with Given Geometric Constraints

Von der Fakultät für Mathematik, Informatik und Naturwissenschaften der RWTH Aachen University zur Erlangung des akademischen Grades eines Doktors der Naturwissenschaften genehmigte Dissertation

vorgelegt von

Tom Frederik Görtzen, M.Sc.

aus Neuss

Berichter: Universitätsprofessorin Dr. Alice C. Niemeyer

Universitätsprofessor Dr. Daniel Robertz

Tag der mündlichen Prüfung: 17.07.2024

Diese Dissertation ist auf den Internetseiten der Universitätsbibliothek verfügbar.

Abstract

Simplicial surfaces encode the incidence relationships between vertices, edges, and faces of triangulated surfaces, providing a combinatorial description of these structures. By assigning a three-dimensional point to each vertex, we again obtain a triangulation, which we view as an embedded simplicial surface in the context of this thesis.

The primary aim of this thesis is the construction of simplicial surfaces under specified geometric constraints, with a particular emphasis on symmetry. Symmetry, in mathematical terms, can be expressed using the language of group theory. Starting with a geometric object, we can determine its automorphism group by identifying all transformations that leave the object invariant. Conversely, from a group theoretic perspective, we can study groups independently and explore whether a geometric object exists such that its automorphism group matches a given group.

Our first main result demonstrates that for any given finite group, we can construct a simplicial surface whose automorphism group is isomorphic to that group. In specific instances, these vertices can be embedded to produce embedded simplicial surfaces with given symmetry.

Additionally, embedded simplicial surfaces can characterise other symmetric properties. For example, we explore systems of interlocked three-dimensional bodies, known as topological interlocking assemblies, which rely solely on their geometric properties. We demonstrate that the theory of planar crystallographic groups can be applied to construct a wide variety of interlocking assemblies. Moreover, we develop the mathematical foundations of interlocking assemblies containing a definition, a method for verifying the interlocking property and many examples. Furthermore, extending the action of planar crystallographic groups allows the creation of surfaces with doubly periodic symmetry.

Embedded simplicial surfaces can be useful in various applications. In the final chapter, we illustrate how the theory of simplicial surfaces can be applied in the context of 3D printing: even if an initial model exhibits degenerations, we can modify it to produce a 3D printable file. Through these explorations, we highlight the practical and theoretical significance of simplicial surfaces in both mathematical research and technological applications, underscoring their versatility and potential for future developments.

Acknowledgements

First and foremost, I would like to express my deepest gratitude to my supervisors, whose guidance and support have been invaluable throughout this journey.

I am profoundly grateful to **Prof. Dr. Alice Niemeyer**, who has been a pillar of support, encouraging me through the complexities of simplicial surfaces and interlocking assemblies, and providing unwavering encouragement and insightful feedback.

My sincere thanks to **Prof. Dr. Wilhelm Plesken**, whose wisdom and fruitful discussions on crystallographic groups have greatly enriched my research. Your guidance has been instrumental in shaping my understanding and approach.

I also wish to extend my heartfelt appreciation to **Prof. Dr. Daniel Robertz**, for his support and co-supervision of my thesis.

Collectively, my supervisors guided me like a navigation system, steering me away from dead ends and often showing me the horizon while I was looking at my feet.

To my colleagues at the Chair of Algebra and Representation Theory, and the Chair of Algebra and Number Theory at RWTH Aachen University, your interest in my work and your own dedication to your research created a motivating atmosphere that I deeply cherished. Thank you for becoming friends and for your support. Special thanks to:

- **Reymond Akpanya**, for sharing an office, his calmness, and our collaborations on fascinating projects.
- **Glal Bacho**, for our inspiring conversations ranging from the best TV series to the best definition of a tangent space.
- **Jonas Hetz**, for the great talks about various topics and for becoming a good friend.
- **Daniel Rademacher**, for his cheerful demeanour and encouraging words.
- **Friedrich Rober**, for our many discussions about LaTeX technicalities, consultations on GAP specifics, and for taking an interest in my geometric constructions.
- **Yannic Rohde**, for his enthusiasm in finding "the one piece" and for the many coffee breaks.

- **Meike Weiß**, **Vanishree Krishna Kirekod**, **Giulia Iezzi**, and **Wolfgang Krass**, for their wonderful presence, support, and the inspiring conversations we had on many topics.
- **SFB team members** who became very good friends with a special thanks to: Sebastian Wiesenhütter, Tobias Neef, Tobias Hatzfeld, Iurii Vakaliuk, and Domen Macek.

I am also very thankful to **Prof. Daisuke Sagaki**, who welcomed me in Tsukuba, Japan, and worked with me on exciting topics. His hospitality, support, kindness, wisdom, and his amazing team members in his lab will forever remain a pleasant memory.

Special thanks to **Prof. Shigeki Akiyama** for his support, encouraging words, and for many fruitful conversations.

My gratitude extends to **Prof. Dr. Andrew Simoson**, who became a good friend, calming and supporting me when I needed help.

To my friends and especially **Dr. Dario Mathiä**, your companionship has been a source of great joy and support.

I am deeply thankful to my parents, **Erika and Peter Görtzen**, for their love, support, and understanding of my sparse visits. Your encouragement has been my foundation.

To my brothers, **Max and Ben Görtzen**, thank you for your interest in what a mathematician does and for your love.

Last but certainly not least, I want to express my deepest love and gratitude to my wife, **Sen**. Your unwavering support, profound understanding, and genuine interest in my thesis, along with your boundless love, have given me the strength to complete this work.

This work emerged as the result of the subproject A04 in the SFB/TRR 280 and was funded by the Deutsche Forschungsgemeinschaft (DFG, German Research Foundation) – SFB/TRR 280. Project-ID: 417002380.

Thank you all for being part of this journey.

Authorship Declaration

This thesis contains work that has been submitted to a journal.

- **Details of the work:** [AG23] Reymond Akpanya and Tom Goertzen. *Surfaces with given Automorphism Group*. 2023. arXiv: 2307.12681 [math.GR].

  Student contribution to work: The author of this thesis contributed fully to all mathematical ideas. The content of this work is contained in Chapter 2 of this thesis. The author of this thesis was responsible for the writing of [AG23, Section 3, 5, 6] and the mathematical ideas of these sections were developed jointly with Akpanya. The writing of [AG23, Section 1, 2] was done in collaboration with all authors. Akpanya was responsible for the writing of [AG23, Section 4, 7] and the mathematical ideas of these sections were developed jointly with the author of this thesis. The implementations used in the respective sections can be found in [Nie+23b].

- **Details of the work:** [Goe24a] Tom Goertzen. *Constructing Interlocking Assemblies with Crystallographic Symmetries*. 2024. arXiv: 2405.15080 [cs.CG].

  Student contribution to work: The author of this thesis solely contributed to the writing and mathematical ideas of the work [Goe24a]. The content of this work is contained in Chapter 3 of this thesis.

- **Details of the work:** [Goe24b] Tom Goertzen. *Mathematical Foundations of Interlocking Assemblies*. 2024. arXiv: 2405.17644 [math.CO].

  Student contribution to work: The author of this thesis solely contributed to the writing and mathematical ideas of the work [Goe24b]. The content of this work is contained in Chapter 3 of this thesis.

- **Details of the work:** [AG24a] Christian Amend and Tom Goertzen. *A Framework for Symmetric Self-Intersecting Surfaces*. 2024. arXiv: 2312.02113 [cs.CG].

  Student contribution to work: The author of this thesis contributed fully to all mathematical ideas. The content of this work is contained in Chapter 5 of this thesis. The author of this thesis was responsible for the writing and developing of the mathematical ideas of [AG24a, Section 4, 5]. The writing and developing of the mathematical ideas of [AG24a, Section 1, 2, 6, 8, 9] was done in collaboration with all authors. Amend was responsible for the writing of [AG24a, Section 3, 7] and the mathematical ideas were developed in joint work with the author of this thesis. The implementations developed for this work are available at [AG24b].

Contents

Chapter 1

Introduction and Preliminaries

1.1 Introduction

To understand our surroundings and the world, it is essential to comprehend surfaces, as they describe the exterior of any geometric object. These objects can be as small as molecules or as large as cars, buildings, landscapes, or even planets.

Surfaces come in various shapes: smooth (like a sphere), non-orientable (such as a Möbius strip), or simple (like pyramids). One of the most basic surfaces is a triangle, which we encounter in school when studying trigonometry and congruent shapes. Triangulated surfaces, which consist only of triangles, can approximate any smooth or piecewise continuous surface. The main advantage of a triangulated surface lies in the simplicity of its basic components: triangles.

A research question, inspired by Prof. M. Trautz, a professor of architecture at RWTH Aachen, is: "How can we approximate a surface using only a few types of congruent triangles?" (see [Bra+17]). This question is complex and requires developing an understanding of how to encode these properties. The mathematical language used to describe triangulated surfaces in this work is that of embedded simplicial surfaces. A simplicial surface describes the combinatorial structure of a triangulated surface, specifically the incidence relations between vertices, edges, and faces (triangles) on the surface, such that certain local regularity conditions are satisfied. For instance, any edge should be incident to at most two triangles, and the triangles incident to a vertex should be ordered in a particular way.

In this work, we address the challenge of constructing simplicial surfaces with given geometric constraints and demonstrate how properties such as symmetry can provide a better understanding of the underlying surface. Symmetry, a natural phenomenon, is key to beauty and can be observed in many aspects of our world. In terms of mathematics, group theory is the natural language for describing symmetries. We aim to connect the concepts of symmetry and surfaces in various ways. One approach to identifying the symmetry of a surface is to consider all transformations of the surface that leave it invariant, known as the automorphism group of the surface.

Simplicial Surfaces with Given Finite Automorphism Group Using the automorphism group of a simplicial surface with a finite number of triangles, we obtain a finite group encoding the symmetries of the surface. Conversely, starting with an (abstract) finite group G, we can ask:

Q1: Can we always find a simplicial surface automorphism group isomorphic to G?

The answer to this question is affirmative, as demonstrated in Chapter 2 of this work. We provide an explicit construction based solely on the given finite group and its generators. This construction leverages the connection between simplicial surfaces and cubic graphs, i.e. graphs where each node is incident to exactly three edges. The face graph of a simplicial surface is a cubic graph formed by representing faces of the surface as nodes and creating edges between nodes if and only if the corresponding faces of the surface are connected by an edge of the surface. Assuming each edge of the surface is incident to exactly two triangles (a property of closed surfaces), we derive a cubic graph.

Conversely, starting with a cubic graph, determining whether it corresponds to a simplicial surface is more challenging and translates to the problem of finding a cycle double cover: a collection of simple cycles in the cubic graph such that each edge in the graph belongs to exactly two cycles. The correspondence to simplicial surfaces is established by associating a vertex with each cycle. One key property of the face graphs of closed simplicial surfaces is the absence of bridges—edges that, when deleted, increase the number of connected components. The following conjecture, first posed by Szekeres in [Sze73], remains open:

Conjecture. *Does every cubic bridgeless graph have a cycle double cover?*

Frucht [Fru49], provides a construction for cubic graphs with a given finite automorphism group. In Chapter 2, we demonstrate that these cubic graphs possess a variety of cycle double covers, which can be employed to construct simplicial surfaces with the given automorphism group.

In some cases, simplicial surfaces can be embedded into three-dimensional space using only equilateral triangles, ensuring that the symmetry group (isometries leaving the surface invariant) matches the automorphism group. These resulting surfaces often feature self-intersecting faces.

Other geometric constraints in this work are motivated by the need to develop geometric objects applicable in various scenarios. This thesis is part of subproject A04 of the larger research project SFB/TRR 280, funded by the DFG (Project-ID: 417002380), which aims to develop "Design Strategies for Material-Minimized Carbon Reinforced Concrete Structures—Principles of a New Approach to Construction". The challenge of finding design strategies for such structures is motivated by the pressing issue of climate change, with the building industry being a significant contributor to greenhouse

gas emissions. Revolutionary approaches are required, and a modular design approach presents a viable solution. This work explores the principle of interlocking assemblies, enabling modular construction without mortar, allowing building blocks to be easily disassembled and reused.

Interlocking Assemblies The idea of interlocking assemblies is based on building "flat-vaults". Conventional masonry structures can be used to construct curved surfaces only, and if we were to flatten these structures, they would simply collapse. In interlocking assemblies, we have a number of blocks, which mathematically can be seen as compact subsets of $\mathbb{R}^3$ satisfying certain relations, that are in contact with each other such that restraining a subset of blocks from moving leads to the immovability of all other blocks within the assembly.

Among the first examples of such assemblies are the ones by Abeille and Truchet given in [Gal35]. Interlocking assemblies are also studied under the names topological interlocking assemblies, Abeille vaults, or flat-vaults in the literature. The study of these assemblies in engineering applications gained momentum with the studies by Dyskin, Estrin, Kanel-Belov, and Pasternak, starting with the work [Dys+01]. In [Dys+03b; Bel+09], construction methods for different types of blocks based on curved or convex shapes are given. Initial formal treatments of these types of assemblies can be found in [Bel+09] and [Wan+19; Wan21]. In the context of this thesis, we deal with the following questions:

Q1: Can we develop a mathematical theory of interlocking assemblies?

Q2: Can we exploit "symmetry" to construct interlocking assemblies?

Q3: Is there a way to evaluate and predict the performance of interlocking assemblies?

In Chapter 3 of this thesis, we establish a mathematical theory and also provide a construction method for interlocking assemblies based on crystallographic symmetries.

We give a mathematical definition and prove that a criterion based on infinitesimal motions introduced in [Wan21] can be used to verify the interlocking properties for assemblies such that the surface of all blocks can be triangulated. Following this, we provide a construction method for candidates of interlocking assemblies with triangulated blocks using the theory of planar crystallographic groups. Here, the main idea is to place two fundamental domains of the same planar crystallographic group in parallel planes and interpolate between them to obtain a block. Indeed, we show that under certain assumptions, the resulting assemblies give rise to interlocking assemblies. Certain blocks that appear in this construction can be assembled in many ways characterized by the theory of Truchet tiles, and we give a combinatorial model predicting how the interlocking takes effect when applied as ceiling construction.

Doubly Periodic Landscapes When constructing interlocking assemblies with a planar crystallographic group, we extend its natural action on the Euclidean plane $\mathbb{R}^2$ to $\mathbb{R}^3$. Similarly, we exploit this extension in Chapter 4 in order to create doubly periodic landscapes which are based on triangles in $\mathbb{R}^3$ such that their projection onto $\mathbb{R}^2$ gives rise to a fundamental domain.

For this construction, we show that for a fixed triangle F in $\mathbb{R}^2$ and any similarity type of triangle determined by the inner angles, we can find a triangle T with a given similarity type such that T projects onto F.

3D-Printing of Simplicial Surfaces 3D-printing of surfaces has become an established tool that allows a better understanding of surfaces. In engineering applications, this tool is especially useful for prototyping. However, when considering embedded simplicial surfaces, certain degenerations can appear, such as self-intersecting surfaces or so-called non-manifold parts, which present challenges when trying to produce a 3D-printable file.

In Chapter 5, we show how to detect such degenerations first and then provide algorithms that produce a 3D-printable file for a given embedded simplicial surface. For detecting self-intersecting surfaces and providing a refined retriangulation of the surface, we demonstrate how to exploit the symmetries of the given surface, leading to a simplification and resulting speed-up in the algorithms.

The creation of images and figures displayed throughout this work employed various software systems, see [Tan24; Nie+23b; Nie+23a; Rid21; Pro24].

1.2 Basic Definitions

In this section, we present the foundational definitions used throughout this thesis. Definitions specific to individual chapters are addressed in their respective chapters.

1.2.1 Simplicial Surfaces

The primary definition relevant to this work is that of simplicial surfaces. This definition provides a combinatorial perspective on a triangulated surface, considering only the incidence relations between vertices, edges, and faces. The following definitions are based on the work presented in [NPR24].

Definition 1.2.1. A *simplicial surface* $(X, <)$ is a countable set X partitioned into non-empty sets X_0, X_1, and X_2 such that the relation $<$, called the *incidence*, is a subset of the union $X_0 \times X_1 \cup X_1 \times X_2 \cup X_0 \times X_2$, satisfying the following conditions. We call the elements of X_0, X_1, and X_2 vertices, edges, and faces, respectively.

1. For each edge $e \in X_1$, there are exactly two vertices $V \in X_0$ with $V < e$.

2. For each face $F \in X_2$, there are exactly three edges $e \in X_1$ with $e < F$ and three vertices $V \in X_0$ with $V < F$. Moreover, any of these three vertices is incident to exactly two of these three edges.

3. For any edge $e \in X_1$, there are exactly two faces $F \in X_2$ with $e < F$.

4. Umbrella condition: For any vertex $V \in X_0$, the number $n = \deg(V)$ of faces $F_i \in X_2$ with $V < F_i$ satisfies $3 \leq \deg(V) < \infty$ and is called the *degree* of the vertex V. The faces F_i can be arranged in a sequence $(F_1, \ldots, F_n)$ such that F_{i+1} and F_i share a common edge e_i with $V < e_i$ for $i = 1, \ldots, n$ and we set $F_{n+1} = F_1$. This sequence can be viewed as a cycle $(F_1, \ldots, F_n)$ called the *umbrella* of V.

The above definition requires each edge to be incident to exactly two faces. We can relax the definition by differentiating between closed surfaces, where each edge is incident to two faces, and open surfaces, containing an edge which is only incident to one face. Furthermore, we can generalize the definition by allowing vertices with degree 2. From now on, when we speak of surfaces, we mean simplicial surfaces in the sense above and omit the incidence relation, whenever it is clear from the context. Definition 1.2.1 allows that two distinct edges share common vertices, and we reintroduce conventional simplicial complexes by introducing vertex-faithful simplicial surfaces as defined below.

A related concept to simplicial surfaces commonly found in the literature are simplicial complexes. In this context, one could ask how far a simplicial surface is "away" from a simplicial complex. The following definition relates a simplicial complex to a simplicial surface.

Definition 1.2.2. A surface X is called *vertex-faithful* if its edges and faces are uniquely described by its incident vertices, i.e. the following map is injective:

$$X \to P(X_0) \coloneqq \{S \subseteq X_0\},\ x \mapsto X_0(x) \coloneqq \{V \in X_0 \mid V < x \text{ or } V = x\}.$$

The image of the above map always yields a simplicial complex in the conventional way.

We define properties such as orientability and the Euler characteristic in the usual sense.

Definition 1.2.3. For a simplicial surface X, we can compute its *Euler characteristic* $\chi(X)$ as

$$\chi(X) = |X_0| - |X_1| + |X_2|.$$

For example, a simplicial sphere has Euler characteristic 2 and a simplicial torus has Euler characteristic 0.

Definition 1.2.4. A simplicial surface X is called *connected* if for all faces $f, f' \in X_2$ there exists a path connecting them, i.e., there exist $n \in \mathbb{N}$ and edges $e_1, \ldots, e_n \in X_1$ and faces $f_0, \ldots, f_n \in X_2$ with $f_0 = f, f_n = f'$ such that $e_i < f_{i-1}, f$ for all $i = 1, \ldots, n$.

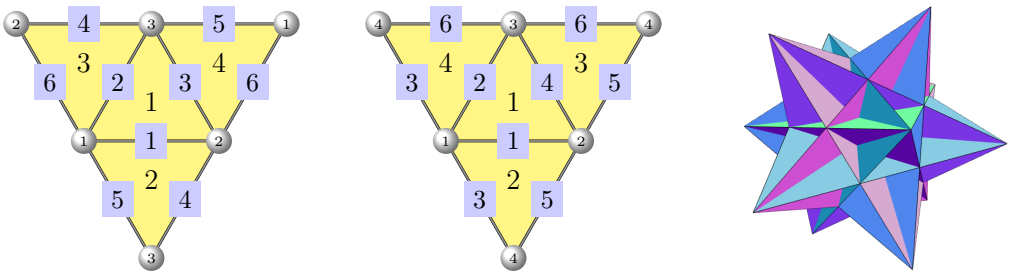

(a) (b) (c)

Figure 1.1: Three depictions of simplicial surfaces: (a) projective plane; (b) tetrahedron (c) icosahedron with embedding as the great icosahedron see [Bra+20]

Example 1.2.5. The following are examples of simplicial surfaces:

1. Three of the five Platonic solids, i.e., the tetrahedron, the octahedron, and the icosahedron, give rise to examples of simplicial surfaces.

2. For a given (closed, connected) simplicial surface X, we can take a (closed, connected) subsurface Y such that each face in Y has exactly two inner and one outer edge. Such surfaces are called *simplex rings*.

3. The projective plane shown in Figure 1.1a gives an example of a simplicial surface which is not vertex-faithful.

Definition 1.2.6. An *orientation* of a simplicial surface X is given by a cyclic ordering of the vertices of each face, such that for any given edge e with vertices $v_1, v_2 < e$ which is incident to two distinct faces f_1, f_2 with vertices $v_1, v_2, v < f_1, v_1, v_2, v' < f_2$, we have that either the ordering of f_1 is (v, v_1, v_2) and the one of f_2 is (v', v_2, v_1) or the ordering of f_1 is (v, v_1, v_2) and f_2 is (v', v_1, v_2). If an orientation for a simplicial surface X exists, we say that X is *orientable*.

Definition 1.2.7. An *embedding* of a vertex-faithful simplicial surface X with vertices V into $\mathbb{R}^3$ is given by an injective map

$$\phi : V \to \mathbb{R}^3.$$

We write (X, ϕ) for a simplicial surface X with embedding ϕ and we refer to (X, ϕ) as an *embedded simplicial*. If a given simplicial surface X is embedded into $\mathbb{R}^3$, we often omit the map ϕ whenever it is clear from the context and identify the vertices, edges, and faces with their respective images under ϕ.

1.2.2 Planar Crystallographic Groups

This section covers the basic concepts of planar crystallographic groups, also known as wallpaper groups, including fundamental domains. Here, a *wallpaper group* is an infinite subgroup of the Euclidean group E(2). The Euclidean group E(2) is isomorphic

to a semidirect product of the orthogonal group $\mathrm{O}(2)$ and the free abelian group $\mathbb{R}^2$. Moreover, an element g of the Euclidean group $\mathrm{E}(2)$ can be viewed as an isometric map $g : \mathbb{R}^2 \to \mathbb{R}^2$, i.e. g is bijective and for all $x, y \in \mathbb{R}^2$ we have $\|x - y\|_2 = \|g(x) - g(y)\|_2$, and we can write $g(x) = Rx + v$, for all $x \in \mathbb{R}^2$, for some orthogonal matrix $R \in \mathrm{O}(2)$ and some vector $v \in \mathbb{R}^2$.

Definition 1.2.8. A *planar crystallographic group* or *wallpaper group* is an infinite group $G \leq \mathrm{E}(2)$ of Euclidean motions acting on the plane $\mathbb{R}^2$ whose orbits

$$G(x) := \{g(x) \mid g \in G\} \text{ for } x \in \mathbb{R}^2$$

satisfy the following two conditions:

1. The orbit of any point in $\mathbb{R}^2$ under the action of G is a *discrete subset* of $\mathbb{R}^2$.
2. There exists a compact subset $F \subset \mathbb{R}^2$, called *fundamental domain*, such that the plane $\mathbb{R}^2$ can be tessellated by the orbits of F under G, i.e.
   (a) $\bigcup_{g \in G} g(F) = \mathbb{R}^2$ and
   (b) there exists a subset $V \subset \mathbb{R}^2$ with $\mathring{F} \subset V \subset F$ and V is a *transversal* of the action of G on $\mathbb{R}^2$, i.e. each orbit of a point $x \in \mathbb{R}^2$ intersects V in exactly one point, i.e. $|G(x) \cap V| = 1$.

The definition of planar crystallographic groups extends to higher dimensions by replacing all occurrences of 2 by n in the definition above, yielding the definition of *crystallographic space groups*. One can prove that there always exists a finite number of isomorphism types of groups. In general, the structure of crystallographic groups can be characterised by the extension of free abelian groups corresponding to translations extended by a finite group, see [Ple96].

Remark 1.2.9. Any wallpaper group G contains a normal subgroup T of translations isomorphic to $\mathbb{Z}^2$ such that the factor group G/T, called *point group*, is finite and can be viewed as a finite group of orthogonal transformations. Each wallpaper group is generated by a finite set of matrices corresponding to a generating set of the point group and two translations spanning a lattice isomorphic to $\mathbb{Z}^2$. This yields a doubly periodic structure of the tessellation of $\mathbb{R}^2$ with a given fundamental domain. For a given fundamental domain F of G the point group acts on F, yielding a *translational cell* that tessellates the Euclidean plane using translation only.

There are 17 wallpaper groups up to isomorphism, see for instance [CBG08], and we refer to them by their *Hermann–Mauguin notation* also known as *international notation* describing certain generating elements of the underlying group, see [IUC02]. This notation refers to special elements with non-trivial representative in G/T, such as 3-fold rotations (in the name p3) or glide reflections (in the name pg). Other well-

known notations include the *orbifold notation*, see [CBG08]. For more on the general theory on wallpaper groups, we refer to [Cox69].

The following examples give the generators for one of the seventeen wallpaper groups. Generators for each of the groups can be found in [IUC02].

Example 1.2.10. A group wallpaper group G of type p3 can be generated by the rotation

$$R = \begin{pmatrix} -\frac{1}{2} & -\frac{\sqrt{3}}{2} \\ \frac{\sqrt{3}}{2} & -\frac{1}{2} \end{pmatrix} \in \mathrm{E}(2)$$

and the translations given by the vectors

$$(0,1)^\intercal, \left(\frac{\sqrt{3}}{2}, -\frac{1}{2}\right)^\intercal \in \mathrm{E}(2).$$

Different fundamental domains F for G are illustrated in Section 3.4 of Chapter 3.

Chapter 2

Simplicial Surfaces with given finite Automorphism Group

2.1 Summary

In [Fru49] Frucht shows that for any finite group G, there exists a cubic graph such that its automorphism group is isomorphic to G. For groups generated by two elements, we simplify his construction to a graph with fewer nodes. In the general case, we address an oversight in Frucht's construction. We prove the existence of cycle double covers of the resulting graphs, leading to simplicial surfaces with given finite automorphism group. For almost all finite non-abelian simple groups, we give alternative constructions based on graphic regular representations. In the general cases C_n, D_n, A_5 for $n \geq 4$, we provide alternative constructions of simplicial spheres. Furthermore, we embed these surfaces into the Euclidean 3-Space with equilateral triangles such that the automorphism group of the surface and the symmetry group of the corresponding polyhedron are isomorphic.

2.2 Introduction

Combinatorial structures such as graphs and simplicial complexes are ubiquitous in mathematical research. The identification and study of these fundamental structures provides a unifying view of phenomena from a wide range of diverse mathematical disciplines. In particular, cubic graphs have been the focus of many studies in graph theory such as the cycle double cover conjecture, see Section 2.3. In this chapter, we investigate the relationship between cubic graphs and simplicial surfaces, with a focus on their respective automorphism groups. Simplicial surfaces describe the incidence relations of triangulated surfaces, and they can be linked to cubic graphs by observing the incidence between faces and edges only.

This chapter is based on research originally published at [AG23].

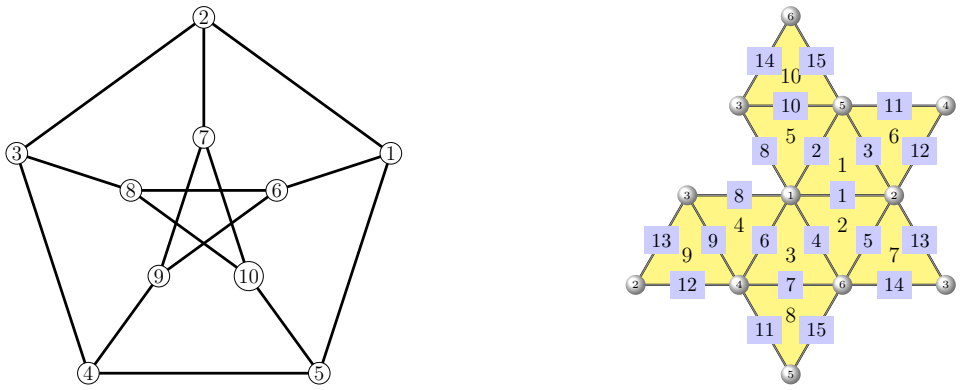

(a) (b)

Figure 2.1: (a) Petersen graph, (b) Surface with face graph isomorphic to the Petersen graph (edges and vertices with the same labels are identified).

In particular, we show in Section 2.7 that a construction by Frucht in [Fru49] yielding a cubic graph with given automorphism group leads to the following result:

Theorem. *Let G be a finite group generated by a set S. There exists a simplicial surface $X_{G,S}$ such that $Aut(X_{G,S}) \cong G$.*

Furthermore, for cyclic groups and dihedral groups we show the following result in Section 2.8:

Theorem. *For $G = C_n$ and $n \geq 3$ or for $G = D_n$ and $n \geq 4$ there exists a simplicial surface X_G with automorphism group isomorphic to G and X_G can be embedded into $\mathbb{R}^3$ with equilateral triangles.*

As an example of a cubic graph consider the Petersen graph shown in Figure 2.1a. A natural question that arises from examining this graph is:

Q1 *How can we link a cubic graph to a simplicial surface, i.e. the combinatorics of a triangulation of a three dimensional polyhedron?*

This question was answered by Szekeres in [Sze73] by interpreting a cubic graph as the graph describing the incidence structure between the faces and edges of a simplicial surface. In this case, the vertices of the surface correspond to the cycles in a cycle double cover of the cubic graph, i.e. a collection of cycles that passes every edge exactly twice. Three cycle double covers of the Petersen graph are given by

$$\{(1,5,4,3,2),(1,6,9,7,2),(1,6,8,3,2,7,10,5),(4,9,6,8,10,5),(3,8,10,7,9,4)\},$$
$$\{(1,5,4,3,2),(1,6,9,7,2),(2,7,10,5,4,9,6,8,3),(1,6,8,10,5),(3,8,10,7,9,4)\},$$
$$\{(1,5,4,3,2),(1,6,9,7,2),(4,9,7,10,5),(3,8,6,9,4),(1,6,8,10,5),(2,7,10,8,3)\}.$$

Here, the third cycle double cover above corresponds to the surface illustrated in Figure 2.1b. If a surface can be constructed from computing a cycle double cover of a given cubic graph, we can compare the automorphism groups:

Q2 *What is the automorphism group of the resulting simplicial surface?*

For the surface in Figure 2.1b, the automorphism group is isomorphic to A_5. This automorphism group corresponds to a subgroup of the automorphism group of the Petersen graph, which leaves the corresponding cycle double cover invariant. Note that the automorphism group of a surface is always isomorphic to a subgroup of the automorphism group of the underlying cubic graph, see Section 2.3.1 for a proof. As a next step, we can try to compute an embedding of the simplicial surface with equilateral triangles, i.e. realize the surface as a polyhedron built from equilateral triangles in the Euclidean 3-space. Computing embeddings by solving a system of equations determined by a given simplicial surface turns out to be a task of high complexity. In [Bra+20] the complexity of solving this system of equations is demonstrated by computing all embeddings of a combinatorial icosahedron with equilateral triangles and non-trivial symmetry groups. The symmetry group of an embedding of a surface is the maximal subgroup in the Euclidean group E(3) leaving the embedding invariant. Such a symmetry group can be embedded into the group of orthogonal transformation O(3). In general, the symmetry group of an embedded surface is a subgroup of the automorphism group of the underlying simplicial surface. Here, we aim to compute embeddings of a simplicial surface with a high number of symmetries as described in the following question:

Q3 *Given a simplicial surface, can we compute an embedding into* $\mathbb{R}^3$ *such that the symmetry group of the surface is isomorphic to the automorphism group of the underlying simplicial surface?*

In this chapter, we elaborate on the translation of cubic graphs with given automorphism group into simplicial surfaces, analyse corresponding embeddings in some cases and therefore give answers to the questions Q1-Q3 for certain classes of cubic graphs and surfaces.

We show that there exists a simplicial surface X_G with $\mathrm{Aut}(X_G) \cong G$ by giving a G-invariant cycle double cover of a cubic graph based on Frucht's construction in [Fru49] or a cubic graph that forms a vertex transitive graph also known as generalized orbital graph. We define a 3-edge colouring to obtain this cycle double cover by applying the methods given in [Sze73] and show that contracting nodes that lie on a 3-cycle can lead to smaller graphs with given automorphism group, see Figure 2.2b.

Note that cubic graphs do not necessarily admit 3-edge colouring. For instance, the Petersen graph, shown in Figure 2.1a, is a well-known example of a vertex-transitive graph that does not admit a 3-edge colouring. Furthermore, for $G = C_n, D_n, A_5$ we provide a simplicial surface X_G with automorphism group isomorphic to G and X_G can be embedded with equilateral triangles. This is shown by exploiting the structure of the groups C_n, D_n, A_5 interpreted as subgroups of O(3). For the cyclic and dihedral cases, we show in Section 2.8.1 that it suffices to consider group orbits of points in $\mathbb{R}^3$ in order to find embeddings with equilateral triangles.

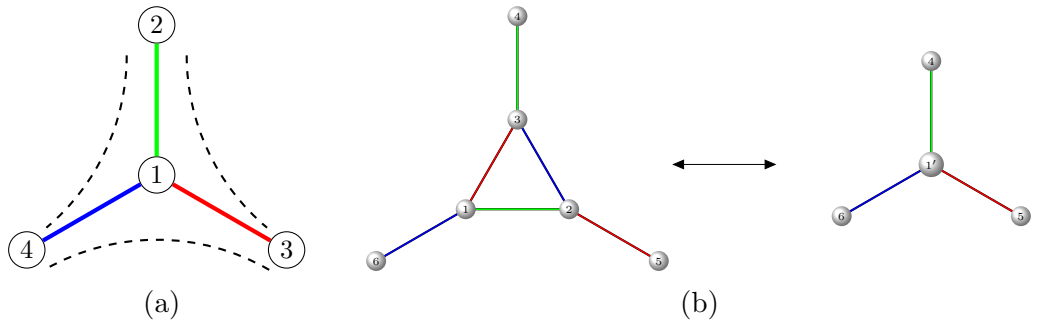

Figure 2.2: (a) We can obtain cycle double colours in 3-edge coloured graphs by defining cycles that alternate between two colours. (b) We can reduce vertices that lie on a 3-cycle inside a 3-edge coloured cubic graph to obtain a smaller cubic graph.

In Section 2.3, we introduce the theory of simplicial surfaces and their connections to cubic graphs. Moreover, we observe that a cubic graph has to be bridgeless in order to associate it to a surface. Section 2.4 deals with Frucht's cubic graph construction from [Fru49] yielding a cubic graph with given automorphism group. Here, we modify the construction for groups with $n > 2$ generators, where Frucht missed a case, see [Fru82; Bab81]. In Section 2.5 we present the graphs with cyclic automorphism group that arise from Frucht's construction and provide an alternative construction that yields cubic graphs with dihedral automorphism groups. We then introduce the construction of vertex-transitive cubic graphs in Section 2.6. In Section 2.7, we show that we can associate a surface to each of the cubic graphs given in the previous sections. Finally, in Section 2.8, we compute infinite families of surfaces based on the cubic graphs presented in Section 2.5 such that the automorphism groups and symmetry groups of these surfaces are isomorphic. All the graph constructions discussed in this chapter, along with the software for the visualization of surfaces and graphs, are implemented in the GAP4 package, SimplicialSurfaces [Nie+23b]. We verify the automorphism groups of the given examples using the algorithms provided in [MP14], which are implemented in GAP4 [GAP].

2.3 Simplicial Surfaces and Graphs

In this section, we introduce the basic notion of simplicial surfaces and their relation to cubic graphs.

Simplicial surfaces describe the incidence structure of triangulated surfaces. Compared to a simplicial complex, where each element is uniquely described by its corresponding vertices, the definition of a simplicial surface allows different faces and edges to have the same vertices by introducing an incidence relation between vertices, edges and faces, see Definition 1.2.1.

Definition 2.3.1. A *homomorphism* between two simplicial surfaces $(X, <_X)$ and $(Y, <_Y)$ is a map $\pi\colon X \to Y$ satisfying the following two conditions.

1. For $A, B \in X$ with $A <_X B$, we have that $\pi(A) <_Y \pi(B)$.

2. For every face $F \in X_2$, the restriction of π to the vertices and edges incident to F is an isomorphism onto the set of vertices and edges that are incident to $\pi(F)$.

Auto-, mono- and epimorphisms are defined in the usual way, and we can define the category of simplicial surfaces.

By observing that the degree of a vertex is invariant under an isomorphism of a simplicial surface, we can define invariants of isomorphic surfaces. One is the *vertex-counter* of a surface X which counts the degrees of the vertices and is defined as a polynomial in the indeterminates $\{v_n \mid n \geq 3\}$, i.e.

$$\prod_{v \in X_0} v_{\deg(v)}.$$

2.3.1 Graphs of Simplicial Surfaces

There are several ways of linking a graph Γ to a surface X. We present some of these graphs based on partial incidence structures of a given simplicial surface, see also [NPR24]. In the rest of the chapter, we refer to the vertices of a graph as nodes in order to distinguish between vertices of a surface and those of a graph.

Definition 2.3.2. Let $(X, <)$ be a simplicial surface.

1. The *incidence graph*, denoted by $\mathcal{I}(X)$, of a surface X has nodes X and there exists an edge between two nodes $A, B \in X$, whenever we have $A < B$ in X.

2. The *vertex(-edge) graph* of X, denoted by $\mathcal{V}(X)$, has nodes X_0 and edges X_1 such that an edge $e \in X_1$ connects the two vertices in $X_0(e)$.

3. The *face(-edge) graph* or *face graph* of X, denoted by $\mathcal{F}(X)$, has nodes X_2 and edges X_1 such that an edge $e \in X_1$ connects the two faces in $X_2(e) = \{F \in X_2 \mid e < F\}$.

Since each face of a (closed) surface X has three edges, the face graph $\mathcal{F}(X)$ is cubic. Typically, vertex-edge graphs are used to associate a graph with a given surface, see for instance [Sze73]. Here, we primarily make use of the graph in (3) as it gives us a strong connection between the theory of cubic graphs and simplicial surfaces. Here, the umbrella condition in Definition 1.2.1 enforces the face graph $\mathcal{F}(X)$ of a surface X to be bridgeless, since each edge must lie on a cycle that is induced by the umbrella of a vertex $V \in X$. Furthermore, it is straightforward to show that a vertex-faithful surface yields a 3-connected graph. The following lemma demonstrates our key tool in establishing a connection between the theory of simplicial surfaces and cubic graphs.

Lemma 2.3.3. *$\mathcal{F}(\cdot)$ is a functor from the category of (closed) simplicial surfaces to the category of bridgeless cubic graphs.*

Proof. Let X, Y be two simplicial surfaces and $\pi\colon X \to Y$ a homomorphism between them. By restricting π to $X_1 \cup X_2$ we get a map $\pi|_{X_1 \cup X_2}\colon \mathcal{F}(X) \to \mathcal{F}(Y)$ which is a graph homomorphism, since $\pi(e) < \pi(f)$ holds for all $e \in X_1, f \in X_2$ with $e < f$. □

Since an automorphism of a simplicial surface yields an automorphism of its face graph we obtain the following result.

Lemma 2.3.4. *For a simplicial surface X we have that* $\mathrm{Aut}(X) \hookrightarrow \mathrm{Aut}(\mathcal{F}(X))$. *Moreover, we have* $\mathrm{Aut}(X) \cong \mathrm{Aut}(\mathcal{F}(X))$ *if and only if for all* $\pi \in \mathrm{Aut}(\mathcal{F}(X))$ *and all vertices $v \in X_0$, the isomorphism π maps the umbrella $(F_1, \ldots, F_n)$ at v onto an umbrella of another vertex of X via $\pi((F_1, \ldots, F_n)) = (\pi(F_1), \ldots, \pi(F_n))$. Thus, each automorphism of $\mathcal{F}(X)$ can uniquely be extended to an automorphism of X.*

Hence, the task of constructing a simplicial surface X with given group G as automorphism group can be reduced to finding a cubic graph Γ with automorphism group isomorphic to G and a surface X with $\mathcal{F}(X) = \Gamma$ such that $\mathrm{Aut}(X) \cong \mathrm{Aut}(\mathcal{F}(X))$. In [Sze73], Szekeres describes how to compute $\mathcal{F}^{-1}(\Gamma)$ for a cubic graph Γ, i.e. the simplicial surfaces with a given face graph. This can be achieved by computing a cycle double cover.

Definition 2.3.5. A *cycle double cover* or *polyhedral decomposition* (see [Sze73]) of a cubic graph Γ consists of a collection of cycles $(C_i)_{i \in I}$ such that for each edge in Γ lies on exactly two cycles.

A simplicial surface can be recovered from its face graph with a cycle double cover, where a cycle C_i corresponds to the umbrella of a vertex of the surface. It follows that a simplicial surface X is vertex-faithful if and only if no two cycles of its corresponding cycle double cover share two common edges. It is still an open problem, whether all cubic bridgeless graphs admit a cycle double cover.

Conjecture 2.3.6 (Cycle double cover conjecture)**.** *In [Sze73], Szekeres conjectures that any cubic graph containing no bridges has a cycle double cover or equivalently is a face graph of a simplicial surface. Moreover, it is conjectured that any bridgeless graph admits a cycle double cover, see [Jae85].*

For the graphs presented in the following sections, we always give a cycle double cover. One of the main tools for finding cycle double covers is the following observation for 3-edge colourable cubic graphs.

Remark 2.3.7. In [Sze73], Szekeres shows that a 3-edge colouring, also called *Tait colouring*, of a cubic graph leads to a cycle double cover. Any cycle of the double cover is obtained by choosing two colour classes and alternating between them. The resulting surface, has a *Grünbaum colouring* of its edges corresponding to this 3-edge colouring.

To show Conjecture 2.3.6 it would suffice to consider cubic graphs that do not admit a 3-edge colouring which are known as snarks in the literature, see [Jae85]. The Petersen graph can be obtained from the graph in Figure 2.3 by contracting three cycles into one node, and both yield examples of non 3-edge colourable cubic graphs. On the other hand, one can subdivide each face into three faces of the surface given in Figure 2.1b to obtain a surface with face graph shown in Figure 2.3.

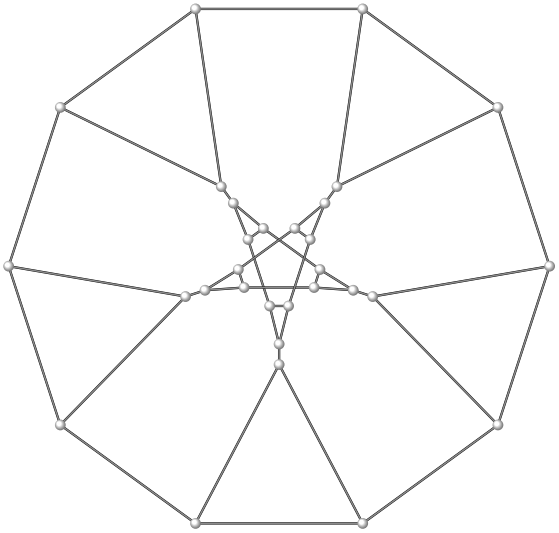

Figure 2.3: Face graph of a surface with automorphism group isomorphic to A_5.

2.3.2 Embedding Simplicial Surfaces with Equilateral Triangles

In order to translate a simplicial surface into a polyhedron with equilateral triangles, one has to solve the *embedding problem*. Solving the embedding problem is equivalent to finding an embedding of a simplicial surface, as defined below.

Definition 2.3.8. Let X be a simplicial surface. A map $\phi\colon X_0 \to \mathbb{R}^3$ such that all neighbouring vertices v_1 and v_2 satisfy

$$\|\phi(v_1) - \phi(v_2)\|^2 = 1$$

in the Euclidean norm is called an *embedding* of X with equilateral triangles.

More general, for 3-edge coloured simplicial surfaces, we can identify each colour with an edge length and ask for embeddings with a given congruence class of triangles.

The question of computing an embedding with congruent triangles introduces a system of quadratic equations, see also [Bra+20; Bra+17]. In general, it remains an unsolved problem whether there exists an embedding of a given simplicial surface, constructed from triangles of a certain congruence type.

Example 2.3.9. If X is a simplicial surface, whose vertex graph $\mathcal{V}(X)$ contains a clique of size $n \geq 5$, there cannot exist an embedding of X constructed from equilateral

triangles. This can be seen as follows: Assume X has an embedding constructed from equilateral triangles. Let $v_1, \ldots, v_5$ be 3-dimensional coordinates corresponding to vertices of the given clique. It follows that, the embedded vertices v_1, v_2, v_3 give rise to an equilateral triangle. Without loss of generality we can assume that this triangle with edge lengths 1 is given by

$$(v_1, v_2, v_3) = \left((0,0,0)^\intercal, (1,0,0)^\intercal, (\frac{1}{2}, \frac{\sqrt{3}}{2}, 0)^\intercal \right).$$

Clearly, v_4 and v_5 have to be on the intersection of the unit spheres with centres at the points v_1, v_2, v_3. Since the intersection equals

$$\left\{ \left(\frac{1}{2}, \frac{1}{2\sqrt{3}}, \sqrt{\frac{2}{3}})^\intercal, (\frac{1}{2}, \frac{1}{2\sqrt{3}}, -\sqrt{\frac{2}{3}} \right)^\intercal \right\}$$

and $v_4 \neq v_5$, we can assign v_4 to the first and v_5 to the second coordinate in the set. However, it follows that $\|v_4 - v_5\| = 2\sqrt{\frac{2}{3}}$ which contradicts the existence of such an embedding.

For example, the minimal triangulation of the torus T consisting of 7 vertices, 21 edges and 14 triangles and incidence relations depicted as in Figure 2.4 does not have an embedding consisting of equilateral triangles, since the graph $\mathcal{V}(T)$ is isomorphic to the complete graph on 7 vertices. Although this simplicial surface cannot be embedded into the Euclidean space as a polyhedron constructed from equilateral triangles, its combinatorial structure can be visualized in a folding plan as seen in Figure 2.4.

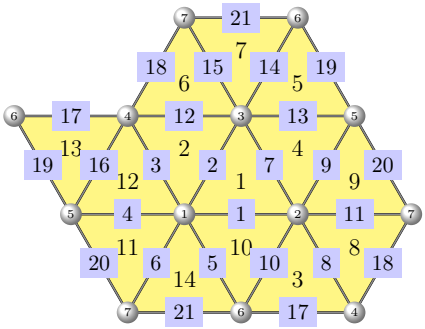

Figure 2.4: A minimal triangulation of the torus.

Even when considering simplicial spheres, it remains unknown if an embedding constructed from equilateral triangles always exists. General non-existing results are for instance known for tori obtained from iteratively gluing together the faces of regular tetrahedra, see [Mas72].

In the context of this chapter, we aim to also find embedded simplicial surfaces such that their embedding also has a prescribed symmetry. The *symmetry group* $\mathrm{Aut}(\phi(X))$ of an embedded simplicial surface X with embedding ϕ is defined as the group of all

orthogonal transformations $\pi \in \mathrm{O}(3)$ leaving $\phi(X)$ invariant, i.e. $\pi(\phi(X)) = \phi(X)$. For a simplicial surface X with an embedding ϕ, the following holds:

$$\mathrm{Aut}(\phi(X)) \hookrightarrow \mathrm{Aut}(X) \hookrightarrow \mathrm{Aut}(\mathcal{F}(X)).$$

2.4 Frucht's cubic graphs

In this section, we recall Frucht's cubic graph construction introduced in [Fru49]. For a given finite group G with generators $S = \{g_1, \ldots, g_n\}$, Frucht constructs a cubic graph with the property that the automorphism group of the obtained graph is isomorphic to G. In his construction he distinguishes between cyclic and non-cyclic groups. Here, we give a slightly simplified construction for a group G generated by two elements. Furthermore, we present a modified construction for a group G generated by more than three elements, as in this case, Frucht's construction in general does not yield a graph with the given group as automorphism group. Moreover, we show that our constructed graph has a three-edge colouring and hence yields a cycle double cover, as described in [Sze73]. Other constructions for cubic graphs with given automorphism group can be found in [Lov07; Bab81]. For a general finite group G generated by n elements $g_1, \ldots, g_n \in G$, the cubic graph constructed by Frucht has $2(n+2)|G|$ nodes. For $n = 2$, we can modify the graph by contracting 3-cycles such that the resulting graph has $2(2+1)|G| = 6|G|$ nodes and still has the same automorphism group.

Frucht's construction is based on Cayley graphs, which are directed edge coloured graphs.

Definition 2.4.1. Let G be a finite group generated by $S = \{g_1, \ldots, g_n\}$ with $S^{-1} = S$. The nodes of the Cayley graph $\mathcal{C}_{G,S}$ are given by the elements of G and its edges by $\{(g, gs) \mid g \in G, s \in S\}$. The n-edge colouring is given as follows: $\{(g, g \cdot s) \mid g \in G, s \in S\} \to \{1, \ldots, n\}, (g, g \cdot g_i) \mapsto i$.

In Figure 2.5a, we see a corresponding uncoloured and undirected version of a Cayley graph with 2 generators. The automorphism group of a Cayley graph corresponds to the left-action of the group G on itself.

Lemma 2.4.2. *The automorphism group of a Cayley graph $\mathcal{C}_{G,S}$ respecting its edge colouring is isomorphic to G and is given by the maps $\pi_g \colon G \to G, h \mapsto g \cdot h$, for all $g \in G$.*

For a finite group G generated by n elements, Frucht defines a cubic graph based on the construction of a Cayley graph by splitting the nodes corresponding to a group element $g \in G$ into several nodes $x_{i,g}, i = 1, \ldots, 2n+4$, as shown in Figure 2.5b.

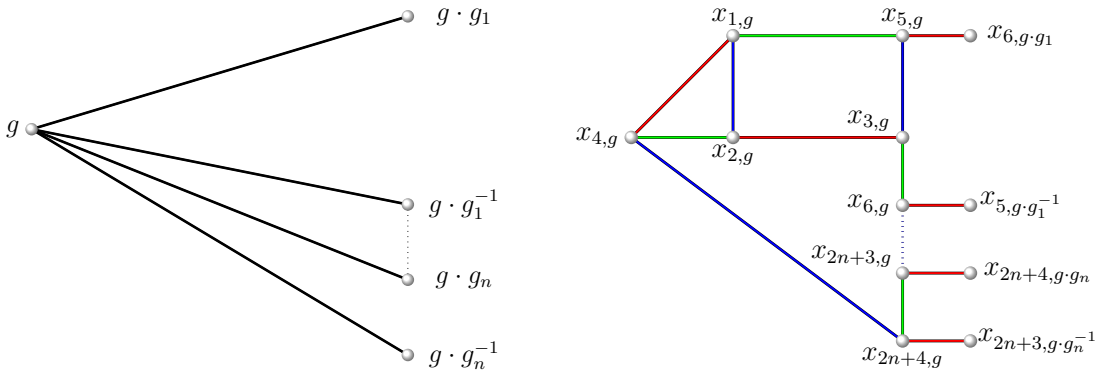

(a) (b)

Figure 2.5: (a) Undirected Cayley graph, (b) Part of Frucht's original cubic graph construction.

To formalise this, we make use of quadratic forms to define cubic graphs.

Remark 2.4.3. A cubic graph can be defined by a quadratic form, which is related to the adjacency matrix of the graph in the following way: Let $x = (x_1, \ldots, x_n)$ denote formal variables corresponding to the nodes of a graph Γ with n nodes. Let $A = (a_{ij})$ denote the adjacency matrix of Γ, and define

$$Q = \frac{1}{2} x A x^{\intercal}.$$

Each monomial of Q corresponds to an edge in Γ and we can obtain A from Q via $a_{ij} = Q(e)$, with $e = e_i + e_j$, where e_i denotes the vector with a 1 at the ith position and 0's everywhere else. The importance of this point of view is the observation that the automorphism group of the graph Γ is isomorphic to the group of permutations of the variables that preserve the quadratic from Q.

Let $h = |G|$ and $S = \{g_1, \ldots, g_n\}$ such that $\langle S \rangle = G$ and $1_G \in S$. We denote the other elements of G by $g_{n+1}, \ldots, g_h$ and define a graph via a quadratic form with nodes corresponding to the indeterminates x_{i,g_j}, with $i = 1, \ldots, 2n+4, j = 1, \ldots, h$. For $i \neq j$ we define the quadratic form

$$Q_{ij} = \sum_{k=1}^{h} x_{i,g_k} x_{j,g_k}.$$

Based on Q_{ij}, Frucht defines the quadratic forms Q and R that yield a cubic graph:

$$Q = Q_{1,2}+Q_{1,4}+Q_{1,5}+Q_{2,3}+Q_{2,4}+Q_{3,5}+Q_{3,6}+Q_{4,2n+4}+\sum_{i=2}^{n} Q_{2i+3,2i+4}+\sum_{i=2}^{n} Q_{2i+2,2i+3}+R,$$

$$R = \sum_{k=1}^{h} \sum_{j=1}^{n} x_{2j+3,g_k} x_{2j+4,g_j \cdot g_k}.$$

For two generators $S = \{g_1, g_2\}$, Frucht proves in [Fru49] that the automorphism group of the resulting cubic graph is isomorphic to G. However, for three generators this is not true in general. For instance, consider $G = A_5$ with generators $\{g_1 = (1,5)(2,4), g_2 = (1,2,4,3,5), g_3 = (2,5,3)\}$. The automorphism group of the resulting cubic graph is isomorphic to $C_2 \times A_5$ and thus does not lead to a cubic graph with given automorphism group. Note that the order of the generators matters in the construction by Frucht, i.e. in general reordering generators yields a non-isomorphic graph.

We modify Frucht's construction slightly to correct his proof and, in the case $|S| = 2$, simplify the graph as illustrated in Figure 2.6b and Figure 2.6a. Both of these constructions are based on contracting 3-cycles.

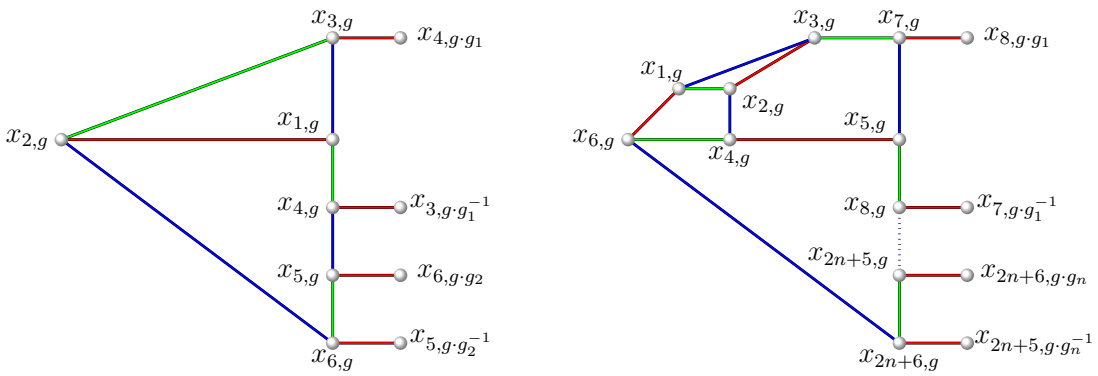

(a) (b)

Figure 2.6: (a) Simplified construction for two generators, (b) Modified construction for more than two generators.

In his proof, Frucht uses the notion of a cycle triplet of a node v in a cubic graph Γ.

Definition 2.4.4. Let e_1, e_2, e_3 be the edges incident to v in Γ and $c_{i,j}$ the length of a minimal cycle passing through the edges e_i, e_j. Then the cycle triplet of v is defined as the multi-set $\{c_{1,3}, c_{2,3}, c_{1,2}\}$.

Next, Frucht shows that for a given finite group G with generators S the constructed graph $\Gamma_{G,S}$ has an automorphism group isomorphic to G by using the following lemma.

Lemma 2.4.5. *For a given automorphism $\pi\colon \Gamma_{G,S} \to \Gamma_{G,S}$, nodes have to be mapped to nodes with the same cycle triplet, since cycles are mapped to cycles with the same length by graph automorphisms.*

For $n = 2$ resp. $n > 2$ we can define the cubic graph obtained from the Cayley graph by substituting each node with a component of the form as shown in Figure 2.6a resp. Figure 2.6b. We set $h = |G|$ and for $n = 2$ resp. $n > 2$ we define a graph with nodes corresponding to the variables x_{i,g_j},with $j = 1, \ldots, h$ and $i = 1, \ldots, 6$ resp. $i = 1, \ldots, 2n + 6$.

For $n = 2$, we define a cubic graph $\Gamma_{G,S}$ by the quadratic forms

$$Q_{simp} = Q_{2,1}+Q_{2,3}+Q_{1,3}+Q_{1,4}+Q_{2,6}+Q_{5,6}+Q_{4,5}+R_{simp},$$
$$R_{simp} = \sum_{k=1}^{h} x_{3,g_k}x_{4,g_k\cdot g_1} + x_{5,g_k}x_{6,g_k\cdot g_2}.$$

For $n > 2$, the graph $\Gamma_{G,S}$ is given by the following quadratic forms

$$\begin{aligned} Q_{mod} =& Q_{1,6}+Q_{1,2}+Q_{1,3}+Q_{2,3}+Q_{3,7}+Q_{2,4}+Q_{4,5}+Q_{4,6} \\ &+Q_{5,7}+Q_{5,8}+Q_{6,2n+6}+\sum_{i=2}^{n} Q_{2i+5,2i+6}+\sum_{i=2}^{n} Q_{2i+4,2i+5}+R_{mod}, \\ R_{mod} =& \sum_{k=1}^{h}\sum_{j=1}^{n} x_{2j+5,g_k}x_{2j+6,g_k\cdot g_j}. \end{aligned}$$

In Figure 2.6a, both nodes $x_{1,g}$ and $x_{2,g}$ have the same cycle triplet $\{3, 5, 6\}$. However, the node $x_{4,g}$ is incident to two nodes that lie on a three-cycle, i.e. $x_{1,g}$ and $x_{3,g\cdot g_1^{-1}}$, but node $x_{6,g}$ is only incident to a single node that lies on a three-cycle, i.e. $x_{2,g}$. Thus, for an automorphism π and a node $x_{i,g}$ we have that $\pi(x_{i,g}) = x_{i,g'}$ for some $g' \in G$. Similarly, in Figure 2.6b, components are mapped onto components, since $x_{6,g}$ is the only node that has cycle triplet $\{4, 6, 2 + 2n\}$ and the rest follows, from the incidence structure of the underlying cubic graph. The remaining part of the proof is analogous to the proof given by Frucht in [Fru49] and is based on showing that the automorphism group of the cubic graphs is isomorphic to the automorphism group of the corresponding edge-coloured Cayley graphs. Altogether, we have the following theorem due to Frucht. Note that Frucht handles cyclic groups and the trivial group separately in [Fru49], as described in the following section.

Theorem 2.4.6. *Let $G = \langle g_1, \ldots, g_n\rangle$ be a finite group. Then there exists a cubic graph Γ with $\mathrm{Aut}(\Gamma) \cong G$. Moreover, using the modified construction above, the graph Γ has $6|G|$ nodes for $n = 2$ and $(2n + 6)|G|$ nodes for $n > 2$.*

Frucht's original cubic graphs can be 3-edge coloured using a function $c\colon E(\Gamma) \to \{r, g, b\}$, where we identify the quadratic form Q with the edges of Γ as follows:

$$\begin{aligned} &c\left(R \cup Q_{1,4} \cup Q_{2,3}\right) = r,\ c\left(Q_{1,5} \cup Q_{2,4} \cup Q_{3,6} \cup \bigcup_{i=2}^{n} Q_{2i+3,2i+4}\right) = g, \\ &c\left(Q_{1,2} \cup Q_{3,5} \cup Q_{4,2n+4} \cup \bigcup_{i=2}^{n} Q_{2i+2,2i+3}\right) = b. \end{aligned} \tag{2.1}$$

We can obtain 3-edge colouring for the simplified and modified graphs by contracting and adding 3-cycles, respectively. For our simplified graph, i.e. in the case of $n = 2$

generators, this yields a 3-edge colouring c_{simp} for Q_{simp} as follows:

$$c_{simp}\left(R_{simp} \cup Q_{2,1}\right) = r,\ c_{simp}\left(Q_{2,3} \cup Q_{1,4} \cup Q_{5,6}\right) = g,\ c_{simp}\left(Q_{1,3} \cup Q_{2,5} \cup Q_{4,5}\right) = b.$$

It is straightforward to check that the quadratic forms Q and Q_{simp} define three-edge coloured cubic graphs with edge colouring c and c_{simp}, respectively.

In Figure 2.7a an example of Frucht's original construction for Q_8 with two generators is shown.

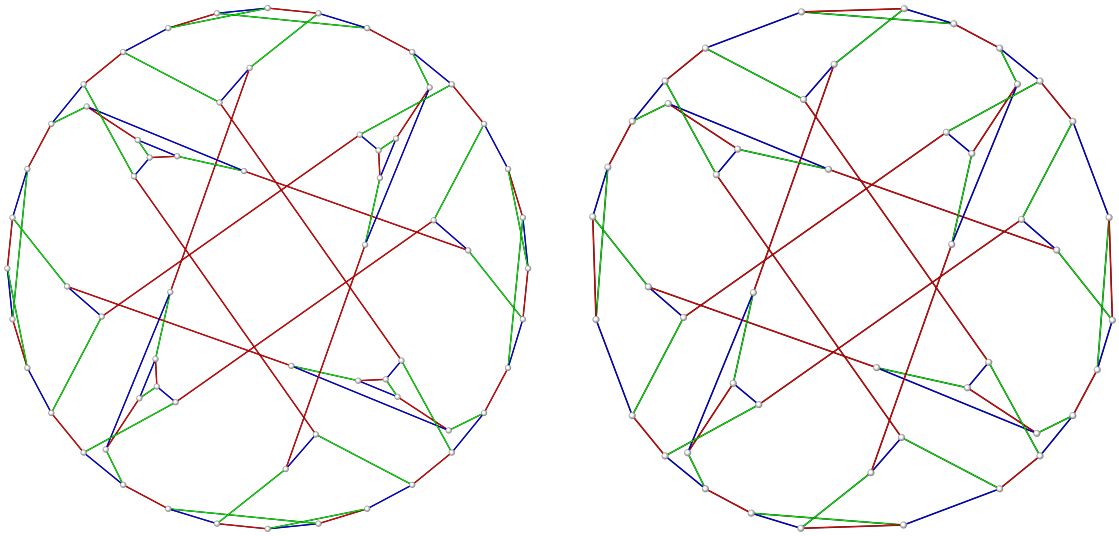

(a) (b)

Figure 2.7: Cubic graphs with automorphism groups isomorphic to Q_8: (a) Frucht's original construction on 64 nodes, (b) Our modified construction on 48 nodes.

The graph shown in Figure 2.7a has 8 vertices of degree 3 and contracting these vertices corresponds to the simplification of Frucht's graph construction for groups generated by two elements. In Figure 2.7b, we see the resulting cubic graph on 48 nodes corresponding to our simplified construction with automorphism group isomorphic to Q_8. Iterating the process of contracting vertices of degree 3 leads to a cubic graph with larger automorphism group on 32 nodes.

2.5 Cubic Graphs with Cyclic or Dihedral Automorphism Group

For a cyclic group C_n with $n > 2$, Frucht defines a graph Γ_{C_n} with $6n$ vertices and cyclic automorphism group of order n. Let $a_i, b_i, c_i, d_i, e_i, f_i$ for $i = 1, \ldots, n$ be indeterminates corresponding to the nodes of the graph Γ_{C_n}, where the edges are given by the following

quadratic form:

$$Q_{C_n} = \sum_{i=1}^{n}(a_ib_i+a_ie_i+a_if_i+b_if_i+c_id_i+c_if_i+c_ie_i)+\sum_{j=1}^{n-1}(b_{j+1}e_j+d_jd_{j+1})+b_1e_n+d_1d_n.$$

In Figure 2.8a a planar embedding of this graph construction is shown for $n = 4$.

Theorem 2.5.1 (Frucht,[Fru49]). *For $n > 2$, the quadratic form Q_{C_n} defines a cubic graph Γ_{C_n} with automorphism group isomorphic to C_n.*

The dihedral groups D_n of order $2n$ are covered by Frucht's more general construction, as presented in the previous section. However, for $n \geq 4$, we can define a cubic graph Γ_{D_n} with $4n$ instead of $6n$ nodes such that $\mathrm{Aut}(\Gamma_{D_n}) \cong D_n$ as follows. For this, let a_i, b_i, c_i, d_i for $i = 1, \ldots, n$ denote indeterminates corresponding to the nodes of the graph Γ_{D_n}, where the edges are given by the following quadratic form:

$$Q_{D_n} = \sum_{i=1}^{n}(a_ib_i + a_ic_i + c_id_i + b_ic_i) + \sum_{j=1}^{n-1}(a_jb_{j+1} + d_jd_{j+1}) + a_nb_1 + d_1d_n.$$

Proposition 2.5.2. *For $n \geq 4$, the automorphism group of the cubic graph Γ_{D_n}, defined by the quadratic form Q_{D_n} above, is isomorphic to D_n.*

Proof. Let π be an automorphism of Γ_{D_n}. The graph Γ_{D_n} has exactly n cycles of length 3, i.e.

$$(a_1, b_1, c_1), \ldots, (a_n, b_n, c_n).$$

Since the image of a cycle under π has to be a cycle of the same length, π permutes the cycles of length 3 and there exists an $i = 1, \ldots, n$ with $\pi((a_1, b_1, c_1)) = (a_i, b_i, c_i)$. It follows that the vertices $d_1, \ldots, d_n$ must be permuted in such a way that $(\pi(d_1), \ldots, \pi(d_n))$ corresponds to the cycle $(d_1, \ldots, d_n)$. We conclude that for all $j = 1, \ldots, n$, we have $\pi(d_{1+j}) = d_{i+j}$ or $\pi(d_{1+j}) = d_{i-j}$, where read the subscripts $1 + j, i + j, i - j$ modulo n. If $\pi(d_{1+j}) = d_{i+j}$, then $\pi(c_{1+j})$ is equal to c_{i+j} and thus it follows that $a_{i+j} = a_{i+j}$ and $b_{i+j} = b_{i+j}$. Therefore, π can be written as the i-th power of the permutation $\omega = (a_1, \ldots, a_n) \ldots (d_1, \ldots, d_n)$. If $\pi(d_{1+j}) = d_{i-j}$, we deduce that π maps a_{i+j}, b_{i+j}, c_{i+j} onto b_{i-j}, a_{i-j} c_{i+j}, respectively, using the same argument. Thus, π is given by the product of ω^i and the involution

$$s = \prod_{j=0}^{\lfloor \frac{n}{2} \rfloor}(a_{1-j}, b_{1+j})(d_{1-j}, d_{1+j})(c_{1-j}, c_{1+j}).$$

Hence, it follows that $\mathrm{Aut}(\Gamma_{D_n}) = \langle \omega, s \rangle \cong D_n$. □

Next, we compute straight-line embeddings of the cubic graphs Γ_{C_n} for $n \geq 3$ and Γ_{D_n} for $n \geq 4$. For simplicity, we denote the set of vertices of the graphs Γ_{C_n} and Γ_{D_n} by V and V', respectively.

We make use of the following remark to construct the corresponding embeddings of the graphs above.

Remark 2.5.3. Let $n \geq 3$ be a natural number. The permutation

$$\pi = (a_1, \ldots, a_n) \ldots (f_1, \ldots, f_n)$$

yields an automorphism of Γ_{C_n} with $\pi^n = id$. Thus, we conclude that $\mathrm{Aut}(\Gamma) = \langle \pi \rangle$ and that the automorphism group of the graph satisfies

$$\mathrm{Aut}(\Gamma_{C_n}) \cong \langle \underbrace{\begin{pmatrix} \cos(\alpha) & -\sin(\alpha) \\ \sin(\alpha) & \cos(\alpha) \end{pmatrix}}_{M_\alpha :=} \rangle \leq \mathrm{GL}_2(\mathbb{R}),$$

where $\alpha = \frac{2\pi}{n}$.

We can embed the vertices of V into $\mathbb{R}^2$ such that we obtain an embedding of Γ_{C_n} that is invariant under the action of M_α defined in the remark above.

Remark 2.5.4. Let $n \geq 3$ be a natural number. We define $v, w_1, w_2 \in \mathbb{R}^2$ by $v := (1,0)^\intercal$, $w_1 := (\cos(\alpha) - 1, \sin(\alpha))^\intercal$ and $w_2 := (\sin(\alpha), 1 - \cos(\alpha))^\intercal$, and define the function $\phi \colon V \to \mathbb{R}^2$ as follows

$$\phi(a_1) = v + \frac{1}{2}w_1, \phi(b_1) = v + \frac{1}{4}w_1, \phi(c_1) = v + \frac{1}{2}w_1 + 2w_2,$$
$$\phi(d_1) = v + \frac{1}{2}w_1 + 3w_2, \phi(e_1) = v + \frac{3}{4}w_1, \phi(f_1) = v + \frac{1}{2}w_1 + w_2,$$

and

$$\phi(a_{i+1}) = (M_\alpha)^i \phi(a_1),\ \phi(b_{i+1}) = (M_\alpha)^i \phi(b_1),\ \phi(c_{i+1}) = (M_\alpha)^i \phi(c_1),$$
$$\phi(d_{i+1}) = (M_\alpha)^i \phi(d_1),\ \phi(e_{i+1}) = (M_\alpha)^i \phi(e_1),\ \phi(f_{i+1}) = (M_\alpha)^i \phi(f_1)$$

where $\alpha = \frac{2\pi}{n}$ and $i \in \{1, \ldots, n-1\}$. Then it is straightforward to see that ϕ induces a planar straight line embedding of Γ_{C_n}.

In Figure 2.8a and 2.8b, we see the constructed planar graph embeddings for Γ_{C_n} with $n = 4$ and $n = 7$. The group $\langle M_\alpha \rangle$ in Remark 2.5.3 can be also embedded into the automorphism group of Γ_{D_n} and we can also use it to construct a planar embedding of Γ_{D_n}.

Remark 2.5.5. Let $n \geq 4$ be a natural number. Let $v, w_1, w_2 \in \mathbb{R}^2$ be defined as $v := (1,0)^\intercal$, $w_1 := (\cos(\alpha) - 1, \sin(\alpha))^\intercal$ and $w_2 := (\sin(\alpha), 1 - \cos(\alpha))^\intercal$ and define the

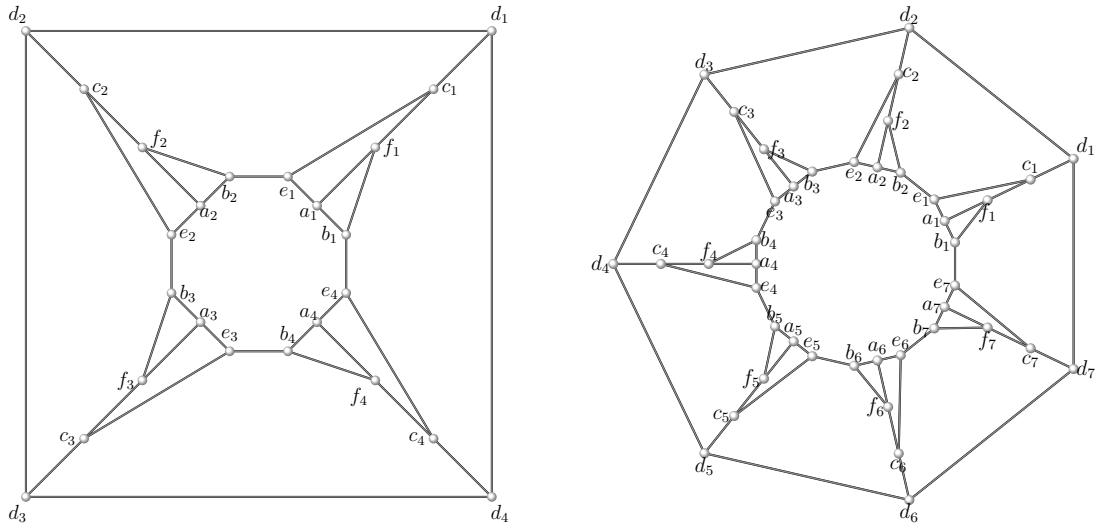

Figure 2.8: (a) Planar embedding of Γ_{C_4}, (b) Planar embedding of Γ_{C_7}.

function $\phi\colon V' \to \mathbb{R}^2$ as

$$\phi(a_1) = v + \frac{3}{4}w_1,\ \phi(b_1) = v + \frac{1}{4}w_1,$$
$$c_1) = v + \frac{1}{2}w_1 + w_2,\ \phi(d_1) = v + \frac{1}{2}w_1 + 2w_2$$

and

$$\phi(a_{i+1}) = (M_\alpha)^i\phi(a_1),\ \phi(b_{i+1}) = (M_\alpha)^i\phi(b_1),$$
$$\phi(c_{i+1}) = (M_\alpha)^i\phi(c_1),\ \phi(d_{i+1}) = (M_\alpha)^i\phi(d_1),$$

where $\alpha = \frac{2\pi}{n}$ and $i \in \{2, \ldots, n\}$. As before, it is straightforward to show that ϕ yields to a planar straight line embedding of Γ_{D_n}.

In Figure 2.9a and Figure 2.9b we see the graph embeddings of Γ_{D_n} for $n = 4, 7$.

In [Tut63], Tutte introduces a crossing-free embedding for any simple planar 3-vertex-connected graph Γ into the Euclidean plane, such that the outer face of the graph forms a convex polygon, and each vertex is positioned at the barycentre of its neighbouring vertices. The linear system of equations that arises from enforcing the above properties on the embedding of Γ has a unique solution, and this embedding is known as the *Tutte-Embedding*. As an example, we consider the graph $\Gamma = (V, E)$ given by

$$V = \{1, 2, 3, 4, 5, 6, 7, 8\}$$
$$E = \{\{1, 2\}, \{1, 4\}, \{1, 5\}, \{2, 3\}, \{2, 6\}, \{3, 4\},$$
$$\{3, 7\}, \{4, 8\}, \{5, 6\}, \{5, 8\}, \{6, 7\}, \{7, 8\}\}$$

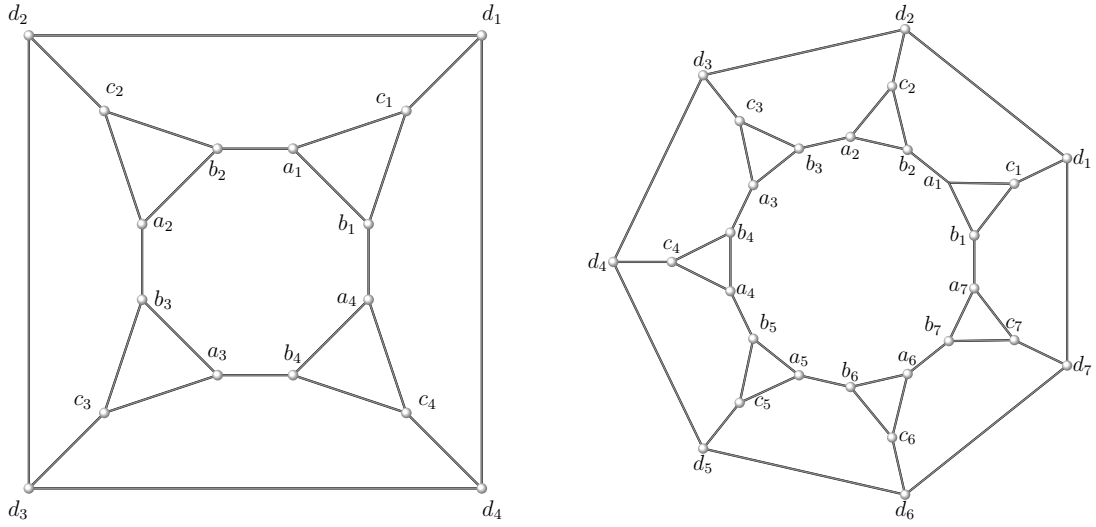

Figure 2.9: (a) Planar embedding of Γ_{D_4}, (b) Planar embedding of Γ_{D_7}.

which can be obtained as the face graph of an octahedron. Enforcing the face given by the vertices $\{1, 2, 3, 4\}$ to form a square, given by $(0, 0)^\intercal, (0, 1)^\intercal, (1, 1)^\intercal, (1, 0)^\intercal$, leads to the embedding identified by the following ordered list of coordinates:

$$\left[(0,0)^\intercal, (0,1)^\intercal, (1,1)^\intercal, (1,0)^\intercal, \left(\frac{1}{3}, \frac{1}{3}\right)^\intercal, \left(\frac{1}{3}, \frac{2}{3}\right)^\intercal, \left(\frac{2}{3}, \frac{2}{3}\right)^\intercal, \left(\frac{1}{3}, \frac{2}{3}\right)^\intercal\right].$$

Here, the coordinates of vertex i, in the Tutte Embedding, are given by the i-th entry in the above list. Figure 2.10 shows the resulting visualisation of Γ. For a non-

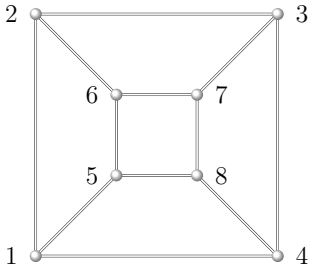

Figure 2.10: Planar embedding of the face graph of the octahedron.

planar cubic graph, see for instance Figure 2.11a, the existence of a unique embedding with all the vertices positioned at the barycentre of their neighbouring vertices is not guaranteed. However, we still obtain a system of linear equations, which can be solved, yielding a highly symmetric embedding of a given graph.

2.6 Cubic Vertex-Transitive Graphs

Frucht's construction yields a cubic graph that has a given group as automorphism group. More precisely, for a given group G generated by two resp. n elements we obtain a cubic graph Γ on $6|G|$ resp. $(2n+6)|G|$ nodes with $\mathrm{Aut}(\Gamma) \cong G$. In general, these graphs are not G-vertex-transitive, i.e. G does not act transitively on the vertices of Γ. Therefore, we focus on the construction of G-vertex-transitive graphs in this section. In the mathematical literature, such graphs are also known as (generalised) orbital graphs, see [LS16].

If a group G acts transitively on a given vertex-transitive graph Γ it can be shown that Γ is isomorphic to a Schreier coset graph, such that the nodes of Γ correspond to the right-cosets G/G_v, where G_v is the stabilizer of an arbitrary node in Γ. Since such a orbital graph has exactly $|G|/|G_v| = |G/G_v|$ vertices, it follows that this graph has considerably less nodes than the graph based on Frucht's construction. Note that if G_v is trivial, then the graph Γ is a Cayley graph. In the following two sections, we distinguish between the two cases $G_v \cong \{1\}$ and $G_v \ncong \{1\}$.

For a subgroup H of a given group G, we define the generalized orbital graph as follows:

Definition 2.6.1. Let G be a finite group and $H \leq G$ be a subgroup of G. Let $S = \{g_1, \ldots, g_n\} \subset G$. Then the graph with nodes G/H and edges $\bigcup_i \{H, g_i H\}^G$ is called a generalized orbital graph, denoted by $\Gamma_{G/H,S}$. If $H = \{\mathrm{id}\}$ we call it a *Cayley graph*. A Cayley graph with automorphism group isomorphic to G is called a *graphic regular representation* (short GRR).

2.6.1 Cubic Cayley Graphs

Here, we discuss possible constructions based on cubic Cayley graphs. Moreover, we illustrate these constructions for the group $G = A_5$ as an example.

Theorem 2.6.2 ([XZZ22])**.** *Except for a finite number of cases, all finite non-abelian simple groups have a cubic GRR.*

Combined with the following conjecture, we can find cycle double covers of cubic GRRs by 3-edge colourings.

Conjecture 2.6.3 ([HKM14])**.** *Every cubic Cayley graph admits a 3-edge colouring.*

Below, we see that Conjecture 2.6.3 can be easily verified in many cases. Alternatively, we can obtain cycle double covers of a Cayley graph as shown below.

Remark 2.6.4. 1. Let $S = \{s_1, s_2, s_3\} \subset G$ be a set of three distinct involutions such that $G = \langle S \rangle$. By colouring the edges accordingly to the corresponding involutions, we see that the Cayley graph given by G and S is a cubic 3-edge colourable graph.

2. Let $S = \{s, x, x^{-1}\} \subset G$ be a set of an involution s and an element x with even order such that $G = \langle S \rangle$. Then the Cayley graph given by G and S is 3-edge colourable by colouring the edges corresponding to the involution s in one colour and the edges obtained by the even cycles of x in alternating colours. More general, we can define a cycle double cover, via the cycles generated by x and sx: for $g \in G$ we have that g lies on the cycle $(g, g \cdot x, g \cdot x^2, \ldots, g \cdot x^{-1})$, where $x^{-1} = x^{|x|-1}$ and on the cycle $(g, g \cdot s, g \cdot s \cdot x, \ldots, g \cdot sx^{-1}, g \cdot sx^{-1} \cdot s)$. The union of these cycles for all elements $g \in G$ yields a cycle double cover invariant under the action of G.

Let $G = A_5$ and $S = \{(1,2)(4,5), (1,5)(3,4), (1,5)(2,4)\}$. Then we have that $G = \langle S \rangle$ and we can verify that the Cayley graph $\mathcal{C}_{A_5,S}$ is a GRR, as shown in Figure 2.11a. The 3-edge colouring obtained as in the remark above leads to a simplicial surface with Euler characteristic 1.

2.6.2 Cubic Orbital Graphs

Next, we focus on the case that $|G_v| > 1$. We construct a cubic vertex-transitive graph Γ on $|G|/|H|$ nodes for subgroups $H \leq G$, giving rise to candidates for small cubic graphs with given automorphism group. However, in general we have that $G < \mathrm{Aut}(\Gamma)$.

For generalized orbital graphs, we need to be more careful. For $1 \neq H \leq G$ it is possible that for an element $g \in G$, the orbit $\{H, gH\}^G$ contains other elements of the form $\{H, g'H\}$ for $g' \neq g \in G$. A (generalized) orbital graph is defined by $H \leq G$ and $S = \{g_1, \ldots, g_n\} \subset G$ with vertices G/H and edges given by the orbit of G (with element-wise actions) on the set $\{\{H, g_1H\}, \ldots, \{H, g_nH\}\}$. Let $g_1, \ldots, g_m$ with m minimal such that $\{\{H, g_1H\}, \ldots, \{H, g_nH\}\}^G = \{\{H, g_1H\}, \ldots, \{H, g_mH\}\}$. Then the resulting orbital graph is regular of degree m. We can use this construction, to obtain all vertex-transitive graphs Γ, with G acting transitively on the nodes of Γ. It is still unknown whether any vertex-transitive graph Γ admits a cycle double cover.

Remark 2.6.5. Let Γ denote a cubic vertex-transitive graph as above. If the edges of Γ are given by three orbitals, we can define a 3-edge colouring by colouring each orbital in a different colour and thus obtain a cycle double cover by alternating colour-cycles. If the edges are given by less than three orbitals, it is no longer guaranteed that we obtain a 3-edge colourable graph.

Let $H = \langle (2,3)(4,5) \rangle \leq A_5$ and consider generators $S = \{(1,5)(3,4), (1,4,2,3,5)\}$ with $\langle S \rangle = A_5$. We obtain a cubic orbital graph Γ on 30 nodes with automorphism group isomorphic to A_5 which admits exactly one 3-edge colouring (up to interchanging colours) and thus it is not a snark, see Figure 2.11b. By considering all vertex-transitive graphs of A_5, we find that this graph is the smallest vertex-transitive cubic graph with automorphism group isomorphic to A_5. Furthermore, a G-invariant cycle double cover consisting of 10 cycles of length 6 and 6 cycles of length 5, which is respected by its

automorphism group, is given as follows:

$$(14,27,28,24,19,17),(9,30,25,18,13,10),\quad (8,26,29,20,23,11),(7,15,16,21,22,12),$$
$$(3,28,27,12,7,4),(3,13,18,23,20,4),\quad (2,11,8,17,14,5),(2,25,30,21,22,5),$$
$$(1,9,10,24,19,6),(1,16,15,29,26,6),\quad (3,28,24,10,13),(2,25,18,23,11),$$
$$(1,16,21,30,9),(6,26,8,17,19),\quad (5,22,12,27,14),(4,20,29,15,7)$$

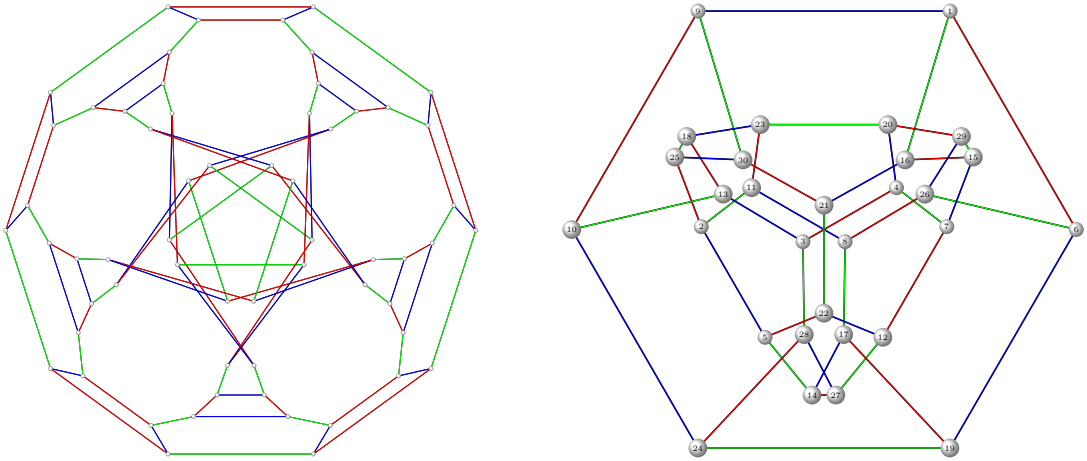

(a) (b)

Figure 2.11: Two vertex-transitive graphs with automorphism group A_5 (a) 3-edge colourable GRR, (b) Orbitalgraph on 30 nodes.

2.7 Cycle Double Covers and Simplicial Surface Constructions

In this section, we show that we can obtain a simplicial surface with a given group G as automorphism group. In both, Frucht's construction and the construction of cubic generalized orbital graphs, we achieve this by computing a G-invariant cycle double cover. Such a cycle double cover can be constructed by exploiting 3-edge colourings or the structure of the group G. Here, the number of faces (triangles) of the resulting surface equals the number of nodes of the given cubic graph. For certain groups, we can obtain smaller surfaces (in the number of faces) by considering vertex-faithful cubic graphs.

2.7.1 Frucht surfaces

We show that Frucht's cubic graphs defined in Section 2.4 give rise to simplicial surfaces. Note that the cyclic case $G = C_n$ for $n > 2$ is covered by Theorem 2.7.5. Furthermore, for $|G| \leq 2$ Frucht gives two cubic graphs with automorphism group of order 2 and 1

(see Fig. 1 and Fig. 2 in [Fru49]) which both yield simplicial spheres with isomorphic automorphism groups.

Theorem 2.7.1. *Let G be a finite non-cyclic group generated by a set S. There exists a simplicial surface $X_{G,S}$ such that $Aut(X_{G,S}) \cong G$.*

Proof. Using Theorem 2.4.6, we obtain a cubic graph $\Gamma = \Gamma_{G,S}$ with $\mathrm{Aut}(\Gamma) \cong G$. Moreover, Γ has a 3-edge colouring as shown in (2.1). This yields a cycle double cover by considering all cycles defined by alternating between two colours, see [Sze73]. We obtain a simplicial surface $X_{G,S}$, where faces and edges are given by the graph and vertices by the cycles such that $\mathcal{F}(X_{G,S}) = \Gamma$ and $\mathrm{Aut}(X_{G,E}) \leq \mathrm{Aut}(\Gamma)$. In order to show equality it suffices to show that the given cycle double cover is G-invariant. The automorphism group of the graph $\mathrm{Aut}(\Gamma)$ is isomorphic to G via the automorphisms of type

$$\sigma_m(x_{i,g_k}) = x_{i,g_m g_k},$$

for $m = 1, \ldots, h = |G|$. We have that $\sigma_m(Q_{i,j}) = Q_{i,j}$ and for $|S| = 2$ resp. $|S| > 2$ we have $\sigma_m(R_{simp}) = R_{simp}$ resp. $\sigma_m(R_{mod}) = R_{mod}$. Hence, the cycle double cover is invariant under σ_m and thus vertices of $X_{G,S}$ are mapped onto each other. It follows that $\mathrm{Aut}(X_{G,S}) \cong G$. □

For the surface construction based on the 3-edge coloring of the graphs given in Figure 2.6a and Figure 2.6b, we give the vertex degrees corresponding to the cycle-lengths.

Remark 2.7.2. Let $G = \langle S \rangle$ be a finite group with generators $S = \{g_1, \ldots, g_n\}$. Then we can give the length of the cycles in the cycle double cover above as follows: For $n = 2$ or $n > 2$ the blue-green cycles yield $|G|$ cycles of length 6 or $6 + 2n$, respectively. For the blue-red cycles, we have $|G|/|g_1 \cdot g_2|$ cycles of length $6|g_1 \cdot g_2|$ for $n = 2$ and $|G|/|g_1 \cdots g_n|$ cycles of length $6|g_1 \cdots g_n|$ for $n > 2$. The green-red cycles yield $|G|/|g_i|$ cycles of length $2|g_i|$ for $i = 2, \ldots, n$ and $|G|/|g_1|$ cycles of length $4|g_1|$. In total we have the vertex counters

$$v_6^{|G|} \cdot v_{6|g_1 \cdot g_2|}^{|G|/|g_1 \cdot g_2|} \cdot v_{4|g_1|}^{|G|/|g_1|} \cdot v_{2|g_2|}^{|G|/|g_2|},$$

for $n = 2$ and

$$v_{2n+6}^{|G|} \cdot v_{6|g_1 \cdots g_n|}^{|G|/|g_1 \cdots g_n|} \cdot v_{4|g_1|}^{|G|/|g_1|} \cdot \prod_{i=2}^{n} v_{2|g_i|}^{|G|/|g_i|},$$

for $n > 2$. Knowing the number of vertices it is straightforward to compute the Euler

characteristic of the resulting simplicial surface $X_{G,S}$ as follows:

$$\chi\left(X_{G,S}\right) = \begin{cases} |G| \cdot \left(\frac{1}{|g_1 g_2|} + \frac{1}{|g_1|} + \frac{1}{|g_2|} - 2\right), & n = 2 \\ |G| \cdot \left(\frac{1}{|g_1 \cdots g_n|} + \sum_{i=1}^{n} \frac{1}{|g_i|} - n - 2\right), & n > 2. \end{cases}$$

The surfaces obtained from the 3-edge colouring are not vertex-faithful, i.e. do not describe a simplicial complex in the usual sense, since the blue-red cycle shares at least two edges with every green-red cycle. Likewise, the blue-green cycle shares all its blue-edges with the blue-red cycle.

However, we can define an alternative cycle double cover, leading to a vertex-faithful surface in many cases.

Remark 2.7.3. Let G be a group with generators $\{g_1, \ldots, g_n\}$ such that for all $i = 1, \ldots, n$ we have that $\langle g_i \rangle \cap \langle g_1 \cdots g_n \rangle = 1$ is the trivial group. Considering Figure 2.6a, we can define a vertex-faithful surface X_G with given automorphism group G. Therefore, we give a cycle double cover of the graphs given in Section 2.4 and show that the group of graph automorphisms which are isomorphic to G leave this cover invariant. Furthermore, the cover has the additional property that no two cycles share two edges. For the rank 2 case, the cover is given as follows:

$$\left(x_{1,g}, x_{2,g}, x_{3,g}\right), \left(x_{1,g}, x_{2,g}, x_{6,g}, x_{5,g}, x_{4,g}\right),$$

for all $g \in G$,

$$\left(x_{6,g}, x_{5,g}, x_{6,g\cdot g_2}, x_{5,g\cdot g_2}, \ldots, x_{6,g\cdot g_2^{|g_2|-1}}, x_{5,g\cdot g_2^{|g_2|-1}}\right),$$

for all orbit representatives g of the right action of $\langle g_2 \rangle$ on G,

$$\left(x_{4,g}, x_{1,g}, x_{3,g}, x_{4,g*g_1}, x_{1,g\cdot g_1}, x_{3,g\cdot g_1}, \ldots, x_{4,g\cdot g_1^{|g_1|-1}}, x_{1,g\cdot g_1^{|g_1|-1}}, x_{3,g\cdot g_1^{|g_1|-1}}\right),$$

for all orbit representatives g of the right action of $\langle g_1 \rangle$ on G, and the cycles

$$\left(x_{6,g}, x_{2,g}, x_{3,g}, x_{4,g\cdot g_1}, x_{5,g\cdot g_1}, x_{6,g\cdot g_1\cdot g_2}, \ldots, x_{6,g}\right),$$

for all orbit representatives g of the right action of $\langle g_1 \cdot g_2 \rangle$ on G. It is straightforward to show that automorphisms of the underlying graph leave this cycle basis invariant since elements of the form $x_{i,g}$ are mapped onto elements of the form $x_{i,g\cdot h}$ for $h \in G$. We can also describe the vertex-counter of the resulting surface as follows:

$$v_3^{|G|} \cdot v_5^{|G|} \cdot v_{2|g_2|}^{|G|/|g_2|} \cdot v_{4|g_1|}^{|G|/|g_1|} \cdot v_{5|g_1 g_2^{-1}|}^{|G|/|g_1 g_2|}.$$

For rank $n > 2$, we can analogously define a cycle double cover and obtain the

following result.

Theorem 2.7.4. *For every finite group $G = \langle g_1, \dots, g_n \rangle$, there exists a simplicial surface X with $\mathrm{Aut}(X) \cong G$. Furthermore, X is vertex-faithful (a simplicial complex) if $\langle g_i \rangle \cap \langle g_1 \cdots g_n \rangle = \{1\}$ for all $i = 1, \dots, n$.*

In some cases, we can give alternative cycle double covers of Frucht's graph to get a vertex-faithful surface. Consider the quaternion group $Q_8 = \langle i, j | i^4 = j^4 = 1, i^2 = j^2, ij = j^{-1}i \rangle$ with generators $g_1 \coloneqq i, g_2 \coloneqq j$ as an example. In [Bab72], it is shown that no graph with automorphism group Q_8 can be embedded onto a sphere. Below, we describe a cycle double cover of the graph shown in Figure 2.7b yielding a vertex-faithful simplicial surface of Euler characteristic 0:

$$\big(x_{1,g}, x_{2,g}, x_{3,g}\big), \big(x_{1,g}, x_{2,g}, x_{6,g}, x_{5,g}, x_{4,g}\big),$$

for all $g \in Q_8$ and

$$\big(x_{3,g}, x_{1,g}, x_{4,g}, x_{3,g\cdot i^{-1}}, x_{2,g\cdot i^{-1}}, x_{6,g\cdot i^{-1}}, x_{5,g\cdot i^{-1}\cdot j^{-1}}, x_{6,g\cdot i^{-1}\cdot j^{-1}}, x_{5,g\cdot i^{-1}\cdot j^{-1}\cdot j^{-1}}, x_{4,g\cdot i^{-1}\cdot j^{-1}\cdot j^{-1}}\big),$$

for all $g \in Q_8$ (note that some elements $g \in Q_8$ are yielding the same cycle).

2.7.2 Surface with Cyclic or Dihedral Automorphism Group

In Section 2.5, cubic graphs with cyclic or dihedral automorphism group are introduced. Here, we present cycle double covers for the two families of cubic graphs giving rise to spherical surfaces. Moreover, these constructions show that the underlying cubic graphs are planar.

Theorem 2.7.5. *For $n > 2$, there exists a vertex-faithful simplicial sphere X_{C_n} with face graph Γ_{C_n} and automorphism group isomorphic to C_n. Furthermore, the graph Γ_{C_n} is a 3-connected planar cubic graph.*

Proof. We fix $n > 2$. For $i = 1 \dots, n$, we define a cycle double cover of the graph Γ_{C_n} as follows:

$$(a_i, b_i, f_i), (a_i, f_i, c_i, e_i), (e_i, c_i, d_i, d_{i+1}, c_{i+1}, f_{i+1}, b_{i+1}),$$
$$(d_1, \dots, d_n), (b_1, a_1, e_1, \dots, b_n, a_n, e_n),$$

with addition modulo n. The automorphism group of the graph is leaving the cycle cover invariant and thus the resulting surface has the same automorphism group as their underlying face graph. We obtain a surface X_{C_n} with automorphism group isomorphic to C_n. The corresponding vertex-counter of X_{C_n} is then given by $v_3^n v_4^n v_7^n v_n v_{3n}$. It follows that the surface X_{C_n} is spherical, since its Euler characteristic is given by $(n + n + n + 2) - 9n + 6n = 2$ and thus X_{C_n} is a vertex-faithful simplicial sphere.

Steinitz Theorem says that a 3-connected cubic graph is planar if and only if it is the face graph of a simplicial sphere. It follows that the graph Γ_{C_n} is planar. □

For $n > 3$, we give an analogous result for the dihedral group D_n.

Theorem 2.7.6. *For $n > 3$, there exists a vertex-faithful simplicial sphere X_{D_n} with face graph Γ_{D_n} and automorphism group isomorphic to D_n. Furthermore, the graph Γ_{D_n} is a 3-connected planar cubic graph.*

Proof. Analogously to the proof above, we construct a cyclic double cover

$$(a_i, b_i, c_i), (a_i, c_i, d_i, d_{i+1}, c_{i+1}, f_{i+1}, b_{i+1}), (d_1, \ldots, d_n), (a_1, b_1, a_2, b_2, \ldots, a_n, b_n),$$

for $i = 1, \ldots, n$ with addition modulo n. We obtain a simplicial surface X_{D_n} with vertex counter $v_3^n v_6^n v_n v_{2n}$ and due to $4n + (n + n + 2) - 6n = 2$ it follows that X_{D_n} is a vertex-faithful simplicial sphere and thus the graph Γ_{D_n} is planar. □

2.7.3 Face-Transitive Surfaces

The cubic graphs that arise from Frucht's construction yield simplicial surfaces by introducing suitable cycle double covers. Note that in general, the automorphism group of such a surface is a proper subgroup of the automorphism group of the underlying face graph. Thus, we do not necessarily obtain face-transitive surfaces, i.e. surfaces whose automorphism group acts transitively on the set of faces of the surface. However, for a graphic regular representation of a given group G, we can always associate a face-transitive surface. Here, we give an example construction for $G = A_5$ that leads to a surface X_G based on such a GRR with $\mathrm{Aut}(X_G) = G$.

In [HLM91], it is shown that Cayley graphs possess a cycle double cover. In the cubic case, this can be linked to 3-edge colourings as follows:

Remark 2.7.7. Let G be a finite group with generators S and assume that $\mathcal{C}_{G,S}$ is a cubic Cayley graph. Then one of the following two cases is true:

1. The group G is generated by three distinct involutions $S = \{s_1, s_2, s_3\}$ corresponding to a 3-edge colouring (each involution has a distinct colour). As before, we can obtain a cycle double cover of $\mathcal{C}_{G,S}$ by alternating between colours.

2. The group G is generated by one involution s and another element x with $|x| > 2$. We have seen that if $|x|$ is even, we can obtain a 3-edge colouring of $\mathcal{C}_{G,S}$. However, we can always obtain a cycle double cover using the cycles $(g, g \cdot x, \ldots, g \cdot x^{|x|-1})$ and $(g, g \cdot s, g \cdot sx, \ldots, g \cdot (sx)^{|sx|-1}, g \cdot (sx)^{|sx|-1} \cdot s)$, for $g \in G$.

In both cases the defined cycle double covers are invariant under the action of $G \leq \mathrm{Aut}(\mathcal{C}_{G,S})$ and in the case $\mathrm{Aut}(\mathcal{C}_{G,S}) \cong G$ we always obtain a simplicial surface $X_{G,S}$ with $|G|$ faces and automorphism group isomorphic to G.

Remark 2.7.8. To obtain a simplicial surface from a 3-edge coloured Cayley graph, we can use the same construction as in the previous chapters. Note that for involutions s_1, s_2, s_3, the length of the cycles are given by $|s_i \cdot s_j| \cdot 2$. In the case that $S = \{s, x, x^{-1}\}$, with $|s| = 2$ and $|x| = 2n$ for $n > 1$ the lengths of the cycles are given by $|x|, |s \cdot x| \cdot 2$ and $|s \cdot x^{-1}| \cdot 2$.

The surface $X_{G,S}$ is vertex-faithful if and only if any two cycles in the corresponding cycle double cover do not share two edges. Using the cycle double cover given in Remark 2.7.7 we can formulate the following criterion.

Proposition 2.7.9. *The surface $X = X_{G,S}$ is vertex-faithful if and only if*

1. *We have $S = \{s_1, s_2, s_3\}$ with three distinct involutions or*
2. *$S = \{s, x, x^{-1}\}$ as in Remark 2.7.7 and $\langle sx \rangle \cap \langle x \rangle = \{1\}$.*

Using the techniques from the previous sections, we get a surface with Euler characteristic 1 and automorphism group isomorphic to A_5. Its face graph is shown in Figure 2.11a. For general vertex-transitive graphs which are not Cayley graphs it is in general an open problem to determine a cycle double cover. In Figure 2.11b, we see an example of such a graph yielding a surface on 30 vertices with automorphism group isomorphic to A_5.

2.7.4 Surfaces with Automorphism Group A_5

In the previous sections, three surfaces with automorphism group isomorphic to A_5 are shown. The corresponding face graphs are given in Figure 2.1a, Figure 2.11a and Figure 2.11b. The resulting surfaces are all face-transitive and of Euler characteristic 1. In this section, we see that there exists a simplicial sphere with automorphism group isomorphic to A_5 together with an embedding with equilateral triangles such that resulting automorphism group in O(3) is isomorphic to A_5. The well-known snub dodecahedron, an Archimedean solid, has an automorphism group isomorphic to $G = A_5$ and its vertex-edge graph is isomorphic to a Cayley graph of A_5, obtained via the generators $S = \{(1,2)(3,4), (1,2,3,4,5), (1,3,5)\}$. Replacing the pentagonal faces with 5 triangles, see kis operator, see [CBG08], we get a triangulated sphere with automorphism group isomorphic to A_5, called pentakis snub dodecahedron, see Figure 2.12a. In Figure 2.12b we see the face graph of the pentakis snub dodecahedron, a planar cubic graph with automorphism group isomorphic to A_5.

2.8 Embeddings of Simplicial Surfaces

In this section, we construct two infinite families of simplicial surfaces with cyclic and dihedral symmetry. These families contain the simplicial surfaces with cyclic or

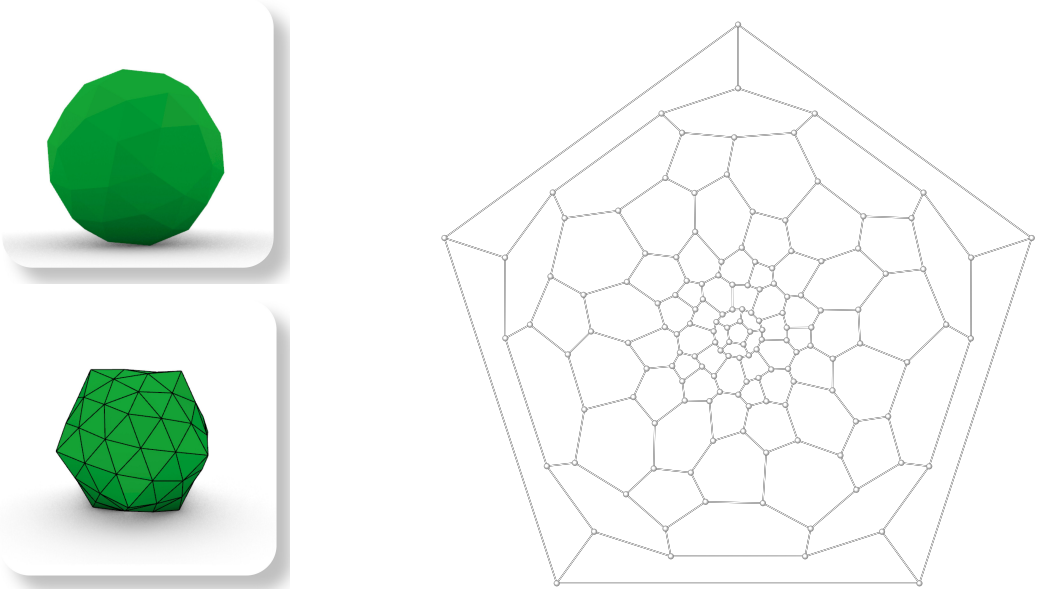

(a) (b)

Figure 2.12: (a) Snub dodecahedron and pentakis snub dodecahedron, (b) Face graph of the pentakis snub dodecahedron.

dihedral automorphism groups constructed in Section 2.7, and we show that we can embed any surface in this family with equilateral triangles such that their symmetry group is isomorphic to their automorphism group as simplicial surfaces. In particular, we show the following:

Theorem 2.8.1. *For $G = C_n$ with $n \geq 3$ or for $G = D_n$ with $n \geq 4$, there exists a vertex-faithful simplicial sphere X_G with automorphism group isomorphic to G and X_G can be embedded into $\mathbb{R}^3$ with equilateral triangles. More precisely, for $n \geq 3$ and $n \geq 4$ we construct families $(X^{(n,k)})_{k\in\mathbb{N}_0}$ and $(Y^{(n,k)})_{k\in\mathbb{N}_0}$, respectively, such that for each n, k there exist embeddings ϕ, ψ with*

$$C_n \cong \mathrm{Aut}(\phi(X^{(n,k)})) \cong \mathrm{Aut}(X^{(n,k)}) \cong \mathrm{Aut}(\mathcal{F}(X^{(n,k)})),$$
$$D_n \cong \mathrm{Aut}(\psi(Y^{(n,k)})) \cong \mathrm{Aut}(Y^{(n,k)}) \cong \mathrm{Aut}(\mathcal{F}(Y^{(n,k)})).$$

Since we aim to construct vertex-faithful surfaces, we can define the surfaces by constructing a subset S of the faces, such that the remaining faces are given by a suitable group action on the vertices. For example, the action of the group $G = \langle(2,3,4,5)\rangle \leq S_6$ can be used to obtain a combinatorial octahedron by computing the union of the following orbits:

$$\begin{aligned}\{1,2,3\}^G \cup \{2,3,6\}^G =&\{\{1,2,3\},\{1,3,4\},\{1,4,5\},\{1,2,5\},\\ &\{2,3,6\},\{3,4,6\},\{4,5,6\},\{2,5,6\}\}.\end{aligned}$$

Here, the group G acts on a subset by permuting the elements of the subset.

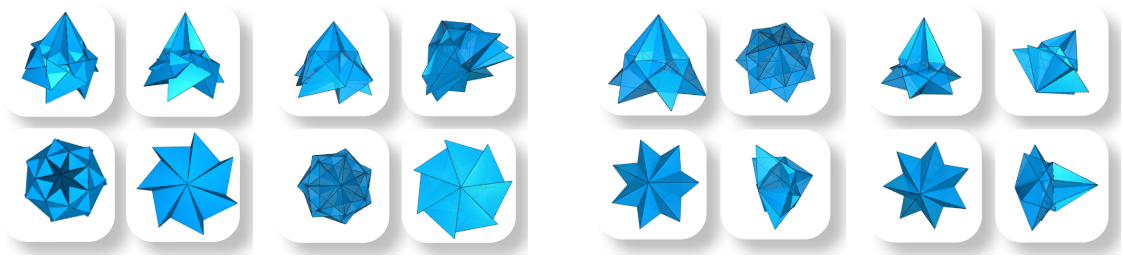

(a) (b)

Figure 2.13: (a) Two different embeddings of the surface $X^{(7,0)}$ by choosing different values for l in the construction above. (b) Two different embeddings of the surface $Y^{(7,0)}$.

Remark 2.8.2. In the following, we identify a face f of a vertex-faithful simplicial surface X with its set of incident vertices, i.e. we write $f = \{v_1, v_2, v_3\}$, if v_1, v_2, v_3 are the three vertices in the surface X that are incident to f.

2.8.1 Constructing a Family of Surfaces with Cyclic Symmetry

In this subsection, we give a detailed construction of the simplicial surfaces X_{C_n} whose face graphs have cyclic automorphism groups. Here, we define the surfaces by computing the corresponding vertices of faces instead of a cycle double cover, as seen in Section 2.7. Furthermore, we present embeddings of these surfaces consisting of equilateral triangles and prove that these surfaces and their computed embeddings also allow cyclic symmetries.

Let therefore $n \geq 3$ be a natural number, k be a non-negative integer and $\Gamma = G_{C_n}$ be the cubic graph, constructed in Section 2.5, satisfying $\mathrm{Aut}(\Gamma) \cong C_n$. Since $\pi = (a_1, \ldots, a_n) \ldots (f_1, \ldots, f_n)$ is an automorphism of Γ with $\mathrm{ord}(\pi) = n$, the automorphism group of Γ is given by $\langle \pi \rangle$.

In the following, we use the action of the cyclic group

$$G = \langle\, g \coloneqq (1, \ldots, n) \ldots ((k+2)n+1, \ldots, (k+3)n) \,\rangle$$

to obtain the vertices of faces of the simplicial surface $X^{(n,k)}$, which fully determine the incidence structure of the surface.

Definition 2.8.3. Let $n \geq 3$ be a natural number, k be a non-negative integer. We define the (vertex-faithful) simplicial surface $X^{(n,k)}$ as the simplicial surfaces with faces

$$\{f_{a_i}, f_{b_i}, f_{c_i}, f_{d_i}, f_{e_i}, f_{f_i} \mid i = 1, \ldots, n\} \cup \{f_{i,j}, \overline{f_{i,j}} \mid i = 1, \ldots, n, j = 1, \ldots, k\}.$$

and vertices incident to the faces $f_{a_1}, f_{b_1}, f_{c_1}, f_{d_1}, f_{e_1}, f_{f_1}$ are given by

$$
\begin{aligned}
f_{a_1} &= \{(k+1)n+1, (k+2)n+1, (k+3)n+2\},\\
f_{b_1} &= \{kn+1, (k+2)n+1, (k+3)n+2\}, f_{c_1} = \{kn+1, kn+2, (k+1)n+1\},\\
f_{d_1} &= \{1, 2, (k+3)n+1\}, f_{e_1} = \{kn+2, (k+1)n+1, (k+3)n+2\},\\
f_{f_1} &= \{kn+1, (k+1)n+1, (k+2)n+1\}
\end{aligned}
$$

and for $0 < j \leq k$ the vertices of faces of $f_{1,j}$ and $\overline{f_{1,j}}$ are given by

$$f_{1,j} = \{(j-1)n+1, (j-1)n+2, jn+1\} \text{ and } \overline{f_{1,j}} = \{(j-1)n+2, jn+1, jn+2\}.$$

The remaining vertices of faces by the action of G on the above faces. In particular, the vertices of the faces $f_{a_{i+1}}, \ldots, f_{f_{i+1}}$, are given by $(f_{a_1})^{g^i}, \ldots, (f_{f_1})^{g^i}$ respectively. In the case $k > 0$, we define the vertices of the faces $f_{i+1,j}$ and $\overline{f_{i+1,j}}$ by $(f_{1,j})^{g^i}$ and $(\overline{f_{1,j}})^{g^i}$, respectively.

We can compute that the surfaces $X^{(n,k)}$ always have Euler characteristic 2 and the face graph of the simplicial surface $X^{(n,0)}$ is isomorphic to G_{C_n}. Next, we seek to embed these simplicial surfaces into $\mathbb{R}^3$ as polyhedra constructed with equilateral triangles, see Definition 2.3.8.

Let l be a natural number with $\gcd(n,l) = 1$ and $\cos(\alpha) \leq \frac{1}{2}$, where $\alpha \coloneqq \frac{2\pi l}{n}$. Furthermore, let ρ and h be scalars defined by

$$\rho \coloneqq \left(\left\| \begin{pmatrix} \cos(\alpha) \\ \sin(\alpha) \end{pmatrix} - \begin{pmatrix} \cos(2\alpha) \\ \sin(2\alpha) \end{pmatrix} \right\|_2 \right)^{-1} = \frac{1}{\sqrt{2\,(1-\cos(\alpha))}},$$

$$h \coloneqq \left\| \begin{pmatrix} \cos(\alpha) \\ \sin(\alpha) \end{pmatrix} - \begin{pmatrix} \cos(\frac{\alpha}{2}) \\ \sin(\frac{\alpha}{2}) \end{pmatrix} \right\|_2 = \sqrt{1 - \rho(2 - \cos(\frac{\alpha}{2}))}.$$

Similar to the construction of the vertices of faces of $X^{(n,k)}$, we embed a subset of the vertices of the surface such that the embedding of the remaining vertices is then obtained by a suitable group action.

Remark 2.8.4. We can embed the simplicial surface $X^{(n,k)}$ with equilateral triangles by means of the function $\phi\colon X_0^{(n,k)} \to \mathbb{R}^3$ as follows:

$$
\begin{aligned}
\phi(jn+1) &= -\,jh\,(0,0,1)^\intercal + \rho\left(\cos\left(j\frac{\alpha}{2}\right), \sin\left(j\frac{\alpha}{2}\right), 0\right)^\intercal,\\
\phi(jn+2) &= -\,jh\,(0,0,1)^\intercal + \rho\left(\cos\left((j+1)\frac{\alpha}{2}\right), \sin\left((j+1)\frac{\alpha}{2}\right), 0\right)^\intercal,
\end{aligned}
$$

for $j = 0, \dots, k$ and

$$\begin{aligned}
\phi((k+3)n+1) =& \sqrt{1-\rho^2}\,(0,0,1)^\intercal\,,\\
\phi((k+3)n+2) =& -\left(kh + \sqrt{1-\rho^2}\right)(0,0,1)^\intercal\,,\\
\phi((k+1)n+1) =& \frac{1}{3}(\phi(kn+1) + \phi(kn+2) + \phi((k+3)n+2))\\
&+ \frac{(\phi((k+3)n+2) - \phi(kn+1)) \times (\phi(kn+2) - \phi((k+3)n+2))}{\|(\phi((k+3)n+2) - \phi(kn+1)) \times (\phi(kn+2) - \phi((k+3)n+2))\|_2},\\
\phi((k+2)n+1) =& \frac{1}{3}(\phi(kn+1) + \phi((k+1)n+1) + \phi((k+3)n+2))\\
&+ \frac{(\phi(kn+1) - \phi((k+3)n+2)) \times (\phi(kn+1) - \phi((k+1)n+1))}{\|(\phi(kn+1) - \phi((k+3)n+2)) \times (\phi(kn+1) - \phi((k+1)n+1))\|_2}.
\end{aligned}$$

The images of the remaining vertices of $X^{(n,k)}$ under ϕ are then given by

$$\phi((jn + (i+1))) = \phi((jn+1)^{g^i}) = (M_\alpha)^i \phi(jn+1),$$

where $i = 1, \dots, n, j = 0, \dots, k$ and M_α is given by

$$\begin{pmatrix} \cos(\alpha) & -\sin(\alpha) & 0 \\ \sin(\alpha) & \cos(\alpha) & 0 \\ 0 & 0 & 1 \end{pmatrix}. \tag{2.2}$$

Since the Euclidean norm is invariant under the multiplication with orthogonal matrices, it suffices to show the edges that are incident to the faces $f_{a_1}, \dots f_{f_1}, f_{1,j}, \overline{f_{1,j}}$ all have length 1. Since these edges have length 1 by construction, ϕ yields an embedding of $X^{(n,k)}$ constructed from equilateral triangles. If clear from the context, we denote this embedding of $X^{(n,k)}$ by $\phi_l^{(n,k)} = \phi_l$.

For $n \geq 3$ the above procedure yields

$$\left|\left\{l \mid 1 \leq l \leq \frac{n}{2},\, \gcd(n,l) = 1, \cos\left(\frac{2\pi l}{n}\right) \leq \frac{1}{2}\right\}\right|$$

non-congruent embeddings of $X^{(n,k)}$, i.e. embeddings that cannot be transformed into each other by using rigid Euclidean motions. For example, the procedure above yields two different embeddings of the surface $X^{(7,0)}$ as polyhedra consisting of equilateral triangles, see Figure 2.13a. Next, we further analyse the automorphism group of $X^{(n,k)}$ and prove that the automorphism group of $X^{(n,k)}$ and the symmetry group of $\phi_l(X^{(n,k)})$ are both cyclic groups of order n.

Proposition 2.8.5. *Let n, k, l be defined as in the above construction and ϕ_l be an embedding of the simplicial surface $X^{(n,k)}$. Then*

$$\mathrm{Aut}(\phi_l(X^{(n,k)})) \cong \mathrm{Aut}(X^{(n,k)}) \cong C_n.$$

Proof. By construction $\langle M_\alpha \rangle$, where M_α is given in (2.2), is a subgroup of the symmetry group $\mathrm{Aut}(\phi_l(X^{(n,k)}))$. Since we have $\langle M_\alpha \rangle \cong C_n$, it suffices to show that the automorphism group of $X^{(n,k)}$ is also cyclic of order n. Let therefore ϕ be an automorphism of $X^{(n,k)}$ and $(k+2)n+1, \ldots, (k+3)n$ the vertices of degree 3 in $X^{(n,k)}$. Note that there is exactly one vertex of degree $3n$, namely $(k+3)n+2$ and that the image of a vertex under ϕ has to be a vertex with the same vertex degree. Thus, we conclude:

$$\begin{aligned}&\phi((k+2)n+1) = (k+2)n+i \text{ for some } i \in \{1, \ldots, n\} \text{ and}\\ &\phi((k+3)n+1) = (k+3)n+1.\end{aligned}$$

Since $\{(k+1)n+1, (k+2)n+1, (k+3)n+1\}$ is a face of $X^{(n,k)}$, the same holds for its images under ϕ. Hence, $\phi((k+1)n+1)$ has to be a vertex of degree 4, such that $\{\phi((k+1)n+1), (k+2)n+i, (k+3)n+1\}$ forms a face of the simplicial surface. This leads to $\phi((k+1)n+1) = (k+1)n+i$. The restriction of ϕ to the vertices of the surface is given by $((1, \ldots, n) \ldots ((k+2)n+1, \ldots, (k+3)n))^i$. Thus, we obtain

$$C_n \cong \langle M_\alpha \rangle \leq \mathrm{Aut}(\phi_l(X^{(n,k)})) \hookrightarrow \mathrm{Aut}(X^{(n,k)}) \cong C_n.$$

□

2.8.2 Constructing a Family of Surfaces with Dihedral Symmetry

In this subsection, we present the detailed construction of the simplicial surfaces $Y^{(n,k)}$. We compute the incidence structure of the surfaces and the corresponding embeddings consisting of equilateral triangles, as in the cyclic case. Let therefore $n \geq 4$ and $k, l, \alpha, \rho, h, M_\alpha$ be defined as in previous section and let Γ_{D_n} the cubic graph with dihedral automorphism group constructed in Section 2.5.

Definition 2.8.6. Let $n \geq 4$ and k natural numbers. The set of faces of the simplicial surface $Y^{(n,k)}$ is defined by

$$\{f_{a_i}, f_{b_i}, f_{c_i}, f_{d_i} \mid i = 1, \ldots, n\} \cup \{f_{i,j}, \overline{f_{i,j}} \mid i = 1, \ldots, n, j = 1, \ldots, k\}.$$

Moreover, let the vertices of the faces $f_{a_1}, \ldots, f_{d_1}$ be defined by

$$f_{a_1} = \{kn+1, (k+1)n+1, (k+2)n+2\},\ f_{b_1} = \{kn+2, (k+1)n+1, (kn+2)+2\},$$
$$f_{c_1} = \{kn+1, kn+2, (k+1)n+1\},\ f_{d_1} = \{1, 2, (k+2)n+1\}.$$

and for $0 < j \leq k$ the vertices of the faces $f_{1,j}$ and $\overline{f_{1,j}}$ be given by

$$f_{1,j} = \{(j-1)n+1, (j-1)n+2, jn+1\} \text{ and } \overline{f_{1,j}} = \{(j-1)n+2, jn+1, jn+2\}.$$

We can apply the permutation $h = (1, \dots, n) \dots ((k+1)n+1, \dots, (k+2)n)$ to obtain the vertices of the remaining faces of $Y^{(n,k)}$: The vertices of the faces $f_{a_{i+1}}, \dots f_{d_{i+1}}$, are given by $(f_{a_1})^{h^i}, \dots, (f_{h_1})^{h^i}$, respectively. If $k > 0$, the vertices of the faces $f_{i+1,j}$ and $\overline{f_{i+1,j}}$ are given by $(f_{1,j})^{h^i}$ and $(\overline{f_{1,j}})^{h^i}$, respectively.

As in the case of the simplicial surfaces $X^{(n,k)}$, we have that the simplicial surfaces $Y^{(n,k)}$ have Euler characteristic 2 and the face graph of the simplicial surface $Y^{(n,0)}$ is isomorphic to G_{D_n}.

Next, we embed the simplicial surface $Y^{(n,k)}$ into $\mathbb{R}^3$ by assigning 3D-coordinates to the vertices of the simplicial surface as follows:

Remark 2.8.7. If $\cos(\alpha) \leq \frac{1}{2}$, an embedding ψ of the simplicial surface $Y^{(n,k)}$ is given as follows: For $0 < j \leq k$ we define the following images:

$$\psi(j \cdot n + 1) = -j \cdot h\,(0,0,1)^\intercal + \rho\left(\cos\left(j\frac{\alpha}{2}\right), \sin\left(j\frac{\alpha}{2}\right), 0\right)^\intercal \text{ and}$$
$$\psi(j \cdot n + 2) = -j \cdot h\,(0,0,1)^\intercal + \rho\left(\cos\left((j+1)\frac{\alpha}{2}\right), \sin\left((j+1)\frac{\alpha}{2}\right), 0\right)^\intercal.$$

Furthermore, the images of the other vertices are given by

$$\begin{aligned}
\psi((k+2)n+1) =& \sqrt{1-\rho^2}\,(0,0,1)^\intercal,\\
\psi((k+2)n+2) =& -\left(kh + \sqrt{1-\rho^2}\right)(0,0,1)^\intercal,\\
\psi((k+1)n+1) =& \frac{1}{3}(\psi(kn+1) + \psi(kn+2) + \psi((k+3)n+2))\\
&+ \frac{(\psi((k+3)n+2) - \psi(kn+1)) \times (\psi(kn+2) - \psi((k+3)n+2))}{\|(\psi((k+3)n+2) - \psi(kn+1)) \times (\psi(kn+2) - \psi((k+3)n+2))\|}.
\end{aligned}$$

Hence, we can define the images of the other vertices by

$$\psi(in+j) = \psi((in+1)^{g^j}) = {M_\alpha}^j \psi(in+1)$$

where $i \in \{1, \dots, k\}, j \in \{1, \dots, n\}$. Here, it suffices to show the edges of the constructed surfaces that are incident to the faces $f_{a_1}, f_{b_1}, f_{c_1}, f_{d_1}, f_1^i, f_2^i$ all have length 1. These edges have length 1 by construction. This construction therefore yields an embedding of $Y^{(n,k)}$ constructed from congruent triangles.

As presented in the cyclic case, the above construction gives rise to

$$\left|\left\{l \mid 1 \leq l \leq \frac{n}{2},\, \gcd(n,l) = 1, \cos\left(\frac{2\pi l}{n}\right) \leq \frac{1}{2}\right\}\right|$$

different embeddings of $Y^{(n,k)}$ that can not be transformed into each other by using rigid Euclidean motions. So for example, the construction above yields two different embeddings of the simplicial surface $Y^{(7,0)}$, see Figure 2.13b. Next, we show that the surfaces and the embeddings have dihedral automorphism groups.

Proposition 2.8.8. *Let n, k, l be defined as in the construction above, and let $\psi = \psi_l^{(n,k)}$ be the corresponding embedding of the simplicial surface $Y^{(n,k)}$. We have*

$$\mathrm{Aut}(\psi(Y^{(n,k)})) \cong \mathrm{Aut}(Y^{(n,k)}) \cong D_n.$$

Proof. Let α be defined by $\frac{2\pi l}{n}$. The matrix

$$S = \begin{pmatrix} 1 & 0 & 0 \\ 0 & -1 & 0 \\ 0 & 0 & 1 \end{pmatrix}$$

defines a symmetry of the embedding of $Y^{(n,k)}$ with $S^2 = I_3$. Thus, $\langle M_\alpha, S\rangle$ is a subgroup of the symmetry group $\mathrm{Aut}(\psi_l(X^{(n,k)}))$. Since $\langle M_\alpha, S\rangle \cong D_n$, it suffices to show that the automorphism group of $Y^{(n,k)}$ is also dihedral of order $2n$. Let ψ be an automorphism of the surface $Y^{(n,k)}$, and consider the vertices $(k+1)n+1, \ldots, (k+2)n$, which are the vertices of degree 3 in the simplicial surface. Since vertices mapped onto each other under an automorphism must have the same vertex degree, ψ permutes the vertices of degree 3. Thus, there exists an $i = 1, \ldots, n$ such that $\psi((k+1)n+1) = (k+1)n+i$. Furthermore, the image of the face $\{kn+1, kn+2, (k+1)n+i\}$ under ψ must again be a face of the surface $Y^{(n,k)}$. By examining the vertex degrees, we find that $\psi(kn+1) = kn+i$ or $\psi(kn+1) = kn+i+1$. If $\psi(kn+1) = kn+i$, then $\psi(kn+2) = kn+i+1$ and the restriction of ψ to the vertices is given by

$$((1, \ldots, n) \ldots ((k+2)n+1, \ldots, (k+3)n))^i.$$

If $\psi(kn+1) = kn+i+1$, then $\psi(kn+2) = kn+i$ and the restriction of ψ to the vertices of the surface is given by

$$((1, \ldots, n) \ldots ((k+2)n+1, \ldots, (k+3)n))^i \psi_S,$$

where ψ_S is an involution that arises from S by embedding the symmetry group of the embedding into the automorphism group of the simplicial surface. Hence, the automorphism group of $Y^{(n,k)}$ is dihedral. □

Chapter 3

Mathematical Foundations of Interlocking Assemblies

3.1 Summary

In this chapter, we establish a mathematical theory and a construction method for interlocking assemblies. First, we develop a mathematical theory around interlocking assemblies, i.e. give a definition and a method of proving the interlocking property based on infinitesimal motions. Afterwards, we give a method of constructing candidates based on planar crystallographic symmetries for interlocking assemblies. For the wallpaper group consisting only of translational symmetries, we prove that the resulting assemblies are translationally interlocked. For certain blocks that can be assembled in numerous ways, characterised by the combinatorial theory of generalised Truchet tiles, we prove the interlocking property. The main idea is to exploit the symmetries of the underlying assembly to simplify the proof of interlocking. Lastly, we present a method to evaluate interlocking assemblies.

3.2 Introduction

Consider the assembly of blocks shown in Figure 3.1d consisting of several congruent copies of the same convex block, the *Abeille block*, which are in contact with each other.

The assembly in Figure 3.1d has the property that restraining a subset of blocks, called the *frame*, from moving implies that all other blocks cannot move in any direction. For instance, one can see intuitively that for each block, two neighbours restrain it from moving upwards and two neighbours from moving downwards. Such an assembly is known as *(topological) interlocking assembly*, [EKA21]. The assembly in Figure 3.1d was first presented by Joseph Abeille as a way of cutting blocks out of stone in order to give a construction method for a "flat-vault", see [Gal35]. This assembly can

This chapter is based on research originally published at [Goe24a; Goe24b].

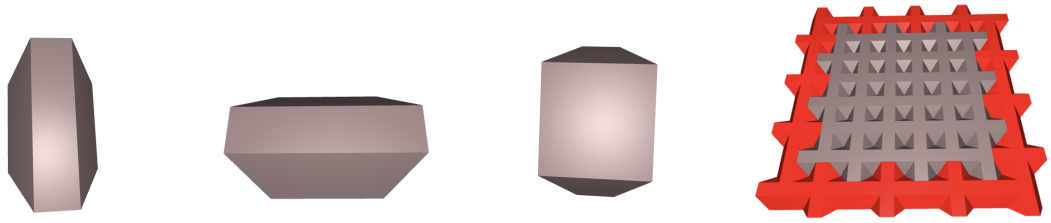

(a) (b) (c) (d)

Figure 3.1: (a,b,c) Several views of the Abeille block, (d) assembly of Abeille blocks with frame consisting of outer blocks in red.

be continued in a doubly periodic way by the means of a certain wallpaper symmetry, i.e. one block can be rotated by $0, 90, 180, 270$ degrees yielding four blocks which can be translated in a doubly periodic way to form an infinite assembly of Abeille blocks. Truchet and Frézier also give assemblies with non-convex blocks with the same symmetry in [Gal35; Fré38]. Wallpaper symmetries are omnipresent in nature, the arts, and engineering applications. For instance, M.C. Escher incorporated wallpaper symmetries into many of his artworks. His approach was to approximate a given shape by a tile, such that the resulting tile gives rise to a *fundamental domain* of a wallpaper group that tiles the Euclidean plane. The approach of obtaining new fundamental domains is also studied by Heesch and Kienzle in [HK63]. We call this approach of deforming fundamental domains the *Escher Trick* which is detailed in Section 3.4. For more background on the general theory of periodic tilings, we refer to [DH87; GS89].

The assembly by Abeille can be linked to an assembly of copies of a regular tetrahedron (a Platonic solid) by considering the intersection of half-spaces given by the planes of the tilted faces of the Abeille blocks. This tetrahedra assembly is considered by Glickman in [Gli84] and by Dyskin et. al in [Dys+01]. Dyskin et. al continued the study of such assembly and show that all Platonic solids [Dys+03a] yield interlocking assemblies, and also generalised the generation of such assemblies to convex blocks [Bel+09]. Moreover, they present a family of non-convex blocks, called *osteomorphic blocks* in [Dys+03b] which can be assembled in a variety of "non-planar" ways. For a recent overview on the research and numerous applications of these assemblies, we refer to [DEP19; EKA21].

In [Wan21], Wang presents an approach to check whether an assembly of blocks with given frame has the interlocking property. This is modelled by infinitesimal versions of contact inequalities leading to a large system of linear inequalities, i.e. for each contact face of two blocks we obtain three inequalities.

In this work, we drop the prefix "topological" and simply refer to the assemblies above as interlocking assemblies. In a mathematical context, the definition of interlocking assemblies presented in this work is purely geometric, and topologically speaking all blocks will be homeomorphic to spheres.

In Section 3.3, we give a mathematical description of interlocking assemblies and

establish a connection between the mathematical definition of interlocking assemblies, first presented in [GNP22], and an infinitesimal definition of such assemblies formulated by Wang in [Wan21]. In Section 3.4, we give a method for constructing candidates for interlocking assemblies by exploiting planar crystallographic symmetries. In Section 3.5, we prove that with additional restrictions on the construction in the previous section, we obtain the interlocking assemblies. In Section 3.6, we show that we can construct blocks that can be assembled in non-unique ways, leading to several interlocking assemblies. In Section 3.7, we provide a heuristic tool for evaluating the load distribution within an assembly and formulate an optimisation problem for finding interlocking assemblies. Throughout this work, we employ methods from crystallographic group theory, Euclidean geometry and analysis.

3.3 Mathematical Foundations of Interlocking Assemblies

In this section, we define the notion of interlocking assemblies. Intuitively speaking, an interlocking assembly is an assembly of blocks such that a subset of blocks, the *frame*, is fixed and no block outside the frame can be removed from the assembly by continuous motions without intersecting other blocks. Before giving the formal definition of interlocking assemblies, we first have to define what an assembly of blocks is and what a motion is. We present several examples of assemblies which either possess the interlocking property or do not. In the last part of this section, we demonstrate how to prove that an assembly possesses the interlocking property based on infinitesimal motions. Parts of this section are based on the work presented in [GNP22].

3.3.1 Rigid and Continuous Motions

Given a subset $X \subset \mathbb{R}^3$, we want to describe motions of X in three-dimensional Euclidean space. It is well-known that a rigid (non-continuous) motion can be obtained by composing a rotation and a translation given by a three-dimensional vector. Altogether, these motions form the so-called *special Euclidean group*. Note that, a rotation in three-dimension space around the origin corresponds to a matrix $R \in \mathbb{R}^{3\times 3}$ such that R is orthogonal and has determinant equal to 1, i.e. $R \cdot R^\intercal = \mathbb{I}$ and $\det R = 1$. The set of all rotational matrices of this form is denoted by SO(3).

Definition 3.3.1. The *special Euclidean group* also known as the set of rigid motions, denoted by SE(3), consists of elements which can be represented as pairs (R, v), where $R \in \mathrm{SO}(3)$ is a rotation matrix and v a translation vector. The group SE(3) is isomorphic to the semidirect product $\mathrm{SO}(3) \ltimes \mathbb{R}^3$ with multiplication given by $(R, v) \cdot (R', v') = (R \cdot R', R \cdot v' + v)$.

The *special Euclidean group* acts on $\mathbb{R}^3$ as summarised in the next remark.

Remark 3.3.2. The *special Euclidean group* acts naturally on $\mathbb{R}^3$ via the following group action

$$\mathrm{SE}(3) \times \mathbb{R}^3 \to \mathbb{R}^3, ((R, v), x) \mapsto R \cdot x + v,$$

where $R \cdot x$ is the vector x rotated by the rotation matrix R. The following matrix representation of SE(3) for a fixed basis of $\mathbb{R}^3$ can be used to encode the above action

$$\rho : \mathrm{SE}(3) \to \mathrm{GL}(4), (R, v) \mapsto \begin{pmatrix} R & v \\ 0 & 1 \end{pmatrix}. \tag{3.1}$$

For this, we identify $\mathbb{R}^3$ with the set $\mathrm{Aff}(\mathbb{R}^3) = \left\{ \begin{pmatrix} x \\ 1 \end{pmatrix} \mid x \in \mathbb{R}^3 \right\} \subset \mathbb{R}^4$, also known as the *affine space*, and SE(3) then acts on $\mathbb{R}^3$ as follows

$$\mathrm{SE}(3) \times \mathbb{R}^3 \to \mathbb{R}^3, \left((R, v), \begin{pmatrix} x \\ 1 \end{pmatrix} \right) \mapsto \rho((R, v)) \cdot \begin{pmatrix} x \\ 1 \end{pmatrix} = \begin{pmatrix} R & v \\ 0 & 1 \end{pmatrix} \cdot \begin{pmatrix} x \\ 1 \end{pmatrix} = \begin{pmatrix} R \cdot x + v \\ 1 \end{pmatrix}.$$

From now on, we identify SE(3) with its image of the above mentioned matrix representation into GL(4). By $\mathbb{I} \in \mathrm{GL}(4)$, we denote the identity matrix and call it the *trivial motion*. If the context allows, we refer to certain elements in SE(3) just by their corresponding rotation matrices or translation vectors. The set of rigid motions SE(3) inherits a topology as an isomorphic image of a subset of $\mathbb{R}^{4\times4}$ equipped with the operator norm $|||\cdot|||_2$ which, for a given matrix $A \in \mathbb{R}^{4\times4}$, is defined via

$$|||A|||_2 = \max_{x \in \mathbb{R}^4, \|x\|_2 = 1} \|A \cdot x\|_2,$$

where $A \cdot x \in \mathbb{R}^4$ is the matrix-vector product of A and x, and

$$\|x\|_2 = \sqrt{x_1^2 + x_2^2 + x_3^2 + x_4^2}$$

is the Euclidean norm on $\mathbb{R}^4$.

As shown in the previous remark, the elements of the *special Euclidean group* act on $\mathbb{R}^3$ as rigid motions. In order to define immovability of blocks in an assembly, we continue with the more applicable definition of continuous motions.

Definition 3.3.3. A *continuous motion* is a map $\gamma\colon [0, 1] \to \mathrm{SE}(3) \subset \mathrm{GL}(4)$ such that γ is continuous (using the topology given in Remark 3.3.2) and $\gamma(0) = \mathbb{I}$ is the identity matrix in SE(3). Furthermore, we say γ is *admissible* if γ is a continuous motion and differentiable in 0. We say that γ is trivial if $\gamma(t) = \mathbb{I}$ for all $t \in [0, 1]$ and we write $\gamma \equiv \mathbb{I}$. For admissible motions, we further enforce that for non-trivial maps γ the derivate at zero is non-zero, i.e. $\dot{\gamma}(0) \neq 0$.

The assumption that the first derivative of a non-trivial admissible motion does not

vanish is needed to establish a connection between the usual definition of interlocking assemblies and the infinitesimal version, see proof of Proposition 3.3.18.

Remark 3.3.4. The group SE(3) is a Lie group. An admissible motion γ can be differentiated in 0 to obtain an element in the corresponding Lie algebra $\mathfrak{se}(3)$. This is due to the fact, that we can extend the map γ to a differentiable map $\tilde{\gamma} : [-1, 1] \to \mathrm{SE}(3)$ by

$$\tilde{\gamma}(t) = \begin{cases} \gamma(t), & t \geq 0, \\ \gamma(-t)^{-1}, & t < 0 \end{cases}$$

and the definition of the Lie algebra as the tangent space at the identity element of the underlying Lie group, see [KN96, Chapter 1.4]. The Lie algebra $\mathfrak{se}(3)$ is a $6-$dimensional vector space with elements of the form $(\omega, t) = (\omega_1, \omega_2, \omega_3, t_1, t_2, t_3)$ which can be embedded into the $\mathbb{R}^{4\times 4}$ matrix-space as follows

$$\begin{pmatrix} 0 & -\omega_3 & \omega_2 & t_1 \\ \omega_3 & 0 & -\omega_1 & t_2 \\ -\omega_2 & \omega_1 & 0 & t_3 \\ 0 & 0 & 0 & 0 \end{pmatrix}$$

and thus we can define a multiplication of elements $(\omega, t) \in \mathfrak{se}(3)$ with elements in $p \in \mathbb{R}^3$ via

$$(\omega, t).p = \begin{pmatrix} 0 & -\omega_3 & \omega_2 & t_1 \\ \omega_3 & 0 & -\omega_1 & t_2 \\ -\omega_2 & \omega_1 & 0 & t_3 \\ 0 & 0 & 0 & 0 \end{pmatrix} \cdot \begin{pmatrix} p \\ 1 \end{pmatrix} = \begin{pmatrix} \omega \times p + t \\ 1 \end{pmatrix},$$

where $\times : \mathbb{R}^3 \times \mathbb{R}^3 \to \mathbb{R}^3$ denotes the cross product given by

$$\omega \times p = \begin{pmatrix} \omega_2 p_3 - \omega_3 p_2 \\ \omega_3 p_1 - \omega_1 p_3 \\ \omega_1 p_2 - \omega_2 p_1 \end{pmatrix}.$$

For more on the correspondence of SE(3) and $\mathfrak{se}(3)$, we refer to [CK16, Chapter 6].

3.3.2 Assemblies of Blocks

In order to define interlocking assemblies, we first need to define the notion of an assembly of blocks.

Definition 3.3.5. Let $\emptyset \neq X \subset \mathbb{R}^n$ be a connected, compact set (in the standard Euclidean topology) with $\overline{\overset{\circ}{X}} = X$, i.e. X equals the closure of its interior. We call X a *block* with boundary denoted by ∂X.

The constraints applied to a block X are inspired by practical applications and the geometric shapes of objects in three-dimensional space. Additionally, the use of the condition $\overline{\mathring{X}} = X$ serves to exclude any type of degenerations. Frequently, extra restrictions are imposed on X. For example, when $n = 3$, we focus on blocks X that have a polyhedral boundary.

Next, we define assemblies of blocks.

Definition 3.3.6. An *assembly* is a family of blocks $(X_i)_{i \in I}$ for a non-empty countable index set I such that $X_i \cap X_j = \partial X_i \cap \partial X_j$ for all $i, j \in I$ with $i \neq j$.

This condition enforces that two distinct blocks of an assembly only touch at their boundary and do not "penetrate" each other, i.e. their interiors do not intersect. Furthermore, we allow infinite assemblies of blocks, which is compatible with the assemblies constructed in Section 3.4 that carry a doubly-periodic symmetry.

In the following, we provide several intuitive examples of interlocking and non-interlocking assemblies before giving the formal definition of an interlocking assembly in the following section. We start with two ways of assembling cubes.

Figure 3.2a displays a canonical way of assembling cubes in a doubly-periodic way, i.e. we translate a given cube in two directions using two vectors $x, y \in \mathbb{R}^3$. When assembling cubes, as shown in Figure 3.2a, it is always possible to move cubes by shifting them upwards, even when neighbouring cubes are constrained from moving. In Figure 3.2b, we see an alternative way of assembling cubes in a doubly-periodic fashion. We can place the assembly between two parallel planes such that the midsection of each cube, i.e. its intersection with the plane going through the middle of the assembly, is given by a hexagon. This assembly can be generated with the method presented in [Bel+09], which is based on the well-known statement that any convex body can be constructed by a finite intersection of half-spaces, see [Grü03]. In Example 3.3.14, we show the assembly in Figure 3.2b indeed gives rise to an interlocking assembly.

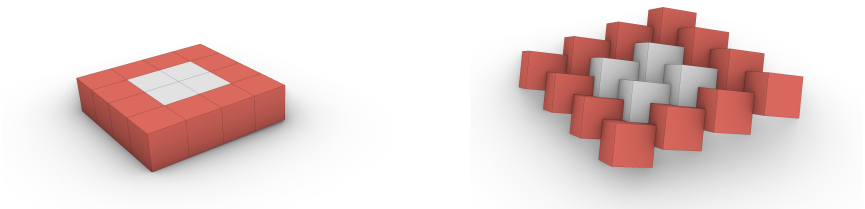

(a) (b)

Figure 3.2: Two ways of assembling cubes in a doubly-periodic fashion: (a) a simple cube assembly where grey cubes can be moved even when fixing the red cubes from moving. (b) An interlocking assembly of cubes which can be generated by the methods presented in [Bel+09].

An assembly of regular tetrahedra as shown in Figure 3.3a (see [Dys+03a; Gli84]) gives another example of an interlocking assembly by choosing a frame consisting of

the red tetrahedra to be fixed. Then it follows that the grey blocks cannot be removed from the assembly by continuous motions without causing penetrations with other blocks. Figure 3.3b and 3.3c show similar assemblies with non-regular tetrahedra, i.e. tetrahedra whose faces are not equilateral triangles. A frame is not shown in Figure 3.3b and 3.3c, and a possible frame could consist of the outer tetrahedra. All the assemblies shown in Figures 3.2b-3.3c are based on regular tessellations of the plane with wallpaper symmetries and can be obtained by the intersections of half-spaces as described in [Bel+09]. In Section 3.4 we describe an alternative approach to construct similar assemblies by deforming fundamental domains of planar crystallographic groups.

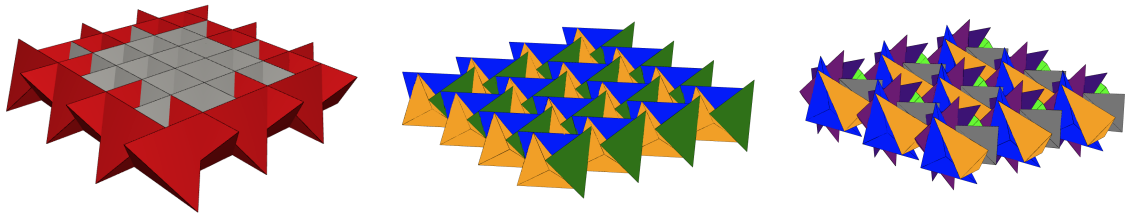

(a) (b) (c)

Figure 3.3: Collection of assemblies with tetrahedra: (a) regular tetrahedra interlocking with p4-symmetry frame in red, see [Gli84; Dys+01], (b) non-regular tetrahedra assembly with p3-symmetry, see [Pie20] for a similar block, (c) and p6-symmetry.

Before we define interlocking assemblies formally, we provide another example of an assembly of modified cubes which does yield an interlocking assembly, even though a single block cannot be removed from the assembly while fixing all other blocks and especially its neighbouring blocks. This block is obtained by modifying a cube in such a way that on one side a pyramid is added, which is removed from a different side of the cube, see Figure 3.4a.

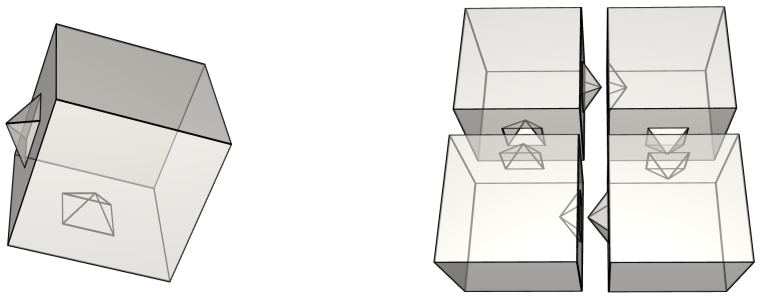

(a) (b)

Figure 3.4: (a) Modified cube. (b) Exploded view of assembling four copies of the modified cube.

We can assemble this block in groups of four similarly to the cube assembly given in Figure 3.2a. However, the assembly shown in Figure 3.5a is not an interlocking assembly, as interlocking only occurs in groups of four blocks. The set consisting of

the four gray blocks can simultaneously be moved without causing intersections by applying the admissible motion $[0,1] \to \mathrm{SE}(3), t \mapsto (\mathbb{R}^3 \to \mathbb{R}^3, x \mapsto x + (0,0,t)^\intercal)$, see Figure 3.5c.

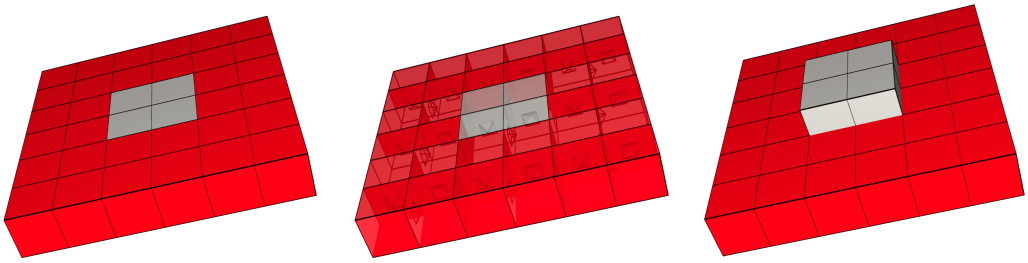

(a) (b) (c)

Figure 3.5: (a,b) An assembly with modified cubes. (c) Even though each block is restrained by its neighbours, four blocks can be moved simultaneously.

3.3.3 The Definition of Interlocking Assemblies

The following definition ensures that in an interlocking assembly, moving any finite subset of blocks leads to a violation of the assembly condition.

Definition 3.3.7. An *interlocking assembly* is an assembly of blocks $(X_i)_{i\in I}$ together with a subset $J \subset I$, called *frame*, such that for all finite non-empty sets $\emptyset \neq T \subset I \setminus J$ and for all non-trivial admissible motions $(\gamma_i)_{i\in T}$ there exists $t \in [0,1]$ and $i, j \in I$ (set $\gamma_\ell \equiv \mathbb{I}$ if $\ell \notin T$ for $\ell \in \{i,j\}$) with

$$\gamma_i(t)(X_i) \cap \gamma_j(t)(X_j) \neq \partial\gamma_i(t)(X_i) \cap \partial\gamma_j(t)(X_j). \tag{$\bowtie$}$$

If we restrict the motions to translations, we say that the assembly is a *translational interlocking assembly*.

This definition is equivalent to saying that we cannot move a finite number of blocks not contained in the frame without causing intersections of blocks.

Remark 3.3.8. The term *topological interlocking assembly* is commonly used in the engineering and architecture literature to describe interlocking assemblies with a peripheral frame or "force" holding together the blocks, see [EKA21]. In a mathematical context, this terminology may lead to confusion, as it implies a topological classification (e.g., spheres or tori based on their genus) that diverges from the primarily geometric nature of these assemblies. To avoid such confusion and ensure clarity, we employ the term *interlocking assembly*, omitting the prefix topological. This decision puts an emphasis on the geometric aspects of these structures and aims to avoid the potential confusion between topological and geometric concepts.

Moreover, the concept of *interlocking puzzles* is also compatible with our definition above. Here, a special block in the assembly labelled as the "key" is used to lock the

whole assembly, i.e. the key viewed as an element inside the block together with any other block yields the frame of an interlocking assembly as given in Definition 3.3.7.

The concepts of topological interlocking and interlocking puzzles both deal with the potential for assembly and disassembly. Specifically, if the frame is no longer fixed, the parts of the assembly can be taken apart. This idea is connected to *assembly planning*, which focuses on the possibility of moving blocks from a starting position to an ending position without causing any penetrations, as outlined in [Wil92].

3.3.4 Infinitesimal Interlocking Criterion

In this section, we build on the observation that the definition of interlocking assemblies incorporates admissible motions which are differentiable maps of the form

$$\gamma\colon [0,1] \to \mathrm{SE}(3), \gamma(0) = \mathbb{I}$$

and we can differentiate γ in 0 to obtain an element in the Lie algebra $\mathfrak{se}(3)$, also known as the algebra of infinitesimal motions acting on $\mathbb{R}^3$, see Remark 3.3.4. This action can be exploited in order to give a linearised version of Definition 3.3.7 based on infinitesimal motions, which turns out to be the one given in [Wan21]. For this, we consider two blocks X_i, X_j inside an assembly of blocks with polyhedral boundary $(X_i)_{i\in I}$ and assume that the common boundary of the two blocks, i.e. $\partial X_i \cap \partial X_j$ can be triangulated by contact triangles. For each contact triangle f given by three vertices, we compute a normal vector n pointing towards the block X_j. Let p be one of the vertices of the given contact triangle f. When given two admissible motions γ_i, γ_j for the blocks X_i, X_j, we can differentiate them in 0 to obtain elements in $\dot{\gamma}_i(0) = (\omega_i, t_i), \dot{\gamma}_j(0) = (\omega_j, t_j) \in \mathfrak{se}(3)$ and act with them on the point p. In Proposition 3.3.18, it is shown that the interlocking criterion ($\bowtie$) translates into the inequality

$$((\omega_j, t_j).p - (\omega_i, t_i).p) \cdot n = (\omega_j \times p + t_j - (\omega_i \times p + t_i)) \cdot n \geq 0,$$

which, using the rule that for all $\omega, p \in \mathbb{R}^3$, $(\omega \times p) \cdot n = (p \times n) \cdot \omega$, can be equivalently formulated as

$$((-p \times n)^\intercal, -n^\intercal, (-p \times n)^\intercal, -n^\intercal) \cdot \begin{pmatrix} \omega_i \\ t_i \\ \omega_j \\ t_j \end{pmatrix} \geq 0. \tag{3.2}$$

The system of inequalities of the form above for a whole assembly are given in Definition 3.3.11 and in Proposition 3.3.18, we show that these inequalities indeed enforce the interlocking property, as given in Definition 3.3.7. In Figure 3.6, we see a schematic illustration of this approach of modelling face to face contact using infinitesimal motions.

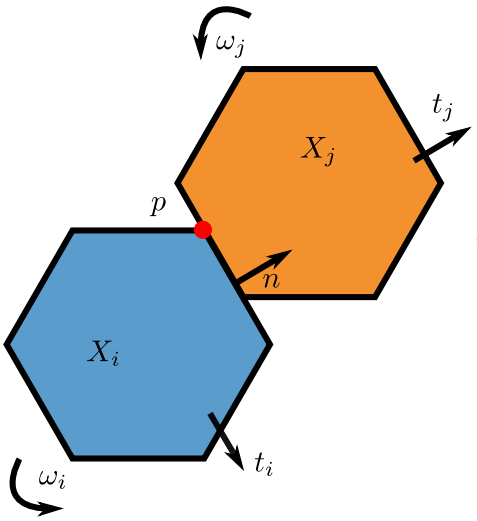

Figure 3.6: Schematic figure for interlocking criteria (after [Wan21]): For two blocks X_i, X_j and a contact point p at a contact face with normal n pointing towards the block X_j, we can derive an inequality corresponding to a non-penetration rule. Here, the motions of each block are associated with a tuple of infinitesimal motions, consisting of an angular momentum ω and a translation t.

Remark 3.3.9. In [Wan+19] an alternative infinitesimal interlocking criteria for convex blocks is presented. The idea is to replace the contact point p in Inequality (3.2) by $p - c_i$ and $p - c_j$, where c_i and c_j are the centres of the two convex blocks X_i and X_j, respectively. Moreover, it is shown in [Wan+19] that this criterion can be translated into an equilibrium analysis using Farkas lemma, which gives a connection between linear inequalities and linear equalities. This approach of relying on the centres of blocks is generalised to non-convex blocks in [Stü+23]. In this work, we focus on the definition of infinitesimal interlocking assemblies as presented in [Wan21], which does not use the centres of each block. This method can be also used for assemblies with non-convex blocks, and we establish a connection to the definition of interlocking assemblies in Proposition 3.3.18.

Since, we also consider infinite assemblies, we first define matrix-vector multiplications of infinite matrices.

Remark 3.3.10. Let $(a_{ij}) = A \in \mathbb{R}^{\mathbb{N}\times\mathbb{N}}$ be an infinite dimensional matrix such that for all $i \in \mathbb{N}$ the set $\{j \mid a_{ij} \neq 0\}$ is finite, i.e. in each row there are only finitely many non-zero entries. Then we can define the matrix-vector multiplication with a vector $x \in \mathbb{R}^{\mathbb{N}}$ in the usual way. In some cases, we restrict to vectors with finite support. Here, we write $\operatorname{supp}(x) = \{i \mid x_i \neq 0\}$ and say that x has finite support if $|\operatorname{supp}(x)| < \infty$.

The following definition, based on the work [Wan21], establishes a connection between an assembly of blocks with triangulated polyhedral boundary and a set of inequalities described by a matrix modelling face-to-face contacts.

Definition 3.3.11. Let $X = (X_i)_{i\in I}$ be an assembly of polyhedra with triangulated polyhedral boundary, such that if the intersection of two blocks at their boundary

has area larger than zero it is already given by common triangular faces. Let $J \subset I$ be a subset of I (possibly empty). Let C be the number of contact triangles between blocks inside the assembly, which are each defined by three vertices. Then we define the *infinitesimal interlocking matrix* $A_{X,J}$ with $3 \cdot C$ rows indexed by the defining vertices of all contact triangles and $6 \cdot |I \setminus J|$ columns corresponding to possible admissible motions $(\omega, t) \in \mathbb{R}^6$ for each block not contained in the frame. For each contact triangle F of blocks $i, j \in I \setminus J$, where p is a defining vertex of F and n is a normal vector of F pointing towards the block j, we obtain a row of $A_{X,J}$ of the form

$$\big(0, \dots, \underbrace{(-p \times n)^\intercal, -n^\intercal}_{i}, 0, \dots, 0, \underbrace{(p \times n)^\intercal, n^\intercal}_{j}, 0, \dots, 0\big).$$

For a block $i \in I \setminus J$ having contact with a block $j \in J$, we obtain a row of the form

$$\big(0, \dots, \underbrace{(-p \times n)^\intercal, -n^\intercal}_{i}, 0, \dots, 0, \dots, 0\big).$$

The assembly is called *infinitesimally interlocked* with *frame* J if

$$A_{X,J} \cdot x \geq 0 \text{ implies } x = 0,$$

for any x with finite support (the inequality ≥ 0 is understood componentwise). Here, we identify x with the family $(\gamma_i)_{i \in I}$ of infinitesimal motions, where $\gamma_i \in \mathfrak{se}(3)$ is of the form $\gamma_i = (\omega_i, t_i) \in \mathbb{R}^6$. By considering identical rows only once, we can reduce the system into an equivalent system with fewer inequalities and call the resulting matrix the *reduced infinitesimal interlocking matrix*. We define the assembly to be *infinitesimal translational interlocked* if there are no translational admissible motions, i.e. we set $\omega_i = 0$ for each block and thus only consider for each block X_i infinitesimal motions of the form $(0, t_i)$. In this case, we only need one row for each face-to-face contact, as we no longer dependent on the points p. The *infinitesimal interlocking space* is defined as the (convex) set of vectors x with finite support and $A_{X,J} \cdot x \geq 0$ (componentwise equal or larger than 0).

Using the cross product in the definition above is tied to the three-dimensional case as the dimension of SE(3) equals 3, and for general values n the dimension of SE(n) equals $\frac{n(n-1)}{2}$.

Remark 3.3.12. Both the interlocking and infinitesimal interlocking definition can be generalised to any dimension. In the case of the infinitesimal interlocking definition, we have to adapt the definition of the rows of the interlocking matrix by changing the part corresponding to infinitesimal rotations ω which is derived from the fact $(p \times n) \cdot \omega = (\omega \times p) \cdot n$, see Proposition 3.3.18.

Before showing that the infinitesimal definition implies the regular definition of an

interlocking assembly, we give several examples of how to compute the interlocking matrix and showcase that even for assemblies with relatively few blocks, the matrix A can be quite large. We start with the simple cube assembly given in Figure 3.2a, and show that its interlocking matrix has a non-trivial kernel with elements corresponding to admissible motions.

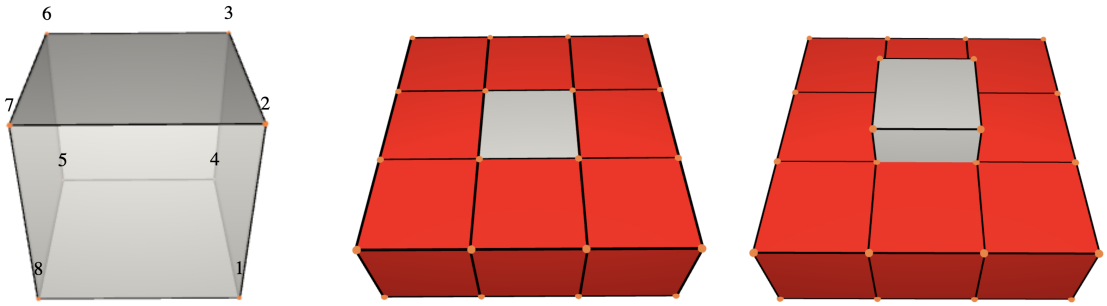

(a) (b) (c)

Figure 3.7: (a) Cube with vertex labels, (b) 3×3 assembly of cubes, (c) 3×3 assembly of cubes with middle cube shifted by the translation $(0, 0, \frac{1}{2})^\intercal$.

Example 3.3.13. We consider a 3×3 assembly of cubes as shown in Figure 3.7b. The outer cubes are fixed and only the inner cube is allowed to move. This cube in the middle can be obtained as the convex hull of the coordinates in the ordered list:

$$[(0,0,1)^\intercal, (0,0,0)^\intercal, (0,1,0)^\intercal, (0,1,1)^\intercal, (1,1,1)^\intercal, (1,1,0)^\intercal, (1,0,0)^\intercal, (1,0,1)^\intercal]$$

and the other cubes are obtained by translations of this cube in the directions $(1,0,0)$ and $(0,1,0)$. The contact-faces of the middle cube to its neighbouring cubes are given by the faces

$$[1,2,3,4], [1,2,7,8], [3,4,5,6], [5,6,7,8],$$

see Figure 3.7a. The corresponding outer normals of the faces above are given by

$$(-1,0,0)^\intercal, (0,1,0)^\intercal, (0,-1,0)^\intercal, (1,0,0)^\intercal.$$

By fixing a triangulation of the cube, we can use Definition 3.3.11 to obtain the infinitesimal interlocking matrix with rows of the form $(-(p \times n)^\intercal, -n^\intercal)$, where n is an outer normal and p is a point belonging to a corresponding face. Note, that we only need four inequalities for each contact square, as a triangulation leads to redundant inequalities (some triangles share points and normals). Thus, we only obtain 16 instead of 24 rows and the reduced infinitesimal interlocking matrix is given as follows:

$$A^\intercal = \begin{bmatrix} 0 & 0 & 0 & 0 & 1 & 0 & 0 & 1 & 0 & -1 & 0 & -1 & 0 & 0 & 0 & 0 \\ 1 & 0 & 0 & 1 & 0 & 0 & 0 & 0 & 0 & 0 & 0 & 0 & -1 & 0 & 0 & -1 \\ 0 & 0 & -1 & -1 & 0 & 0 & -1 & -1 & 0 & 0 & 1 & 1 & 1 & 1 & 0 & 0 \\ 1 & 1 & 1 & 1 & 0 & 0 & 0 & 0 & 0 & 0 & 0 & 0 & -1 & -1 & -1 & -1 \\ 0 & 0 & 0 & 0 & -1 & -1 & -1 & -1 & 1 & 1 & 1 & 1 & 0 & 0 & 0 & 0 \\ 0 & 0 & 0 & 0 & 0 & 0 & 0 & 0 & 0 & 0 & 0 & 0 & 0 & 0 & 0 & 0 \end{bmatrix}.$$

The computation $A \cdot (0,0,0,0,0,1)^\intercal = 0$ implies that an element of the form $(\omega, t)^\intercal = (0,0,0,0,0,1)^\intercal$ lies in the kernel of A. This can be interpreted as shifting a cube outside the assembly along the translation $t = (0,0,1)^\intercal$, see Figure 3.5c. Indeed, we can use the map $\gamma : [0,1] \to \mathrm{SE}(3), t \mapsto (\mathbb{R}^3 \to \mathbb{R}^3, x \mapsto x + (0,0,t)^\intercal)$ to shift out the cube in the middle, and it holds that $\dot{\gamma}(0) = (0,0,1)^\intercal$. In general, we observe that for the matrix A to have a trivial kernel, a necessary condition is that there have to be at least three normal vectors of faces n_1, n_2, n_3 with $\langle n_1, n_2, n_3 \rangle = \mathbb{R}^3$.

Next, we consider the assembly of stacked cubes as given in Figure 3.8.

(a) (b) (c)

Figure 3.8: (a) 3×3 Interlocking assembly of cubes, (b) contact faces of the middle cube with its neighbours, (c) orientation of cubes with integer coordinates.

Example 3.3.14. In order to describe the example shown in Figure 3.8 geometrically, we again consider the unit cube given by the points and faces, as in the previous example.

In order to embed the assembly shown in Figure 3.8a in a way that the coordinates of all cubes are integers, we scale the unit cube by a factor 2 such that its side length are all equal to 2. Hence, we get the coordinates

$$[(0,0,2)^\intercal, (0,0,0)^\intercal, (0,2,0)^\intercal, (0,2,2)^\intercal, (2,2,2)^\intercal, (2,2,0)^\intercal, (2,0,0)^\intercal, (2,0,2)^\intercal].$$

Now, we obtain the assembly shown in Figure 3.8c by applying the translations $v_1 = (1,1,2)^\intercal, v_2 = (-1,2,1)^\intercal$ to the cube above by translating the cube with $i \cdot v_1 + j \cdot v_2$ and $i, j \in \{0,1,2\}$. The contact faces of the grey cube in the middle are shown in Figure 3.8b and the resulting interlocking matrix determined by the contact faces is then given as follows:

$$A^\intercal = \begin{bmatrix} -3 & -3 & -4 & -4 & 4 & 4 & 5 & 5 & 0 & 0 & 0 & 0 & 0 & 0 & 0 & 0 & 4 & 4 & 3 & 3 & -5 & -5 & -4 & -4 \\ 0 & 0 & 0 & 0 & 0 & 0 & 0 & 0 & 3 & 3 & 4 & 4 & -4 & -4 & -5 & -5 & 0 & -1 & -1 & 0 & 1 & 2 & 2 & 1 \\ 1 & 2 & 2 & 1 & 0 & -1 & -1 & 0 & -5 & -4 & -4 & -5 & 4 & 3 & 3 & 4 & 0 & 0 & 0 & 0 & 0 & 0 & 0 & 0 \\ 0 & 0 & 0 & 0 & 0 & 0 & 0 & 0 & 1 & 1 & 1 & 1 & -1 & -1 & -1 & -1 & 0 & 0 & 0 & 0 & 0 & 0 & 0 & 0 \\ 1 & 1 & 1 & 1 & -1 & -1 & -1 & -1 & 0 & 0 & 0 & 0 & 0 & 0 & 0 & 0 & 0 & 0 & 0 & 0 & 0 & 0 & 0 & 0 \\ 0 & 0 & 0 & 0 & 0 & 0 & 0 & 0 & 0 & 0 & 0 & 0 & 0 & 0 & 0 & 0 & 1 & 1 & 1 & 1 & -1 & -1 & -1 & -1 \end{bmatrix}.$$

Using a linear program solver such as the one available in [JOP+24], one can compute that the kernel of the matrix is trivial and there is no $0 \neq x \in \mathbb{R}^6$ with $Ax \geq 0$. Alternatively, we can centre the middle cube at the origin to receive the following matrix

$$B^\intercal = \left[\begin{array}{cccccccccccccccccccccc} 1&1&0&0&0&0&0&1&1&0&0&0&0&0&0&0&0&0&-1&-1&-1&-1&0&0\\ 0&0&0&0&0&0&0&0&0&-1&-1&0&0&0&0&-1&-1&1&0&0&1&0&1&1&0\\ 0&1&1&0&1&0&0&1&-1&0&0&-1&0&-1&-1&0&0&0&0&0&0&0&0&0&0\\ 0&0&0&0&0&0&0&0&0&1&1&1&1&-1&-1&-1&-1&0&0&0&0&0&0&0&0\\ 1&1&1&1&-1&-1&-1&-1&0&0&0&0&0&0&0&0&0&0&0&0&0&0&0&0&0\\ 0&0&0&0&0&0&0&0&0&0&0&0&0&0&0&0&0&1&1&1&1&-1&-1&-1&-1 \end{array}\right].$$

With this matrix, it is straightforward to see that a vector $x^\intercal = (\omega, t)$ with $Bx \geq 0$ has to satisfy $t = 0$ and similarly $\omega = 0$. Thus, the assembly is infinitesimally interlocked.

In the following example, we see how admissible motions translate into infinitesimal motions.

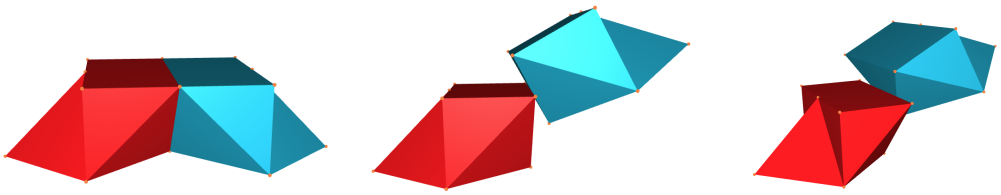

(a) (b) (c)

Figure 3.9: Two *Versatile Blocks* and application of an admissible motion: (a) Initial placement (b,c) views of applying $\gamma(0.5)$ to the right block.

Example 3.3.15. In this example, we consider two copies of a block, called *Versatile Block*, defined in Section 3.6. We consider the two blocks shown in Figure 3.9a with a contact triangle given by the points $(0,0,0)^\intercal, (0,-1,1)^\intercal, (0,1,1)^\intercal$. The map

$$\gamma : [0,1] \to \mathrm{SE}(3), t \mapsto \left(\mathbb{R}^3 \to \mathbb{R}^3, x \mapsto \begin{pmatrix} \cos(t) & 0 & -\sin(t) \\ 0 & 1 & 0 \\ \sin(t) & 0 & \cos(t) \end{pmatrix} \cdot \left(x + \begin{pmatrix} 0 \\ 0 \\ t-1 \end{pmatrix} \right) + \begin{pmatrix} 0 \\ 0 \\ 1 \end{pmatrix} \right)$$

applied to the right (blue) block in Figure 3.9a rotates and shifts it along the upper edge of the contact triangle with the left (red) block, and can be also written as follows:

$$\gamma(t)(x) = \begin{pmatrix} \cos(t) & 0 & -\sin(t) & -\sin(t)\cdot(t-1) \\ 0 & 1 & 0 & 0 \\ \sin(t) & 0 & \cos(t) & \cos(t)\cdot(t-1)+1 \\ 0 & 0 & 0 & 1 \end{pmatrix} \cdot x,$$

where x lies in the affine space $\mathrm{Aff}(\mathbb{R}^3)$. We see that $\gamma(0) = \mathbb{I}$ is the identity map and differentiating entrywise in 0 yields:

$$\dot{\gamma}(0) = \begin{pmatrix} 0 & 0 & -1 & 1 \\ 0 & 0 & 0 & 0 \\ 1 & 0 & 0 & 2 \\ 0 & 0 & 0 & 0 \end{pmatrix} \in \mathfrak{se}(3).$$

The map γ is a continuous motion that applied to the right block in Figure 3.9a

does not lead to any intersections, assuming that the left block in Figure 3.9a is restrained from moving. However, the points $\gamma(t)\left((0,-1,1)^\intercal\right), \gamma(t)\left((0,1,1)^\intercal\right)$ do not lie on the right side of the left block for any $t > 0$. In order to show that this example is compatible with Definition 3.3.11, we have to show that for the points $p \in \{(0,0,0)^\intercal, (0,-1,1)^\intercal, (0,1,1)^\intercal\}$ and the normal vector $n = (1,0,0)^\intercal$ of the contact triangle of the two blocks pointing towards the block on the right, the following inequality is satisfied

$$(p \times n, n) \cdot \dot{\gamma}(0) \geq 0,$$

where we identify $\dot{\gamma}(0)$ with $(0,-1,0,1,0,2)$. Indeed, for $p = (0,-1,1)$ we have

$$((p \times n)^\intercal, n^\intercal) \cdot \dot{\gamma}(0) = (0,1,1,1,0,0)^\intercal \cdot (0,-1,0,1,0,2) = 0,$$

for $p = (0,0,0)^\intercal$ we get

$$((p \times n)^\intercal, n^\intercal) \cdot \dot{\gamma}(0) = (0,0,0,1,0,0)^\intercal \cdot (0,-1,0,1,0,2) = 1$$

and for $p = (0,1,1)^\intercal$ we obtain

$$((p \times n)^\intercal, n^\intercal) \cdot \dot{\gamma}(0) = (0,1,-1,1,0,0)^\intercal \cdot (0,-1,0,1,0,2) = 0.$$

In order to show that the infinitesimal interlocking property implies the usual interlocking property, we need to define the *positive side* of a plane which depends on a fixed choice of a vector normal to the plane.

Definition 3.3.16. The *positive side* of a plane $P = (n,d)$ given by a normal vector n and a point $d \in \mathbb{R}^3$ which is contained in P is defined as all points p that are obtained by summing a point of the plane together with its normal multiplied by a non-negative factor, i.e. there exists $a \geq 0$ such that $p = a \cdot n + d + v$ with $n \cdot v = 0$.

We can reformulate Definition 3.3.16 as shown in the following lemma.

Lemma 3.3.17. *Let $P = (n,d)$ be a plane given by its normal vector n and a point $d \in \mathbb{R}^3$ which is contained in P. Let $p \in \mathbb{R}^3$ be a point. Then p is contained on the positive side of P if and only if $(p-d) \cdot n \geq 0$.*

Proof. The point p is contained on the positive side of P if and only if there exists $a \geq 0$ such that $p = a \cdot n + d + v$ with $n \cdot v = 0$. It follows that $p \cdot n = a \cdot \|n\|_2^2 + d \cdot n \geq d \cdot n$ and thus $(p-d) \cdot n \geq 0$. The point p lies on the other side of P, if $a < 0$ and in this case we can show analogously that $(p-d) \cdot n \leq 0$. □

As highlighted in Remark 3.3.4, the Lie algebra of the Lie group SE(3) is given by $\mathfrak{se}(3)$. The 6-dimensional algebra $(\omega, t) \in \mathfrak{se}(3)$ acts on a point $p \in \mathbb{R}^3$ via $\mathrm{SE}(3) \times \mathbb{R}^3 \to \mathbb{R}^3, \omega \times p + t$. The main difficulty of relating the infinitesimal definition to the definition of an interlocking assembly is translating the condition ($\bowtie$) in Definition 3.3.7 into an infinitesimal version.

Proposition 3.3.18. *Let $(X_i)_{i\in I}$ be an assembly together with a subset $J \subset I$. If for all finite subsets $\emptyset \neq T \subset I \setminus J$ and infinitesimal motions $x = (\gamma_i)_{i\in I}$, with $\gamma_i \in \mathbb{R}^6$ and $\gamma_i = 0$ for all $i \in I \setminus T$ (x has finite support) with*

$$A_{X,J} \cdot x \geq 0$$

implies that $x = 0$, then $(X_i)_{i\in I}$ is an interlocking assembly with frame J.

Proof. If there is an admissible family of non-trivial motions $(\gamma_i)_{i\in T}$ for a non-empty finite subset of the blocks $T \subset I \setminus J$, we can assume that for at least one $i \in T$, we have that $\dot{\gamma_i}(0) \neq 0$. Now, let p be a contact point of a contact face with vertices p, p', p'' of the blocks X_i, X_j with normal n_i pointing towards X_j. Since the motions γ_i for $i \in T$ do not lead to penetrations, it follows that for all admissible motions γ_i, γ_j of the underlying assembly there either exists $\varepsilon > 0$ such that for all $t \in [0, \varepsilon)$ the point $\gamma_j(t)(p)$ is contained in the positive side of the plane $P = (\gamma_i(t)(n_i), \gamma_i(t)(p))$ and with Lemma 3.3.17 this is equivalent to

$$(\gamma_j(t)(p) - \gamma_i(t)(p)) \cdot \gamma_i(t)(n_i) \geq 0,$$

or if there is no such ε (see Example 3.3.15), we instead consider the points $p - \frac{v}{k}$ for $k \in \mathbb{N}$, $v = \frac{(p'-p)+(p''-p)}{3}$ and get

$$\left(\gamma_j(t)\left(p - \frac{v}{k}\right) - \gamma_i(t)\left(p - \frac{v}{k}\right)\right) \cdot \gamma_i(t)(n_i) \geq 0,$$

for $t \in [0, \varepsilon_k)$ and take the limit $k \to \infty$. It follows that

$$\begin{aligned} 0 &\leq (\gamma_j(t)(p) - \gamma_i(t)(p)) \cdot \gamma_i(t)(n_i) \\ &= (\gamma_j(t)(p) - p - (\gamma_i(t)(p) - p)) \cdot \gamma_i(t)(n_i) \end{aligned}$$

which is equivalent to the following by multiplying with $\frac{1}{t}$ for $t > 0$:

$$\begin{aligned} 0 &\leq \frac{1}{t}(\gamma_j(t)(p) - p - (\gamma_i(t)(p) - p)) \cdot \gamma_i(t)(n_i) \\ &= \left(\frac{\gamma_j(t)(p) - p}{t} - \frac{\gamma_i(t)(p) - p}{t}\right) \cdot \gamma_i(t)(n_i). \end{aligned}$$

Since γ_i, γ_j are differentiable and thus continuous we have

$$\lim_{t\to 0} \gamma_i(t)(n_i) = n_i$$

and thus it follows that

$$0 \leq (\dot{\gamma_j}(0)(p) - \dot{\gamma_i}(0)(p)) \cdot n_i.$$

For an admissible motion γ, the derivative at 0 given by $\dot{\gamma}(0)$ is an element in the Lie algebra $\mathfrak{se}(3)$ and can be represented as a 6−dimensional vector (ω, t), see Remark 3.3.4. If $\dot{\gamma}_j(0)$ corresponds to (ω_j, t_j) and $\dot{\gamma}_i(0)$ to (ω_i, t_i) we get

$$0 \leq (\omega_j \times p + t_j - (\omega_i \times p + t_i)) \cdot n_i.$$

For vectors $a, b, c \in \mathbb{R}^3$, we have that

$$(a \times b) \cdot c = (b \times c) \cdot a,$$

since the determinant of the matrix $(a, b, c) \in \mathbb{R}^{3\times 3}$ can be expressed as $(a \times b) \cdot c$ and thus it follows that

$$(a \times b) \cdot c = \det(a, b, c) = \det(b, c, a) = (b \times c) \cdot a.$$

With this we can compute the following:

$$\begin{aligned}
0 &\leq (\omega_j \times p + t_j - (\omega_i \times p + t_i)) \cdot n_i \\
&= \omega_j \times p \cdot n_i + t_j \cdot n_i - \omega_i \times p \cdot n_i - t_i \cdot n_i \\
&= p \times n_i \cdot \omega_j + t_j \cdot n_i - p \times n_i \cdot \omega_i - t_i \cdot n_i \\
&= -p \times n_i \cdot \omega_i - n_i \cdot t_i + p \times n_i \cdot \omega_j + n_i \cdot t_j \\
&= (-p \times n_i, -n_i, p \times n_i, n_i) \cdot (\omega_i, t_i, \omega_j, t_j).
\end{aligned}$$

In total, we conclude that

$$0 \leq (-p \times n, -n, p \times n, n) \cdot (\omega_i, t_i, \omega_j, t_j).$$

It follows that we obtain the infinitesimal interlocking matrix $A_{X,J}$ of the underlying assembly in this way. If we assume that there is no $x \neq 0$ with finite support such that $A_{X,J} \cdot x \geq 0$, then there is no non-trivial admissible motion γ since we enforce that for such motions the corresponding infinitesimal motion given by the derivate of γ in 0 is non-trivial, i.e. $\dot{\gamma}(0) \neq 0$. □

Given this infinitesimal criterion, the question arises how it can be used to prove the interlocking property given in Definition 3.3.7. In general, we proceed as follows with a given interlocking matrix A:

1. Show that for any x, the existence of a row index i with $(Ax)_i > 0$ implies that $|\text{supp}(x)| = \infty$.

2. Show that the kernel of A is trivial.

This proves that the only admissible infinitesimal motion is the zero vector.

In general, we need to consider not only inequalities arising from face-to-face contacts.

Remark 3.3.19. In Definition 3.3.11, we only consider contacts of face pairs. In Section 3.5, we show that this suffices to prove the interlocking property for certain assemblies.

In general, restricting to face pairs only is not sufficient to prove the interlocking property, see [Wan+19; Stü+23]. In these situations one needs to model further contact types leading to further inequalities, i.e.

- vertex-vertex contact,
- vertex-edge contact,
- vertex-face contact,
- edge-edge contact,
- edge-face contact,
- face-face contact.

Considering these additional contact types increases the complexity of the problem immensely. In certain situations, we can simplify these contact relations using symmetries of the underlying assembly.

3.4 Constructing Assemblies with Wallpaper Symmetries

In the literature, many known examples of (topological) interlocking assemblies admit *planar crystallographic symmetries*, also known as *wallpaper symmetries*. These symmetries correspond to doubly-periodic tilings, such that the neighbours of each tile are arranged the same. Well-known examples include assemblies with Platonic solids (tetrahedra, octahedra, cubes, icosahedra and dodecahedra) [Dys+03a] that can be generated using the method presented in [Bel+09]. Wallpaper symmetries are omnipresent in nature, arts and engineering applications. For instance, M.C. Escher incorporated wallpaper symmetries in many of his artworks. His approach was to approximate a given shape by a tile, such that the resulting tile gives rise to a *fundamental domain* of a wallpaper group that tiles the Euclidean plane.

In this section, we describe how we construct candidates for interlocking assemblies with wallpaper symmetries based on an "Escher-like approach".

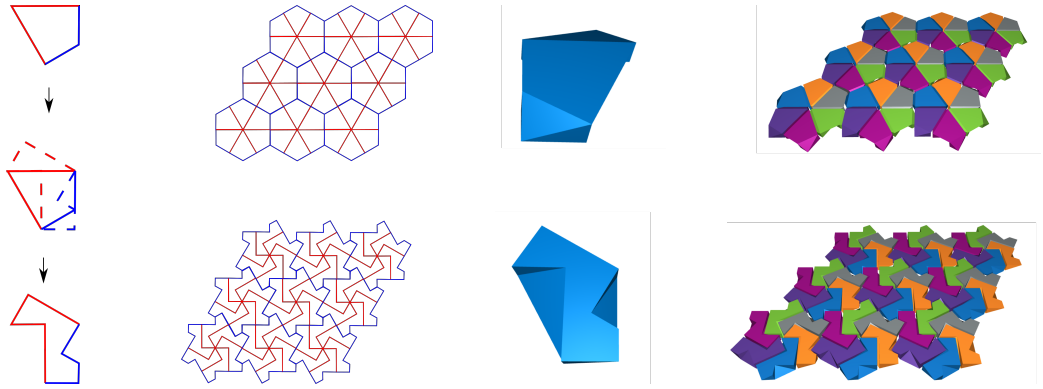

(a) (b) (c) (d)

Figure 3.10: Example of steps for generating interlocking blocks exploiting a wallpaper group of type p6. (a) Applying the *Escher Trick*, i.e. deforming fundamental domains into each other, (b) related tessellations of the two domains, (c) block obtained by interpolating between the two domains, (d) resulting assembly with blocks coloured according to their arrangement.

Example 3.4.1. For the example in Figure 3.10, we consider a wallpaper group G of type p6 (using the international notation [IUC02]). This group is generated by the following isometries acting on the Euclidean plane $\mathbb{R}^2$: a rotation matrix

$$R_{60} = \begin{pmatrix} \frac{1}{2} & -\frac{\sqrt{3}}{2} \\ \frac{\sqrt{3}}{2} & \frac{1}{2} \end{pmatrix},$$

which rotates points by 60 degrees around the origin, and two translations corresponding to the vectors $t_1 = (2,0)^\intercal$ and $t_2 = \left(1,\sqrt{3}\right)^\intercal$. A kite F, upper domain in Figure 3.10a, given by the points $(0,0)^\intercal, (1,0)^\intercal, \left(1,-\frac{\sqrt{3}}{3}\right)^\intercal, \left(1,-\frac{\sqrt{3}}{2}\right)^\intercal$, yields a funda-

mental domain for this group. The domain F tiles the plane by repeatedly applying the rotation matrix R_{60} and the translations t_1, t_2, i.e. for $i = 1, \dots, 6$ the six kites $R_{60}^i(F) = R_{60 \cdot i}(F)$ which are obtained by rotations around the origin yield a hexagon which tiles the plane by applying the translations t_1, t_2, see the top part of Figure 3.10b. Edges of the kite that are identified under this group action are coloured the same in Figure 3.10b, and we can choose intermediate points defining a piecewise linear path to deform these edges. This yields a new fundamental domain F', shown at the bottom of Figure 3.10a, and we call this method of obtaining a new domain the *Escher Trick*, which is described in more detail in the following sections. Finally, we can place the two domains F, F' in different parallel planes and interpolate between them to obtain a block X, shown in Figure 3.10c. This interpolation corresponds to a triangulation of the boundary of the block X. The block X can be assembled by extending the action of the motions R_{60}, t_1, t_2 onto the Euclidean space $\mathbb{R}^3$ by acting only on the first components of each vector, see Remark 3.4.3. This block is first introduced in [Vak+22] to develop shell structures based on interlocking blocks.

We can generalise this construction for any given wallpaper group G, by considering the set of all fundamental domains of G, i.e.

$$\mathcal{F} = \{F \mid F \text{ is a fundamental domain of } G\}$$

and considering a continuous (with regard to the Hausdorff metric) map $\lambda : [0,1] \to \mathcal{F}$ such that the set

$$X_\lambda = \{(x_1, x_2, t) \in \mathbb{R}^3 \mid (x_1, x_2) \in \lambda(t), t \in [0,1]\} \subset \mathbb{R}^3$$

gives rise to a block. Each intersection of X_λ with planes parallel to $\{(x, y, 0) \mid x, y \in \mathbb{R}\}$ corresponds to an element of $\mathcal{F}$. Copies of the block X_λ can be arranged by the action of G such that we obtain an assembly, see Theorem 3.4.17. Note that, the map λ can be recovered from the block X_λ using the projection map $\pi\colon \mathbb{R}^3 \to \mathbb{R}^2, (x_1, x_2, x_3) \mapsto (x_1, x_2)$ by taking $\lambda(t) = \pi(X_\lambda \cap \{x \in \mathbb{R}^3 \mid x_3 = t\})$. In this section, we restrict ourselves to blocks with piecewise linear boundary and polygonal fundamental domains. For that reason, we describe a triangulation of the surface of a block X, as in the example above.

Remark 3.4.2. In [Sub+19; Akl+20] a similar construction considering only Voronoi domains is presented which can be described as follows. Given a curve $\gamma\colon [0,1] \to \mathbb{R}^2$ such that $\gamma(t)$ is a point in general position for all $t \in [0,1]$, one can obtain X_λ as above by setting $\lambda(t) = D(\gamma(t))$, where $D(\gamma(t))$ is the Voronoi domain of the point $\gamma(t)$. This construction based on Voronoi Domains can be generalised to settings independent of wallpaper groups and leads to many blocks which are candidates for interlocking assemblies, see [Ebe+24; Mul+22]. In [Pie20], several constructions of interlocking blocks are given which are inspired by Frézier blocks [Fré38] that can be also constructed by using the methods presented in this section.

The main goal of this section is to construct three-dimensional assemblies with wallpaper symmetries. Thus, we need to extend the canonical action of a wallpaper group $G \leq E(2)$ onto $\mathbb{R}^3$.

Remark 3.4.3. Each element in $g \in \mathrm{E}(2)$ can be written as follows: $g : \mathbb{R}^2 \to \mathbb{R}^2, x \mapsto R \cdot x + v$, where $R \in \mathrm{O}(2)$ is an orthogonal matrix, $v \in \mathbb{R}^2$ a translation vector and $R \cdot x$ is a matrix-vector-product. The element g can be identified with a matrix of the form $\begin{pmatrix} R & v \\ 0 & 1 \end{pmatrix} \in \mathrm{GL}(3)$ acting by vector matrix-multiplication on the affine space $\mathrm{Aff}(\mathbb{R}^2) = \left\{ \begin{pmatrix} x \\ 1 \end{pmatrix} \mid x \in \mathbb{R}^2 \right\}$. Using this identification, we can embed such matrices into E(3) via the following map

$$\mathrm{E}(2) \to \mathrm{E}(3), \begin{pmatrix} R & v \\ 0 & 1 \end{pmatrix} \mapsto \begin{pmatrix} R & 0 & v \\ 0 & 1 & 0 \\ 0 & 0 & 1 \end{pmatrix}.$$

Thus, we can extend the action of a wallpaper group G onto the space $\mathbb{R}^3$.

In the following, we illustrate the construction of blocks as in Example 3.4.1. For this, we review the basic concepts of fundamental domains for planar crystallographic groups. We then explain the details of the Escher Trick, which allows us to derive a new fundamental domain, F', from an initial one, F, by deforming its edges. Subsequently, we introduce the method for constructing interlocking blocks based on this approach. Finally, we extend this method to create additional blocks.

3.4.1 Fundamental Domains and the Escher Trick

In this section, we give examples of fundamental domains and describe how we can obtain new fundamental domains from a given one. Before we introduce so-called *Dirichlet domains*, we start by giving an example of fundamental domains for wallpaper groups of type p3.

Example 3.4.4. Consider the wallpaper group G of type p3 with generators given as in Example 1.2.10. In Figure 3.11, we see several examples of fundamental domains for this group. In Figure 3.11a, the point x is chosen to be the centre of the given fundamental domain. Moreover, it has the property that no non-trivial element $\mathbb{I} \neq g \in G$ fixes x, i.e. $g(x) \neq x$. The fundamental domain can then be obtained by considering all points that are closer to x, than any other point in the orbit $G(x)$. Such a domain is known as *Dirichlet domain* or *Voronoi domain* (see the definition below). The two domains depicted in Figure 3.11b and Figure 3.11c can be obtained from the first one, by "deforming" its edges. This method, called the *Escher Trick* after the Dutch artist M.C. Escher, is detailed below.

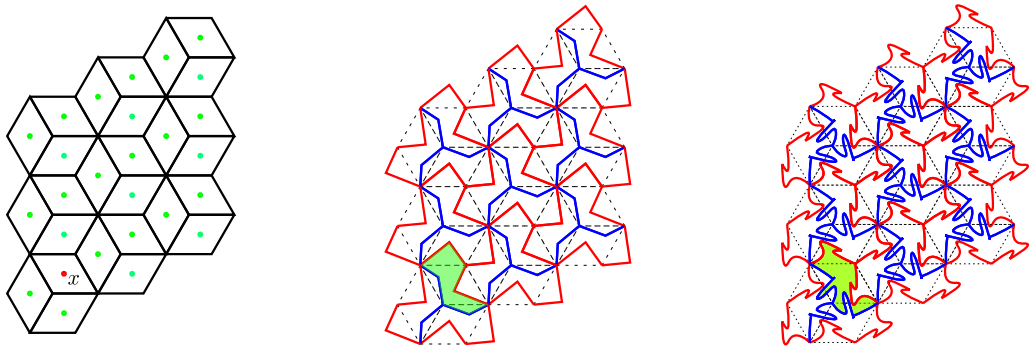

(a) (b) (c)

Figure 3.11: Several examples of fundamental domains for a wallpaper group G of type p3 (see Example 1.2.10): (a) Dirichlet domain defined by a point x with trivial stabiliser (in red) and orbit (in green) (b,c) *Escher Trick* used to obtain new fundamental domains from the domain in (a) by deforming edges. Edges that are mapped onto each other by the action of the underlying group G are coloured the same.

In the following, let G be a planar crystallographic group.

Definition 3.4.5. We say that a point $x \in \mathbb{R}^2$ is a *point in general position* if x satisfies $g(x) \neq x$ for all $\mathbb{I} \neq g \in G$. The *Dirichlet domain* or *Voronoi domain* for a point x in general position is defined to be the set of all points $y \in \mathbb{R}^2$ which are closer to x than to any other point in the orbit $G(x)$, i.e.

$$D(x) := \{y \in \mathbb{R}^2 \mid \|x - y\|_2 \leq \|g(x) - y\|_2 \text{ for all } g \in G\}.$$

Dirichlet domains exists for all crystallographic groups and yield examples of fundamental domains with a polyhedral boundary.

Lemma 3.4.6 ([Ple96])**.** *The Dirichlet domain $D(x)$, for a point x in general position, is a bounded convex polyhedral fundamental domain.*

We can cut one fundamental domain into several parts to obtain a new one. In Figure 3.12, this process is exemplified with two of the three domains given in Figure 3.11. Note that the two domains have the same area.

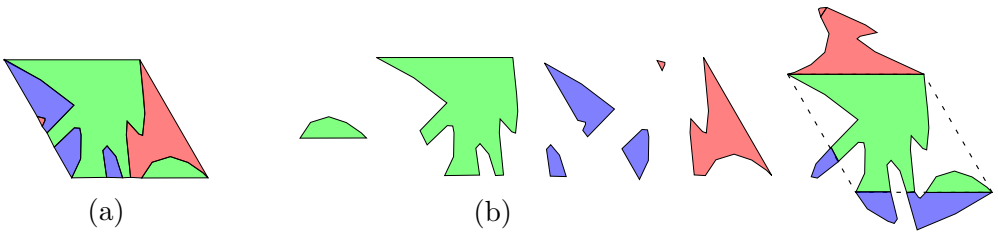

(a) (b) (c)

Figure 3.12: (a) The fundamental domain depicted in Figure 3.11a can be subdivided into different coloured regions corresponding to the coloured paths in Figure 3.11c. (b) This process yields multiple pieces. (c) These pieces are then assembled respecting identified edges to form the fundamental domain shown in Figure 3.11c.

In the proof of the following lemma, we see that the process of cutting up one fundamental domain to obtain another one is intuitive and can be generalised to crystallographic groups of any dimensions.

Lemma 3.4.7. *Any two fundamental domains of an $n-$dimensional crystallographic group G have the same volume.*

Proof. We sketch a simple proof of this lemma. Let F_1, F_2 be two fundamental domains for G. Then we can write $F_2 = \bigcup_{g\in G}(F_2 \cap gF_1)$ and since the domain F_2 is compact and G acts discretely there exist finitely many $g_1, \dots, g_k \in G$ with $F_2 \cap g_iF_1 \neq \emptyset$ and we have $F_2 = \bigcup_{g\in G}(F_2 \cap gF_1) = \bigcup_{i=1}^{k}(F_2 \cap g_iF_1)$. If vol denotes the n-dimensional volume, it follows that

$$\mathrm{vol}(F_2) = \sum_{i=1}^{k} \mathrm{vol}(F_2 \cap g_iF_1) = \sum_{i=1}^{k} \mathrm{vol}(g_i^{-1}F_2 \cap F_1) = \mathrm{vol}(F_1),$$

since the group elements are volume preserving. □

In the following, we restrict our attention to wallpaper groups G such that G does not fix any lines. If an edge of a fundamental domain F for G is fixed under the action of G it would make the fundamental domain rigid, i.e. it is not possible to deform the domain. Therefore, using crystallographic notation (see [IUC02]), G can be one of the following types: p1, p2, pg, p2gg, p3, p4 or p6 (see [IUC02] for generators of the groups).

In order to deform edges of a given fundamental domain for a wallpaper group of the above type, we identify edge pairs of fundamental domains. This is summarised in the following lemma.

Lemma 3.4.8. *Let G be a wallpaper group of type* p1, p2, pg, p2gg, p3, p4 or p6 *and F a polyhedral fundamental domain for G such that $\overline{\mathring{F}} = F$. Then it follows that the edges of F can be grouped into pairs such that the edges of each pair lie in the same orbit under the action of G, i.e. we can order the edges $e_1, \dots, e_n$ of F such that we have $n = 2m$ and there exist $g_1, \dots, g_m$ with $g_i(e_i) = e_{i+m}$. Here, we identify each edge e_i as a set containing two vertices $v_i, w_i \in \mathbb{R}^2$ with $e = e_i = \{v_i, w_i\}$.*

Proof. Since G does not fix any line, it follows that no edge of F is left invariant under G. Now, assume that for a given edge $e = \{v, w\}$ of F there exist $\mathbb{I} \neq g', g'' \in G$ and e', e'' edges of F such that $e' = g'(e), e'' = g''(e)$. Take a point p on $\mathrm{conv}(e) = \{\lambda v + (1-\lambda)w \mid \lambda \in [0,1]\}$ such that there exists $\varepsilon > 0$ with $B_\varepsilon(p)$ is divided by e into two non-empty sets B, B' such that $B \subset F$. Such a point p exists by the assumption $\overline{\mathring{F}} = F$ and the fact that G acts discretely. Then it follows that $g'(B'), g''(B') \subset F$ since $h(B) \not\subset F$ for all $h \in G$ with $g \neq h$ and thus $g' = g''$. It follows that the edges of F can be paired under the action of G. □

The existence of Dirichlet domains for any wallpaper group allows us to start with a given fundamental domain and deform the edges in such a way that we obtain a new fundamental domain. This method can be also used to approximate a given set by a fundamental domain, see [KS00]. For a visualisation of wallpaper groups and this method, we refer to the software [SHC].

Remark 3.4.9. The Escher Trick can be summarised in the following steps:

1. Start with a given fundamental domain F for a wallpaper group G, for instance a Dirichlet domain.

2. Identify edge pairs of F, i.e. edges that are identified under the action of the underlying group.

3. For each edge pair (e, e'), choose an edge e and an injective curve γ_e with values in $\mathbb{R}^2$ and same endpoints as e such that the orbit under the action of G of all curves γ_e do not "cross" but are allowed to "touch" (this condition is precisely stated for piecewise linear paths defined by three points in Definition 3.4.11).

4. We obtain a new fundamental domain with boundary given by the orbit of the curves γ_e.

In Figure 3.13, we see an example of the Escher Trick. Here, we exploit the symmetries of p1 to create a free-form fundamental domain resembling a bird. The initial domain is given by a rhomb, i.e. a quadrilateral with all side lengths the same, which is a Dirichlet domain (choose its centre as defining point as in Figure 3.11a). Edges that are identified are coloured the same, and we can define a curve for each such edge.

Since, we enforce that the curves start and end at the defining points of the edges, we obtain a closed curve by concatenating all curves. Due to Jordan's curve theorem, proved by Jordan in [Jor87], we obtain a bounded set, yielding a fundamental domain for the underlying wallpaper group G.

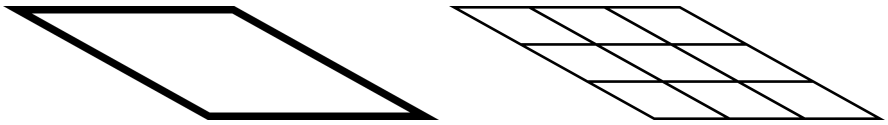

(a) Dirichlet domain and corresponding tiling for wallpaper group of type p1.

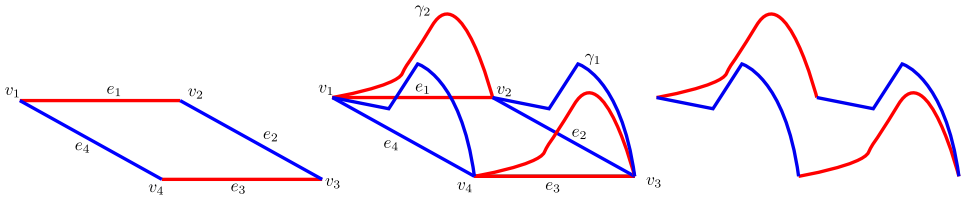

(b) Steps of the Escher Trick for wallpaper group of type p1 using non-linear deformations.

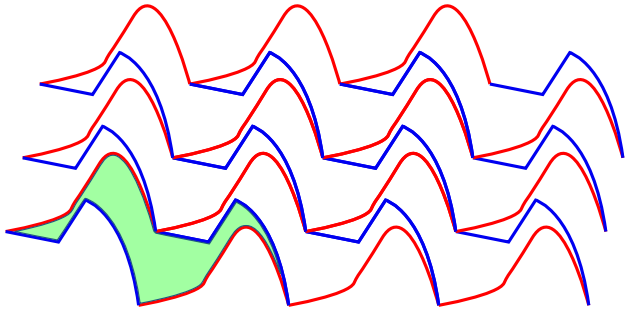

(c) Resulting tiling from Figure (b) with one tile highlighted in green.

Figure 3.13: Example for the construction steps of the Escher Trick for wallpaper group of type p1: (a) We start with a given fundamental domain; (b) Identify edge pairs and deform edges using paths to obtain a new fundamental domain. (c) The acquired domain also gives rise to a tesselation of the plane.

The condition in step 3. above that the paths do not cross is enforced in order to obtain a unique fundamental domain. For two differentiable curves, γ, γ', we can define crossing points for t, t' with $\gamma(t) = \gamma'(t')$ by checking if $\dot{\gamma}(t) \neq \dot{\gamma}'(t')$ holds. Since we neither want to restrict ourselves to differentiable curves nor want to allow all curves, we reformulate this condition for piecewise linear curves defined by three points, two of which are the endpoints of a given edge. First, we define piecewise linear paths.

Definition 3.4.10. For $v_1, v_2 \in \mathbb{R}^2$, we define the *piecewise linear path* or *line segment* connecting v_1, v_2 as the continuous map $\gamma_{v_1,v_2} : [0,1] \to \mathbb{R}^2, \mapsto v_1 + t \cdot (v_2 - v_1)$. Moreover, we define the *piecewise linear path* defined for $n \geq 3$ points $v_1, \ldots, v_n$ as the continuous map $\gamma_{v_1,\ldots,v_n} : [0,1] \to \mathbb{R}^2$ defined inductively via

$$\gamma_{v_1,\ldots,v_n}(t) = \begin{cases} \gamma_{v_1,\ldots,v_{n-1}}(2 \cdot t), & t \in [0, \frac{1}{2}], \\ \gamma_{v_{n-1},v_n}\left(2 \cdot \left(t - \frac{1}{2}\right)\right), & t \in [\frac{1}{2}, 1] \end{cases}.$$

In Figure 3.14, we see several examples of crossing and non-crossing piecewise linear paths defined on three points. In the following definition, we formalise these observations.

Definition 3.4.11. Let $v_1, p_1, v_2, v_3, p_2, v_4 \in \mathbb{R}^2$ and consider the piecewise linear paths $\gamma_1 = \gamma_{v_1,p_1,v_2}, \gamma_2 = \gamma_{v_3,p_2,v_4}$. We say that the two piecewise linear maps defined by three

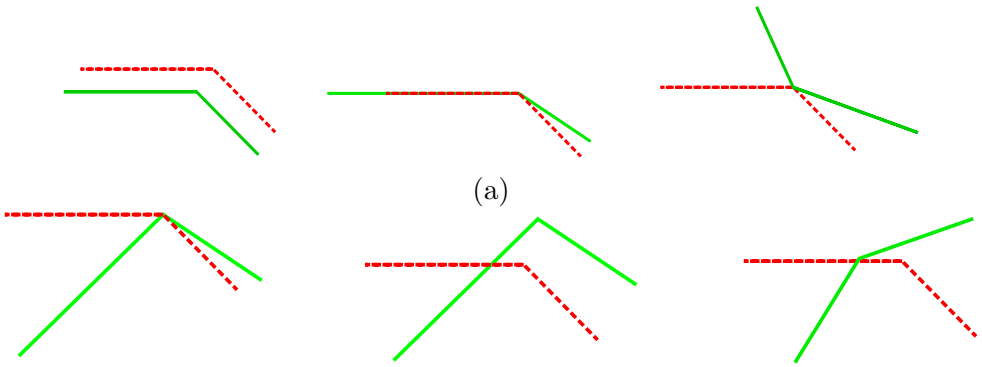

(a)

(b)

Figure 3.14: (a) Non-crossing or touching paths, (b) crossing paths.

points cross if they share a common point other than their endpoints, and for the line segment L of the first path γ_1 that intersects the second path γ_2, we have that γ_2 lies on both sides of L. This can be formalised as follows:

1. there exist $t_1, t_2 \in (0,1)$ with $\gamma_1(t_1) = \gamma_2(t_2)$ (shared point);
2. there exist $t, t' \in (0,1)$ such that $\gamma_2(t)$ can be written as $\gamma_2(t) = p_1 + a \cdot (v_1 - p_1) + b \cdot (v_2 - p_1)$ with $a, b \geq 0, a + b > 0$ and $\gamma_2(t)$ can be written as $\gamma_2(t') = p_1 + a' \cdot (v_1 - p_1) + b' \cdot (v_2 - p_1)$ with $a < 0$ or $b < 0$.

In the following section, we see that this approach is consistent with the goal of obtaining triangulated surfaces.

Lemma 3.4.12. *Let F be a polyhedral fundamental domain for a wallpaper group G of type p1, p2, pg, p2gg, p3, p4 or p6 with $\overline{\overset{\circ}{F}} = F$ (as in Lemma 3.4.8). Let $v_1, \dots, v_n$ and $e_1, \dots, e_n$ be the vertices and edges of F, respectively, such that e_i is incident to the vertices v_i and v_{i+1} for $i = 1, \dots, n-1$ and e_n is incident to the vertices v_n and v_1. Then we have that $n = 2m$ is even, and we can reorder the edges such that all edges can be obtained from the edge representatives $e_1, \dots, e_m$ under the action of G. Choose points $p_1, \dots, p_m$ such that the paths $G(\{\gamma_{v_i,p_i,v_{i+1}} \mid i = 1, \dots, m\})$ do not cross (Definition 3.4.11). Then we obtain a new fundamental domain F' with boundary given by the path $\gamma_{v_1,p_1,v_2,\dots,v_n,p_n,v_1}$.*

In the following, we often refer to the points $p_1, \dots, p_m$ above as *intermediate points*, as they define piecewise linear paths of the form $\gamma_{v_i,p_i,v_{i+1}}$. Moreover, we say that an edge e is *deformed* by an intermediate point p, if p is not contained in the convex hull of e, i.e. does not lie on the edge.

Proof. Jordan's curve theorem states that for a closed continuous curve in $\mathbb{R}^2$, $\gamma : [0,1] \to \mathbb{R}^2$ with $\gamma(0) = \gamma(1)$ and $\gamma_{[0,1)}$ injective, we obtain a unique bounded domain. If the concatenation of the paths has this property, we are done. If two paths touch, we can split the resulting path into two disjoint paths that both define a bounded region. Since no paths cross, this domain is a fundamental domain. □

Before we go to the main goal of this section, defining three-dimensional interlocking blocks, we show that we can interpolate between the domains F and F' defined in the previous lemma.

Lemma 3.4.13. *Consider the two domains F, F' as defined in Lemma 3.4.12. We can interpolate between the boundaries of F and F' with closed paths such that every path in between is the boundary of a fundamental domain, i.e. there exists a continuous map $\lambda : [0,1] \times [0,1] \to \mathbb{R}^2$ with $\lambda(0,[0,1]) = \partial F$ and $\lambda(1,[0,1]) = \partial F'$, and for every $z \in [0,1]$ we have that $\lambda(z,[0,1])$ is the boundary of a fundamental domain.*

Proof. Before we define the map λ, we define a continuous map $\Gamma_i : [0,1] \times [0,1] \to \mathbb{R}^2$ for each path, $\gamma_i = \gamma_{v_i,p_i,v_{i+1}}$, such that $\Gamma_i(0,[0,1]) = e_i$ $\Gamma_i(1,[0,1]) = \gamma_i$ for all $i = 1,\dots,m$. For a piecewise linear path γ_{v_1,p,v_2} defined by three points $v_1, p, v_2 \in \mathbb{R}^2$, the map $\Gamma = \Gamma_{v_1,p,v_2}$ is given as follows:

$$\Gamma_{v_1,p,v_2} : (0,1) \times [0,1] \to \mathbb{R}^2,$$
$$(z,t) \mapsto \begin{cases} v_1 + \left(\frac{2t}{z}\right) z\,(p - v_1)\,, & t \in [0, \frac{z}{2}], \\ z\,(p - v_1) + v_1 + \left(\left(t - \frac{z}{2}\right) \frac{1}{1-z}\right)(z\,(v_1 - v_2) + v_2 - v_1)\,, & t \in [\frac{z}{2}, 1 - \frac{z}{2}], \\ z\,(p - v_2) + v_2 - \left(\left(t - \left(1 - \frac{z}{2}\right)\right) \frac{2}{z}\right) z\,(p - v_2)\,, & t \in [1 - \frac{z}{2}, 1]. \end{cases}$$

For each $z \in (0,1)$, the map $t \mapsto \Gamma(z,t)$ can be viewed as a reparametrisation of the piecewise linear path $\gamma_{v_1,v_1+z(p-v_1),v_1+z(p-v_1),v_2}$. We can extend Γ continuously to a map on $[0,1] \times [0,1]$ by setting

$$\Gamma(0,t) = v_1 + t \cdot (v_2 - v_1)$$

and

$$\Gamma\,(1,t) = \begin{cases} v_1 + 2t\,(p - v_1)\,, & t \in [0, \frac{1}{2}], \\ p + (2t-1)\,(v_2 - p)\,, & t \in [\frac{1}{2}, 1]. \end{cases}$$

We define λ as the concatenation of all paths Γ_i. Next, it follows similarly as in the proof of Lemma 3.4.12, that the maps $\Gamma_i(t)$ lead to a fundamental domain for all $t \in [0,1]$ such that the boundary is transformed continuously. □

Instead of considering piecewise linear paths with a single intermediate point, we can generalise the approach by also considering other types of non-crossing paths. For this, let F be a fundamental domain with edge representatives given by $e_1, \dots, e_m$. We consider paths γ_i for $i = 1, \dots, m$ with the following properties: assume that for each edge e_i the path γ_i is obtained by a map $\Gamma_i \colon [0,1] \times [0,1] \to \mathbb{R}^2$ such that

1. Γ_i is continuous,
2. for all $x \in [0,1]$, the map $\Gamma_i(x) \colon [0,1] \to \mathbb{R}^2$ is injective,

3. $\Gamma_i(0)$ parameterises e_i and $\Gamma_i(1) = \gamma_i$,

4. $\{\Gamma_i(x)(0), \Gamma_i(x)(1)\} = e_i$ for all $x \in [0,1]$ and

5. for all $x \in [0,1]$ any paths in $G(\{\Gamma_i(x) \mid i = 1, \ldots, m\})$ do not cross,

where for $x \in [0,1]$, $\Gamma_i(x)$ is defined as the map $[0,1] \to \mathbb{R}^2, t \mapsto \Gamma_i(x,t)$. Then we can define for each $x \in [0,1]$ a fundamental domain F_x with boundary given by the orbit $G(\{\Gamma_i(0)\})$. Since the maps Γ_i are continuous, we obtain a three-dimensional manifold $\bigcup_{x\in[0,1]} F_x$.

3.4.2 Assemblies with Wallpaper Symmetries

Using the map λ as defined in Lemma 3.4.13, we can associate a fundamental domain F_z for each $z \in [0,1]$ to $\lambda(z)$ and define the following set

$$X_\lambda = \{(x_1, x_2, x_3 \cdot c)^\intercal \in \mathbb{R}^3 \mid (x_1, x_2) \in F_{x_3} \text{ for } x_3 \in [0,1]\}, \tag{3.3}$$

for some $c \in \mathbb{R}_{>0}$. In this section, we show that we can triangulate the boundary of this block X_λ, i.e. ∂X_λ is a polyhedron. For this, we define the surface of a block by a triangulation X such that its intersection with planes of the form $P_z = \{(x,y,z)^\intercal \mid (x,y)^\intercal \in \mathbb{R}^2\}$ is the boundary of a fundamental domain for $z \in [0,c]$ for some $c > 0$. It turns out that the boundary of the fundamental domains $X \cap P_0$ and $X \cap P_c$ corresponds to the boundary of F and F', respectively, as defined in Lemma 3.4.12.

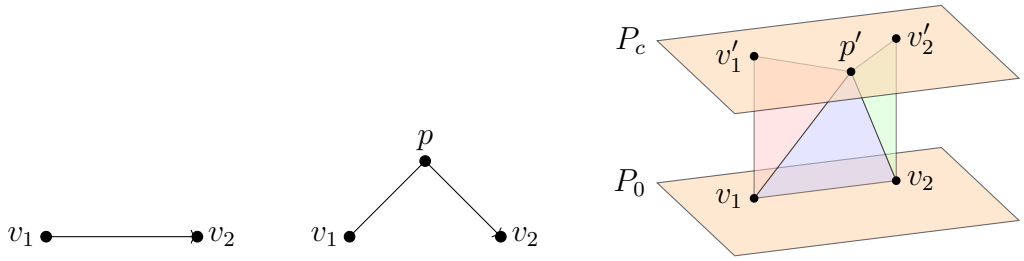

(a) (b) (c)

Figure 3.15: Deforming an edge and a corresponding triangulation: (a) initial edge with vertices v_1, v_2, (b) introducing intermediate point p (as in Lemma 3.4.12) resulting in two edges with vertices v_1, p and v_2, p, (c) interpolating between edges by setting $v_1' = v_1 + (0,0,c)^\intercal, v_2' = v_2 + (0,0,c)^\intercal, p' = p + (0,0,c)^\intercal$ for some $c > 0$. Note that the points p', v_1', v_2' and the points v_1, v_2, p lie in the planes P_c and P_0, respectively.

The points p in the construction shown in Figure 3.15c can be chosen in the same way as in Lemma 3.4.12 in order to obtain a triangulation given below.

Definition 3.4.14. Let F, F' be as in Lemma 3.4.12. We place F and F' in parallel planes and define $X_{F,F'}$ as a triangulation with embedded triangles of the following type:

For each edge e of F with vertices v_1, v_2 and corresponding intermediate point $p \in \mathbb{R}^2$ we have the triangle $\{v_1, v_2, p'\}$ called *tilted face* and the triangles $\{v_1, v_1', p'\}, \{v_2, v_2', p'\}$ called *vertical faces*. Additionally, we add a fixed triangulation of the domains F, F'.

This triangulation can be viewed as an embedded simplicial surface described by the embedded vertices $\{v_1, \dots, v_n\} \cup \{v_1', \dots, v_n'\} \cup \{p_1', \dots, p_m'\} \subset \mathbb{R}^3$ and faces given by the triangulation $X_{F,F'}$ as defined above. We have *vertical faces* of the form $\{v_i, p_i', v_i'\}, \{v_{i+1}, p_i', v_{i+1}'\}$ and *tilted faces* of the form $\{v_i, p_i', v_{i+1}\}$. By omitting the triangulation of F and F', the vertical and tilted faces yield an embedded simplex ring.

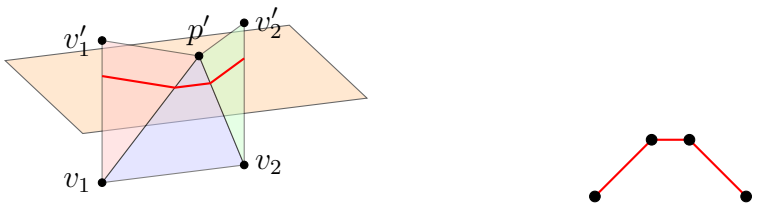

(a) (b)

Figure 3.16: (a) Intersection of the triangulation with the plane P_z. (b) Intersection is given by a piecewise linear path given by $\Gamma_{v_1,p,v_2}(z)$ as defined in the proof of Lemma 3.4.13

Lemma 3.4.15. *The boundary of the block X_λ is given by the triangulation $X_{F,F'}$.*

Proof. This follows immediately from the fact, that the intersection of the triangles of $X_{F,F'}$ with the plane P_z are given by $\lambda(z)$. □

Remark 3.4.16. We can summarise the steps to construct a block X_λ with boundary $X_{F,F'}$ based on a wallpaper group G as follows:

1. Start with a polygonal fundamental domain F of G, for instance, a Dirichlet domain.
2. Identify the edge pairs, i.e. edges of F that are mapped onto each other by group elements of G.
3. For each edge pair, choose an "intermediate" point satisfying certain conditions leading to a piecewise linear path.
4. Merge these paths to obtain a new fundamental domain F'.
5. Place the two domains $F, F' \subset \mathbb{R}^2$ in parallel planes in $\mathbb{R}^3$ and interpolate between them with a function λ such that the boundary of the resulting block X_λ is given by a triangulation $X_{F,F'}$.

Theorem 3.4.17. *We can act with G on the blocks $X = X_\lambda$ constructed as described in Remark 3.4.16 to obtain an infinite assembly with symmetry group given by G.*

Proof. This follows immediately from the construction of X_λ, since "slices" with planes P_z correspond to fundamental domains whose images under G only meet at their boundary. We need to check that for two group elements g, g' we have that $g(X) \cap g'(X) = \partial g(X) \cap \partial g'(X)$. Since the boundary of the block X is characterised by the intermediate layers which are fundamental domains of G, this follows immediately from the definition of planar crystallographic groups, see Definition 1.2.8. □

We can compute the volume of X_λ as described in the following remark.

Remark 3.4.18. The volume of X_λ is given by $c \cdot \mathrm{vol}(F)$, where F is the initial fundamental domain and c is the height of X_λ. This follows immediately from the facts that each fundamental domain has the same volume (Lemma 3.4.7), the block X_λ is a polyhedron and Cavalieri's principle.

Next, we give several examples of the construction presented so far.

Example 3.4.19. An equilateral triangle gives a fundamental domain for the wallpaper group G of type p6. However, we view this triangle as a quadrilateral since one edge is split as it contains a point fixed by G. In Figure 3.17, we see how we construct an interlocking block based on this domain.

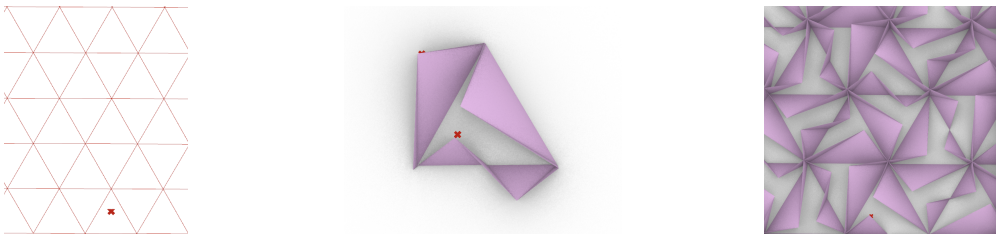

(a) (b) (c)

Figure 3.17: (a) An equilateral triangle can be viewed as a fundamental domain of a wallpaper group G of type p6. (b) One edge of the triangle is split into two, and we can construct a block using intermediate points. (c) The resulting assembly (without top and bottom faces) is obtained by using the action of G.

Example 3.4.20. In this example, we start with a tiling of the plane by fundamental domains of a wallpaper group G of type p3.

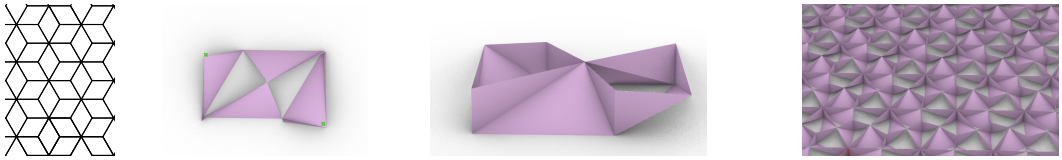

(a) (b) (c) (d)

Figure 3.18: (a) Fundamental domain of wallpaper group G of type p3. (b,c) Views of constructed block. (d) Assembly based on this block using the action of G.

As a final step in processing the geometry of X_λ and its triangulation, we focus on eliminating any irregularities or non-manifold elements. These are features that could

interfere with subsequent analyses or computations. To accomplish this, we apply a set-theoretic approach by considering the closure of the interior of X_λ, expressed as $\overline{\mathring{X}_\lambda}$. This method ensures that every point defined as part of X_λ also encompasses those on its boundary, effectively removing problematic areas without changing the essential structure of the shape. For certain choices of intermediate points, we can do this directly as given below.

Remark 3.4.21. If $p_i = p_j$ for some i, j we identify the corresponding vertices and if $p_i = p_{i+1}$ we omit the faces that appear two times. In Section 3.6, we see several examples of the latter type: one being the *Versatile Block* and one being the *RhomBlock*.

The other case, when an intermediate point equals the starting point of another edge, can be treated using the methods presented in Chapter 5. Below, we give an example of this case.

Example 3.4.22. Consider a wallpaper group G of type p4 generated by the rotation matrix $\begin{pmatrix} 0 & 1 \\ -1 & 0 \end{pmatrix}$ that rotates a point by 90 degrees and translations given by the vectors $(2,0)^\intercal, (0,2)^\intercal$. A square with coordinates given by $(0,0)^\intercal, (0,-1)^\intercal, (1,-1)^\intercal, (1,0)^\intercal$ is a fundamental domain F for G. The edge pair representatives are given by $e_1 = \{(0,0)^\intercal, (0,-1)^\intercal\}$ and $e_2 = \{(0,-1)^\intercal, (1,-1)^\intercal\}$. For e_1 and e_2 we choose $(1,-1)^\intercal$ and $(0,-2)^\intercal$ as intermediate points, respectively. We obtain a new fundamental domain F' according to Lemma 3.4.12 with height $c = 1$. The resulting block X interpolating between F and F' is shown in Figure 3.19a. Note that, it contains a triangle that vanishes when considering the closure of the interior of X, shown in Figure 3.19b. In Figure 3.19e, we see an assembly of the blocks, where all blocks are shifted away from the centre of the assembly.

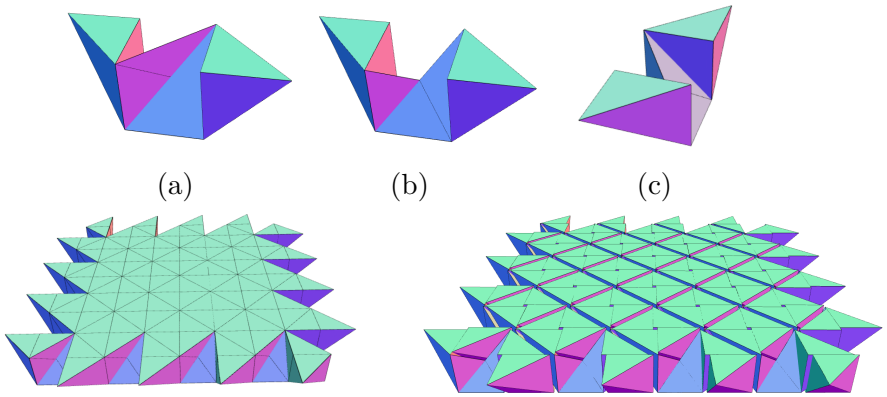

Figure 3.19: (a) Block based on construction with wallpaper group of type p4, (b,c) different views after removing artefacts, (d) view of the assembly, (e) exploded view of the assembly of the resulting block.

As demonstrated in the following remark, the block X_λ acts as a fundamental domain for a three-dimensional crystallographic group $\tilde{G}$. Consequently, this structure

enables the construction of space-filling assemblies, indicating that multiple instances of X_λ, when appropriately arranged according to an action given by $\tilde{G}$, can completely fill three-dimensional space without gaps or overlaps.

Remark 3.4.23. The block X_λ is a fundamental domain for the three-dimensional crystallographic group generated by the embedding of G into SE(3), as given in Remark 3.4.3, together with the translation $(0, 0, 2c)^\intercal$ and the element $\begin{pmatrix} 1 & 0 & 0 \\ 0 & 1 & 0 \\ 0 & 0 & -1 \end{pmatrix} \in \mathrm{O}(3)$.

Proof. This follows from the fact that each planar crystallographic group can be extended to a space group in this way, [IUC02]. □

The generation of an assembly $(g(X))_{g\in G}$ with wallpaper symmetry leads to several questions:

1. Does it yield an interlocking assembly?
2. Can we put together the assembly by adding one block after another?
3. What are its structural benefits?

In Section 3.5, we show in Theorem 3.5.7 that as long as for each edge representative e the piecewise linear path γ_e mentioned above is not a line, the block created above yields a translational interlocking assembly if G is of type p1 as all the edges of the original fundamental domain are deformed. In general, for constructions of blocks based on other wallpaper groups, we can rule out certain motions corresponding to the kernel of the infinitesimal interlocking matrix. The other two questions are briefly discussed in Section 3.7.

3.4.3 Extensions of Block Constructions

We can obtain several new blocks by iterating the approach, mirroring at planes or deforming the initial domain F which is placed in the plane P_0 into both positive and negative direction by setting $c > 0$ and $c < 0$, respectively.

Iterating and Mirroring For instance, instead of assuming that we have a map Γ which deforms a straight edge e into a path γ. We can approximate arbitrary paths γ by piecewise linear paths and iterate this construction to obtain an approximation $\tilde{\gamma}$ of γ. Moreover, we can extend the method from the previous section in several ways to form new assemblies, e.g. by

1. iterating the steps of deforming edges of fundamental domains or
2. mirroring at the bottom or top plane.

These processes can be formalised as follows: Given $\lambda_1 \colon [0,1] \to \mathcal{F}, \lambda_2 \colon [0,1] \to \mathcal{F}$ such that $\lambda_1(1) = \lambda_2(0)$ we can define the following interpolation functions:

1. iterating: $\lambda \colon [0,1] \to \mathcal{F}, \lambda(t) = \begin{cases} \lambda_1(2 \cdot t) & t \in [0, 1/2], \\ \lambda_2(2 \cdot (t - 1/2)) & t \in [1/2, 1] \end{cases}$ and

2. mirroring: $\lambda \colon [0,1] \to \mathcal{F}, \lambda(t) = \begin{cases} \lambda_1(1 - 2 \cdot t) & t \in [0, 1/2], \\ \lambda_1(2 \cdot (t - 1/2)) & t \in [1/2, 1] \end{cases}$.

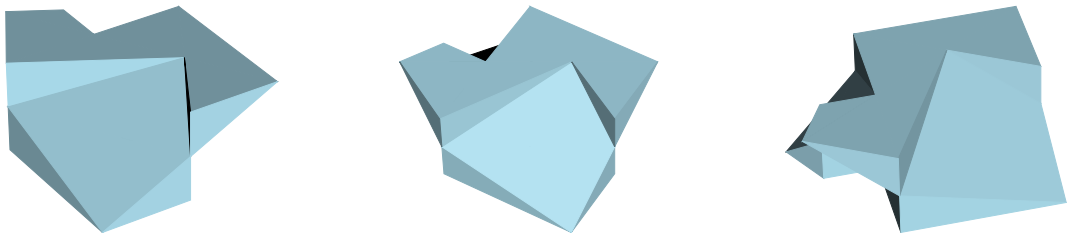

Figure 3.20: We can modify the block given in Figure 3.10c by iterating the construction starting with the mid-section given by a kite and deforming it in both positive and negative direction.

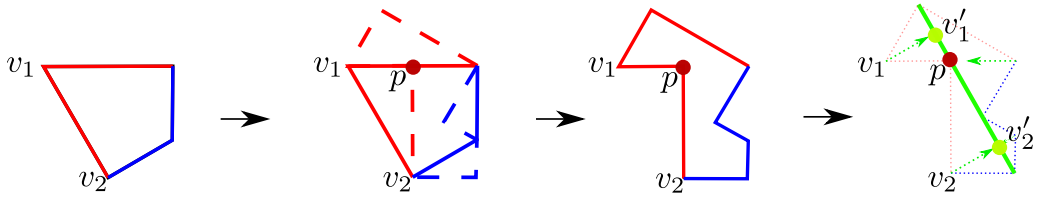

Figure 3.21: Schematic illustration of pushing points towards the interior: we use the Escher Trick to obtain a new fundamental domain F' from a fundamental domain F. The intermediate points are chosen in a way such that they lie on a line. We can modify F' by replacing its vertices v_i by vertices v_i' on this line.

Subsets of Fundamental Domains Another approach is to deform blocks along the z-axis by means of a *growth-function*, i.e. a bijective increasing continuous map $f \colon [0,1] \to [0,1]$, and considering the block given by $X_{\lambda \circ f}$. We can also generalise our construction by allowing certain geometrically defined subsets $\tilde{\lambda}(t)$ of fundamental domains, i.e. instead of considering the set of all fundamental domains $\mathcal{F}$, we consider the set of all subsets of fundamental domains $\tilde{\mathcal{F}}$. Deforming a fundamental domain into a subset of another fundamental domain can be achieved, by modifying the points v_1', v_2' of the triangulation given in Definition 3.4.14 by replacing them by points inside the fundamental domain F' placed in the plane P_c. This generalisation leads to more possible candidates for interlocking assemblies, and the examples of assemblies with tetrahedra given in Figures 3.2b-3.3c, obtained using the method given in [Bel+09], can be constructed this way.

Example 3.4.24. Consider the block in Figure 3.20. In the previous section, we deformed an edge with endpoints v_1, v_2 of a fundamental domain F using an intermediate point p, leading to a new fundamental domain F' containing edges with points v_1, p and p, v_2. Instead, we can also consider subsets of fundamental domains that can be obtained by shifting the points v_1, v_2 in the F' towards the interior such that the subset still contains the intermediate points, see Figure 3.21. In this example, the intermediate points are chosen in such a way such that we can choose a line as a subset containing the intermediate points. We can keep the triangulation of the underlying block and obtain a new block with smaller surface area and still sharing "tilted faces" with their neighbours, see Figure 3.22.

In [Pie20; GNP22], similar constructions for several examples are presented. Note that, we can obtain several well-known assemblies in this way. For instance, the tetrahedra assembly presented in [Gli84; Dys+01] can be obtained by a block presented by Frézier in [Fré38].

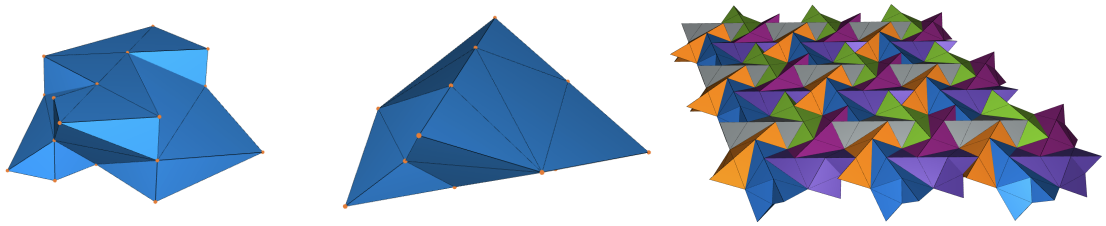

(a) (b) (c)

Figure 3.22: (a) The block shown in Figure 3.20 can be further modified by taking subsets to obtain another block. (b) Resulting block by shifting points towards the interior. The block shown in (b) is completely contained inside the block (a). In (c) we see an assembly using the block in (b).

As illustrated above, we can classify and construct assemblies admitting a wallpaper symmetry in numerous ways, by also considering subsets of fundamental domains.

Next, we show how to approximate fundamental domains with smooth boundary curves.

Approximating Curves and Smooth Surfaces We can approximate any curve by piecewise linear paths. For instance, consider the curve given by the function $f\colon [0,1] \to \mathbb{R}^2, t \mapsto (t, \sin(2\pi t))$, approximated by piecewise linear paths in Figure 3.23.

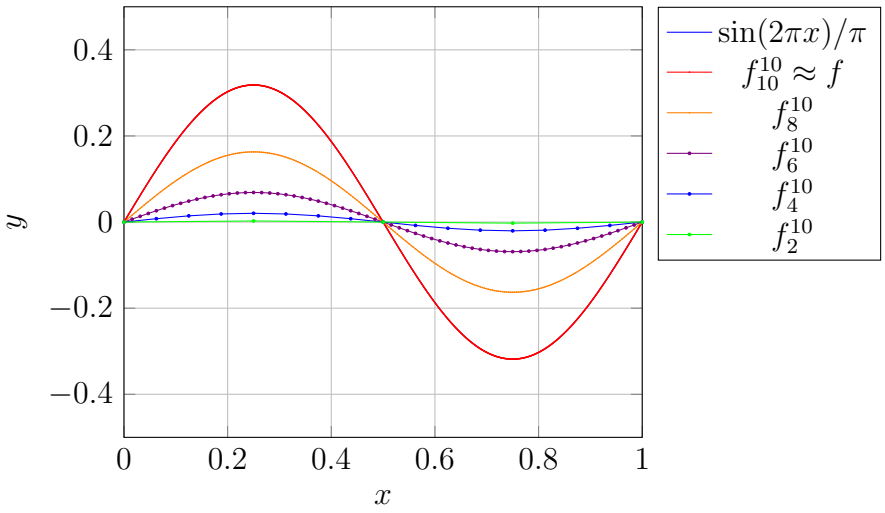

Figure 3.23: Approximating $f\colon [0,1] \to \mathbb{R}^2, t \mapsto (t, \sin(2\pi t))$ by piecewise linear paths, see Definition 3.4.25.

We can iterate the Escher Trick n-times while simultaneously modifying the method slightly with the goal of approximating smooth surfaces. The aim is to define a homotopy deforming the function f above, into the curve defining the line segment $[0,1]\times\{0\}$ and to use this as a parametrisation of piecewise linear curves with the Escher Trick.

In the following, we observe one way of approximating a continuous curve $f\colon [0,1] \to \mathbb{R}^2$ with piecewise linear function in a compatible way with the Escher Trick.

Definition 3.4.25. For a given continuous and injective function $f\colon [0,1] \to \mathbb{R}^2$ with $f(0) = (0,0)^\intercal$ and $f(1) = (1,0)^\intercal$, we define the following piecewise functions $f_0, \dots, f_n$ for given $a, N \in \mathbb{N}$: let $n = 1, \dots, N$ then $f_n^N : [0,1] \to \mathbb{R}^2$ is the piecewise linear path interpolating between the points $f(0), (\frac{n}{N})^a \cdot (f(\frac{i}{2^n}) - (\frac{i}{2^n}, 0)) + (\frac{i}{2^n}, 0), f(1)$ for $i = 1, \dots, 2^n - 1$.

These piecewise linear paths approximate f as shown in the following lemma.

Lemma 3.4.26. *For a function f as given above, the functions f_N^N converge uniformly to f.*

Proof. This follows immediately from the fact that f is uniformly continuous on the compact interval $[0,1]$ and the way f_N^N is defined. □

Remark 3.4.27. The series of functions are chosen in a way to be compatible with iterating the Escher Trick. The setup is as follows: we deform the edge with points $(0,0)^\intercal, (1,0)^\intercal \in \mathbb{R}^2$ by applying the Escher Trick iteratively with functions f_n^N. The outline of the fundamental domain in the nth step is then given by f_n^N. For the resulting block, we set the height of each layer to $(\frac{n}{N})^a$ for a fixed $a \in \mathbb{N}$. Such ways of approximating curves are known as polygonal approximation in the literature, and other ways of approximating curves with piecewise linear functions can be found, for instance in [II88].

Example 3.4.28. In this example, we give a construction of a block for a wallpaper group G of type p4 by deforming straight edges of a square into segments of the sine function. We start with a square given by $(0,0)^\intercal, (1,0)^\intercal, (1,1)^\intercal, (0,1)^\intercal \in \mathbb{R}^2$ such that the edges given by the points $(0,0)^\intercal, (1,0)^\intercal$ and $(0,0)^\intercal, (0,1)^\intercal$, respectively $(1,0)^\intercal, (1,1)^\intercal$ and $(1,1)^\intercal, (0,1)^\intercal$ are identified under the action of G. We deform the edge $(0,0)^\intercal, (1,0)^\intercal$ using the function $f(t) = (t, \frac{\sin(2\pi \cdot t)}{\pi})^\intercal$ and obtain the block in Figure 3.24 as described in Remark 3.3 by setting $N = 10, a = 3$. In this way, we obtain a block whose outer perimeter approximates a piecewise smooth surface.

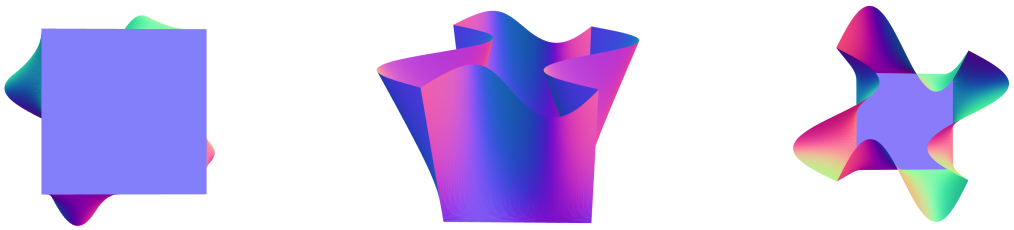

(a) (b) (c)

Figure 3.24: Views of the constructed block in Example 3.4.28 from (a) below, (b) front and (c) above.

3.5 Interlocking Property of Assemblies with Wallpaper Symmetry

In this section, we establish interlocking properties of assemblies constructed with the methods based on continuously deforming fundamental domains of a given wallpaper group G into each other, as presented in the previous section. From these infinite assemblies, we can also obtain interlocking assemblies with finitely many blocks by only considering finite portions, see Corollary 3.5.9. For this purpose, we first show that the infinitesimal interlocking property (Definition 3.3.11) of the infinite assemblies construction in Section 3.4 can be decoded into a convex set living in infinite dimensional space carrying the same symmetries as the underlying assembly. This observation allows a simplification for proving the interlocking property. Next, we show that no "sliding" motions are possible for any constructed assemblies satisfying certain conditions.

Definition 3.5.1. Let $(X_i)_{i\in I}$ be an assembly of blocks and $\gamma = (\gamma_i)_{i\in I}$ be admissible motions such that $\gamma_i \equiv 0$ for almost all $i \in I$. We say that γ consists of *sliding motions* if the infinitesimal interlocking matrix A of the assembly $(X_i)_{i\in I}$ satisfies

$$Ax = 0,$$

where $x = (\dot{\gamma}_i(0))_{i\in I}$.

In Example 3.3.13 we show that assembling cubes can lead to sliding motions which can be viewed as motions such that contact faces remain in contact when applying the motion. In Proposition 3.5.6, we establish that the assemblies constructed in the previous section do not admit any sliding motion if we assume sufficient edge deformations specified as Criterion 3.5.3.

Using this, we show that we can classify assemblies with a translational interlocking property and p1 symmetry using the notion of "infinite interlocking chains".

Definition 3.5.2. Let $(X_i)_{i\in I}$ be an assembly of blocks, A its infinitesimal interlocking matrix and let $\gamma = (\gamma_i)_{i\in I}$ be admissible motions. The infinitesimal motion $x = (\dot{\gamma}_i(0))_{i\in I}$ is an *infinite interlocking chain* if $Ax \geq 0$ and x has infinite support.

Consider an assembly coming from the construction in Section 3.4 by continuously deforming a fundamental domain F of a wallpaper group G into another domain F' of the same group leading to a block X that can be assembled using the extended action of G onto $\mathbb{R}^3$, i.e. we consider the infinite assembly of blocks $(X_g)_{g\in G} = (g(X))_{g\in G}$. If there exists a finite set $H \subset G$ such that $H(F) = H(F')$ it follows that we can simultaneously shift the blocks corresponding to H upwards using the admissible motion $\gamma\colon t \mapsto \big(x \mapsto (x_1, x_2, x_3 + t)\big)$. This leads to the following interlocking criterion.

Criterion 3.5.3. *The assembly $(X_g)_{g\in G}$ is a translational interlocking assembly with*

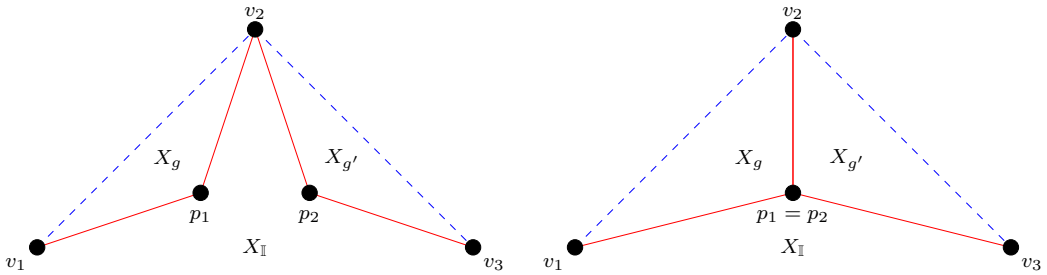

Figure 3.25: We can deform two neighbouring edges with vertices $\{v_1, v_2\}$ and $\{v_2, v_3\}$ of an initial fundamental domain F by introducing intermediate points p_1, p_2. The choices of p_1, p_2 determine the contact of the resulting block $X = X_{\mathbb{I}}$ to other blocks $X_g, X_{g'}$ inside the assembly. (a) If $p_1 \neq p_2$ then the resulting triangles associated to the edges meet with a single block. (b) If $p_1 = p_2$, we obtain a contact triangle between the blocks $X_g, X_{g'}$.

empty frame if and only if there is no finite set $\emptyset \neq H \subset G$ *such that* $\bigcup_{h\in H} h(F) = \bigcup_{h\in H} h(F')$. *This is equivalent to saying that for each finite set* $\emptyset \neq H \subset G$ *the edges on the boundary of* $\bigcup_{h\in H} h(F)$ *are deformed (see discussion after Lemma 3.4.12).*

Indeed, we prove the following for wallpaper groups of type p1 in Theorem 3.5.7.

Theorem. *If G is of type p1, the assemblies $(X_g)_{g\in G}$ are translational interlocked if and only if Criterion 3.5.3 holds.*

The general interlocking property is harder to prove, since we have to consider translations as well as rotations. For a special block, called the "RhomBlock", we show this full interlocking property in Section 3.6, where we use the fact that the vertical walls of the RhomBlock come in parallel pairs. Furthermore, the translational interlocking property for blocks coming from wallpaper groups of type p1 carries on for other assemblies with certain blocks such as the Versatile Block, see Section 3.6.

3.5.1 A Convex Set with Wallpaper Symmetry

Let X be a block coming from the construction in Section 3.4 which can be assembled using the action of a planar crystallographic group G, see Theorem 3.4.17. Hence, there is an assembly of the form $(X_g)_{g\in G}$ with $X = X_{\mathbb{I}}$, where $\mathbb{I}$ is the identity element of G. In the construction of X we consider edge representatives $e_1, \ldots, e_n \subset \mathbb{R}^2$ of an initial fundamental domain F together with intermediate points $p_1, \ldots, p_n \in \mathbb{R}^2$ determining a triangulation of the surface of X. For a given edge e_i of F, we distinguish between the two cases $p_{i-1} \neq p_i \neq p_{i+1}$ and $p_{i-1} = p_i$ or $p_i = p_{i+1}$, see Remark 3.4.21.

The contact faces of the block X to the neighbouring blocks can be determined by considering each edge independently. For an edge with intermediate point satisfying the first case above (see Figure 3.25a), we obtain rows in the interlocking matrix (Definition

3.3.11) of the following form, since the resulting triangles all are in contact with a single block X_g:

$$\begin{matrix} X & X_g \\ \begin{bmatrix} * & * \\ * & * \\ * & * \end{bmatrix} \end{matrix}$$

This means that the three triangles coming from the deformation of the given edge are all in contact with another block. For the special case $p_i = p_{i+1}$ (see Figure 3.25b) we have fewer faces, see Remark 3.4.21, and for each edge e_i, there are two blocks $X_g, X_{g'}$ that intersect with X at the faces defined at e_i leading to a matrix of the form

$$\begin{matrix} X & X_g & X_{g'} \\ \begin{bmatrix} * & * & 0 \\ * & * & 0 \\ 0 & * & * \end{bmatrix} \end{matrix}.$$

Each block contact is contained in the matrices of the form above. Since we assumed that the block X is constructed with the techniques given in the previous section, its boundary is given by the triangulation $X_{F,F'}$, where F, F' are two fundamental domains. For each vertical or tiled face T with normal vector n of $X_{F,F'}$ that is in contact with another block in the assembly corresponding to a group element $g \in G$, we can find an edge representative $e \in \{e_1, \dots, e_m\}$ of F such that T is obtained w.l.o.g. by the deformation of e as in Figure 3.15. For each vertex p of T, we obtain a quadruple (e, p, n, g), which we call an *edge representing quadruple*. In order to put together all contacts of blocks within the assembly, we define the following set:

$$\begin{aligned} \mathrm{IA}_{X,G} = \{&(\gamma_g)_{g\in G} \in \mathbb{R}^{6\times G} \mid (e,p,n,g) \text{ edge representing quadruple, } |\mathrm{supp}((\gamma_g)_{g\in G})| < \infty \\ &(-((R(p)+t)\times R(n))^\intercal, -R(n)^\intercal, ((R(p)+t)\times R(n))^\intercal, R(n)^\intercal)\cdot(\gamma_{g'}, \gamma_{g'\cdot g}) \geq 0, \\ &\forall g' = (R,t) \in G\}. \end{aligned}$$

Since each contact triangle comes from an edge, we have described all contact faces that determine the inequalities in the set above and thus have the following result.

Proposition 3.5.4. *The set* $\mathrm{IA}_{X,G}$ *is the infinitesimal interlocking space as defined in Definition 3.3.11.*

Proof. We need to show that the inequalities defining the set $\mathrm{IA}_{X,G}$ are exactly those coming from the interlocking matrix A in Definition 3.3.11. Let p be a contact point of a contact face with normal n two blocks $X_{g'}, X_{g''}$ coming from a deformed edge e. It follows that $g'^{-1}(e) \in \{e_1, \dots, e_n\}$ and we write $g = g'^{-1} \cdot g''$. By the definition of the

underlying assembly, we have that $(R(e)+t, R(p)+t, R(n), g)$ is an edge representing quadruple, where $g'^{-1} = (R,t) \in G$. Thus, we obtain all inequalities of A and vice versa, each inequality in the definition of $\mathrm{IA}_{X,G}$ comes from A. □

3.5.2 The Kernel of the Infinitesimal Interlocking Matrix

In this section, we show that no sliding motions are possible for the blocks constructed in Section 3.4 as long as they fulfil Criterion 3.5.3. For this, let $(X_g)_{g\in G}$ be an assembly constructed with the methods in Section 3.4 and fulfilling Criterion 3.5.3. Then we compute its infinitesimal interlocking matrix, which we call A.

Lemma 3.5.5. *Let $(\gamma_g)_{g\in G} \in \mathbb{R}^{6\times G}$ be a vector (with finite support) of infinitesimal motions for each block. A "deformed side" of a block means that for the bottom plane corresponding to the tiling with F there is an edge with corresponding intermediate point deforming, the edge leading to three faces with distinct normal vectors having contact. Assume that one "deformed side" of a block X has contact to another block X', which is not moving. Then we can simplify the computation of the kernel to a reduced matrix.*

Proof. Let $e \subset \mathbb{R}^2$ be an edge with vertices $v_1, v_2 \in \mathbb{R}^2$, and let $p \in \mathbb{R}^2$ be a point. We embed the vertices v_1, v_2 into $\mathbb{R}^3$ by appending a 0 and let v_1', v_2' be the points which are obtained by appending 1 instead of 0 and also embed p into $\mathbb{R}^3$ by appending a 1. We then consider the three triangles in $\mathbb{R}^3$ given by the points $T_2 := \{v_1, v_1', p\}, T_1 := \{v_1, v_2, p\}, T_3 := \{v_2, v_2', p\}$ and normal vectors n_i of T_i given by $n_1 := (v_2 - v_1) \times (p - v_1), n_2 := (v_1' - v_1) \times (p - v_1), n_3 := (v_2' - v_2) \times (p - v_2)$. We obtain the following 9×6 sub-matrix of A of the form corresponding to the contacts of blocks X and X':

$$A_e = \begin{pmatrix} (p \times n_1)^\intercal & n_1^\intercal \\ (v_1 \times n_1)^\intercal & n_1^\intercal \\ (v_2 \times n_1)^\intercal & n_1^\intercal \\ (p \times n_2)^\intercal & n_2^\intercal \\ (v_1 \times n_2)^\intercal & n_2^\intercal \\ (v_1' \times n_2)^\intercal & n_2^\intercal \\ (p \times n_3)^\intercal & n_3^\intercal \\ (v_2 \times n_3)^\intercal & n_3^\intercal \\ (v_2' \times n_3)^\intercal & n_3^\intercal \end{pmatrix}.$$

Since we need to show that A_e has rank 6, we can use row operation on A_e to obtain

the following matrix with the same rank

$$A'_e = \begin{pmatrix} (p \times n_1)^\intercal & n_1^\intercal \\ ((v_1 - p) \times n_1)^\intercal & 0 \\ ((v_2 - p) \times n_1)^\intercal & 0 \\ (p \times n_2)^\intercal & n_2^\intercal \\ ((v_1 - p) \times n_2)^\intercal & 0 \\ ((v'_1 - p) \times n_2)^\intercal & 0 \\ (p \times n_3)^\intercal & n_3^\intercal \\ ((v_2 - p) \times n_3)^\intercal & 0 \\ ((v'_2 - p) \times n_3)^\intercal & 0 \end{pmatrix}.$$

Now, it suffices to show that n_1, n_2, n_3 are linearly independent and one of the following matrices have rank 3:

$$\begin{pmatrix} ((v_1 - p) \times n_1)^\intercal \\ ((v_1 - p) \times n_2)^\intercal \\ ((v_2 - p) \times n_3)^\intercal \end{pmatrix} \text{ or } \begin{pmatrix} ((v_2 - p) \times n_1)^\intercal \\ ((v_1 - p) \times n_2)^\intercal \\ ((v_2 - p) \times n_3)^\intercal \end{pmatrix}.$$

For a 3×3 matrix M with $\det M \neq 0$ it holds that

$$(Ma) \times (Mb) = \operatorname{cof}(M) \cdot (a \times b),$$

where $\operatorname{cof}(M) = \det(M) \cdot (M^{-1})^\intercal$ is the *cofactor matrix* of M. Hence, we can assume that $v_1 = (0,0)^\intercal, v_2 = (1,0)^\intercal$ and the matrices simplify to

$$M_1 = \begin{pmatrix} -p_2^2 - 1 & p_1 & p_1 \\ -(1-p_1)\, p_2 & p_2 & p_2 \\ p_1 - 1 & -p_1^2 - p_2^2 & -(1-p_1)^2 - p_2^2 \end{pmatrix},$$
$$M_2 = \begin{pmatrix} -p_2^2 - 1 & p_1 & p_1 - 1 \\ p_1 p_2 & p_2 & p_2 \\ p_1 & -p_1^2 - p_2^2 & -(1-p_1)^2 - p_2^2 \end{pmatrix}.$$

Then we obtain the following determinants of the matrices dependent on the values of p:

$$\det M_1 = -p_2(p_1 - 1)(p_1^2 + p_2^2 + 1), \det M_2 = -p_1 p_2 (p_1^2 + p_2^2 - 2p_1 + 2).$$

Since p is not contained on the line v_1, v_2, we can assume that $p_2 \neq 0$ and if $p_1 = 1$ it follows that M_2 has non-zero determinant and if $p_1 \neq 1$ it follows that M_1 has non-zero determinant. □

Proposition 3.5.6. *The infinitesimal interlocking matrix A has trivial kernel if and only if Criterion 3.5.3 holds.*

Proof. In the discussion preceding Criterion 3.5.3, it is shown that we can find a non-trivial admissible motion shifting out blocks if there is a finite set $\neq H \subset G$ with $H(F) = H(F')$. Moreover, this motion correspond to the translation $(0, 0, 1)$ and indeed gives rise to a sliding motion.

Assuming the opposite, we show that there are no sliding motions, i.e. the matrix A has trivial kernel. Let x with finite support and $Ax = 0$, we identify x with the family of infinitesimal motions $(\gamma_g)_{g\in G}$ such that $\gamma_g = 0$ for almost all $g \in G$. We show by induction that $x = 0$. For this, we need to prove that there is always an edge in the sense of Lemma 3.5.5. But since there is always at least one block having contact to a block which is moved by x, such an edge exists. For each non-open edge e, there is at least one block with points "above" e. Since the number of blocks that are considered is finite, we find an open edge e, since at least one edge admits deformations. □

3.5.3 Interlocking Chains

From the infinitesimal interlocking space formulation, we obtain a matrix A such that vectors x with finite support and $Ax \geq 0$ correspond to admissible infinitesimal motions. We show that, in the case where G is of type p1 and only translations are considered, the inequality $(Ax)_i > 0$ for some row index i implies that x has infinite support. Therefore, it suffices to consider x with $Ax = 0$. This can be demonstrated by proving the existence of an infinite intersection chain.

Theorem 3.5.7. *Any assembly $(X_g)_{g\in G}$ coming from the construction of the previous section with G of type p1 is translational interlocked if and only if Criterion 3.5.3 is fulfilled.*

Proof. If there exists a set H as in Criterion 3.5.3, we can simply shift out the corresponding blocks using upward translations. Proposition 3.5.6 implies that there are no non-trivial motions inside the kernel of the interlocking matrix. Thus, it suffices to rule out motions γ such that there exists k with $(A \cdot \gamma)_k > 0$. If there exists such an entry, it follows that there exists a block X_i with non-trivial motion t_i and a normal n of a face with $t_i \cdot n > 0$. Then for any face of the block X_i with normal n' such that $t_i \cdot n' < 0$ implies that the neighbouring block at this face has to move as-well. This automatically leads to an infinite chain. □

Remark 3.5.8. The proof above can be extended to assemblies such that each neighbouring block has the same normals. In Section 3.6, this leads to infinitely many translational interlocking assemblies for several blocks.

Corollary 3.5.9. *Let $(X_i)_{i\in I}$ be an infinite interlocking assembly and $J \subset I$ a finite subset in I, such that the elements in J can be written as a tuple $(j_1, \ldots, j_n)$ such that the blocks $X_{j_l}, X_{j_{l+1}}$ for $l = 1, \ldots, n-1$ and the blocks X_{j_1}, X_{j_n} share a common face. Then there is a finite subset $J \subset \tilde{I} \subset I$ such that $\big((X_i)_{i\in\tilde{I}}, J\big)$ is a topological*

interlocking assembly. Moreover, this subset can be chosen to be the blocks inside the region spanned by the blocks corresponding to the elements in J.

3.6 VersaTiles - Versatile Block and RhomBlock

In this section, we introduce a construction method for tiles and interlocking blocks, characterised by generalised *Truchet tiles*, which can be assembled in numerous ways. We employ the theory of wallpaper groups and fundamental domains (see Section 3.4) to derive the tile construction method. The deformation of tiles leads to a family of tiles with combinatorially equivalent tiling rules.

A block arising from this construction is the *Versatile Block*, initially introduced in [GNP22]. This block can be assembled in various planar and non-planar configurations, as first discussed in [Akp+23].

As an illustrative example, we demonstrate the continuous deformation of a *lozenge* into a hexagon, resulting in a polyhedron in three-dimensional space. This polyhedron gives rise to interlocking assemblies corresponding to tilings with lozenges, and we refer to this block as the *RhomBlock*, given its rhombic bottom shape.

3.6.1 Wallpaper Groups with Equilateral Quadrilateral Fundamental Domains

In the following, we primarily focus on the following wallpaper groups: p1, pg, p3 and p4 (see Section 3.4). In general, there is no canonical choice of a fundamental domain for a given wallpaper group G. Convex constructions of fundamental domains include Dirichlet domains, also known as Voronoi domains, leading to a fundamental domain for any point $x \in \mathbb{R}^2$ in general position, i.e. x has a trivial stabiliser in G, see Definition 3.4.5.

For a given wallpaper group G of type p1$= \langle t_1, t_2 \rangle \cong \mathbb{Z}^2$, it is necessary to give a lattice basis. If we choose $t_1 = (0,1)^\intercal$ and $t_2 = (\cos\alpha, \sin\alpha)^\intercal$, for $0 < \alpha < \pi$, there exists a fundamental domain in the form of a rhombus (all side lengths are the same) displayed in Figure 3.26. For different angles α, the rhombus yields an example of a fundamental domain for several wallpaper groups, as described in the following.

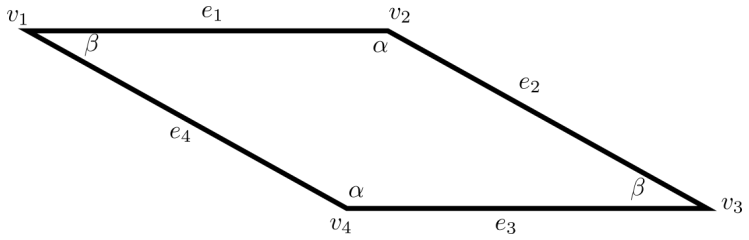

Figure 3.26: Fundamental domain for p1 in the form of a rhombus with $\alpha + \beta = \pi$.

In general, the fundamental domain in Figure 3.26 also gives a fundamental domain for the group pg, generated by the glide reflection defined by first applying the reflection matrix $\begin{pmatrix} -1 & 0 \\ 0 & 1 \end{pmatrix}$ and the translations defined by the vectors $(1,0)^\intercal, (0, \sin\alpha)^\intercal$. Hence,

the group pg can be generated by the translations $t_1, 2 \cdot t_2$ and the glide reflection above. The two groups lead to two periodic ways of assembling a rhombus, as shown in Figure 3.27c and Figure 3.27d. For the special choices $\alpha = \beta = \pi/2$ respectively $\alpha = \pi/3, \beta = 2\pi/3$, we obtain two more periodic tilings, where the rhombi have the form of squares respectively lozenges and the underlying wallpaper groups have a point group of 4-fold respectively 3-fold rotations, see Figure 3.27. These choices give rise to fundamental domains for p1 and pg as well as for p4 respectively p3.

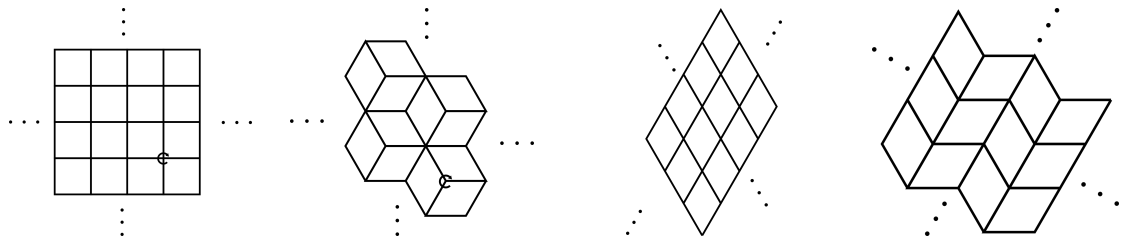

(a) (b) (c) (d)

Figure 3.27: Rhombi tiled periodically: (a) p4-symmetry ($\alpha = \beta = \frac{\pi}{2}$) (squares), (b) p3-symmetry with lozenges ($\alpha = \frac{\pi}{3}, \beta = \frac{2\pi}{3}$) (c) p1-symmetry, (d) pg-symmetry.

The different periodic ways of tiling rhombi, shown in Figure 3.27, can be combined to obtain aperiodic tilings. In the next subsection, we show that we can generalise this construction to obtain fundamental domains leading to tiles with a rich combinatorial way of assembling them.

3.6.2 Constructing VersaTiles

In this section, we formulate a versatility condition leading to the construction of VersaTiles and blocks like the Versatile Block, introduced in [GNP22], that can be assembled in non-unique ways.

The VersaTile Condition

In this subsection, we provide a method for obtaining fundamental domains which can be assembled in non-unique ways. Starting with a parallelogram as in Figure 3.26 which is always a fundamental domain for a certain wallpaper groups of type p1 and pg. We identify the edges using the group action of a wallpaper group G on the plane and deform them using two curves γ_1, γ_2 connecting the vertices of the two edge-representatives such that any two curves in the G-orbit of γ_1, γ_2 can touch but do not cross. This leads to a new fundamental domain defined by the two curves γ_1, γ_2, as described in Section 3.4. In order to create VersaTiles, we consider the following three

sets of domains, which are fundamental domains for more than one wallpaper group:

$$\mathcal{F}_1 = \mathcal{F}_1(\alpha,\beta) = \{F | F \text{ is a fundamental domain for p1 and pg}\},$$
$$\mathcal{F}_4 = \mathcal{F}_4(\alpha,\beta) = \{F | F \text{ is a fundamental domain for p1, pg and p4}\} \text{ and}$$
$$\mathcal{F}_3 = \mathcal{F}_3(\alpha,\beta) = \{F | F \text{ is a fundamental domain for p1, pg and p3}\}.$$

Note that we use compatible groups in the respective sets, i.e. the translational lattice has to be the same, defined by the angles α, β of the respective parallelogram (see Figure 3.26) and for $\mathcal{F}_4(\alpha,\beta)$ it follows that $\alpha = \beta = \pi/2$ and for $\mathcal{F}_3(\alpha,\beta)$ it follows that $\alpha = \pi/3, \beta = 2\pi/3$. With this choice of angles, the inclusions $\mathcal{F}_3 \subset \mathcal{F}_1$ and $\mathcal{F}_4 \subset \mathcal{F}_1$ hold. Moreover, a rhombus with certain angles is contained in each set.

Remark 3.6.1. The idea of the VersaTiles construction is to apply the Escher Trick on the rhombus shown in Figure 3.26 while respecting the symmetries of several wallpaper groups simultaneously. This can be formulated for p1 and pg as the *first versatility condition*, as follows:

(1) The paths for the edges e_1 and e_2 (see Figure 3.26) are axis-symmetric, i.e. for $e \in \{e_1, e_2\}$ and γ_e a path with the same endpoints v, w as e, the image of γ_e in $\mathbb{R}^2$ is invariant under reflection along the perpendicular bisector of the edge e. Moreover, the paths for e_3 and e_4 are determined by the paths of e_1 and e_2 under the translations $v_4 - v_1$ and $v_3 - v_2$, respectively.

This condition is enforced by the two ways the edges are identified. For respecting the symmetries of p4 or p3, we also need to consider a dependence between the edges e_1 and e_2. This is formulated in the following *second versatility condition*:

(2) The path for the edge e_2 is determined by the path of e_1 by rotating it around the angle α.

This way, we can construct infinitely many combinatorially equivalent tiles, which we call *VersaTiles*. Furthermore, the path approach in Section 3.4, Lemma 3.4.26, yields three-dimensional blocks that give rise to candidates for interlocking assemblies. Both steps together yield a region that contains a path segment determining the whole boundary of the resulting tile, see red triangle in Figure 3.28. In the special cases p4 and p3 these construction steps can be also understood as operations inside the wallpaper groups p4gm and p3m1, respectively.

In the following subsection, we consider the special cases $\mathcal{F}_4, \mathcal{F}_3$ of this construction to construct both VersaTiles and interlocking blocks.

Generalised Truchet Tiles and Combinatorics

In this subsection, we propose a generalised version of Truchet tiles made from parallelograms with unit side lengths in order to classify tilings with VersaTiles. This

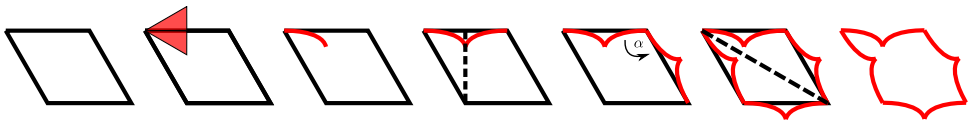

Figure 3.28: Construction steps for generalised Truchet tilings with versatility conditions enforced on paths visualised by dashed lines: 1. Start with a rhombus; 2. Identify regions to draw a path segment; 3. Draw a path segment; 4. Mirror it to enforce condition (1); 5. Rotate it to enforce condition (2); 6. Obtain the remaining paths by translations; 7. Put together all paths to obtain a VersaTile.

approach is strongly related to the theory of *dimer models* which are polygons that consist of two *atoms*, where an atom can be an equilateral triangle, a square, a cube or a similar shape. For further reading on dimer models, we refer to [KO05] for an introduction and [Ken09] for the fundamental theory.

In [Tru04], Truchet describes square tiles with a diagonal, where one triangle is coloured black and the other triangle is coloured white. Moreover, he proves the existence of infinitely many possible assemblies. Smith and Boucher explore the connection of Truchet tiles to other tiles and provides additional insights into their combinatorics in [SB87]. We can generalise Truchet tiles to rhombs in two canonical ways, see Figure 3.29.

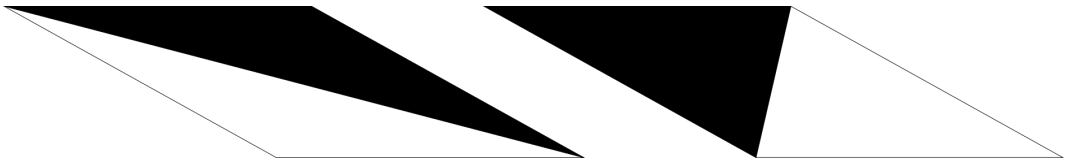

(a) (b)

Figure 3.29: (a,b) Two ways of generalising Truchet tiles.

The generalisation of Truchet tiles is motivated by the following tiling/assembling rule, see [Akp+23]:

Two different Truchet tiles only touch at different colours.

In Figure 3.30, we see how we can assemble such tiles for different angles.

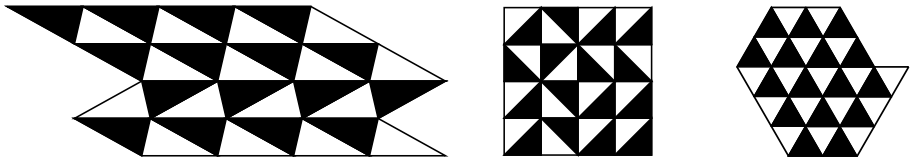

(a) (b) (c)

Figure 3.30: Generalised Truchet tilings based on wallpaper symmetries (a) p1 and pg, (b) p1,pg and p4, (c) p1,pg and p3.

For $\alpha = \beta = \pi/2$, we obtain a square and for $\alpha = \pi/3, \beta = 2\pi/3$ a lozenge as

Truchet tile. These choices of angles lead to two more possible planar assemblies, corresponding to the wallpaper groups p4 and p3. In the extreme case p4 which is handled in [Akp+23] it is straightforward to understand the combinatorics behind Truchet tiles and the tiling rule given above.

Lemma 3.6.2. *There are 2^{n+m} tilings in an $n \times m$ grid.*

Proof. This follows directly from the fact that the tiling is uniquely determined by the upper and left boundary colours. For an alternative proof, see Lemma 1 in [Akp+23]. □

In the other extreme case, corresponding to the wallpaper group p3, tilings are classified by the theory of lozenge tilings, see [Gor21]. For the theory of lozenges, it is much harder to classify tilings. However, the following result is well-known.

Lemma 3.6.3 ([Gor21])**.** *A hexagon with side lengths $a, b, c \in \mathbb{Z}_{>0}$ has*

$$\prod_{i=1}^{a}\prod_{j=1}^{b}\prod_{k=1}^{c}\frac{i+j+k-1}{i+j+k-2}$$

-many tilings with lozenges.

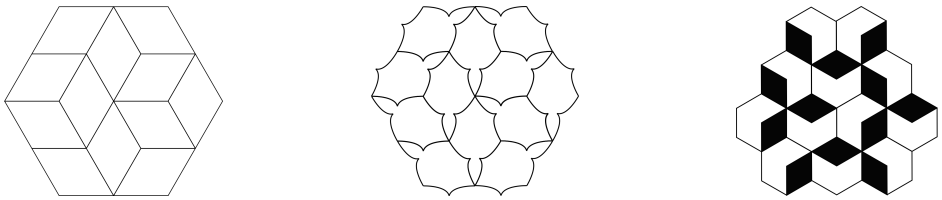

(a) (b) (c)

Figure 3.31: (a) Tiling of hexagon with lozenge tiles (b,c), same tiling with generalised lozenge tiles. The black parts in (c) indicate the initial orientation of the equivalent tilings in (a,b).

3.6.3 Limit Case p4 - The Versatile Block

We now describe the construction of the *Versatile Block*, which was first introduced in [GNP22]. We can tile the plane $\mathbb{R}^2$ with unit squares with edges identified based on the wallpaper group p4. Afterwards, we deform the square with side length $\sqrt{2}$ into a rectangle with side lengths 2 and 1, which are also known as *Aztec tiles* in the literature, see [Gor21]. We can still rotate the resulting block and put an assembly together by shifting groups of four blocks using translations. Note that both the square and the rectangle given above are fundamental domains for the wallpaper groups pg, p4 and p1.

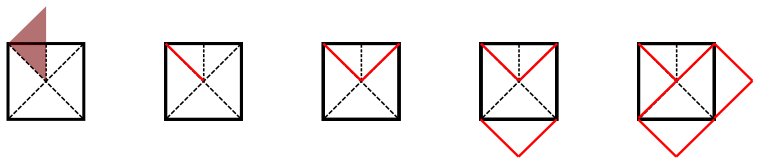

Figure 3.32: Versatile Block construction.

Since, we are using piecewise linear paths with a single intermediate point in Figure 3.32, we can apply the methods presented in Section 3.4. Thus, we can interpolate between the square and the rectangle to obtain intermediate domains, see Figure 3.33, together with a block, called *Versatile Block*, see Figure 3.34.

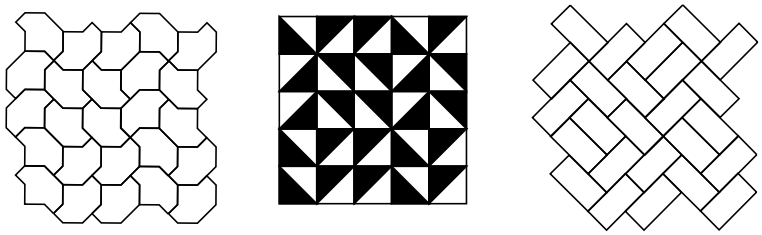

Figure 3.33: Combinatorial equivalent tilings based on VersaTile construction in Figure 3.32.

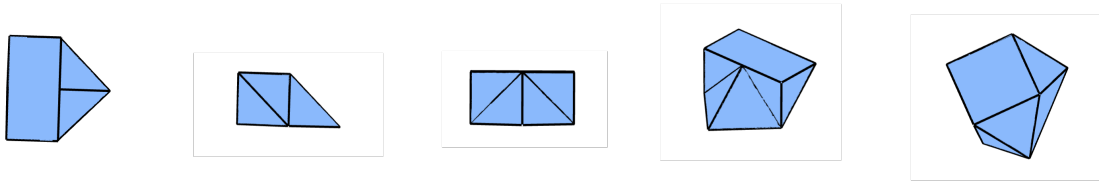

Figure 3.34: Different views of the Versatile Block constructed above, see [GNP22].

The Versatile Block described in Figure 3.32 is called versatile as it admits different periodic assemblies based on the groups pg, p4 and p1 as shown in Figure 3.35.

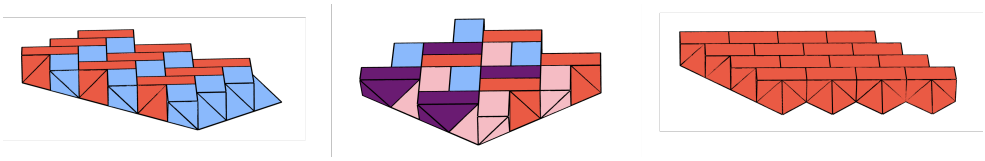

Figure 3.35: The Versatile Block described in Figure 3.32 admits different assemblies with wallpaper symmetries. Blocks of the same colour are obtained by applying translations, see [GNP22].

The list of coordinates in $\mathbb{R}^3$ for the nine vertices of the *Versatile Block* is given by:

$$
\begin{array}{ccccc}
v_1 & v_2 & v_3 & v_4 & v_5 \\
(0,0,0)^\intercal & (1,1,0)^\intercal & (2,0,0)^\intercal & (1,-1,0)^\intercal & (0,1,1)^\intercal \\
v_6 & v_7 & v_8 & v_9 & \\
(1,1,1)^\intercal & (1,0,1)^\intercal & (1,-1,1)^\intercal & (0,-1,1)^\intercal. &
\end{array}
$$

We refer to a particular vertex by its position in this ordered list, indicated by the index of v_i for $i = 1, \ldots, 9$. For the underlying incidence structure of the triangulation the faces are given by the following lists of incident vertices.

$$[[1,2,3],[1,2,5],[1,3,4],[1,4,9],[1,5,9],[2,3,7],[2,5,6],$$
$$[2,6,7],[3,4,7],[4,7,8],[4,8,9],[5,6,7],[5,7,9],[7,8,9]].$$

Remark 3.6.4. The height of the Versatile Block is chosen to be 1. In this way, we can also assemble two copies in a non-planar way. In total, there are six ways of assembling two copies of the Versatile Block up to symmetry, shown in Figure 3.36.

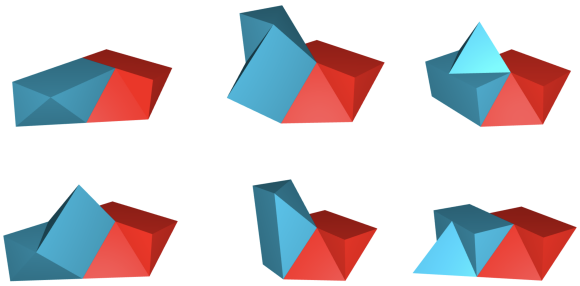

Figure 3.36: There are exactly 6 possible ways, up to isomorphism, to assemble two copies of the Versatile Block such that inclined faces of one block meet declined faces of the other, see [Akp+23].

Assembling two copies of the Versatile Block between the planes $z = 0$ and $z = 1$ given by $\langle (1,0,0),(0,1,0)\rangle$ and $\langle (1,0,0),(0,1,0)\rangle + (0,0,1) = \{(x,y,1) \mid x,y \in \mathbb{R}\}$ as displayed in the left-most pictures in Figure 3.36, leads to a wide range of possible assemblies, called *planar assemblies*. Since the Versatile Block construction is based on VersaTiles, the planar interlocking assemblies with the Versatile Block can be classified by square Truchet tiles. Apart from planar tilings, the Versatile Block admits different space-tessellations. In Figure 3.37 we see some of those tessellations with their corresponding translation cells. Given that all coordinates of the Versatile Block

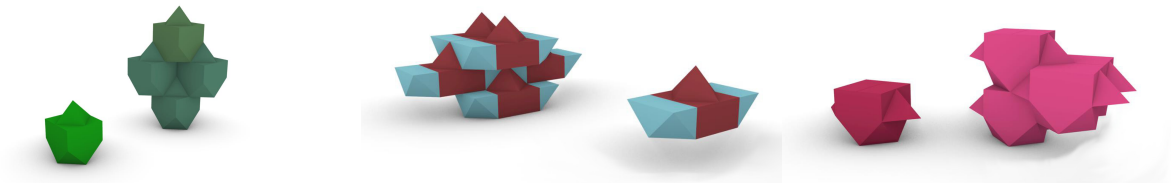

Figure 3.37: Space-filling assemblies of copies of the Versatile Block, see [Akp+23].

are in $\mathbb{Z}^3$, the natural question arises regarding whether the coordinates of potential assemblies also belong to the integer lattice.

Remark 3.6.5. Let A be an assembly with copies of the Versatile Block, such that contact faces are as shown in Figure 3.36. For two blocks, it can be shown that all coordinates lie in $\mathbb{Z}^3$: we can proceed by induction, where we remove blocks from an

assembly with $n > 3$ blocks. It follows that all coordinates have integer components by checking the coordinates of the starting configurations in Figure 3.36.

We can also employ the construction method presented in Section 3.4 to approximate a smooth surface. For this, we consider the VersaTile constructed in Figure 3.38.

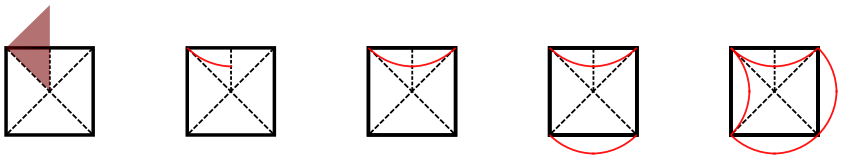

Figure 3.38: Smooth VersaTile construction.

We can approximate the smooth curve by piecewise linear paths and iterate the block construction to obtain the block in Figure 3.39.

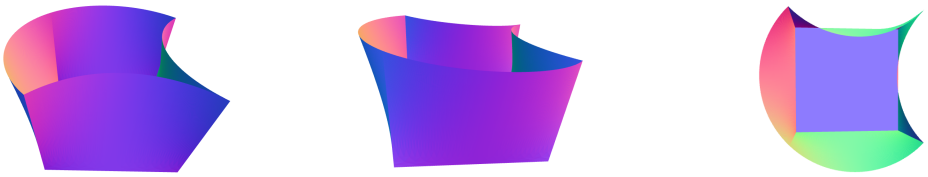

(a) (b) (c)

Figure 3.39: Several views of the resulting block from the VersaTile construction in Figure 3.38: (a) front view, (b) side view, and (c) top view.

3.6.4 Limit Case p3 - The RhomBlock

In this subsection, we describe a block coming from the deformation of a lozenge tile (rhomb) into a hexagon and yielding a candidate to an interlocking block, thus the name *RhomBlock* which can be also seen as a hexagonal version of the Versatile Block. The interlocking property of assemblies with copies of RhomBlocks is proved in the following sections.

Construction

Using the construction described in Section 3.4, we can construct a block based on Figure 3.40.

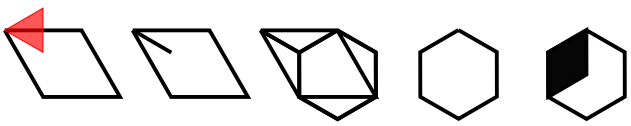

Figure 3.40: Construction steps for VersaTile with p3 symmetriy with linear path and black lozenge implying former orientation.

The surface of the resulting block can be triangulated using the coordinates

$$\begin{array}{ccccc} v_1 & v_2 & v_3 & v_4 & v_5 \\ (0,0,0)^\intercal & \left(\frac{1}{2},\frac{\sqrt{3}}{2},0\right)^\intercal & (1,0,0)^\intercal & \left(\frac{1}{2},-\frac{\sqrt{3}}{2},0\right)^\intercal & \left(0,0,\sqrt{\frac{2}{3}}\right)^\intercal \\ v_6 & v_7 & v_8 & v_9 & v_{10} \\ \left(\frac{1}{2},\frac{\sqrt{3}}{6},\sqrt{\frac{2}{3}}\right)^\intercal & \left(1,0,\sqrt{\frac{2}{3}}\right)^\intercal & \left(1,-\frac{\sqrt{3}}{3},\sqrt{\frac{2}{3}}\right)^\intercal & \left(\frac{1}{2},-\frac{\sqrt{3}}{2},\sqrt{\frac{2}{3}}\right)^\intercal & \left(0,-\frac{\sqrt{3}}{3},\sqrt{\frac{2}{3}}\right)^\intercal \end{array}$$

and corresponding vertices of faces:

$$[[1,2,3],[1,3,4],[1,5,6],[1,2,6],[2,3,6],[3,6,7],[3,7,8],[3,4,8],[4,8,9],[4,9,10],$$
$$[1,4,10],[1,5,10],[5,6,7],[5,9,10],[7,8,9],[5,7,9]].$$

In Figure 3.41 we see the resulting block.

Figure 3.41: Two views of the RhomBlock.

Similarly, as in the p4-case, we can construct a smooth version of the RhomBlock.

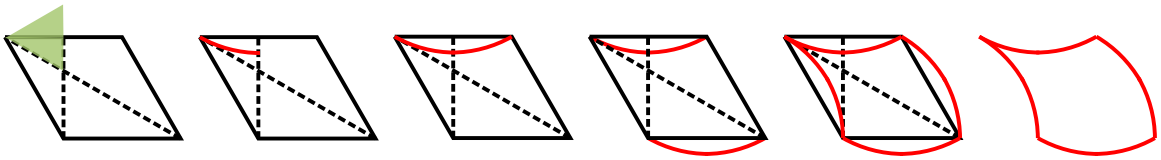

Figure 3.42: Smooth VersaTile construction for p3.

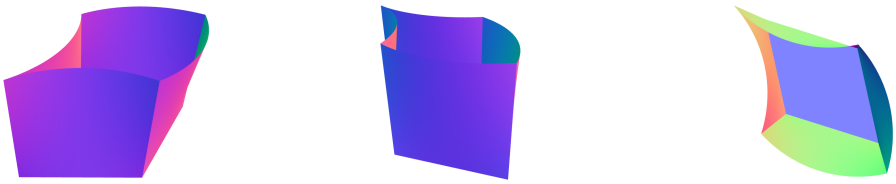

(a) (b) (c)

Figure 3.43: Several views of the resulting block from the VersaTile construction in Figure 3.42: (a) front view, (b) side view, and (c) top view.

Combinatorics of the RhomBlock

Since lozenges carry a $C_2 \times C_2$ symmetry, we can associate a lozenge tiling to a VersaTile tiling in two ways by switching between the two bipartite colouring of the hexagonal

plane.

Lemma 3.6.6. *Each lozenge tiling leads to two VersaTile tilings.*

There are various ways of associating a graph to a lozenges tiling. One way is to consider the regular hexagonal tiling of the plane, where each hexagon can be subdivided into six equilateral triangles. Then, a lozenge tiling corresponds to a perfect matching when considering the *face graph*, also called *standard graph* (see below), of this equilateral triangle tiling. In the following definition, we present some graph construction with examples in Figure 3.45.

Definition 3.6.7. Given a lozenge tiling T, we define the following graphs with additional information:

1. The *standard graph* $\mathcal{G}_T$ of T is defined to be the undirected graph with nodes corresponding to equilateral triangles contained in the lozenges tiling (place T inside the hexagonal plane) and the edges of $\mathcal{G}_T$ correspond to edges of T connecting two triangles. In order to recover T from $\mathcal{G}_T$, we can define a perfect matching connecting two triangles whenever they belong to the same lozenge tile. In the language of simplicial surfaces, a lozenge tiling can be recovered as a perfect matching of parts of the face graph of the hexagonal plane.

2. The *edge graph* $\mathcal{E}_T$ of T is defined to be the undirected graph with nodes corresponding to the edges of $\mathcal{G}_T$ and two nodes are connected by an edge if they belong to the same triangle. The tiling T can be recovered with a maximal independent set which correspond to the perfect matching of $\mathcal{G}_T$.

3. The *directed graph* $\mathcal{D}_T$ of T is defined to be the directed graph with nodes corresponding to the lozenges and arcs corresponding to neighbouring tiles. The direction is based on the underlying bipartite hexagonal lattice, where two tiles t_1, t_2 are connected with an arc (t_1, t_2) if the black part of t_1 neighbours the white part of t_2.

Here, we associate a lozenge to a single hexagon, according to the RhomBlock construction whose upper face is given by a hexagon, and it only remains to say how it is oriented regarding it bottom face. In Figure 3.44a, we see a lozenge tiling based on a substitution rule and its embedding in the bipartite hexagonal plane. Here, the substitution starts with an initial placement of the 6 lozenges in the middle and then lozenges are added for each tile iteratively at their tip.

(a) (b)

Figure 3.44: (a) Lozenge tiling, (b) lozenge tiling embedded bicoloured.

In Figure 3.45, we see three graphs with additional information that encode the tiling from Figure 3.44a.

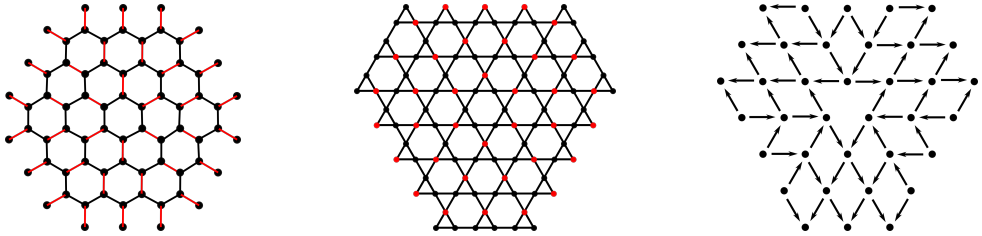

(a) (b) (c)

Figure 3.45: Three graphs representing tiling shown in Figure 3.44a (a) standard graph with perfect matching (in red), (b) edge graph with maximal independent set (in red), (c) directed graph.

The graph, in Figure 3.45a, has nodes corresponding to the equilateral triangles and edges corresponding to the edges of the hexagonal plane. The lozenge tiling then corresponds to a so-called *perfect matching*, i.e. a subset of the edges such that each node is contained in exactly one edge. The graph, in Figure 3.45b, has three nodes for each white face of the bipartite hexagonal plane corresponding to the edges. Here, a *maximal independent set* of nodes directly corresponds to the perfect matching of the graph shown in Figure 3.45a yielding the corresponding lozenge tiling. The directed graph in Figure 3.45c, can be obtained from the graph in Figure 3.45b as follows: for each white triangle we have exactly one node and arcs pointing from black towards red nodes. In Section 3.7, we define a cost function on the arcs of such directed graphs, yielding a flow network with applications for evaluating interlocking assemblies.

Below we summarise the interplay between the defined graphs above.

Proposition 3.6.8. *Each graph together with its additional data yields a unique tiling with lozenges up to isomorphism.*

Proof. Each graph is uniquely determined by the other graphs. We can embed the vertices of the standard graph inside the hexagonal plane, such that two neighbouring triangles are connected by an edge. In this way, we obtain a lozenge tiling via a perfect matching. □

Remark 3.6.9. The standard graph $\mathcal{G}_T$ is often used to enumerate lozenges in the literature, see [Gor21] as it links lozenge tilings to perfect matchings of certain planar graphs. Kasteleyn theory, see [Gor21], gives a way of counting perfect matchings in a planar graph and enables the enumeration of lozenge tilings of certain domains, such as given in Lemma 3.6.3.

RhomBlock Interlocking

In this section, we prove that any infinite tiling with lozenges leads to an interlocking assembly with RhomBlocks.

Theorem 3.6.10. *For a given infinite tiling of the plane with lozenges, we can associate two infinite interlocking RhomBlock assembly.*

Proof. By Lemma 3.6.6, we can associate two RhomBlock assemblies to a given lozenges tiling. We can proceed similarly as in Theorem 3.5.7. However, since the vertical walls of the RhomBlock come in parallel pairs, we can create interlocking chains even when considering infinitesimal rotational motions. In order to prove that this assembly is indeed an interlocking assembly, we consider its infinitesimal interlocking matrix A and show that for any γ with finite support, and $A \cdot \gamma \geq 0$ it follows that $\gamma = 0$. This is proven in two steps: first we show that for any such γ there is no i with $(A \cdot \gamma)_i > 0$ and then we show that the kernel of the matrix A is trivial. So assume that, there exists a row index i with $(A \cdot \gamma)_i > 0$. If i is associated to a vertex of a vertical face, we can construct an infinite chain as follows: The entry $(A \cdot \gamma)_i > 0$ corresponds to an inequality of the form $(-(p \times n)^\intercal, -n^\intercal, (p \times n)^\intercal, n^\intercal) \cdot (\gamma', \gamma) > 0$ according to Definition 3.3.11. If $((p \times n)^\intercal, n^\intercal) \cdot \gamma > 0$ it follows that $((p \times -n)^\intercal, -n^\intercal) \cdot \gamma = (((p-n) \times -n)^\intercal, -n^\intercal) \cdot \gamma < 0$ and thus there must be γ'' with $(((p-n) \times n)^\intercal, n^\intercal) \cdot \gamma'' > 0$, where $p - n$ is a point of the face of another block. Proceeding iteratively, we obtain an infinite chain of moving blocks in direction $-n$, which is not possible as we assumed that γ has finite support and thus $(A \cdot \gamma)_i = 0$ for any point associated to a vertical face. This already implies that γ consists only of upward translations (otherwise a row index i with the above would exist). If i with $(A \cdot \gamma)_i > 0$ then belongs to a tilted face, it follows that upward translation lead to another infinite chain by chosing opposing tilted faces. Hence, the case $A\gamma = 0$ remains which follows from the more general Proposition in Section 3.5. □

3.7 Evaluation Criteria for Interlocking Assemblies

When considering and comparing interlocking assemblies, two questions naturally arise:

1. Why do we consider interlocking assemblies?
2. How can we compare interlocking assemblies?

Answers to the first question, i.e. motivation and reason for considering interlocking assemblies are listed in the literature as interlocking assemblies have several real-world applications, see [EKA21]. For us, it suffices that we can look at these assemblies from a pure mathematical point of view, while real-world applications provide us with a clear conscience to do so. In this section, we focus on the second question, which is about comparing several assemblies. Requirements on interlocking assemblies are given by real-world applications and lead to evaluation criteria which can be applied to find optimal interlocking assemblies. Here, are several typical requirements on interlocking assemblies:

1. There shall be only a few types of blocks (easier manufacturing).
2. Blocks shall be "easy" to assemble (fast and efficient assembly methods).
3. Blocks can be used in various situations (modular building approach).
4. The assembly shall be tolerant to missing blocks (safety concerns).
5. Interlocking assemblies shall be "stable" (what stable means is discussed below).

The first four requirements can be formulated mathematically in various ways and can be already implemented in the construction of interlocking blocks. For instance, the method in Section 3.6 yields candidates satisfying the first three requirements, such as the Versatile Block and RhomBlock. Moreover, we can construct blocks leading to assemblies which are tolerant to missing blocks, i.e. after removing blocks the resulting assembly is still an interlocking assembly. Additionally, we can relate this problem to creating interlocking assemblies with identical blocks such that the number of blocks belonging to the frame is relatively small. The fifth requirement is vague as it is not clear what "stable" means and the same interlocking assembly could be useful in certain real-world applications, for instance as a ceiling construction, and bad in certain other situations, for instance as wall-construction. In this section, we focus on the following evaluation criteria:

1. How are "forces" distributed within the assembly?
2. How to deform the assembly to remove a block?

For this, we consider *planar assemblies*, i.e. interlocking assemblies which are placed between two parallel planes. The force distribution is then modelled using flow networks where the nodes of the network correspond to the blocks and the arcs to neighbouring blocks which support a block from below and the cost function to the fraction the block is supported. This model is called "interlocking flows" and is first introduced in [Goe+23] for considerations of assembly strategies with the Versatile Block. In the following, we start by defining the cost function for this network. We show that the second question leads to an optimisation problem with the goal of computing an optimal block geometry with a given surface area.

3.7.1 Projection and Cost Function on Contact Areas

In this section, we introduce a cost function for all pairwise block contacts within a specified assembly $(X_i)_{i\in I}$. We assume that all blocks within the assembly are congruent to a single block X with polyhedral boundary, assembled using the action of a wallpaper group G leading to planar assemblies. Consequently, each block, along with its neighbours, behaves locally in the same manner. The neighbours of a block X, supporting it from both below or above upon shifting X in direction $(0, 0, \pm\varepsilon)$, yield intersections with neighbouring blocks.

Remark 3.7.1. It suffices to consider supporting blocks only from below, as the block X itself supports such blocks from above, and the rest follows using the action of G.

To be more specific, let $X_1, \dots, X_n$ denote the n neighbours of the block $X = X_0$, where n is a natural number. The intersection of X with its neighbours is given by

$$X \cap X_i = \partial X \cap \partial X_i.$$

Example 3.7.2. When considering assemblies based on the Versatile Block, there are exactly two blocks supporting it from below. Moreover, when considering the projection of the respective contact areas onto the plane $\mathbb{R}^2$, this region is one half of the area of the bottom square.

We aim to quantify how X is supported from below through its neighbours. To achieve this, we associate a real number $c_i \in [0, 1]$ with each neighbour, satisfying $\sum c_i = 1$.

Definition 3.7.3. Let $F_1, \dots, F_n$ be sets such that $F_i \subset X \cap X_i = \partial X \cap \partial X_i$ is maximal and each F_i is the union of triangles $\{f_1^i, \dots, f_{m_i}^i\}$ with non-empty area and associated normals $\{n_1^i, \dots, n_{m_i}^i\} \subset \mathbb{R}^3$ pointing towards X and $n_3 > 0$ for all $n \in \{n_1^i, \dots, n_{m_i}^i\} \subset \mathbb{R}^3$ such that $f_l^i \cap f_k^i$ has empty area for $l \neq k$. We consider the projection $\pi(f_j) = \{(x_1, x_2) \mid x \in f_j \subset \mathbb{R}^3\} \subset \mathbb{R}^2$ of the faces f_j onto $\mathbb{R}^2$ and define a

function $c : \{1, \dots, n\} \to \mathbb{R}, i \mapsto c_i$, for $i \in \{1, \dots, n\}$ as follows:

$$c_i = \frac{\sum_{j=1}^{m_i} \text{Area}(\pi(f_j^i))}{\sum_{i=1}^{n} \sum_{j=1}^{m_i} \text{Area}(\pi(f_j^i))}, \tag{3.4}$$

where $\text{Area}(\cdot)$ gives the area of a measurable set in $\mathbb{R}^2$.

Consider the projection of the contact area of all neighbouring blocks of X onto a given plane. For a given block X_i neighbouring X, the quantity c_i measures the relative contact area of X_i. Thereby, c_i simulates the load transferred from block X onto X_i (see the following section).

Remark 3.7.4. For the construction of a block X together with an assembly using the methods presented in Section 3.4, we can maximise the contact area to neighbouring blocks $A = \sum_i \text{Area}(\pi(F_i))$ by carefully choosing the intermediate points.

Below, we see several examples of computing the cost function.

Example 3.7.5. For several examples presented in Section 3.4 and Section 3.6, we can compute the values c_i as follows:

1. Versatile Block and RhomBlock: $c_i = \frac{1}{2}$, $i = 1, 2$.
2. Block based on wallpaper group of type p6 in Example 3.4.1: $c_1 = \frac{4}{5}$, $c_2 = \frac{1}{5}$.
3. Block based on wallpaper group of type p3 in Example 3.4.20: $c_i = \frac{1}{2}$, $i = 1, 2$.
4. Block based on wallpaper group of type p4 in Example 3.4.22: $c_i = \frac{1}{2}$, $i = 1, 2$.

It appears that most blocks in the previous example are not distinguishable in terms of the values c_i. However, we note that the projected contact area of the Versatile Block equals $\frac{1}{2}$, whereas the projected contact area of the block given in Example 3.4.22 equals 1.

3.7.2 Interlocking Flows

In this section, we present a tool, called *Interlocking Flows*, which simulates how load is distributed within a planar interlocking assembly $(X_i)_{i \in I}$ with a frame given by the set $J \subset I$. This tool is based on the cost function presented in the previous section and the concept of *Directional Blocking Graphs* and is first introduced in the context of assemblies with the Versatile Block in [Goe+23], where it is shown that the predictions obtained from the Interlocking Flow method agrees with the results of an FEM analysis.

Directional Blocking Graphs (short DBG) are a discrete tool to study interlocking assemblies. These graphs are introduced in [Wil92; WL94] and investigated in the

context of interlocking assemblies in [WSP18]. The nodes of a DBG correspond to the blocks of the assembly, and the edges to the contacts of the blocks (connect two blocks when they "support" each other). Below, we give an adapted version of the definition of such a graph for interlocking assemblies by treating blocks that lie on the frame differently. In order to define DBG, we first need to define when two blocks restrain each other from moving.

Definition 3.7.6. Let $(X_i)_{i\in I}$ be a planar interlocking assembly with a frame given by the set $J \subset I$. We say that a block X_i is *restrained* in direction d by another block X_j if shifting the X in the direction d leads to an intersection with X_j. This means that for $i \in I \setminus J$ and $j \in I$, the translated block $X_i - d \coloneqq \{x - d \mid x \in X_i\}$ intersects with X_j, i.e.

$$(X_i - d) \cap X_j \neq \partial(X_i - d) \cap \partial X_j.$$

Furthermore, we say that a block in the frame restrains itself from moving (independent of the choice of d).

Definition 3.7.7. For $d \in \mathbb{R}^3$, the *Directional Blocking Graph* (short *DBG*), denoted by $\mathcal{G}((X_i)_{i\in I}, d)$, is defined as the directed graph with

1. nodes given by the set I and
2. arcs of the form $i \to j$ if the block X_i is restrained by X_j in direction d for $i, j \in I$.

We use a DBG $\mathcal{G}$ to model how a given load is transferred onto the frame of the underlying assembly. This is facilitated by using the cost function c defined in the previous section, yielding a flow network where the *sinks* are nodes that represent the blocks on the frame.

Example 3.7.8. We can extend the graph shown in Figure 3.45c, by introducing loops to the outer nodes, in order to obtain such a DBG for a RhomBlock assembly.

From now on, we consider the more specific situation where $d = (0, 0, -\varepsilon)$ for a small positive value $0 < \varepsilon \ll 1$. In the previous section we have associated real numbers to neighbours of blocks which can be used to define a cost function on the edges of a DBG resulting in a flow network.

Definition 3.7.9. For an assembly $(X_i)_{i\in I}$ of blocks $X_i \subset \mathbb{R}^3$ with frame $J \subset I$, we define its *interlocking flow network* as the following flow network:

1. The directed graph structures is given by the DBG $\mathcal{G} = \mathcal{G}((X_i)_{i\in I}, d)$ with $d = (0, 0, -\varepsilon)$ for a small positive value $0 < \varepsilon \ll 1$;
2. Each arc $a = i \to j$ of $\mathcal{G}$ is labelled $c(a)$ as follows: if $i \in I \setminus J$ we can compute the cost function c (Equation 3.4 in Section 3.7.1) of the block $X = X_i$ with its neighbouring block X_j within the assembly, and we associate the value c_j to the given arc. If $i \in J$, it follows that $i = j$ and we give a the the value 1.

We define the *interlocking flow matrix* as the matrix $B \in \mathbb{R}^{I \times I}$ with entries given by

$$B_{ij} = \begin{cases} c\,(i \to j)\,, & i \to j \text{ is an arc,} \\ 0, & \text{otherwise,} \end{cases}$$

for $i, j \in I$.

The interlocking flow matrix can be viewed as a weighted *adjacency matrix* of a DBG $\mathcal{G}$, yielding a flow network with capacity function c. It turns out, that this matrix is a stochastic matrix, as shown in the following lemma.

Lemma 3.7.10. *The interlocking flow matrix B is a right stochastic matrix.*

Proof. This follows immediately from the fact that the values c are chosen in a way that the rows of B sum up to 1. □

The following example is based on the work presented in [Goe+23] and deals with the special case that the underlying assembly is given by copies of the Versatile Block, see Section 3.6. It exemplifies how we can model load distribution within an assembly with a frame given by $J \subset I$ composed of Versatile Blocks. The load onto the assembly is modelled as a vector $x \in \mathbb{R}^I_{\geq 0}$ with $x_j = 0$, for all $j \in J$, and the distribution is based on the interlocking flow network with interlocking matrix B defined below.

Example 3.7.11. Planar assemblies based on the Versatile Block can be classified by Truchet tiles, as shown in Section 3.6. We assume that the set I corresponds to an $m \times n$ grid of Truchet tiles and the set $J \subset I$ of the most-outer tiles. In the following, we identify I with the set $\{1, \ldots, n \cdot m\}$. It follows that the interlocking flow and the associated interlocking flow matrix can be computed as follows: the nodes correspond to Truchet tiles and the arcs are of the form $i \to j$ for two tiles i, j which meet at different colours, such that i is coloured white and j is coloured black. The value on an arc $a = i \to j$ is given as presented in Example 3.7.5, i.e.

$$c(a) = \begin{cases} \frac{1}{2}, & \text{if } i \neq j, \\ 1, & \text{if } i = j. \end{cases}$$

We can interpret this model as a discretisation of load distribution in the following way: let $x \in \mathbb{R}^I_{\geq 0}$ be a vector with $x_j = 0$, if $j \in J$ and $x_i \in \mathbb{R}_{\geq 0}$ for $i \in I \setminus J$. Thus, we can interpret the entries of x as the applied loads in direction d on each block. Below, x is chosen to be $x_i = 1$ for $i \in I \setminus J$ and $x_j = 0$ for $j \in J$. The model of load transfer can then be discretised by considering the matrix-vector multiplication

$$B^k \cdot x$$

for discrete time steps $k = 0, \ldots, \ell$, where $\ell \gg k$ is chosen to be large with $B^n \cdot x$ being close to the convergence load transfer on the frame given the initial load x. Since B

is a stochastic matrix, it follows that the sum over all entries of $B^k \cdot x$ equals the sum over the entries of x, i.e.

$$\sum_{i=1}^{n\times m} (B^k \cdot x)_i = \sum_{i=1}^{n\times m} x_i,$$

which can be interpreted as a discrete version of a conservation of energy law. The matrix vector multiplication $B^k \cdot x$ can be computed by exploiting the flow structure as follows:

1. Create an $n \times m$ grid corresponding to the underlying Truchet tiling of I.
2. Fill the square corresponding to $i \in I$ with the value x_i (initialise vector x).
3. Add $1/2$ times the value of square $i \in I \setminus J$ to square j if the white part of square i touches the black part of square j (this corresponds to the matrix multiplication $B \cdot x$).
4. Iterate the second and third step $k-1$ times with the updated squares.

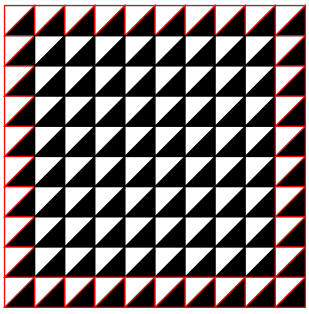

(a) Truchet tiling.

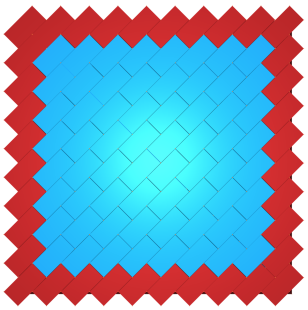

(b) p1 assembly with frame.

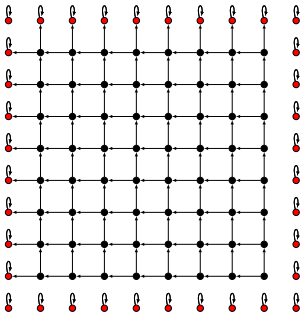

(c) p1 DBG.

0	6.43	5.93	5.32	4.61	3.81	2.92	1.98	1.00	0
6.43	0	0	0	0	0	0	0	0	0
5.93	0	0	0	0	0	0	0	0	0
5.32	0	0	0	0	0	0	0	0	0
4.61	0	0	0	0	0	0	0	0	0
3.81	0	0	0	0	0	0	0	0	0
2.92	0	0	0	0	0	0	0	0	0
1.98	0	0	0	0	0	0	0	0	0
1.00	0	0	0	0	0	0	0	0	0
0	0	0	0	0	0	0	0	0	0

(d) $B^\ell \cdot x$ with entries rounded to two digits for $1 \ll \ell$ large.

Figure 3.46: Combinatorial Interpretation for p1 experiments.

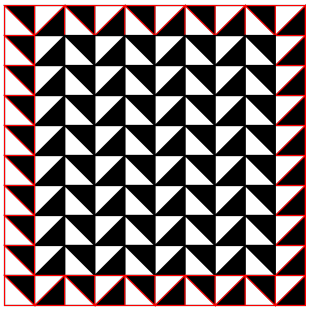

(a) Truchet tiling.

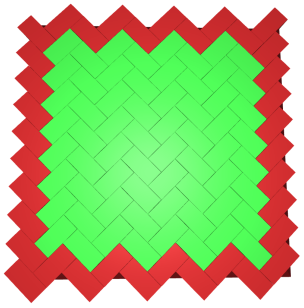

(b) pg assembly with frame.

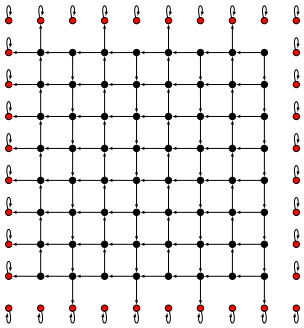

(c) pg DBG.

0	4.44	0	3.71	0	2.82	0	1.66	0	0
4.44	0	0	0	0	0	0	0	0	0
5.52	0	0	0	0	0	0	0	0	0
6.10	0	0	0	0	0	0	0	0	0
6.27	0	0	0	0	0	0	0	0	0
6.05	0	0	0	0	0	0	0	0	0
5.42	0	0	0	0	0	0	0	0	0
4.30	0	0	0	0	0	0	0	0	0
2.55	0	0	0	0	0	0	0	0	0
0	0	4.10	0	3.31	0	2.31	0	1.00	0

(d) $B^\ell \cdot x$ with entries rounded to two digits for $1 \ll \ell$ large.

Figure 3.47: Combinatorial Interpretation for pg experiments.

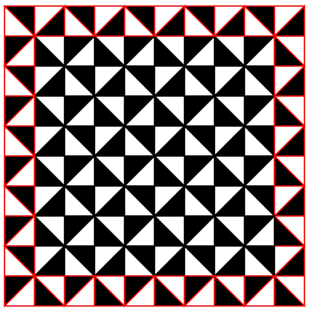

(a) Truchet tiling.

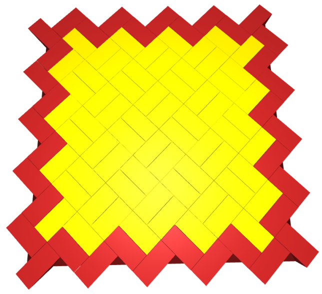

(b) p4 assembly with frame.

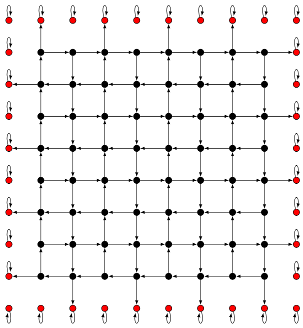

(c) p4 DBG.

0	0	0	0	0	0	0	0	0	0
0	1	1	1	1	1	1	1	1	0
0	1	1	1	1	1	1	1	1	0
0	1	1	1	1	1	1	1	1	0
0	1	1	1	1	1	1	1	1	0
0	1	1	1	1	1	1	1	1	0
0	1	1	1	1	1	1	1	1	0
0	1	1	1	1	1	1	1	1	0
0	1	1	1	1	1	1	1	1	0
0	0	0	0	0	0	0	0	0	0

(d) $x \in \mathbb{R}^I \cong \mathbb{R}^{100} \cong \mathbb{R}^{10\times 10}$.

0	$\frac{1}{2}$	0	$\frac{1}{2}$	0	$\frac{1}{2}$	0	$\frac{1}{2}$	0	0
0	$\frac{1}{2}$	$\frac{1}{2}$	1	$\frac{1}{2}$	1	$\frac{1}{2}$	1	$\frac{1}{2}$	$\frac{1}{2}$
$\frac{1}{2}$	1	1	1	1	1	1	1	$\frac{1}{2}$	0
0	$\frac{1}{2}$	1	1	1	1	1	1	1	$\frac{1}{2}$
$\frac{1}{2}$	1	1	1	1	1	1	1	$\frac{1}{2}$	0
0	$\frac{1}{2}$	1	1	1	1	1	1	1	$\frac{1}{2}$
$\frac{1}{2}$	1	1	1	1	1	1	1	$\frac{1}{2}$	0
0	$\frac{1}{2}$	1	1	1	1	1	1	1	$\frac{1}{2}$
$\frac{1}{2}$	$\frac{1}{2}$	1	$\frac{1}{2}$	1	$\frac{1}{2}$	1	$\frac{1}{2}$	$\frac{1}{2}$	0
0	0	$\frac{1}{2}$	0	$\frac{1}{2}$	0	$\frac{1}{2}$	0	$\frac{1}{2}$	0

(e) $B \cdot x$.

0	2.58	0	4.38	0	4.88	0	4.16	0	0
0	0	0	0	0	0	0	0	0	2.58
4.16	0	0	0	0	0	0	0	0	0
0	0	0	0	0	0	0	0	0	4.38
4.88	0	0	0	0	0	0	0	0	0
0	0	0	0	0	0	0	0	0	4.88
4.38	0	0	0	0	0	0	0	0	0
0	0	0	0	0	0	0	0	0	4.16
2.58	0	0	0	0	0	0	0	0	0
0	0	4.16	0	4.88	0	4.38	0	2.58	0

(f) $B^\ell \cdot x$ with entries rounded to two digits for $1 \ll \ell$ large.

Figure 3.48: Combinatorial Interpretation for p4 experiments.

Indeed, modelling load distribution using interlocking flows promises to be a reliable tool of predicting the distribution of load onto the frame, as is it consistent with the results obtained by the FEM analysis presented in [Goe+23]. Thus, we obtain a fast and discrete evaluation criterion which allows a fast impression how forces distribute in order to pick candidates of numerous interlocking assemblies based on certain applications. For instance, in an 10×10 interlocking assembly with 100 Versatile Blocks, there are $2^{10+10-3} = 2^{17} = 131072$ possible assemblies (up to rotation and mirroring) using the Versatile Block, see Section 3.6, and for an initial prediction, we can evaluate the load distributions onto the frame for all 131072 assemblies in a matter of seconds as it only revolves around matrix-vector multiplications with relatively small matrices.

3.7.3 Homeomorphisms and Stability

In this section, we associate a real value to an assembly, indicating how much we need to "deform" it before it is no longer an interlocking assembly.

Definition 3.7.12. Let $(X_i)_{i\in I}$ be an interlocking assembly with frame $J \subset I$. Let $\varphi\colon \mathbb{R}^3 \to \mathbb{R}^3$ be a homeomorphism such that the family $(\varphi(X_i))_{i\in I}$ is no longer an interlocking assembly with frame J. The *deformation value* D_X of $(X = (X_i)_{i\in I}, J)$ is then defined to be the infimum of

$$\|\mathbb{I} - \varphi\|_{L_2} = \int_{\mathbb{R}^3} \|x - \varphi(x)\|_2 dx$$

over all above φ, i.e.

$$D_X = \inf_{\varphi\colon \mathbb{R}^3 \to \mathbb{R}^3 \text{ hom.}} \|\mathbb{I} - \varphi\|_{L_2}.$$

This leads to the following optimisation problem:

Remark 3.7.13. Let $\mathrm{Area}(X)$ be the surface area of a block X and let $c \in \mathbb{R}_{>0}$ be a constant positive real number. We seek to find X such that $\mathrm{Area}(X) = c$ and the deformation value is as large as possible. In other words, given a surface area, the goal is to find an interlocking block with the largest possible deformation value, i.e.

$$\mathrm{Area}(X) = c, \quad D_X \to \sup\,.$$

For future research, one can combine this approach with the construction of interlocking blocks using wallpaper groups.

The following questions naturally arise:

1. What additional properties are required for φ ?
2. Can homeomorphisms be used to create new interlocking assemblies?
3. Is the L_2-norm suited for the definition above?
4. Is there a discrete way to estimate the deformation number?

Chapter 4

Doubly Periodic Landscapes

4.1 Summary

We show that for any prism with a triangular domain and any similarity type of triangle, we can find a plane through the origin whose intersection with the prism has the desired domain. This result can be combined with the theory of wallpaper groups with a triangular fundamental domain to obtain a doubly periodic structure. We demonstrate that known structures, such as the Miura-Ori pattern, can be obtained in this way. Moreover, we can extend this construction by either using the concept of layer groups or by acting on several triangles at once.

4.2 Introduction

Thirteen of the seventeen types of wallpaper groups can have a triangle as a fundamental domain. Given such a triangle F which is the fundamental domain of a wallpaper group G, we can describe F by three points in the xy-plane P_0, P_1, P_2, we consider the set $C := F + \langle e_3 \rangle$, where $e_3 = (0, 0, 1)^\intercal$. We show in Theorem 4.3.1, that for any given triple of angles (α, β, γ) of an equivalence type of triangles, there exists a plane P through the point P_0 such that $T := P \cap (F + \langle e_3 \rangle)$ forms a triangle with angles (α, β, γ).

Next, we can "lift" the natural group action of G such that G acts on $\mathbb{R}^3$ and thus on the newly created triangle T. The orbit of T under the action of G yields an infinite doubly-periodic embedded simplicial surface in 3D space such that the projection onto the xy-plane is again a wallpaper pattern.

As an extension, we consider the intersections of C with multiple planes and in this way we can find doubly-periodic surfaces with self-intersecting faces. These constructed surfaces can be then applied, for instance, as candidates for shell structures in civil engineering, see [Vak+22].

4.3 Column Plane Cut Theorem

The following theorem is formulated using the terminology of projections. Instead, we can also view it as framed in the introduction, i.e. cutting a prism with a plane.

Theorem 4.3.1. *Suppose F is a triangle determined by three points $P_i \in \mathbb{R}^2$, where we identify P_i with its image under the map $\mathbb{R}^2 \to \mathbb{R}^3, (p_1, p_2) \mapsto (p_1, p_2, 0)$. Then for all $\alpha, \beta \in (0, \pi)$ with $\alpha + \beta < \pi$, there exist $t, r \in \mathbb{R}$ such that the triangle T given by the points $\tilde{P}_0 = P_0, \tilde{P}_1 = P_1 + (0, 0, t), \tilde{P}_2 = P_2 + (0, 0, r)$ has inner angles $\alpha, \beta, \pi - \alpha - \beta$.*

Proof. We show the statement with the following steps:

(1) Show that, we can assume that $P_0 = (0, 0, 0)^\intercal, P_1 = (1, 0, 0)^\intercal, P_2 = (y_1, y_2, 0)^\intercal$ for some $y_1, y_2 \in \mathbb{R}$.

(2) Show that, we can assume $\alpha \in (0, \frac{\pi}{2})$.

(3) Show that, we can write t as an expression in r and $\cos(\alpha)$ and P_2.

(4) Show that, all possible values for $\beta \in (0, \pi - \alpha)$ are achieved for a fixed α using the intermediate value theorem.

Without loss of generality, we can assume that the base triangle is given by three points of the form $P_0 = (0, 0, 0)^\intercal, P_1 = (1, 0, 0)^\intercal$ and $P_2 = (y_1, y_2, 0)^\intercal$. This can be done by applying a suitable affine transformation given by a scalar $a \in \mathbb{R}_{>0}$, an orthogonal matrix R and a translation t, i.e. translate P_0 into the origin and rotate and scale P_1 into the point as given above. Such transformations map triangles onto triangles with same angles, and thus we can continue with the points as above, see (1). Since $\gamma = \pi - \alpha - \beta > 0$, it follows that either γ, α, β lies inside the interval $(0, \frac{\pi}{2})$. Thus, we can assume (2). Now, for $t, r \in \mathbb{R}$ denote the side lengths of the triangle given by the points $\tilde{P}_i$ by a, b, c such that $a = \|\tilde{P}_1 - \tilde{P}_2\|_2, b = \|\tilde{P}_2 - \tilde{P}_0\|_2, c = \|\tilde{P}_0 - \tilde{P}_1\|_2$. We compute

$$
\begin{aligned}
a &= \sqrt{(y_1 - 1)^2 + y_2^2 + (r - t)^2} = \sqrt{y_1^2 - 2y_1 + 1 + y_2^2 + r^2 - 2rt + t^2}, \\
b &= \sqrt{y_1^2 + y_2^2 + r^2}, \\
c &= \sqrt{1 + t^2}.
\end{aligned}
$$

Then by the cosine law, it follows that the inner angles of the triangle given by the

points $\tilde{P}_i$ are given by

$$\cos\alpha = \frac{b^2+c^2-a^2}{2bc} = \frac{y_1^2+y_2^2+r^2+1+t^2-(y_1^2-2y_1+1+y_2^2+r^2-2rt+t^2)}{2\sqrt{1+t^2}\sqrt{y_1^2+y_2^2+r^2}},$$
$$\cos\beta = \frac{a^2+c^2-b^2}{2ac} = \frac{y_1^2-2y_1+1+y_2^2+r^2-2rt+t^2+1+t^2-(y_1^2+y_2^2+r^2)}{2\sqrt{1+t^2}\sqrt{(y_1-1)^2+y_2^2+(r-t)^2}},$$
$$\cos\gamma = \frac{a^2+b^2-c^2}{2ab} = \frac{y_1^2-2y_1+1+y_2^2+r^2-2rt+t^2+y_1^2+y_2^2+r^2-(1+t^2)}{2\sqrt{y_1^2+y_2^2+r^2}\sqrt{(y_1-1)^2+y_2^2+(r-t)^2}}.$$

This simplifies to

$$\cos\alpha = \frac{y_1+rt}{\sqrt{1+t^2}\sqrt{y_1^2+y_2^2+r^2}},$$
$$\cos\beta = \frac{-y_1+-rt+t^2}{\sqrt{1+t^2}\sqrt{(y_1-1)^2+y_2^2+(r-t)^2}},$$
$$\cos\gamma = \frac{y_1^2-y_1+y_2^2+r^2-rt}{\sqrt{y_1^2+y_2^2+r^2}\sqrt{(y_1-1)^2+y_2^2+(r-t)^2}}.$$

The first equality implies (later, we see that we can assume that both sides are non-negative for certain values of t, r and thus also equivalence holds)

$$\cos^2\alpha = \frac{(y_1+tr)^2}{(1+t^2)(y_1^2+y_2^2+r^2)},$$

this expression is quadratic in t and is equivalent to

$$\begin{aligned}0 &= \cos^2\alpha\left(1+t^2\right)\left(y_1^2+y_2^2+r^2\right)-(y_1+tr)^2\\ &= \left(\cos^2\alpha\left(y_1^2+y_2^2+r^2\right)-r^2\right)t^2+(-2y_1r)\,t+\left(\cos^2\alpha\left(y_1^2+y_2^2+r^2\right)-y_1^2\right).\end{aligned}$$

Solving this quadratic equation for t yields

$$t = \frac{1}{D}\left(y_1r \pm \sqrt{y_1^2r^2-DC}\right),$$

where $D = \cos^2\alpha\,(y_1^2+y_2^2+r^2)-r^2, C = \cos^2\alpha\,(y_1^2+y_2^2+r^2)-y_1^2$. Thus, we obtained an expression for t dependent only on $\cos\alpha, r$ and y_1, y_2. In the following, we only consider the expression

$$t = \frac{1}{D}\left(y_1r + \sqrt{y_1^2r^2-DC}\right),$$

and show that all possible values for $\cos\beta$ can be achieved by appropriate choices of r. This expression is well-defined and continuous in r unless $D = 0$ or $y_1^2r^2-DC < 0$.

We have $D = 0$ if and only if

$$|r| = \sqrt{\frac{\cos^2\alpha\,(y_1^2+y_2^2)}{1-\cos^2\alpha}}$$

and $y_1^2 r^2 - DC < 0$ if and only if

$$|r| < \sqrt{\frac{\cos^2\alpha\,(y_2^2+y_1^2)-y_1^2}{1-\cos^2\alpha}} < \sqrt{\frac{\cos^2\alpha\,(y_1^2+y_2^2)}{1-\cos^2\alpha}}.$$

Moreover, if $\cos^2\alpha\,(y_2^2+y_1^2) < y_1^2$ then the discriminant is always non-negative. Thus, we have that the expression of t above is defined in the intervals

$$\begin{aligned}
&\left(-\infty, -\sqrt{\frac{\cos^2\alpha\,(y_1^2+y_2^2)}{1-\cos^2\alpha}}\right),\\
&\left(-\sqrt{\frac{\cos^2\alpha\,(y_1^2+y_2^2)}{1-\cos^2\alpha}}, -\sqrt{\frac{\cos^2\alpha\,(y_2^2+y_1^2)-y_1^2}{1-\cos^2\alpha}}\right],\\
&\left[\sqrt{\frac{\cos^2\alpha\,(y_2^2+y_1^2)-y_1^2}{1-\cos^2\alpha}}, \sqrt{\frac{\cos^2\alpha\,(y_1^2+y_2^2)}{1-\cos^2\alpha}}\right),\\
&\left(\sqrt{\frac{\cos^2\alpha\,(y_1^2+y_2^2)}{1-\cos^2\alpha}}, \infty\right).
\end{aligned}$$

We want to understand the values of $\cos\beta$ on the intervals above, where we view $\cos\beta$ as a function of r, using the expression of t. Now, we can compute the following limit

$$\begin{aligned}
\lim_{r\to\pm\infty}\cos\beta &= \lim_{r\to\pm\infty} \mp\frac{\frac{y_1-1}{r} + t\left(1-\frac{t}{r}\right)}{\sqrt{1+t^2}\cdot\sqrt{\frac{(y_1-1)^2+y_2^2}{r^2}+\left(1-\frac{t}{r}\right)^2}}\\
&= \mp\frac{\frac{\sqrt{\cos^2\alpha-\cos^4\alpha}}{\cos^2\alpha-1}}{\sqrt{1+\left(\frac{\sqrt{\cos^2\alpha-\cos^4\alpha}}{\cos^2\alpha-1}\right)^2}}\\
&= \pm\cos\alpha.
\end{aligned}$$

Moreover, we see that the values of $\cos\beta$ agree on $r = \pm\sqrt{\frac{\cos^2\alpha\left(y_2^2+y_1^2\right)-y_1^2}{1-\cos^2\alpha}}$. It remains to check the limits of $\cos\beta$ for $r \to \pm\sqrt{\frac{\cos^2\alpha\left(y_1^2+y_2^2\right)}{1-\cos^2\alpha}}$. Since both the nominator and denominator of t vanish for $r \to -\mathrm{sgn}(y_1)\sqrt{\frac{\cos^2\alpha\left(y_1^2+y_2^2\right)}{1-\cos^2\alpha}}$ we can use L'Hospital rules to show that the limit exists in $\mathbb{R}$ and thus extend $\cos\beta$ as a function in r continuously.

Additionally, we compute

$$\lim_{r\to \operatorname{sgn}(y_1)\sqrt{\frac{\cos^2\alpha\left(y_1^2+y_2^2\right)}{1-\cos^2\alpha}}} \cos\beta = 1.$$

Putting everything together, it follows that $\cos\beta$ is continuous on the intervals and by the intermediate value theorem it follows that $\cos\beta$ achieves all values in the interval $(-\cos\alpha, 1)$ (we assumed $\cos\alpha > 0$ in the beginning). Since $\cos : [0,\pi] \to [-1,1]$ is bijective and strongly decreasing, it follows that possible values for β are exactly given by the interval $(0, \pi-\alpha)$ using the fact $-\cos\alpha = \cos(\pi-\alpha)$. It remains to show that the expression of $\cos\alpha$ is positive on a region, where $\cos\beta$ achieves all possible values. In terms of the expression of $\cos\alpha$, we have

$$\cos\alpha > 0 \text{ if and only if } y_1 + rt > 0,$$

where we assume the expression $t = \frac{1}{D}\left(y_1 r + \sqrt{y_1^2 r^2 - DC}\right)$. For this, we distinguish between the two cases $y_1 < 0$ and $y_1 \geq 0$ and show that for $y_1 < 0$, we have that $\cos\alpha > 0$ holds on $\left(-\infty, -\sqrt{\frac{\cos^2\alpha\left(y_1^2+y_2^2\right)}{1-\cos^2\alpha}}\right)$ and for $y_1 \geq 0$ we have that $\cos\alpha > 0$ holds on the intervals $\left(-\infty, -\sqrt{\frac{\cos^2\alpha\left(y_1^2+y_2^2\right)}{1-\cos^2\alpha}}\right)$, $\left(-\sqrt{\frac{\cos^2\alpha\left(y_1^2+y_2^2\right)}{1-\cos^2\alpha}}, -\sqrt{\frac{\cos^2\alpha\left(y_2^2+y_1^2\right)-y_1^2}{1-\cos^2\alpha}}\right]$ and $\left[\sqrt{\frac{\cos^2\alpha\left(y_2^2+y_1^2\right)-y_1^2}{1-\cos^2\alpha}}, \sqrt{\frac{\cos^2\alpha\left(y_1^2+y_2^2\right)}{1-\cos^2\alpha}}\right)$. By the computations above, $\cos\beta$ achieves all values in $(-\cos\alpha, 1)$ in both cases. In the case $y_1 < 0$, we have

$$\begin{aligned} 0 <& y_1 + t\cdot r \\ =& \frac{Dy_1 + y_1 r^2 + r\sqrt{y_1^2 r^2 - DC}}{D}, \end{aligned}$$

which is equivalent to the expression below, obtained by multiplying with $0 < -D$

$$\begin{aligned} 0 <& -Dy_1 + -y_1 r^2 - r\sqrt{y_1^2 r^2 - DC} \\ =& y_1 r^2 - \cos^2\alpha\left(y_1^2 + y_2^2 + r^2\right) y_1 - y_1 r^2 - r\sqrt{y_1^2 r^2 - DC} \\ =& \underbrace{-\cos^2\alpha\left(y_1^2 + y_2^2 + r^2\right) y_1}_{\geq 0} \underbrace{-r\sqrt{y_1^2 r^2 - DC}}_{>0} \end{aligned}$$

on $\left(-\infty, -\sqrt{\frac{\cos^2\alpha\left(y_1^2+y_2^2\right)}{1-\cos^2\alpha}}\right)$ for $\operatorname{sgn}(y_1) = -1$.

In case $y_1 \geq 0$, we have to consider all other intervals. On $\left(-\infty, -\sqrt{\frac{\cos^2\alpha\left(y_1^2+y_2^2\right)}{1-\cos^2\alpha}}\right)$

we have

$$\begin{aligned}0 <& y_1 + t \cdot r \\ =& \frac{Dy_1 + y_1 r^2 + r\sqrt{y_1^2 r^2 - DC}}{D} = \frac{\cos^2\alpha\left(y_1^2 + y_2^2 + r^2\right) y_1 + r\sqrt{y_1^2 r^2 - DC}}{D}\end{aligned}$$

multiply with $0 < -D$ yields

$$\begin{aligned}0 <& - Dy_1 + -y_1 r^2 - r\sqrt{y_1^2 r^2 - DC} \\ &= y_1 r^2 - \cos^2\alpha\left(y_1^2 + y_2^2 + r^2\right) y_1 - y_1 r^2 - r\sqrt{y_1^2 r^2 - DC} \\ &= -\cos^2\alpha\left(y_1^2 + y_2^2 + r^2\right) y_1 \underbrace{-r\sqrt{y_1^2 r^2 - DC}}_{\geq 0}\end{aligned}$$

and this holds if and only if

$$\begin{aligned}&0 < \cos^2\alpha\left(y_1^2 + y_2^2 + r^2\right) y_1 < -r\sqrt{y_1^2 r^2 - DC} \\ \Leftrightarrow& \left(\cos^2\alpha\left(y_1^2 + y_2^2 + r^2\right) y_1\right)^2 < r^2\cos^2\alpha\left(y_1^2 + y_2^2 + r^2\right)\left(r^2 + y_1^2 - \cos^2\alpha\left(y_1^2 + y_2^2 + r^2\right)\right) \\ \Leftrightarrow& \cos^4\alpha\left(y_1^2 + y_2^2 + r^2\right)^2\left(y_1^2 + r^2\right) < r^2\cos^2\alpha\left(r^2 + y_1^2\right)\left(y_1^2 + y_2^2 + r^2\right) \\ \Leftrightarrow& 0 < r^2 - \cos^2\alpha\left(y_1^2 + y_2^2 + r^2\right) = -D\end{aligned}$$

which holds true on the interval. Now for the remaining intervals we have $D > 0$ and thus

$$0 < \cos^2\alpha\left(y_1^2 + y_2^2 + r^2\right) y_1 + r\sqrt{y_1^2 r^2 - DC}$$

this clearly holds on $\left[\sqrt{\frac{\cos^2\alpha\left(y_2^2+y_1^2\right)-y_1^2}{1-\cos^2\alpha}}, \sqrt{\frac{\cos^2\alpha\left(y_1^2+y_2^2\right)}{1-\cos^2\alpha}}\right)$ since both summands are non-negative so it remains to consider $\left(-\sqrt{\frac{\cos^2\alpha\left(y_1^2+y_2^2\right)}{1-\cos^2\alpha}}, -\sqrt{\frac{\cos^2\alpha\left(y_2^2+y_1^2\right)-y_1^2}{1-\cos^2\alpha}}\right]$. Analogously to the computation above, we have (using that $D > 0$ on this interval):

$$0 < \cos^2\alpha\left(y_1^2 + y_2^2 + r^2\right) y_1 + r\sqrt{y_1^2 r^2 - DC}$$

holds if and only if

$$0 < -r\sqrt{y_1^2 r^2 - DC} < \cos^2\alpha\left(y_1^2 + y_2^2 + r^2\right) y_1$$

which holds for $0 < D$. In summary, we have shown for any possible value y_1, and given α, β with $0 < \alpha < \frac{\pi}{2}$ and $0 < \alpha + \beta < \pi$ we can find t, r the triangle given by the points $\tilde{P}_0 = P_0, \tilde{P}_1 = P_1 + (0, 0, t), \tilde{P}_2 = P_2 + (0, 0, r)$ has inner angles $\alpha, \beta, \pi - \alpha - \beta$.

□

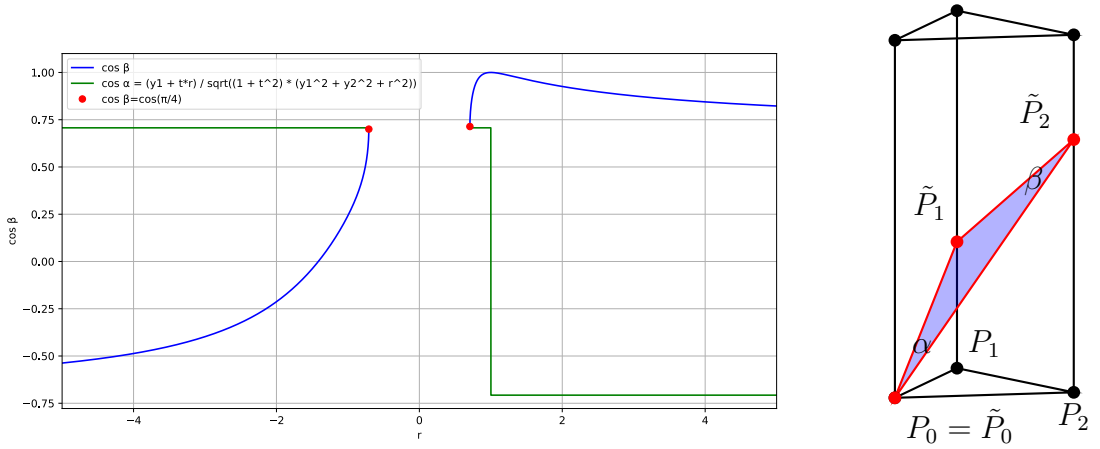

(a) (b)

Figure 4.1: We consider a column with base triangle F given by the points $P_0 = (0,0,0)^\intercal, P_1 = (1,0,0)^\intercal, P_2 = (0.5, \sqrt{3}/2, 0)^\intercal$ if T is a triangle projecting onto F with points $\tilde{P}_0 = (0,0,0)^\intercal, \tilde{P}_1 = (1,0,t)^\intercal, \tilde{P}_2 = (0.5, \sqrt{3}/2, r)^\intercal$ such that the angle at $\tilde{P}_0$ is $\alpha = \frac{\pi}{4}$. (a) The angle β at $\tilde{P}_2$ can be written as a function, depending on r if choosing t such that we always have the angle α at $\tilde{P}_0$. (b) Choosing $\alpha = \beta$, we can compute $t = \sqrt{2}$ and $r = \frac{1}{\sqrt{2}}$.

Example 4.3.2. We consider an equilateral triangle F with unit side lengths given by the points $P_0 = (0,0,0)^\intercal, P_1 = (1,0,0)^\intercal, P_2 = (1/2, \sqrt{3}/2, 0)^\intercal$. We want to find a triangle T that projects onto F with inner angle $\alpha = \frac{\pi}{4}$. By Theorem 4.3.1, we know that we can obtain such a triangle with angles $\alpha = \frac{\pi}{4}, \beta, \gamma$ with points of the form $\tilde{P}_0 = (0,0,0)^\intercal, \tilde{P}_1 = (1,0,t)^\intercal, \tilde{P}_2 = (1/2, \sqrt{3}/2, r)^\intercal$. Both t and $\cos\beta$ can be written as terms dependent only on r, i.e.

$$t = \frac{1}{D}\left(\frac{1}{2}r + \sqrt{\frac{1}{4}r^2 - DC}\right),$$

where $D = \frac{1}{2}(1+r^2) - r^2, C = \frac{1}{2}(1+r^2) - \frac{1}{4}$ since $\cos\alpha = \cos\frac{\pi}{4} = \frac{1}{\sqrt{2}}$. Now,

$$\cos\beta = \frac{-y_1 + -rt + t^2}{\sqrt{1+t^2}\sqrt{(y_1-1)^2 + y_2^2 + (r-t)^2}},$$

with $y_1 = 1/2$ and $y_2 = \sqrt{3}/2$ and we can plot the possible values of $\cos\beta$ depending on the values of r by using the expression of t above, see Figure 4.1. For instance, we find that a triangle with angles $\alpha, \beta = \alpha, \pi/2$ can be found using the values

$$r = \pm\sqrt{\frac{\cos^2\alpha\,(y_2^2 + y_1^2) - y_1^2}{1 - \cos^2\alpha}} = \pm\frac{1}{\sqrt{2}}$$

and compute t based on this. Since the base triangle F is equilateral, we can even

exchange values for r and t. For instance, in Figure 4.1 we see the resulting triangle for $t = \sqrt{2}$ and $r = \frac{1}{\sqrt{2}}$.

4.4 Doubly Periodic Landscapes

We consider a planar crystallographic group G with a fundamental domain F for G such that F is a triangle, i.e. the convex hull of three points in $\mathbb{R}^2$. Using the Hermann-Mauguin notation, also known as international notation (see [IUC02]), this is possible for the following types of wallpaper groups: p2, pg, cm, p2mg, p2gg, c2mm, p4, p4mm, p4gm, p3m1, p31m, p6, p6mm. We use the construction presented in the previous section to obtain a triangle T in $\mathbb{R}^3$ such that the projection of T onto $\mathbb{R}^2$ equals F. Next, the idea is to extend the action of G onto $\mathbb{R}$ in order to act on T, with the aim of obtaining a doubly periodic surface.

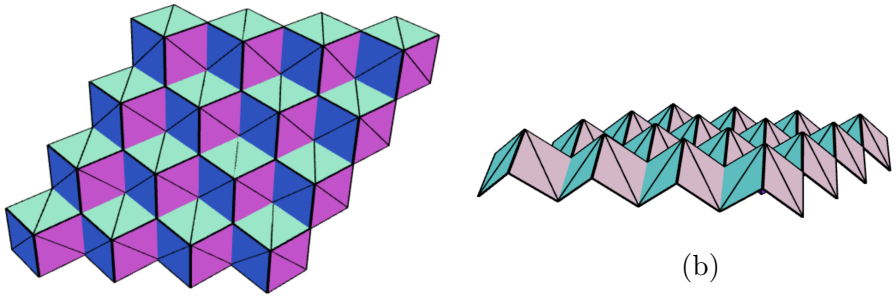

(a) (b)

Figure 4.2: Example construction based on the wallpaper group of type p3m1.

Example 4.4.1. Consider the triangle constructed in Example 4.3.2. We can use reflections at each side of the prism to obtain the doubly periodic landscape depicted in Figure 4.2. This corresponds to considering the wallpaper group of type p3m1 which has an equilateral triangle as a fundamental domain and is generated by reflections along each edge.

However, in some cases, i.e. p2, pg, p2mg, p2gg, c2mm, p4 and p6, we have that for the corresponding triangles one of the following is true

1. a point lies on an edge other than a vertex is fixed under the action of the underlying group is fixed or

2. a point is obtained by the vertices of another triangle in the tessellation given the domain F.

Hence, in these cases the domain F can rather be understood as a quadrilateral with one inner angle being equal to 180 degrees.

So we first restrict our attention to groups of type cm, p4mm, p4gm, p3m1, p31m or p6mm, and consider a fundamental domain F in the shape of a triangle.

In order to understand how to extend the action of G, we first investigate the edges of the underlying triangular fundamental domains and distinguish between mirror and rotation edges.

Mirror Edges If all edges are mirror edges, we can simply extend the action of G by using the following map and understand G as a subgroup of SE(2)

$$\mathrm{SE}(2) \to \mathrm{SE}(3), \begin{pmatrix} R & t \\ 0 & 1 \end{pmatrix} \mapsto \begin{pmatrix} R & 0 & t \\ 0 & 1 & 0 \\ 0 & 0 & 1 \end{pmatrix}.$$

Similarly, we can embed the other groups into SE(3) to obtain doubly periodic surfaces with the additional requirement that rotations map edges to edges.

Rotation Edges If we are in the case that a point fixed under the action of G lies on an edge it follows that there exists a 180-degree rotation in G around this point. Since rotating a triangle T with points in $\mathbb{R}^3$ in this way does not necessarily map edges to edges as long as both points of the rotation do not share the same third coordinate, we need to extend the corresponding group element in a way different to the one above.

One idea is to rotate along the corresponding point in T in the plane containing T. A question that naturally arise in these cases is: What does this do to the projection?

Lemma 4.4.2. *Let T be a triangle in $\mathbb{R}^3$ and $p \in \mathbb{R}^3$ a midpoint of one of the edges of T. Then we can compute the rotation of T by 180 degrees around p in the plane given by T and project it on P_0. It follows that the projection is the rotated projection of T along the projected point p.*

Proof. Let $R \in \mathbb{R}^{3\times 3}$ a rotation matrix and $t \in \mathbb{R}^3$ such that $R(T) + t$ is a triangle in the plane. Then the rotation around p by 180 degrees can be written as

$$R^{-1}R_{180}R(T-p) + p = -(T-p) + p = -T + 2p,$$

where R_{180} is just the scalar matrix $-\mathbb{I}$. We can assume that T is defined by points A, B, C and $p = \frac{A+B}{2}$. Then it follows that the triangle rotated around the point p by 180 degrees has the points

$$-(A-p)+p = B, -(B-p)+p = A, -(C-p)+p = -C + A + B.$$

When projected onto $\{(x, y, 0) \mid x, y \in \mathbb{R}\}$ this triangle is exactly the rotation of the projection $\pi(T)$ around the points $\pi(p)$ by 180 degrees. □

Other type of rotations as present in the groups of type p4, p6 can be extended to elements of E(3) in the same way as we have extended mirror symmetries. However, in

this case, we need to put the additional restriction on T that edges are again mapped onto each after repeatedly acting with the rotation. It follows that T has to be an isosceles triangle.

Hence, we can put the extensions above together to embed G into E(3) given a triangle T.

Proposition 4.4.3. *Let G be a planar crystallographic group with fundamental domain F in the shape of a triangle. If T is a triangle in $\mathbb{R}^3$ that projects onto F, we can extend the action of G onto $\mathbb{R}^3$ such that we obtain a doubly periodic surface when acting on T.*

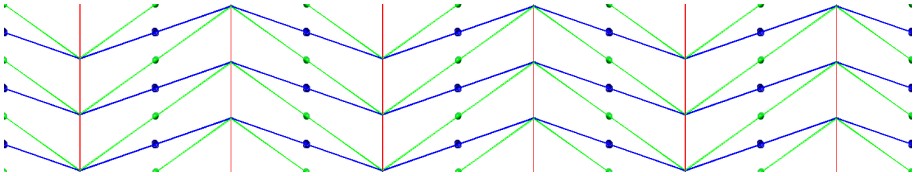

Figure 4.3: Fundamental domain for wallpaper group of type p2mg. The red edge is a mirror edge and the blue and green edges are rotation edges.

In the following example, we illustrate that we can obtain the famous Miura-Ori pattern, named after its inventor Koryo Miura [Miu85], using our presented methods.

Example 4.4.4 (Miura-Ori)**.** We consider the planar crystallographic group G of type p2mg which has a triangular fundamental domain with one mirror edge and two rotation edges. A group presentation is given by

$$\langle a, b, c \mid a^2, b^2, c^2, abcacb \rangle,$$

see [NPR24; IUC02]. We use the following action: a mirrors, b rotates around the point of its middle edge as in Lemma 4.4.2 and c rotates 180 degrees (also see Figure 4.3). Then we can find a triangle such that the projection yields a fundamental domain for G and the edge corresponding to c is parallel to the projection plane. The resulting pattern yields an example of a *Miura-Ori* pattern and is foldable. In fact, all *Miura-Ori* patterns can be obtained in this way.

4.5 Generalisations and Outlook

There are two immediate ways of generalising the construction given in the previous section:

1. Use more than one triangle.

2. Extend the group action in order to obtain a larger structure.

The first option can be used to construct so-called self-intersecting surfaces by choosing self-intersecting triangles with the same projection. In the following chapter, we see that we can obtain a retriangulation such that we no longer have self-intersecting faces, i.e. faces only intersect at common edges or vertices. The second option can be linked to the so-called layer groups (see [KL02]) which are doubly periodic subgroups of three-dimensional crystallographic space groups. There are exactly 80 layer groups, and those of interest arise exactly as group extensions of the wallpaper groups considered in the previous section. In Figure 4.4, we see how to generalise the construction given in Figure 4.2.

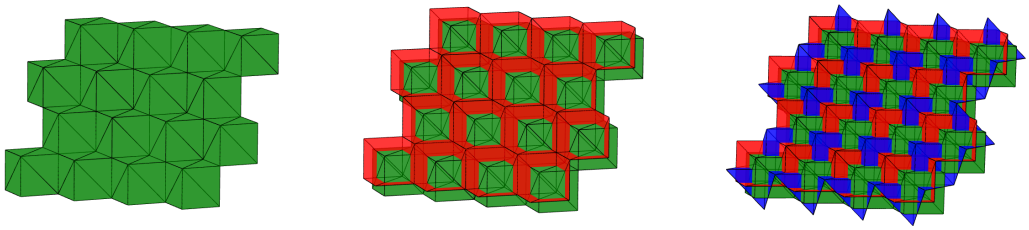

(a) (b) (c)

Figure 4.4: Generalising the construction.

Chapter 5

3D Printing of Self-Intersecting Surfaces

5.1 Summary

3D printing of surfaces has become an established method for prototyping and visualisation. However, surfaces often contain certain degenerations, such as self-intersecting faces or non-manifold parts, which pose problems in obtaining a 3D printable file. Therefore, it is necessary to examine these degenerations beforehand.
Surfaces in three-dimensional space can be represented as embedded simplicial complexes describing a triangulation of the surface. We use this combinatorial description, and the notion of embedded simplicial surfaces (which can be understood as well-behaved surfaces) to give a framework for obtaining 3D printable files. This provides a new perspective on self-intersecting triangulated surfaces in three-dimensional space. Our method first retriangulates a surface using a minimal number of triangles, then computes its outer hull, and finally treats non-manifold parts. To this end, we prove an initialisation criterion for the computation of the outer hull. We also show how symmetry properties can be used to simplify computations. Implementations of the proposed algorithms are given in the computer algebra system GAP4. To verify our methods, we use a dataset of self-intersecting symmetric icosahedra. Exploiting the symmetry of the underlying embedded complex leads to a notable speed-up and enhanced numerical robustness when computing a retriangulation, compared to methods that do not take advantage of symmetry.

This chapter is based on research originally published at [AG24a]. We make code available at [AG24b].

5.2 Introduction

Triangulated surfaces in three-dimensional space are an essential tool in 3D printing and in geometric modelling. These surfaces are usually described by their incidence structure, consisting of vertices, edges and faces and coordinates for each vertex. For applications like 3D printing, certain regularity properties are often assumed, such as the absence of *self-intersecting faces* or *non-manifold parts*, as these lead to artefacts in the printed models. These degenerations frequently appear in surfaces, and it is thus necessary to treat them before obtaining a 3D printable file. In this context, non-manifold parts are either *non-manifold edges* that are incident to more than two faces or *non-manifold vertices*, where the incident faces cannot be ordered in a connected face-edge path. Non-manifold edges in particular cause parts to be disconnected when printing. For instance, when identifying two cubes at an edge, we obtain a surface with a non-manifold edge as shown in Figure 5.1a. Common *slicer software* that prepares a file for 3D printing often neglects these edges, leading to 3D printed cubes that no longer share a common edge. Self-intersecting faces yield another problem, as they hinder the computation of the outer-hull, which is necessary to determine a printing path. This is because inner parts of the model are usually disregarded in the printing process. In Figure 5.1b an example of this with two intersecting cubes is shown.

(a) (b)

Figure 5.1: (a) Identifying two cubes at an edge leads to a non-manifold edge. In 3D printing applications, this edge is often neglected, leading to two separated cubes. (b) Two intersecting cubes are shown together with a view of its interior. The interior part can be omitted by reduction to the outer-hull.

In order to obtain 3D printable files that can be realised as models depicting the key features of the original surface, it is necessary to address the aforementioned problems. In Figure 5.2, two modified versions of these cubes are shown that are geometrically as close as possible (for instance using the *Hausdorff distance*) such that 3D printed copies do not display artefacts. Additionally, the underlying surface is well-behaved in the context above, i.e. does not possess self-intersections or non-manifold parts.

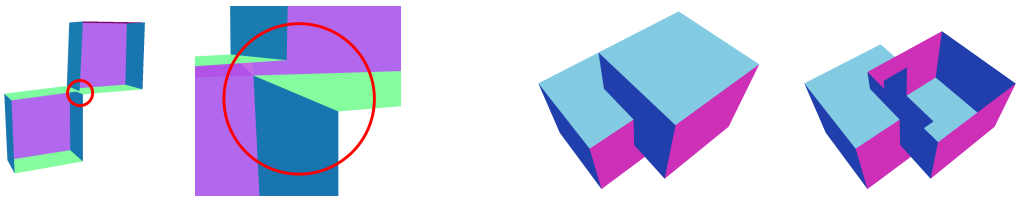

(a) (b)

Figure 5.2: (a) We can modify the two cubes in Figure 5.1a by operations replacing the part containing the non-manifold edge. When 3D printing the adapted surface, the two cubes are connected. (b) For 3D printing applications, only the outer-hull is printed. Thus, we obtain a modified surface by neglecting inner parts.

In this chapter, we address these challenges by introducing a framework that modifies surfaces to obtain 3D printable files. To this end, we first introduce the notion of *(embedded) simplicial surfaces* in Section 5.3, which are triangulated surfaces without non-manifold parts. This notion is based on the work presented in [Bra+17; NPR24]. Next, we describe our method, which starts with a triangulated surface, containing self-intersections or non-manifold parts and yields an embedded simplicial surface. Here, we focus on methods allowing the exploitation of symmetries of the model, leading to a robust way of detecting and rectifying self-intersections, see Section 5.6. The guiding examples we consider in this work are the 35 symmetric icosahedra of edge length 1 classified in [Bra+20].

Our approach proceeds as follows:

1. Compute all self-intersections of the model in Section 5.4.
2. Retriangulate the original faces such that the resulting complex has no self-intersections in Section 5.5.
3. Compute the outer hull, chambers and correctly (outward) oriented normals of the retriangulated complex in Section 5.7.
4. Remedy non-manifold parts in Section 5.8.

Note that the order in which these steps are performed is essential for our approach: for the outer hull, all self-intersections have to be removed, and for tackling non-manifold parts, one needs to reduce to the outer hull with outward oriented normals. More details on this can be found in the respective sections. In the following, we highlight steps 1.-3. with the great icosahedron. In this case, step 4 is not necessary, as no non-manifold parts are present.

The implementation of our methods in GAP4 [GAP] are available in our GAP4 package [AG24b].

The Great Icosahedron A prominent example of a self-intersecting polyhedron is the great icosahedron, shown in Figure 5.3. The great icosahedron is a non-convex regular polyhedron with icosahedral symmetry and part of the Kepler-Poinsot polyhedra, see [Cox+82]. Like the regular icosahedron, a Platonic solid, it has 20 faces, 30 edges and 12 vertices and thus Euler characteristic 2. Moreover, it is invariant under the full icosahedral group of order 120. However, it has many self-intersections: each of the 20 faces intersects with 15 faces non-trivially. For processing this surface for applications like 3D printing or meshing, it is natural to ask how the symmetry of the given surface can be exploited to simplify our preprocessing. Specifically, we can investigate how symmetry simplifies the computation of the outer hull or that of a retriangulation. For the computation of a new triangulation that corresponds to the embedding of the great icosahedron in $\mathbb{R}^3$, we can proceed as follows: we note that each face can be mapped to any other face by at least one of the 120 symmetries, i.e. the symmetry group acts transitively on the faces. It follows that it suffices to first retriangulate one face, and in a second step transfer this retriangulation to the entire surface. Similarly, we can use the symmetry group when computing self-intersections of face pairs. Without the use of symmetry, one would need to consider all $\binom{20}{2} = 190$ face pairs when searching for self-intersections. In the case of the great icosahedron, symmetry group acting on pairs of faces has 5 orbits, meaning it suffices to consider 5 face pairs instead of all 190 to compute all self-intersections. Using an algorithm that guarantees to consider a minimal number of triangles, see Section 5.5, we retriangulate one triangle, and transfer this triangulation to all other triangles. This is shown in Figure 5.4. Next, we can compute the outer hull to obtain a surface with 180 faces, 92 vertices and 270 edges with icosahedral symmetry.

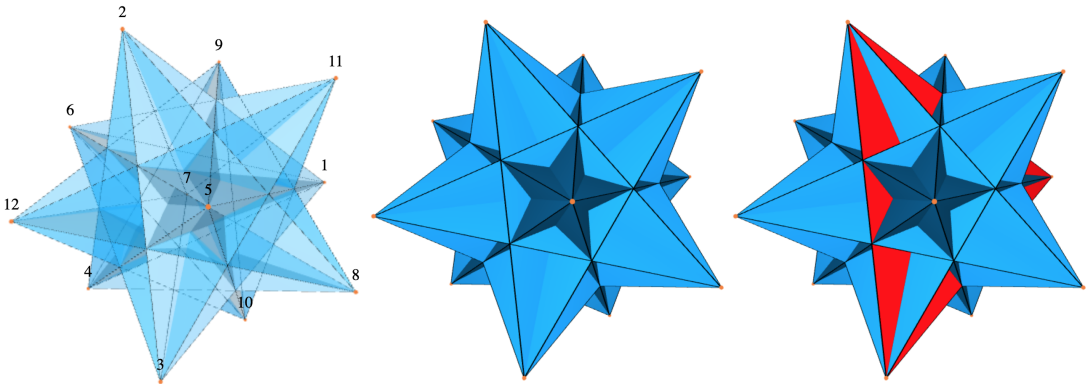

(a) (b) (c)

Figure 5.3: (a) The great icosahedron has 12 embedded vertices, 30 edges and 20 faces, and the same incidence structure as the regular icosahedron (a Platonic solid). (b,c) Each of the 20 faces intersects with 15 faces non-trivially, and we can compute the intersections of all face pairs by only considering one face (face in red) and in a next step use the symmetry group to compute the remaining intersections.

To be more specific, we can choose the coordinates of the vertices of the great

icosahedron in such a way that all edge lengths are of unit length:

$$\overset{v_1}{\left(0, \frac{1}{2\varphi}, \frac{1}{2}\right)}, \overset{v_2}{\left(0, \frac{1}{2\varphi}, -\frac{1}{2}\right)}, \overset{v_3}{\left(-\frac{1}{2\varphi}, -\frac{1}{2}, 0\right)}, \overset{v_4}{\left(\frac{1}{2\varphi}, -\frac{1}{2}, 0\right)}, \overset{v_5}{\left(-\frac{1}{2}, 0, -\frac{1}{2\varphi}\right)}, \overset{v_6}{\left(\frac{1}{2}, 0, -\frac{1}{2\varphi}\right)},$$
$$\overset{v_7}{\left(\frac{1}{2}, 0, \frac{1}{2\varphi}\right)}, \overset{v_8}{\left(-\frac{1}{2}, 0, \frac{1}{2\varphi}\right)}, \overset{v_9}{\left(\frac{1}{2\varphi}, \frac{1}{2}, 0\right)}, \overset{v_{10}}{\left(0, -\frac{1}{2\varphi}, \frac{1}{2}\right)}, \overset{v_{11}}{\left(-\frac{1}{2\varphi}, \frac{1}{2}, 0\right)}, \overset{v_{12}}{\left(0, -\frac{1}{2\varphi}, -\frac{1}{2}\right)},$$

where $\varphi = \frac{1+\sqrt{5}}{2}$ is the *golden ratio*. The vertices of the faces are then given by the following list:

$$[v_1, v_2, v_3], [v_1, v_2, v_4], [v_1, v_4, v_5], [v_1, v_5, v_6], [v_1, v_3, v_6], [v_2, v_3, v_7],$$
$$[v_2, v_4, v_8], [v_4, v_5, v_9], [v_5, v_6, v_{10}], [v_3, v_6, v_{11}], [v_2, v_7, v_8], [v_4, v_8, v_9],$$
$$[v_5, v_9, v_{10}], [v_6, v_{10}, v_{11}], [v_3, v_7, v_{11}], [v_7, v_8, v_{12}], [v_8, v_9, v_{12}], [v_9, v_{10}, v_{12}],$$
$$[v_{10}, v_{11}, v_{12}], [v_7, v_{11}, v_{12}].$$

For 3D printing purposes and other applications, it is essential to disregard inner parts of a model by computing the outer-hull. In order to tackle this algorithmically, we first identify all intersecting face pairs and disregard their parts that lie in the interior. In Figure 5.4, we see the steps that are performed to compute the intersection of the face marked in red in Figure 5.3.

We observe that the symmetry group of the great icosahedron is isomorphic to the full icosahedral group which itself is isomorphic to $C_2 \times A_5$ (a direct product of the cyclic group of order 2 with the alternating group of order 5) and can be generated by the following three reflection matrices

$$\begin{pmatrix} -1 & 0 & 0 \\ 0 & 1 & 0 \\ 0 & 0 & 1 \end{pmatrix}, \begin{pmatrix} \frac{\varphi}{2} & -0.5 & \frac{1}{2\varphi} \\ -0.5 & -\frac{1}{2\varphi} & \frac{\varphi}{2} \\ \frac{1}{2\varphi} & \frac{\varphi}{2} & 0.5 \end{pmatrix}, \begin{pmatrix} 1 & 0 & 0 \\ 0 & 1 & 0 \\ 0 & 0 & -1 \end{pmatrix}.$$

As mentioned above, this group acts transitively on the faces. Thus, we can reduce the number of face pair intersections that need to be considered, as the stabiliser of a single face is isomorphic to a symmetry group of an equilateral triangle. This implies that we can compute all intersections using only one face, which is shown in Figure 5.4.

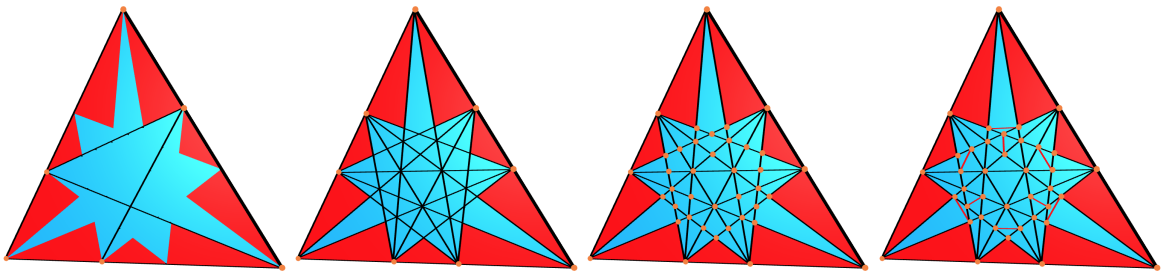

(a) (b) (c) (d)

Figure 5.4: (a) Intersections of one face of the great icosahedron with other faces up to symmetry. (b) The *stellation diagram* of a face of the great icosahedron, showing lines where other face planes intersect with this one [Cox+82], can be obtained from (a) by rotations and reflections. (c) Computing all intersection points of intersection within the face. (d) Triangulating non-triangle parts, yielding a *simplicial disc*. This retriangulation can be carried over to all 20 faces of the great icosahedron using its symmetry group in order to obtain a surface without self-intersections.

For understanding the internal structure, we have to find the *chambers* of the great icosahedron given by the connected components of the following set

$$\mathbb{R}^3 \setminus \bigcup_{f \in F} \operatorname{conv}(f),$$

where $\operatorname{conv}(f)$ is the *convex hull* of the vertices defining f, see Definition 5.3.5. In Figure 5.5, we show an *exploded view* of the 413 internal chambers of the great icosahedron obtained using the retriangulation as described above. Each chamber is shifted away from the centre with the same magnitude: let $p \in \mathbb{R}^3$ be the centre of the great icosahedron and for a given chamber C with centre $c \in \mathbb{R}^3$, we shift the chamber C using the translation $m \cdot (c - p)$ with magnitude $m \in \mathbb{R}_{>0}$.

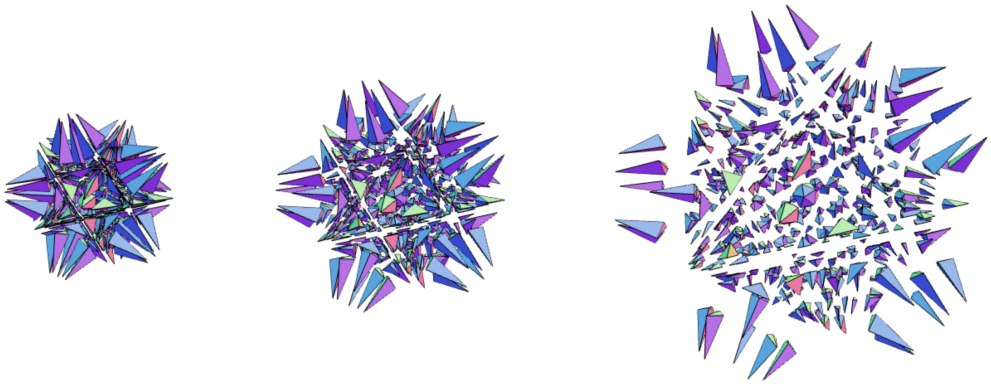

(a) $m = 1$ (b) $m = 2$ (c) $m = 4$

Figure 5.5: Exploded views of the 413 internal chambers of the great icosahedron with different magnitudes m.

The centre chamber of the great icosahedron with edge lengths 1 is given by the regular icosahedron with faces corresponding to the central equilateral triangle of the

stellation diagram in Figure 5.4 with edge lengths

$$\left(\frac{2}{7+3\sqrt{5}}\right) \approx 0.145898.$$

In fact, all but one (final stellation) of the 59 icosahedra presented in [Cox+82] can be obtained by taking a subset of the chambers that is invariant under the icosahedral group.

In this work, we mainly focus on another class of icosahedra, classified in [Bra+20], which contain all icosahedra that are combinatorially equivalent to the regular icosahedron, carry a non-trivial symmetry and have edge length 1. There are exactly 35 such icosahedra, of which 33 possess self-intersections, and the regular icosahedron and the great icosahedron are also among them.

Related Work Self-intersections and non-manifold parts of models are very active fields of research. This is because of the obstructions they cause in many fields, such as meshing, scanning of 3D models, and 3D printing [Att18; Chu+19; WLG03; ZHY19]. In [Att18], an algorithm, along with an initialization criterion, to compute the outer hull of a complex is presented. In [ZHY19], a robust method is described to rectify self-intersections of a complex using a subdivision based on Delaunay triangulation with certain constraints to retriangulate the initial complex.
Focusing on self-intersections in triangulated complexes, there are several approaches for finding all self-intersections or testing whether two given triangles intersect, for instance [MG22; Möl97]. Also, see [Ska23] for a recent review on algorithms for the detection of self-intersections. Repairing and retriangulation methods can be found in [Att14] for a direct approach, which is also suitable for the computation of outer hulls, [LB18] for a method using immersion techniques and [YS09] for a method employing edge swap techniques. In [CK10], a method is presented to change the topology of a polygonal mesh that combines an adaptive octree with nested binary space partitions (BSP), i.e. subdivisions of a Euclidean space into convex sets using hyperplanes as partitions. Alternative methods on remedying non-manifold parts can be found in [DPH09; RC99; WLG03]. Another similar direction is the treatment of meshes and their repair, as done in [Chu+19]. As an input to our model, we use the symmetries of a given complex, which leads to simplification and speed up the algorithms. Of course, this is an idea that can be applied to different settings, such as in model segmentation in [GF09]. In conjunction with the ideas we present, one can consider detection of symmetries in surfaces, as in [BBS23; Li+16].

5.3 Embedded Simplicial Surfaces

In this section, we introduce the main terminology used in this work with a focus on *embedded simplicial surfaces*, which yield well-behaved triangulations in the context of meshing and 3D printing applications. We start by giving a definition of a version of simplicial complexes adapted to a triangular surface, motivated by the combinatorial theory of simplicial surfaces, see [Bau20; NPR24]. In the literature, an (abstract) simplicial complex X is commonly defined as a subset $X \subset \mathcal{P}(V) = \{\emptyset \neq A \subset V\}$ where V is a set, and we have that for all $t \in X$ and for all $\emptyset \neq x \subset t$ it follows that $x \in X$. In the context of this chapter, we restrict ourselves to the case where the maximal elements of X are sets of size 3 and the elements of X fulfil further conditions which are natural in the context of triangulations.

Definition 5.3.1 (Simplicial Complex)**.** Let V be a finite set. A (closed) *simplicial complex* X with vertices V is a subset of $\mathcal{P}_3(V) = \{A \subset V : |A| \leq 3\}$ such that the following conditions hold.

(i) For all $v \in V$, $\{v\} \in X$. Additionally, $\emptyset \notin X$.

(ii) For all $t \in X$ and $\emptyset \neq x \subset t$, it follows that $x \in X$.

(iii) For each $t \in X$ with $|t| < 3$, there exists $t' \in X$ with $t \subset t'$ and $|t'| > |t|$.

(iv) For each $f \in X$ with $|f| = 3$ and any $v_1, v_2 \in f$, we can find $f' \neq f$ such that $v_1, v_2 \in f'$.

We call the three-element sets in X the *faces* or *triangles*, the two-element sets in X the *edges* and the one-element sets in X the *vertices*. The faces, edges and vertices are denoted by X_2, X_1 and X_0, respectively. We also say a vertex $v \in X$ is incident to an edge $e \in X$ if $v \subset e$, and an edge $e \in X$ is incident to a face $f \in X$ if $e \subset f$. Additionally, a vertex $v \in X$ is incident to a face $f \in X$ if $v \subset f$. Since we do not consider complexes other than simplicial ones, we sometimes omit the word simplicial in the following.

The conditions in the definition above all correlate to natural assumptions for a simplicial complex consisting of triangles. For example, since we consider $\mathcal{P}_3(V)$, the faces are triangles. The conditions (i)-(iv) in the definition above are interpreted as follows:

(i) ensures that the vertex set, on which a complex is built, is part of the complex.

(ii) implies that if we take a face or edge, its parts are also included in the description of the complex.

(iii) enforces that each vertex is part of an edge and each edge is part of a face.

(iv) forces the surface to be closed, thus every edge has to be incident to at least two faces.

In summary, we observe that a simplicial complex X is uniquely determined by the incident vertices of its faces.

We give the following definition of faces associated to a given vertex.

Definition 5.3.2. Let X be a simplicial complex and take a vertex v of X. Define the faces incident to v to be the set $X_2(v) \coloneqq \{f \in X : v \in f \text{ and } |f| = 3\}$.

A more regular object is a (closed) vertex-faithful simplicial surface, see Definition 1.2.1, which enforces further properties compared to a simplicial complex, which corresponds to the absence of non-manifold parts. For example, the condition that each edge is incident to exactly two faces directly corresponds to no *non-manifold edges* being present in a given complex. Moreover, vertices in a simplicial complex that do not fulfil the *umbrella condition* are called *non-manifold vertices* (see also Section 5.8 for this).

In Figure 5.6, we see several distinct embeddings of the same underlying simplicial surface.

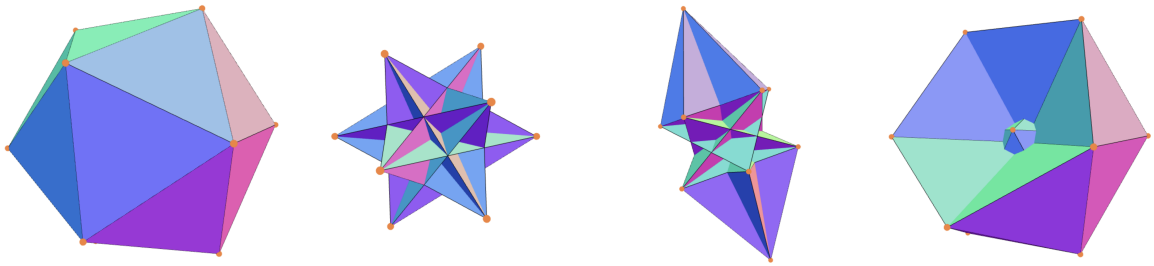

(a) (b) (c) (d)

Figure 5.6: One simplicial surface (icosahedron) with distinct embeddings of unit edge length [Bra+20]: (a) platonic solid, (b) the great icosahedron, (c) icosahedron$_{3,1}$, (d) icosahedron$_{3,2}$ (notation given in [Bra+]).

Remark 5.3.3. The map ϕ in Definition 1.2.7 can be represented as a list with $|V|$ entries in $\mathbb{R}^3$, or alternatively as a matrix in $\mathbb{R}^{|V|\times 3}$. Thus, one can switch from the combinatorial structure of an embedded simplicial complex to one used in application, such as a coordinate representation or an STL file. Here, it suffices to store the embedding data suitably, for example, via a list of lists.

An orientation of a simplicial surface, see Definition 1.2.6, can be used to associate a normal vector to each face of an orientable surface.

Remark 5.3.4. If an embedded surface is orientable, we can define the outer normals for each face as follows: Let $f = \{v_1, v_2, v_3\}$ such that the vertices are ordered as (v_1, v_2, v_3), then the outer normal is given by the right-hand rule

$$(v_2 - v_1) \times (v_3 - v_1).$$

Note that if the outer hull of our surface is given as the boundary of an open set, it is well-known to be orientable (one can use the outer normals). In applications such as 3D printing, this is to be expected after removing artefacts.

As an alternative to the combinatorial approach of defining an orientation and related outer normals for an embedding, we give a geometric definition of chambers and the outer hull for an embedded complex as follows.

Definition 5.3.5 (Chambers and outer hull)**.** The *chambers* of an embedded complex X are defined as the connected components of

$$\mathbb{R}^3 \setminus \bigcup_{f \in X_2} \operatorname{conv}(f),$$

where $\operatorname{conv}(f)$ is the convex hull given by the vertices of f, i.e.

$$\operatorname{conv}(f) = \{\lambda_1 \cdot v_1 + \lambda_2 \cdot v_2 + \lambda_3 \cdot v_2 \mid 0 \leq \lambda_1, \lambda_2, \lambda_3 \leq 1, \sum_{i=1}^{3} \lambda_i = 1, f = \{v_1, v_2, v_3\}\}.$$

The *outer hull* X_{out} is defined as the boundary of the unique chamber with infinite volume. The other chambers of X are called the *finite* chambers.

Note that since we require an embedded complex X to be finite, the outer hull in Definition 5.3.5 exists and is non-empty.

With this in mind, we can also define when a point is contained inside the embedded complex.

Definition 5.3.6. Let X be an embedded simplicial complex. We say that a point $p \in \mathbb{R}^3$ is *contained* in X if $p \in C$ for a finite chamber C of X or $p \in \operatorname{conv}(f)$ for a face $f \in X$. More generally, we say that for two elements in the embedded complex $x, y \in X$ that x is contained in y if $\operatorname{conv}(x) \subset \operatorname{conv}(y)$. This naturally extends to points $p \in \mathbb{R}^3$: p is contained in an element $x \in X$ if $p \in \operatorname{conv}(x)$.

Below, we define *intersection points*, which parameterise the intersection of two faces of an embedded complex.

Definition 5.3.7 (Intersection points)**.** Let (X, ϕ) be an embedded simplicial complex. We say that X is a *self-intersecting complex* or has *self-intersections* if there exist two faces $f_1 \neq f_2$ and a point $p \in \mathbb{R}^3$ such that

$$p \in \operatorname{conv}(\phi(f_1)) \cap \operatorname{conv}(\phi(f_2)) \setminus \operatorname{conv}(\phi(f_1) \cap \phi(f_2)),$$

i.e. p is not a common vertex of f_1 and f_2, does not lie on a common edge and lies inside both faces. Since the intersection of convex sets is again convex, we have that $\operatorname{conv}(\phi(f_1)) \cap \operatorname{conv}(\phi(f_2))$ can be written as the convex hull of finitely many points, called *intersections points*, contained in the edges of f_1 and f_2. We write $I(X, \phi)$ for the collection of all intersection points and $I(X, \phi, f) := I(X, \phi) \cap \operatorname{conv}(\phi(f))$ for the

collection of all intersection points of a fixed face f. If the set of intersection points $I(X, \phi)$ is empty, we call the embedded complex *intersection-free*, else we say that it has *self-intersections*.

For computation of self-intersections of a complex, one can consider all possible face-pairs and check if they intersect. One way to determine whether two faces have an intersection is to check if any of the edges of one of the faces intersects with the other face, and vice versa. By examining the computed intersection points, as seen in Section 5.4, we determine if an intersection is present or not.

Definition 5.3.8. Let X, X' be two embedded complexes. We say that X, X' are *geometrically equivalent* if they give rise to the same chambers and in this case we call X' a *retriangulation* of X. We say that X' *rectifies* X if both embedded complexes are geometrically equivalent and X' has no self-intersections.

In Section 5.7, we show that we can compute the outer-hull of a complex X without self-intersections. Then together with the embedding, the normal vectors are sufficient to create a 3D model of the simplicial complex, as seen in [SM03]. But if an embedding has a self-intersection, the following needs to be considered.

Remark 5.3.9. The outer hull of an embedded complex X is well-defined, even in the case that the embedding has self-intersections. However, then our description of X via coordinates of vertices is not sufficient to compute the outer hull, as can be seen in Figure 5.7.This is because faces can lie in multiple chambers simultaneously, making it impossible to use normals to infer information about the outer hull. In this example, computing the outer hull using normal vectors, as described in Remark 5.3.4, is not possible.

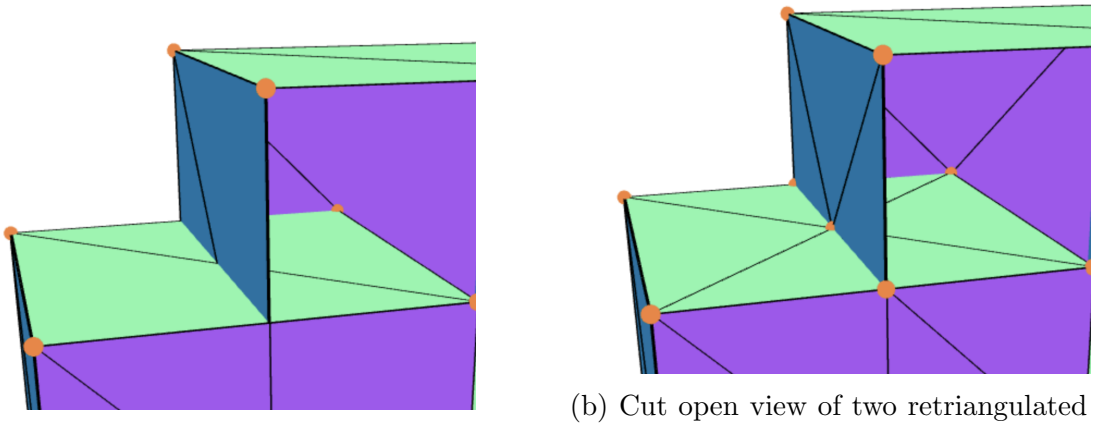

(a) Cut open view of two intersecting cubes.

(b) Cut open view of two retriangulated intersecting cubes.

Figure 5.7: Intersection of triangles in two intersecting cubes. In (b), each face can be associated to exactly two chambers.

5.4 Detecting Self-Intersections

In order to retriangulate a complex with self-intersections, we first need to detect its intersection points (Definition 5.3.7). One objective of our framework lies in using a robust way for detecting self-intersections. For this, we employ a well-known method to check if two triangles intersect. It is sufficient to consider only two triangles at a time, and compare all such face-pairs one after another. Here, efficiency can also be gained using a-priori criteria to omit face-pairs that cannot intersect (for example based on vertex coordinates).
As our methods are modular, one could also use state of the art intersection detection algorithms such as PANG2 (see [MG22]) instead. Below, we present a numerical robust method for detecting self-intersecting triangles.

For this, we assume our initial data is a simplicial complex X with embedding ϕ and consider two faces $f_\ell = \{v_1^\ell, v_2^\ell, v_3^\ell\},\ \ell = 1, 2$ in X. Here, we identify the vertices and edges of X with their images under the embedding ϕ. We determine intersection points by examining the edges of f_1 via the normal equation of the plane $P(f_2)$ spanned by v_1^2, v_2^2 and v_3^2. Afterwards, we check if the found point lies inside the triangle f_2 or not. Finally, after checking for all such intersection points of f_1 and f_2, we can use them to determine if the two triangles intersect.
We first fix our definitions before presenting the method in more detail. There is an alternative characterisation to Definition 5.3.6 (containment in edges and faces) for points, which is more numerically robust. For this, we use the standard Euclidean dot product $\langle \cdot, \cdot \rangle$.

Proposition 5.4.1. *Let f be a triangle with vertices $v_1, v_2, v_3 \in \mathbb{R}^3$ and normal vector n_f, and consider the planes*

$$P_1 := \operatorname{span}(n_f, v_1 - v_2), P_2 := \operatorname{span}(n_f, v_2 - v_3), P_3 := \operatorname{span}(n_f, v_3 - v_1).$$

A point p lies inside f if and only if p lies on the same plane as f and satisfies the following condition:

$$\langle p - v_i, \tilde{n}_i \rangle \geq 0, \quad \text{for } i \in \{1, 2, 3\}, \tag{5.1}$$

where $\tilde{n}_i$ is a normal vector of the plane P_i, pointing towards the interior of f.

This is visualised for the planar case in Figure 5.8. In the sense of Inequality (5.1), p_1 has non-negative scalar product with all normal vectors, while p_2 has negative scalar product with $\tilde{n}_2$.

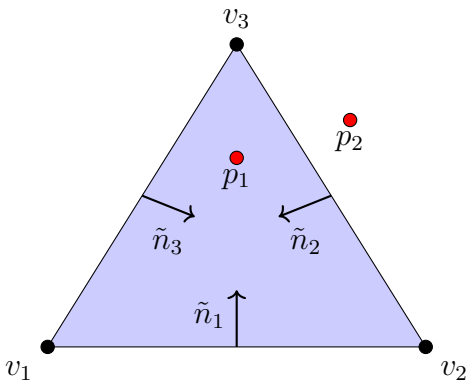

Figure 5.8: Triangle f with vertices v_1, v_2, v_3, normals $\tilde{n}_i$ pointing inwards and point p_1 inside f and point p_2 outside f.

Remark 5.4.2. Let P be a plane with normal vector n and let x be a point in P. Proposition 5.4.1 is based on the observation that if a point p fulfils $\langle p-x, n\rangle \geq 0$, then p lies above the plane (where the above direction is the one given by the orientation of the normal vector).

Another important consideration are numerical errors.

Remark 5.4.3. Consider the equation determining whether a point p lies in a plane P, with normal n and a fixed $x \in P$:

$$p \in P \iff \langle p - x, n\rangle = 0. \tag{5.2}$$

Since numerical computations are not always precise, a point p that does lie in P will only yield $\langle p - x, n\rangle \approx 0$. Thus, for implementation purposes, one actually needs to check whether $\langle p - x, n\rangle \in [-\varepsilon, \varepsilon]$ for a small constant $\varepsilon > 0$. We apply this to all the conditions mentioned in this section, as can be seen in the code in our package.

In the following, we give a detailed description of our method, in the setting as described above. First, we examine the edges of f_1. For an edge $\{v_i^1, v_j^1\} = e \subset f_1$, we have to distinguish the following two cases:

(i) e is not parallel to f_2.

(ii) e is parallel to f_2.

Case (i) holds if and only if $\langle v_j^1 - v_i^1, n_2\rangle \neq 0$, where n_2 is a unit normal vector of the face f_2.

First, assume case (i). If n_2 is a normal vector of the plane $P(f_2)$, containment of a point p in the plane $P(f_2)$ can be described as in Equation (5.2). Letting ℓ_{ij} denote the line connecting v_i^1 and v_j^1, parameterised by $\ell_{ij}(\alpha) := \alpha v_j^1 + (1-\alpha)v_i^1$, we thus get

$$\ell_{ij}(\alpha) \in P(f_2) \iff \alpha = \frac{\langle v_1^2 - v_i^1, n_2\rangle}{\langle v_j^1 - v_i^1, n_2\rangle}. \tag{5.3}$$

Equivalence (5.3) yields a criterion for deciding whether a point $\ell_{ij}(\alpha)$ on the line ℓ_{ij} lies in the plane $P(f_2)$. As we have assumed case (i), there exists α such that $\ell_{ij}(\alpha) \in P(f_2)$. This point $\ell_{ij}(\alpha)$ is part of f_1 if $\alpha \in [0, 1]$. In case this holds, we also need to check if it is contained in the interior of the triangle f_2. For this, we use the geometric condition described in Proposition 5.4.1.

For case (ii), when the edge is contained in the plane $P(f_2)$, the problem reduces to a two-dimensional one and the following subcases need to be differentiated:

(i) The edge is contained in a different but parallel plane as the triangle

(ii) The edge is contained in the same plane as the triangle and one of the following holds

  (a) does not intersect the triangle,

  (b) intersects the triangle,

  (c) lies inside the triangle.

For a theoretical treatment of these subcases, we refer to [Vin05], and for an implementation to our provided package [AG24b].

By using the methods described above, we compute all intersection points I_2 of edges of f_1 with f_2. We also need the reverse: the intersection points I_1 of edges of f_2 with f_1, as seen in Figure 5.9a.
We also have to consider duplicates. Thus, we examine $I := I_1 \cup I_2$, as comparison of I with the vertices of f_1 and f_2 and its cardinality $c := |I|$ determines if the faces intersect.

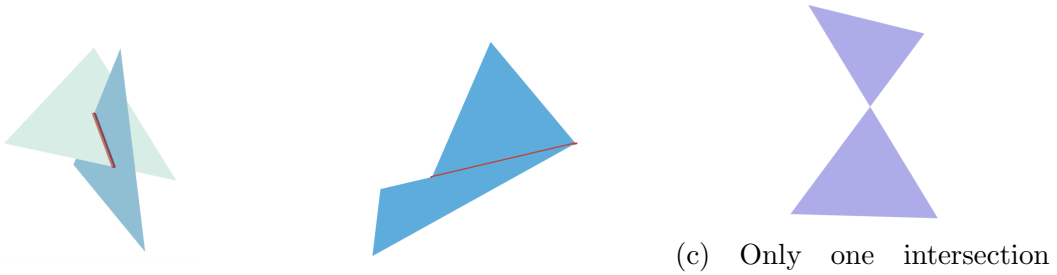

(a) Two intersection points (b) Two intersection points (c) Only one intersection point

Figure 5.9: Intersection of triangles (a, b) vs no intersection (c).

An intersection is present if for instance $c = 2$ and $(I \setminus (f_1 \cup f_2)) \neq \emptyset$, as can be seen in Figures 5.9a and 5.9b. The comparison with the original vertices of f_1 and f_2 is needed since adjacent triangles, compared along their joint edge, would also result in $c = 2$. Thus, the intersection is parameterised by v_1, v_2 with $I_1 \cup I_2 = \{v_1, v_2\}$.
If $c = 1$, and the intersection point is equal to a vertex of only one of the faces (or equal to none), there is also an intersection. We then parameterise it by v, where $I = \{v\}$.

After identifying all intersection points as listed above, we show in the following section how to retriangulate a face f based on its intersection points.

5.5 Retriangulation of Self-Intersecting Complexes

In this section, we introduce an algorithm that yields a retriangulation X' of an embedded complex X such that both complexes are geometrically equivalent and X' has no self-intersections. The key idea is to give the retriangulation of each face a disc structure, with vertices and edges determined by the intersection points with other faces.

In Figure 5.10, we showcase how our method retriangulates a face $f \in X$ with self-intersections.

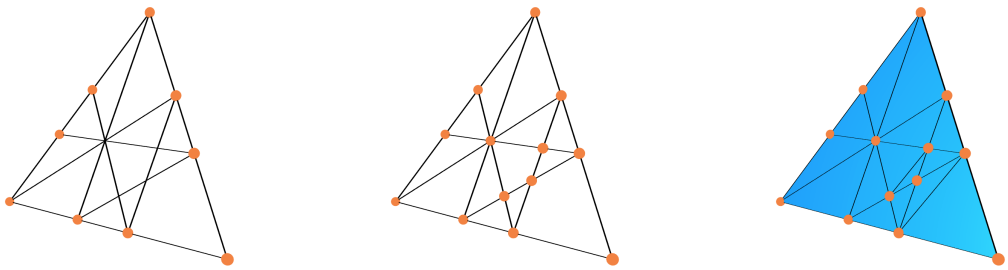

(a) (b) (c)

Figure 5.10: The steps of triangulating a face: (a) all intersections with other faces given as line segments, (b) finding intersection points within the line segments of the underlying face, (c) a simplicial disc giving a retriangulation of the original face.

Remark 5.5.1. It suffices to retriangulate one face after another to obtain a retriangulation, see Definition 5.3.8. Hence, we restrict to the case of a single face $f \in X$ with intersections given by the set $I(X, \phi, f)$, where (X, ϕ) denotes the underlying embedded complex.

We proceed as follows: first, we check whether two intersections within f with two other triangles f', f'' intersect and introduce new vertices if they do. Then, we retriangulate f to obtain a simplicial disc $\tilde{f}$ that is geometrically equivalent to f, i.e. spans the same area.

Definition 5.5.2. A *simplicial disc* D is a simplicial surface with the following properties:

1. D is connected with a single boundary component;
2. D is orientable.

Lemma 5.5.3. *A simplicial disc is uniquely described by the vertices of edges.*

Proof. This follows from the fact that for three edges e_1, e_2, e_3 that can be arranged in a closed cycle such that (e_1, e_2), (e_2, e_3) and (e_1, e_3) share exactly one vertex, we obtain a unique face f with incident edges given by e_1, e_2, e_3. □

Another characteristic of simplicial discs can be given as follows.

Remark 5.5.4. For any simplicial disc D, there exists a simplicial sphere S such that D can be obtained by cutting the sphere S into two parts along a simple closed vertex-edge cycle.

We can compute the Euler Characteristic of a simplicial disc as follows.

Lemma 5.5.5. *The Euler characteristic of a disc D is given by*

$$V + (E + E') - \frac{E + (E + E')}{3} = 1, \tag{5.4}$$

where V is the number of vertices, E the number of inner edges and E' the number of boundary edges of D.

Proof. Gluing together two identical discs along their boundary leads to a sphere with $2V + V'$ vertices and $2E + E'$ edges, where V' is the number of boundary vertices of the disc D. The number of faces in a closed simplicial sphere equals $2E/3$, and its Euler characteristic is equal to 2. Using that the Euler characteristic of a simplicial sphere equals 2, we obtain the following

$$2V + V' - (2E + E') + \frac{2(2E + E'))}{3} = 2.$$

Since the number of boundary vertices V' of a disc equals the number of boundary edges E', we arrive at the statement above. □

Remark 5.5.6. Lemma 5.5.3 yields that we can represent an embedded disc only by the vertices of edges and the coordinates of the given vertices. Thus, we introduce a data structure $\mathcal{D}$ that contains all self-intersections of f with other faces as a list with two entries:

1. The first entry is a list containing all coordinates of the embedded vertices V of f, and all coordinates of the intersections with other faces.

2. The second entry records the edges in a list that connect two vertices of the first list.

Assuming that we computed all intersections of a given face f with all other faces in the underlying complex, the starting step is to search for edge intersections and containment of vertices in edges inside $\mathcal{D}$. For ease of notation, we define for a set Y the set $Y^{(k)} := \{g : \{1, \dots, k\} \to Y \text{ injective}\}$ as the set of k-tuples with pairwise distinct entries, for $k \in \mathbb{N}$.

In the following algorithm, intersecting lines within the given face f are subdivided if they intersect each other. For this, we assume that we can remove duplicates of edges and vertices within f using a helper function CleanData. The output of the algorithm contains the original face f and subdivisions of all its intersections with other faces.

Algorithm 1: RectifyDiscIntersections

input: Triangle together with intersection points given by
$\mathcal{D}[1] \subset \mathbb{R}^3, \mathcal{D}[2] \subset V^{(2)}$

output: Modified $\mathcal{D}$ without self intersecting line segments

begin
- $\mathcal{D} \leftarrow$ CleanData(l)
- $edges \leftarrow \mathcal{D}[2]$
- $vertices \leftarrow \mathcal{D}[1]$
- **for** $v \in vertices$ **do**
  - **for** $e \in edges$ **do**
    - **if** v is contained in e **then**
      - $edges \leftarrow edges \setminus e \cup \{\{v, e[1]\}, \{v, e[2]\}\}$
      - `/* edge` e `is split via vertex` v `*/`
    - **end**
  - **end**
- **end**
- $\mathcal{D} \leftarrow$ CleanData$(\mathcal{D})$
- $edgepairs \leftarrow edges^{(2)}$
- **for** $edgepair \in edgepairs$ **do**
  - **if** $edgepair[1]$ intersects $edgepair[2]$ in $v \notin \mathcal{D}[1]$ **then**
    - $edges \leftarrow edges \setminus \{edgepair[1], edgepair[2]\}$
    - $edges \leftarrow edges \cup \{\{v, edgepair[2][1]\}, \{v, edgepair[2][2]\}$
    - $edges \leftarrow edges \cup \{\{v, edgepair[1][1]\}, \{v, edgepair[1][2]\}\}$
    - `/* edges` $edgepair[1], edgepair[2]$ `intersect in a vertex` v `*/`
  - **end**
- **end**
- $\mathcal{D} \leftarrow$ CleanData$(\mathcal{D})$
- **return** $\mathcal{D}$

end

The output of RectifyDiscIntersections (Algorithm 1) yields a data structure $\mathcal{D}$ that describes a non-intersecting polygon together with inner parts given as line segments. Next, we want to triangulate this output. For this, it suffices to add non-self intersecting edges until condition (5.4) on the Euler characteristic of a simplicial disc is fulfilled. We add minimal non-intersecting edges until we obtain a triangulation. It follows that the resulting triangulation has a minimal number of vertices, as only necessary vertices are added. This algorithm can also be modified to consider more general polygons instead of triangles.

In order to apply condition (5.4) for giving a termination criterion, we first compute the number of boundary vertices V' of $\mathcal{D}$, which equals the number of boundary edges E', and then use that $E + E' = |\mathcal{D}[2]|, V = |\mathcal{D}[1]|$. Since we only need to add inner

edges, we can compute the number of total internal edges as

$$E = 3V - 2E' - 3.$$

Therefore we only need to add $3 \cdot |\mathcal{D}[1]| - 2E' - 3 - |\mathcal{D}[2]|$ edges. This yields an improvement to the greedy algorithm of adding shortest edges, first proposed in [DG70].

Algorithm 2: DiscTriangulation

```
input: 𝒟 without self intersecting line segments
output: A simplicial disc 𝒟
begin
    possibleedges ← V^(2)
    possibleedges ← SortByLength(possibleedges)
    while V − (E + E′) + (E+(E+E′))/3 ≠ 1 do
        e_1 ← possibleedges[1]
        possibleedges ← possibleedges \ e_1
        foundnewedge ← true
        for e_2 ∈ 𝒟[2] do
            if e_1 intersects e_2 then
                foundnewedge ← false
                /* edges e_1 and e_2 intersect */
                break
            end
        end
        if foundnewedge then
            𝒟 ← 𝒟 ∪ {e_1}
        end
    end
    return 𝒟
end
```

DiscTriangulation (Algorithm 2) gives an approximation of a *minimal weight triangulation*, i.e. summing up all edge lengths of the resulting disc is minimal, see [MR08]. In general, solving this problem proves to be NP-hard [MR08]. Since each polygon without self-intersection in two dimensions can be triangulated without introducing new vertices [Ber+00], DiscTriangulation (Algorithm 2) terminates for arbitrary inputs.

5.6 Symmetric Optimisation for Retriangulation

In this section, we consider all orthogonal transformations that leave a given embedded complex X invariant in order to optimise computing its retriangulation. For this, we

need to define the orthogonal group O(3) that acts on $\mathbb{R}^3$.

Definition 5.6.1. The orthogonal group O(3) defined by rotation and reflection matrices acting on the real-space $\mathbb{R}^3$ consists of 3×3-matrices A with $A^{tr} \cdot A = \mathbb{I}$, i.e. matrices A with inverse given by their transposed matrix.

The standard scalar product of two vectors $x, y \in \mathbb{R}^3$ is invariant under multiplication by an orthogonal matrix A, since we have

$$\langle Ax, Ay \rangle = (Ax)^{tr} (Ay) = x^{tr} A^{tr} Ay = x^{tr} y = \langle x, y \rangle.$$

Note that an embedded complex X is determined by the coordinate vectors of its vertices V, together with the combinatorial information given by subsets of $P_3(V)$. From now on, we identify V with a subset of $\mathbb{R}^3$. The action of an element $\pi \in \mathrm{O}(3)$ viewed as a map $\mathbb{R}^3 \to \mathbb{R}^3$ on an embedded complex X is determined by applying π to the 3D coordinates of each vertex. With this, we can define the symmetry group of X.

Definition 5.6.2. The symmetry group of X is defined as the group $\mathrm{Sym}(X) \leq \mathrm{O}(3)$ of all orthogonal transformations leaving X invariant, i.e.

$$\mathrm{Sym}(X) \coloneqq \{\pi \in \mathrm{O}(3) \mid \pi(X) = X\}.$$

In the context of this chapter, we choose the notion $\mathrm{Sym}(X)$ in order to distinguish the symmetry group of the embedded complex from the automorphism group $\mathrm{Aut}(X)$ of the underlying (combinatorial) complex. The symmetry group $\mathrm{Sym}(X)$, as defined above, is not to be confused with the group of all bijective maps $X \to X$, which is also frequently called the symmetry group of X in the mathematical literature.

The symmetry group $\mathrm{Sym}(X)$ of a simplicial complex X acts on the embedded vertices and this action can be extended to edges and faces in a canonical way, i.e. if e is an edge with embedded vertices $\{v_1, v_2\}$ and f is a face with embedded vertices $\{v_1, v_2, v_3\}$, we can define

$$\pi(e) = \{\pi(v_1), \pi(v_2)\} \text{ and } \pi(f) = \{\pi(v_1), \pi(v_2), \pi(v_3)\},$$

for $\pi \in \mathrm{Sym}(X)$. In this way, the group $\mathrm{Sym}(X)$ induces subgroups of the automorphism group $\mathrm{Aut}(X)$ of the underlying simplicial complex X, i.e. permutation subgroups acting on the vertices, edges and faces. These permutation groups can be used when computing face and face-pair orbits. Switching to a discrete permutation group allows both faster and more precise computations without the use of numerical methods.

Before rectifying the self-intersections, as in Section 5.5, we can determine a *transversal* (also called *face transversal*) of the orbits of $\mathrm{Sym}(X)$ on the set of faces, which is

a minimal set of faces $\{f_1, \ldots, f_n\}$ with

$$\bigcup_{i=1}^{n} \mathrm{Sym}(X)(f_i) = X_2.$$

Thus each face of the complex can be obtained by applying certain symmetries to a face in the much smaller set $\{f_1, \ldots, f_n\}$. For instance, if $\mathrm{Sym}(X)$ acts transitively on X_2, we have $n = 1$.

When computing self-intersection, we have to consider pairs of faces (f_1, f_2). We can extend the action of $\mathrm{Sym}(X)$ on the faces X_2 to the pairs of distinct faces, denoted by $X_2^{(2)}$. Hence, it suffices to consider the orbits defined by this group action instead of considering all face pairs,

$$\mathrm{Sym}(X) \times X_2^2 \to X_2^2,\ \big(\pi, (f_1, f_2)\big) \mapsto (\pi(f_1), \pi(f_2)).$$

Here, the faces f_1 and f_2 are mapped to $\pi(f_1) = f_1'$ and $\pi(f_2) = f_2'$, respectively, by applying an element π in the symmetry group $\mathrm{Sym}(X)$. Now we can observe that the faces f_1, f_2 intersect if and only if the faces f_1', f_2' intersect. Let $I_{f_1,f_2} = f_1 \cap f_2$ denote the intersection of two faces. With the notation above, it follows that

$$\pi(I_{f_1,f_2}) = I_{f_1',f_2'}.$$

This means that it suffices to consider only one element of the orbit

$$\mathrm{Sym}(X)((f_1, f_2)) \coloneqq \{(\pi(f_1), \pi(f_2)) \mid \pi \in \mathrm{Sym}(X)\}$$

to determine all intersections of face pairs in this set.

Combining both observations of the group actions of $\mathrm{Sym}(X)$ on the faces X_2 and face pairs $X_2^{(2)}$, it suffices to consider only face pairs of the form (f_i, f) with $i = 1, \ldots, n$ and f_i being part of the chosen face transversal. In order to obtain all such relevant face pairs, we can compute the orbits of the stabiliser $\mathrm{Stab}_{f_i}(X_2^{(2)})$ of the face f_i on the set of faces X_2.

In summary, the symmetry group of an embedded complex X can be used in two ways to simplify computations for self-intersections:

1. Finding self-intersections: given the self-intersections of a pair $\{f_1, f_2\}$ of faces, the self-intersections of all pairs of faces in the orbit of $\{f_1, f_2\}$ under the symmetry group are also known.

2. Retriangulation: it is only necessary to fix self-intersections and retriangulate one face in each orbit of the symmetry group acting on the faces.

These steps are summarised in SymmetricRetriangulation (Algorithm 3).

Algorithm 3: SymmetricRetriangulation

input: Embedded complex X and $\mathrm{Sym}(X)$
output: Embedded complex X' without self-intersection
begin
  FaceRepresentatives= representatives of orbits of $\mathrm{Sym}(X)$ on the faces X_2
  FacePairRepresentatives= [ ]
  for $f \in$ FaceRepresentatives **do**
    /* Add all face pair representatives containing f */
    FacePairRepresentatives$[f]$ = representatives of orbits of Stab_f acting on face pairs (f, f')
  end
  FaceIntersectionsRepresentatives= [ ]
  for $f \in$ FaceRepresentatives **do**
    for $(f, f') \in$ FacePairRepresentatives$[f]$ **do**
      if HasIntersection$((f, f'))$ **then**
        /* Find all representative face pair intersections */
        Add Intersection$((f, f')$ to the list FaceIntersectionsRepresentatives$[f]$
      end
    end
  end
  /* Transfer all representative face pair intersections */
  FaceIntersections= [ ]
  for $f \in$ FaceRepresentatives **do**
    for $\pi \in \mathrm{Stab}_f$ **do**
      FaceIntersections$[f]$ =Concatenate(FaceIntersections$[f]$, π(FaceIntersectionsRepresentatives$[f]$))
    end
  end
  /* Fix intersections and retriangulate face representatives */
  FaceRetriangulations= []
  for $f \in$ FaceRepresentatives **do**
    FaceRetriangulations$[f]$ =Retriangulate(f)
    /* transfer retriangulation to remaining faces */
    for $f' \in$ Orbit of f under action of $\mathrm{Sym}(X)$ **do**
      $\pi = \pi \in \mathrm{Sym}(X)$ such that $\pi(f) = f'$
      FaceRetriangulations$[f'] = \pi$(FaceRetriangulations$[f]$)
    end
  end
  return FaceRetriangulations
end

The resulting speedup compared to methods that do not exploit the symmetry of the given complex is proportional in both steps to the number of orbits. The number of orbits for a group acting on a given set can be computed using a well-known result attributed to Cauchy, Frobenius and Burnside:

Lemma 5.6.3 (Cauchy-Frobenius-Burnside Lemma)**.** *The number of orbits $|\Omega/G|$ of a finite group G acting on a finite set Ω equals the average amount of fixed points, i.e.*

$$|\Omega/G| = \frac{1}{|G|} \sum_{g \in G} \mathrm{Fix}_g(\Omega),$$

where $\mathrm{Fix}_g(\Omega) = |\{\omega \in \Omega \mid g(\omega) = \omega\}|$ is the number of fixed points of a group element g acting on Ω.

For example, if only the identity element of $\mathrm{Sym}(X)$ fixes elements of the set X, we have exactly $|X|/|\mathrm{Sym}(X)|$-orbits. In terms of SymmetricRetriangulation (Algorithm 3), this would result in a speedup proportional to the order of $\mathrm{Sym}(X)$, i.e. the number of symmetries leaving X invariant.

Another advantage of our approach is that we can preserve the symmetry of the resulting self-intersection complex.

Remark 5.6.4. We can obtain an embedded complex X' without self-intersections and

$$\mathrm{Sym}(X) = \mathrm{Sym}(X'),$$

if we account for the preservation of local symmetries of faces, i.e. if f is a face in X and D_f is the resulting disc obtain by retriangulation f together with its intersection with other faces we need to enforce for $\pi \in \mathrm{Sym}(X)$ with $\pi(f) = f$ that $\pi(D_f) = D_f$. This can be combined with a more general approach describing local symmetry-preserving operations, as given in [BGS17; GCV21].

5.7 Computation of Outer Hull and Chambers

For several purposes, such as 3D printing or surface modelling, it is necessary to compute the outer-hull of a self-intersecting complex X to disregard inner parts. For this, we consider an algorithm introduced in [Att18]. This algorithm relies on an initialisation, for which we provide a proof below, with an outer triangle t (so one that is part of the outer hull of X) with normal n pointing outwards. Here, we also write (t, n) for a pair of a triangle and its normal. Moreover, we show that this algorithm can be also applied to obtain any chambers within the complex.

Lemma 5.7.1. *Let X be a closed simplicial complex with vertices given by V and embedding $\phi : V \to \mathbb{R}^3$ such that (X, ϕ) has no self-intersections. We identify vertices,*

edges and faces with their embedding under ϕ and for $p \in \mathbb{R}^3$, we write $p = (p_x, p_y, p_z)$. Now, let $\tilde{v}$ be the vertex with maximal first-coordinate, i.e.

$$\tilde{v}_x = \max\{v_x \mid v \in V\}$$

(we can assume uniqueness after rotating the complex). Let $\tilde{e} = \{\tilde{v}, v'\}$ be the edge in X incident to $\tilde{v}$ such that

$$\frac{|(\tilde{v} - v')_x|}{\|\tilde{v} - v'\|} = \min\left\{ \frac{|(\tilde{v} - v)_x|}{\|\tilde{v} - v\|} \;\middle|\; \tilde{v} \subset e = \{\tilde{v}, v'\} \right\},$$

compare Figure 5.11 (we can also assume uniqueness here with the same argument as above). Let $\tilde{t}$ be the face incident to $\tilde{e}$ with unit normal $\tilde{n} = (\tilde{n}_1, \tilde{n}_2, \tilde{n}_3)$ such that

$$|\tilde{n}_x| = \max\{|n_x| \mid n \text{ is a unit normal of a face } f \text{ with } \tilde{v} \subset \tilde{e} \subset f\}.$$

If $\tilde{n}_x < 0$, negate $\tilde{n}$. Then $\tilde{t}$ is an outer triangle with normal $\tilde{n}$ pointing outwards.

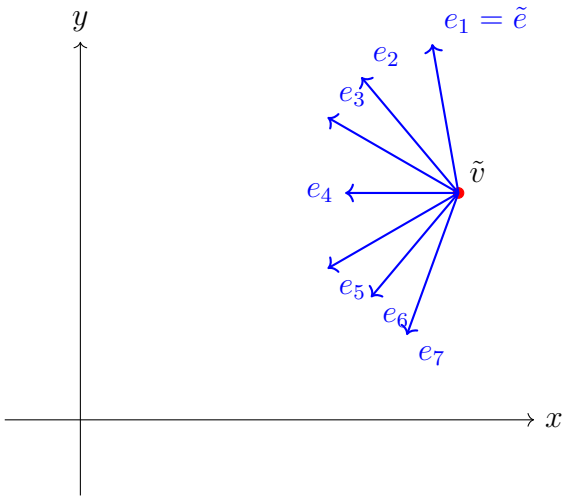

Figure 5.11: Projection of unit edge vectors onto the plane $z = 0$.

Proof. Since the complex is intersection free, either $\tilde{n}$ or $-\tilde{n}$ is a corrected orientated normal if we know that $\tilde{t}$ lies on the outer hull. Additionally, we may assume that, up to rotation, the x-value of $\tilde{v}$ is a strict maximum.
So assume $(\tilde{t}, \tilde{n})$ to be incorrectly oriented, thus either $\tilde{t}$ is not part of the outer hull, or $\tilde{n}$ is pointing inwards. Then from all points $p \in \tilde{t}$, we hit another point $h_p \in X$ when travelling along the line $p + \alpha\tilde{n}$, $\alpha \geq 0$. Since the complex is intersection-free, if p is not a vertex, then $h_p \neq p$.
Label the vertices of $\tilde{t}$ such that the edge $\tilde{e}$ connects $\tilde{v}$ and v', and call $\hat{e}$ the edge connecting the third vertex v_2 to $\tilde{v}$. Then take a sequence of points $\ell_n \in \hat{e}$ that converges to $\tilde{v}$. The corresponding sequence h_{ℓ_n} also converges to $\tilde{v}$ by maximality of $\tilde{v}$ and positive x-coordinate of $\tilde{n}$. Since we only have finitely many faces in our model,

there is a minimal face diameter, thus we can assume that without loss of generality, $h_{\ell_n} \in t'$ for some face t'. The fact that X is intersection-free forces $\tilde{v} \in t'$ and since we can hit t' along $\hat{e}$ via $\tilde{n}$, the other two vertices of t' have to have x-value greater than v_2. Thus, $\tilde{e}$ can be reached via two edge-face paths from t', since X is a closed surface. In at least one direction, there can never be vertices that do not have x-value greater than v_1 as else there would need to be a self-intersection present. Thus, there exists a vertex v with x-value greater than v_1 that is incident to a face t'' that contains $\tilde{e}$ (so that v is not incident to $\tilde{e}$). But this contradicts the choice of the normal $\tilde{n}$, so $(\tilde{t}, \tilde{n})$ is correctly oriented. □

The idea of computing the outer hull is based on depth-first search (DFS) on the faces and edges of the outer hull. For this, we use the initialisation configuration given in Lemma 5.7.1 above for a given face and a normal vector. Next, we need a criterion to decide for each edge which face lies on the surface of the outer hull. In [Att18], Attene introduces an algorithm for the computation of the outer-hull of a complex X without self-intersections. For each edge e in the complex, a *fan of faces* Fan(e), consisting of all faces incident to e in the complex, can be defined.

Definition 5.7.2. Let X be a complex and e an edge of X. We define the fan of e as the set

$$\text{Fan}(e) \coloneqq \{f \mid e \subset f \text{ face in } X\}.$$

An ordering of Fan(e) can be obtained via a face $f_1 \in \text{Fan(e)}$ and its normal vector n, see Figure 5.12. For this, we compute the *upward continuation* of the face f_1, which is defined as the next face $f_2 \in \text{Fan}(e)$ in direction of n. We can associate a normal to f_2 by rotating the normal vector n along the edge e and negating it. The concept of a fan is also used in Section 5.8 when considering non-manifold parts after computing the outer hull.

Since we start with a correct initialisation step and the surface is connected, we can proceed inductively to cover the whole surface of the outer-hull. In [Att18], Attene also covers sheets, i.e. faces that are contained with both sides inside the outer-hull. Because the initial surface is closed, we do not need to consider this case here.

We extend the algorithm in [Att18] to compute not only the outer hull, but all chambers of X given an initialization face t_0 with normal n_0.

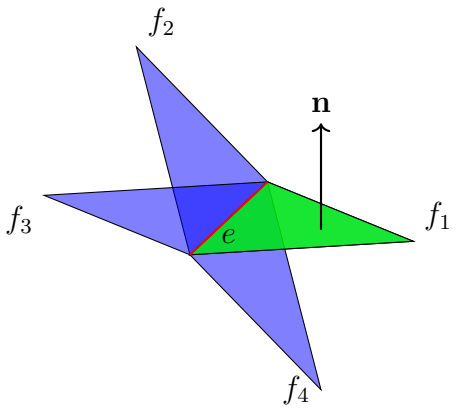

Figure 5.12: For the edge e, Fan(e) is given by four faces f_1, f_2, f_3, f_4. Using the normal vector n of face f_1, we can order the faces in a circle (f_1, f_2, f_3, f_4). The upward continuation of the face f_1 with normal n is then given by f_2.

Algorithm 4: ExtractChamber

input: Intersection-free complex X, initial face t_0 with normal n_0

output: Chamber containing face t_0 with side given by n_0

begin

  e_1, e_2, e_3 = three edges of initialization face t_0

  $B = [\langle t_0, e_1\rangle, \langle t_0, e_2\rangle, \langle t_0, e_3\rangle]$

  mark t_0 as outer

  while $B \neq []$ **do**

    $\langle t_i, e_j\rangle$ =first element of B

    remove $\langle t_i, e_j\rangle$ from B

    t_{new} = upward continuation of t_i at e_j

    if t_{new} = is not tagged as outer **then**

      mark t_{new} as outer

      e_1, e_2 =two edges of face t_{new} not equal to e_j

      Add $\langle t_{new}, e_1\rangle, \langle t_{new}, e_2\rangle$ to the beginning of B

    end

  end

end

For any face f of X with given normal vector n, we obtain a closed connected subcomplex Y of X using ExtractChamber (Algorithm 4), which is the boundary of a chamber of X (see Definition 5.3.5). Here, ExtractChamber (Algorithm 4) associates a set of faces to a chamber.

Lemma 5.7.3. *The set X_2 of faces of an embedded simplicial complex X together with a two-sided orientation of each face can be partitioned using the notion of chambers above, i.e. each side of each face belongs to a unique chamber. The outer-hull can be obtained using the start configuration from Lemma 5.7.1.*

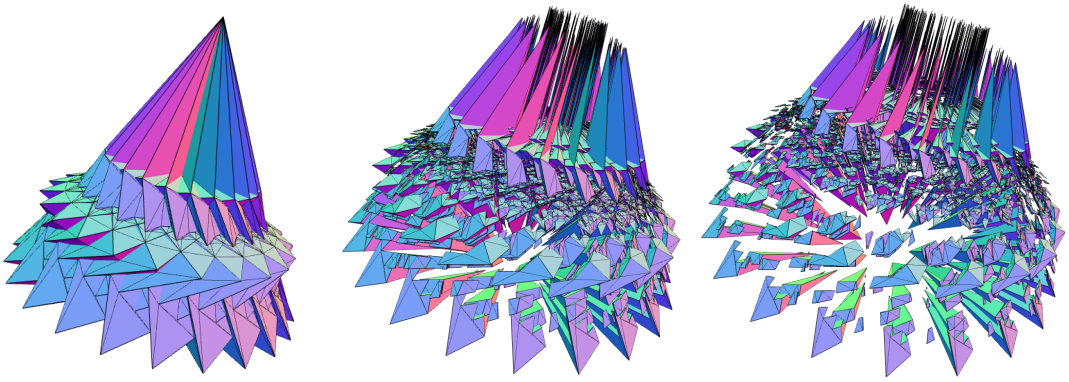

(a) $m = 0$ (b) $m = 1$ (c) $m = 2$

Figure 5.13: Exploded views of the retriangulation of the simplicial surface X_{23} with cyclic symmetry C_{23} with different magnitudes m.

Proof. ExtractChamber (Algorithm 4) stays inside a given chamber. As a chamber is connected and a depth-first search is conducted on the faces in a chamber, the output is independent of the initialisation face of a given chamber. □

Computing chambers and visualising them leads to a more profound understanding of the involved complexes. Volumes and other invariants can be computed in parallel for the whole complex by using a decomposition into chambers.

Example 5.7.4. Consider the self-intersecting complex X_{23}, shown in Figure 5.13a, with symmetry group isomorphic to C_{23} (cyclic group with 23 elements). It belongs to an embedded family of simplicial surfaces with equilateral triangles and cyclic symmetry, see Section 2.8Chapter 2 for exact coordinates. The complex X_{23} has $6 \cdot 23 = 138$ faces, 71 vertices and 207 edges and thus Euler characteristic $71 - 207 + 138 = 2$. The embedding of the vertices of X_{23} is chosen in a way that its symmetry group $G = \mathrm{Sym}(X_{23}) \leq \mathrm{O}(3)$ is given by elements of the form

$$\begin{pmatrix} \cos(\varphi) & -\sin(\varphi) & 0 \\ \sin(\varphi) & \cos(\varphi) & 0 \\ 0 & 0 & 1 \end{pmatrix},$$

where $\varphi \in \{\frac{2\pi \cdot j}{23} \mid 0 \leq j < 23\}$ and it is generated by the rotation matrix

$$\begin{pmatrix} \cos(\frac{2\pi}{23}) & -\sin(\frac{2\pi}{23}) & 0 \\ \sin(\frac{2\pi}{23}) & \cos(\frac{2\pi}{23}) & 0 \\ 0 & 0 & 1 \end{pmatrix},$$

which can be seen by matrix-multiplication and the addition theorem of cos and sin. By labelling the 138 faces by f_1 to f_{138}, we obtain $\binom{138}{2} = 9453$ face pairs. There are exactly $6 = \frac{138}{23}$ orbits of faces under the action of G, with representatives that we call f_1 to f_6. We can find all face pair intersections by the action of G on pairs of the form

$(f_i', f), i = 1, \ldots, 6$, where f is a face of X_{23}. Hence, it suffices to test intersection on these orbit representatives, as every intersection can be obtained by applying a group element to one of these face pairs (see Section 5.6). We retriangulate $f_1, \ldots, f_6$ using DiscTriangulation (Algorithm 2) and then apply G to obtain a retriangulation of the entire surface X_{23}. Transferring, i.e. applying group elements of G, can be achieved in time linear in the number of faces. Thus, we obtain an approximate speedup in the order of G, so by a factor of $23 = |G|$. In Figure 5.13, we see an exploded view of the internal chambers of X_{23}.

5.8 Non-Manifold Parts

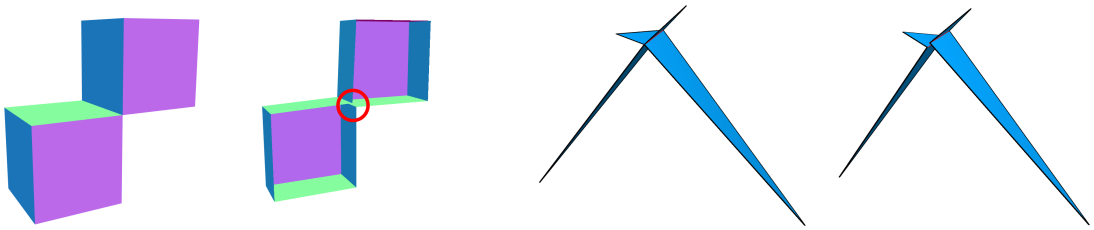

(a) (b)

Figure 5.14: (a) Remedying of two adjoint cubes. On the left, the original complex is shown, while the complex on the right possesses only manifold edges. (b) Our remedy algorithm shown for a single fan around the red edge. This example is taken from icosahedron$_{3,2}$, which can also be seen in Figure 5.15 below.

As illustrated in Figure 5.1 in the introduction, a common issue in models is the presence of non-manifold parts. In 3D printing, non-manifold parts cause issues or instabilities during the printing process, as a 3D printer cannot print sets of zero measure. These parts also occur naturally, such as in the dataset of embedded icosahedra with edge length one, see [Bra+20]. We can deal with non-manifold parts by transforming the complex slightly to obtain a similar but non-degenerate surface. Combinatorially, the process of resolving non-manifold parts in an embedded complex involves converting it into a simplicial surface by modifying the parts that do not meet conditions 3. and 4. in Definition 1.2.1, i.e. edges that are incident to more than two faces and vertices that do not satisfy the umbrella condition. We refer to this process as *remedying* the complex. Examples are provided in Figures 5.14a and 5.15. In order to avoid unnecessary computations, we first fix self-intersections and compute the outer hull (for instance, Figure 5.15a might represent part of an inner chamber). Additionally, identifying non-manifold parts from our combinatorial data can only be done after computing a self-intersection-free complex that is geometrically equivalent to the original, as discussed in Section 5.3. Furthermore, to ensure correct information on modifying edges and vertices, one must first guarantee the outward orientation of normals. Therefore, in the following discussion, we assume a complex with embedding (X, ϕ) that is

intersection-free and reduced to its outer hull.

Non-Manifold Edges

We first introduce some notation and describe our approach, before we illustrate the assignment of new coordinates to vertices.

Definition 5.8.1. *Non-manifold edges* are edges which are incident to more than two triangles, as shown in Figure 5.15a. We differentiate between three types:

(i) *Inner non-manifold edges* have both of their vertices incident to another non-manifold edge;

(ii) *Outer non-manifold edges* are edges where only one vertex is incident to another non-manifold edge;

(iii) *Isolated non-manifold edges* are edges which are not incident to any other non-manifold edge.

It is important to note that one can treat isolated non-manifold edges by subdividing the incident triangles, resulting in two outer non-manifold edges. We thus only discuss the first two cases. Moreover, it follows that inner and outer non-manifold edges occur in paths, with outer non-manifold edges at the start and end, respectively, and inner ones in between. We thus proceed in a path-based framework: First, we gather all the non-manifold edges and then treat edge-paths of non-manifold edges iteratively. This is visualised in Figure 5.15.

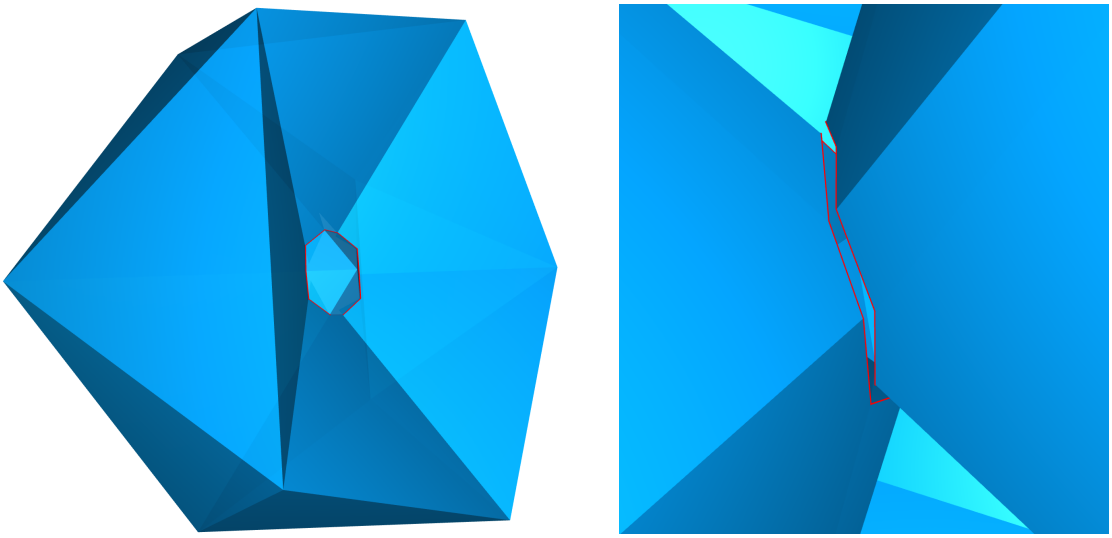

(a) (b)

Figure 5.15: (a) Non-manifold edges marked in red. (b) Interior view that shows split (prior non-manifold) edges.

To remedy an inner non-manifold edge e, we split the vertices v_1, v_2 incident to e, resulting in new vertices v_1^j, v_2^j for $j = 1, 2$. Additionally, we create another edge

$e' = \{v_1^2, v_2^2\}$ and set $e = \{v_1^1, v_2^1\}$. For an outer non-manifold edge, we only split the vertex incident to another non-manifold edge. Both cases can be seen in Figure 5.16. The exact assignment of coordinates to the new vertices is described below.

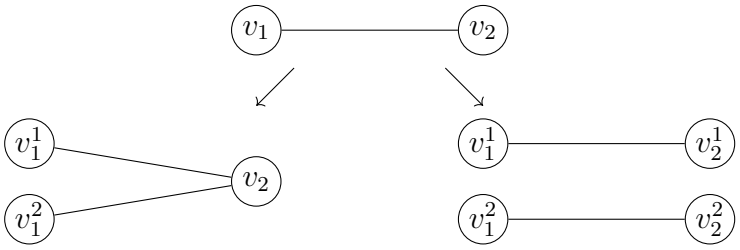

Figure 5.16: Splitting non-manifold Edges based on type: outer (left) and inner (right).

Every path of non-manifold edges of length ℓ that is not a circle starts and ends at an outer non-manifold edge, and thus we only need to split $\ell - 1$ vertices (one for each edge except the last). For circles, one then has to split ℓ vertices.
One also needs to consider *junctions* inside the non-manifold edge paths, which are defined as vertices where more than two non-manifold edges meet. If, while iterating, we come upon a junction, we proceed via a depth first approach and split the remainder up into disjoint paths, since the edges are already fixed by splitting the common vertex. It is possible in certain configurations to produce a single non-manifold vertex after all non-manifold edges are corrected, which is why we deal with edges first and then consider vertices in the following. Our implemented algorithms in [AG24b] also rely on this order, to correctly infer information about the surface.

We now describe the coordinate assignment when splitting vertices.

Definition 5.8.2. Let (X, ϕ) be an embedded simplicial complex, reduced to its outer hull, and $e \in X$ an edge. We call a pair of faces (f_1, f_2) in $\mathrm{Fan}(e)$ an *outward oriented butterfly* if, when rotating f_1 along its normal with rotation axis e, the next face in the fan that one encounters is f_2.

For manifold edges e, the above is not very interesting, since $\mathrm{Fan}(e) = \{f_1, f_2\}$ holds for an outward oriented butterfly (f_1, f_2). Since the initial complex we started with is closed we have the following:

Remark 5.8.3. For a closed embedded simplicial complex that has been reduced to its outer hull, the fan of each non-manifold edge can be decomposed into $|\mathrm{Fan}(e)|/2$ outward oriented butterflies.

To compute the new vertices, we shift them by a small value $\varepsilon > 0$ into a suitable direction s_e, which is given as follows: Choose an outward oriented butterfly $(f_1, f_2) \subset \mathrm{Fan}(e)$ and taking for both f_1, f_2 the vertex w_i that is not incident to e, and set

$$s_e := 1/2(w_1 - v_1) + 1/2(w_2 - v_1).$$

Then we replace v in f_1 and f_2 by $\overline{v} := v + \varepsilon s_e$.

This procedure is iterated for all outward oriented butterflies of Fan(e), which thus remedies e.

Remark 5.8.4. Note that the parameter $\varepsilon > 0$ above can be adapted based on the considered application area. For example, for 3D printing, it can be chosen based on the nozzle width, which guarantees that the resulting surface is printed correctly.

Non-Manifold Vertices

As noted above, it is possible, in certain configurations, for a non-manifold vertex to appear after dealing with a junction of non-manifold edges. These can also be present as artefacts in 3D modelling, for example when adjoining surfaces. Note that it only makes sense to talk about non-manifold vertices here, not about non-manifold points, as these would give rise to self-intersections which we dealt with beforehand. A *non-manifold vertex* in a complex X is a vertex for which the *umbrella condition* in Definition 1.2.1 fails. Thus, the incident faces cannot be ordered in a connected face-edge path. To remedy such a vertex v, we first consider the family C_α of all *local umbrellas* of v (indexed by α).

Definition 5.8.5 (Local Umbrella)**.** For a complex X without non-manifold edges and vertex $v \in X$, the local umbrellas C_α of v in X are defined as follows. Take F to be all the faces incident to v and set C_α to be the equivalence classes of $\mathrm{Pot}(F)$ under the following relation:

$$f_1 =_v f_2 \iff f_1 \text{ can be reached via an edge-face path from } f_2 \text{ by only using edges incident to } v.$$

Thus, the local umbrellas C_α are maximal sets of faces of v under the condition that all faces in the set are edge-connected via edges that are incident to v.

It is important to first remedy non-manifold edges before considering vertices, since if still non-manifold edges are present, the local umbrella could also switch between different sides of the surface. For each local umbrella C_α, we take for all $f \in C_\alpha$ their vertices v_1^f and v_2^f that do not equal v and compute an average direction vector

$$v_\alpha := \frac{1}{|C_\alpha|} \left(\sum_{f \in C_\alpha} \frac{1}{2}(v_1^f - v_0) + \frac{1}{2}(v_2^f - v_0) \right).$$

Next, we replace v by $v' := v_0 + v_\alpha \cdot \varepsilon$ in all the f of our current C_α, where $\varepsilon > 0$ is a small shift parameter.

We thus move v slightly in the direction of the local umbrella, and by doing this for each of the local umbrellas, we obtain m-moved versions of v that are pairwise distinct and manifold, where $\alpha = 1, \ldots, m$ is the number of v-edge-connected components of the faces of v.

5.9 Experiments on Self-Intersecting Icosahedra

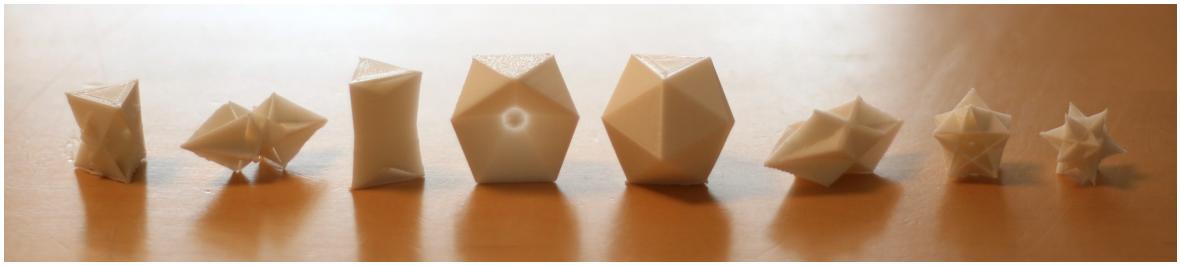

Figure 5.17: 3D printed icosahedra with constant edge length.

In [Bra+20] all 35 symmetric embeddings of icosahedra with equilateral triangles of edge length 1 are classified. This means that the underlying simplicial surface agrees but the embedding varies, see [Bra+] for coordinates and visualizations of the resulting surfaces. From these 35 embeddings, 33 have self-intersections and thus are candidates for testing the algorithms presented in the previous sections. They are named as $\text{icosahedron}_{i,j}$, where $i \in \{1, \dots, 14\}$ and $j \in \{1, \dots, k(i)\}$ for certain numbers $k(i) \in \mathbb{N}$. The numbering comes from the classification based on 14 formal Gram-matrices that give rise to different embeddings. Note that, for a given formal Gram-matrix, all corresponding embeddings have the same symmetry, see [Bra+20].

In Figure 5.5, we see one such an icosahedron, also known as the great icosahedron, with symmetry group isomorphic to the entire icosahedral group. Thus, we can use symmetric optimization as proposed in Section 5.6. Table 5.1 in the Appendix shows that applying our symmetry algorithm leads to large speedup by a factor of 14.68 when first retriangulating the surface and subsequently computing the outer hull. In Figure 5.17 we show a collection of printed versions of the icosahedra, beforehand processed by our algorithm.

The computations were performed on a MacBook Pro with Apple M1 Pro chip and 16GB memory, averaging over 10 run times. We observe a strong correlation between the group sizes and the average speedup when comparing the time needed with or without using the symmetry group.

5.10 Conclusion and Outlook

In Table 5.1 of the Appendix, we can see the speedup for retriangulating and computing the outer hull of all 35 symmetric icosahedra with edge length 1. For an icosahedron with symmetry group size of 2, which corresponds to just a single symmetry in the complex, the average speedup in our data set is still 2.12. Even if no symmetries are known a-priori, symmetry detection methods [BBS23; Li+16] can be used to compute the symmetry group to allow the application of the presented symmetry-driven algorithm in Section 5.6. The symmetry optimisation method can be also applied to infinite

structures if the face-orbits are finite. For instance, crystallographic groups give examples of doubly periodic symmetries with face-orbit representatives sitting inside a fundamental domain, see [GNP22; Wie+23] for examples of such surfaces.
The study of chambers of an embedded complex can be used to compute various geometric properties such as the volume and has the potential of designing interlocking puzzles [Che+22] by subdividing a given complex into its chambers and introducing connectors. With this, we can also subdivide a given surface into chambers by introducing inner triangles leading to a complex inner structure.

The retriangulation method in this chapter is motivated by producing a complex with a minimal number of triangles. The robustness of the underlying algorithm and the possibility of applying symmetries leads to a numerically robust and fast method. The results we obtained for embedded icosahedra and cyclic complexes show that a speedup factor corresponding to the number of non-trivial symmetries is possible without any loss of algorithmic stability.

For further research, optimisation of computing the outer hull of a self-intersecting complex can be studied. For instance, one could consider finding alternative algorithms that compute the outer hull before considering self-intersections, since only the outer hull is relevant in many settings. Additionally, since we rely on the exploitation of the mathematical structure of simplicial complexes, we need suitable assumptions on initial data. One could, then, also consider addressing the problem of turning an arbitrarily degenerate input (like a non-closed surface) into one that can be treated by our framework. Another interesting goal would be to remedy non-manifold parts in a way that preserves the symmetry group of the original complex. Then, algorithms for further processing could benefit from symmetry as well. In general, additional research is required to gain an understanding of how parameters need to be adjusted in order to guarantee a model that satisfies the same properties as the underlying geometric object.

5.11 Appendix

Table 5.1: Timing of computing the outer hull of Icosahedra [Bra+]: run times of algorithm on all 35 symmetric icosahedra with and without using their respective symmetry groups. The average speedup on our data set is approximately 3.17.

Icosahedron	Group Size	Time with Group (ms)	Time without Group (ms)	Speedup
$\text{Icosahedron}_{1,1}$	4	30.6	83.0	2.71
$\text{Icosahedron}_{2,1}$	120	715.4	10502.6	14.68
$\text{Icosahedron}_{2,2}$	120	13.6	67.4	4.96
$\text{Icosahedron}_{3,1}$	20	75.0	385.6	5.14
$\text{Icosahedron}_{3,2}$	20	280.8	116.0	3.80
$\text{Icosahedron}_{4,1}$	12	35.8	80.9	2.31
$\text{Icosahedron}_{4,2}$	12	84.9	424.1	2.26
$\text{Icosahedron}_{5,1}$	4	33.2	144.7	5.00
$\text{Icosahedron}_{5,2}$	4	116.0	622.1	4.36
$\text{Icosahedron}_{6,1}$	20	39.2	140.6	5.36
$\text{Icosahedron}_{7,1}$	12	1090.5	2536.7	2.33
$\text{Icosahedron}_{7,2}$	12	488.8	1343.2	2.75
$\text{Icosahedron}_{7,3}$	12	212.8	517.5	2.43
$\text{Icosahedron}_{8,1}$	4	111.5	325.1	2.92
$\text{Icosahedron}_{9,1}$	4	229.8	409.1	1.78
$\text{Icosahedron}_{9,2}$	4	2074.3	4097.2	1.98
$\text{Icosahedron}_{9,3}$	4	89.8	149.2	1.66
$\text{Icosahedron}_{9,4}$	4	136.8	241.9	1.77
$\text{Icosahedron}_{9,5}$	4	58.3	99.3	1.70
$\text{Icosahedron}_{10,1}$	2	679.9	3024.7	4.45
$\text{Icosahedron}_{10,2}$	2	21.2	66.9	3.16
$\text{Icosahedron}_{11,1}$	10	99.1	248.1	2.50
$\text{Icosahedron}_{11,2}$	10	42.6	111.6	2.62
$\text{Icosahedron}_{12,1}$	6	137.9	213.0	1.54
$\text{Icosahedron}_{12,2}$	6	109.7	163.8	1.49
$\text{Icosahedron}_{12,3}$	6	145.9	240.3	1.65
$\text{Icosahedron}_{12,4}$	6	223.2	380.5	1.70
$\text{Icosahedron}_{13,1}$	2	352.8	567.4	1.61
$\text{Icosahedron}_{13,2}$	2	751.4	1130.4	1.50
$\text{Icosahedron}_{13,3}$	2	460.7	703.2	1.53
$\text{Icosahedron}_{13,4}$	2	467.0	780.6	1.67
$\text{Icosahedron}_{13,5}$	2	153.2	236.4	1.54
$\text{Icosahedron}_{13,6}$	2	243.9	373.4	1.53
$\text{Icosahedron}_{14,1}$	10	57.3	182.9	3.19

Bibliography

[AG23] R. Akpanya and T. Goertzen. “Surfaces with given Automorphism Group”. In: *arXiv e-prints*, arXiv:2307.12681 (July 2023).

[AG24a] C. Amend and T. Goertzen. “A Framework for Symmetric Self-Intersecting Surfaces”. In: *arXiv e-prints*, arXiv:2312.02113 (May 2024).

[AG24b] C. Amend and T. Goertzen. *SelfIntersectingComplexes - GAP package*. `https://github.com/TomGoertzen/SelfIntersectingComplexes`. Version 1.0dev. 2024.

[Akl+20] E. Akleman, V. R. Krishnamurthy, C.-A. Fu, S. G. Subramanian, M. Ebert, M. Eng, C. Starrett, and H. Panchal. “Generalized abeille tiles: Topologically interlocked space-filling shapes generated based on fabric symmetries”. In: *Computers & Graphics* 89 (2020), pp. 156–166.

[Akp+23] R. Akpanya, T. Goertzen, S. Wiesenhuetter, A. C. Niemeyer, and J. Noennig. “Topological Interlocking, Truchet Tiles and Self-Assemblies: A Construction-Kit for Civil Engineering Design”. In: *Proceedings of Bridges 2023: Mathematics, Art, Music, Architecture, Culture*. Ed. by J. Holdener, E. Torrence, C. Fong, and K. Seaton. Phoenix, Arizona: Tessellations Publishing, 2023, pp. 61–68.

[Att14] M. Attene. “Direct repair of self-intersecting meshes”. In: *Graphical Models* 76.6 (2014), pp. 658–668.

[Att18] M. Attene. “As-exact-as-possible repair of unprintable STL files”. In: *Rapid Prototyping Journal* 24.5 (Jan. 2018), pp. 855–864.

[Bab72] L. Babai. “Automorphism groups of planar graphs. I”. In: *Discrete Math.* 2.4 (1972), pp. 295–307.

[Bab81] L. Babai. “On the abstract group of automorphisms”. In: *Combinatorics (Swansea, 1981)*. Vol. 52. London Math. Soc. Lecture Note Ser. Cambridge Univ. Press, Cambridge-New York, 1981, pp. 1–40.

[Bau20] M. Baumeister. “Regularity aspects for combinatorial simplicial surfaces”. Dissertation. Aachen: RWTH Aachen University, 2020.

[BBS23] M. Buric, T. Bosner, and S. Skec. “A Framework for Detection of Exact Global and Partial Symmetry in 3D CAD Models”. In: *Symmetry* 15.5 (2023).

[Bel+09] A. Belov-Kanel, A. Dyskin, Y. Estrin, E. Pasternak, and I. Ivanov-Pogodaev. “Interlocking of Convex Polyhedra: towards a Geometric Theory of Fragmented Solids”. In: *Moscow Mathematical Journal* 10 (Jan. 2009).

[Ber+00] M. de Berg, M. van Kreveld, M. Overmars, and O. Schwarzkopf. *Computational geometry*. revised. Algorithms and applications. Springer-Verlag, Berlin, 2000, pp. xii+367.

[BGS17] G. Brinkmann, P. Goetschalckx, and S. Schein. “Comparing the constructions of Goldberg, Fuller, Caspar, Klug and Coxeter, and a general approach to local symmetry-preserving operations”. In: *Proc. A.* 473.2206 (2017), pp. 20170267, 14.

[Bra+] K.-H. Brakhage, A. C. Niemeyer, W. Plesken, D. Robertz, and A. Strzelczyk. *Documentation of Paper: The icosahedra of edge length 1*. `http://algebra.data.rwth-aachen.de/Icosahedra/visualplusdata.html`. (Accessed on 30/11/2023).

[Bra+17] K.-H. Brakhage, A. C. Niemeyer, W. Plesken, and A. Strzelczyk. “Simplicial surfaces controlled by one triangle”. In: *J. Geom. Graph.* 21.2 (2017), pp. 141–152.

[Bra+20] K.-H. Brakhage, A. C. Niemeyer, W. Plesken, D. Robertz, and A. Strzelczyk. “The icosahedra of edge length 1”. In: *J. Algebra* 545 (2020), pp. 4–26.

[CBG08] J. H. Conway, H. Burgiel, and C. Goodman-Strauss. *The symmetries of things*. New York: A K Peters, Ltd., Wellesley, MA, 2008.

[Che+22] R. Chen, Z. Wang, P. Song, and B. Bickel. “Computational Design of High-Level Interlocking Puzzles”. In: *ACM Trans. Graph.* 41.4 (July 2022).

[Chu+19] L. Chu, H. Pan, Y. Liu, and W. Wang. “Repairing Man-Made Meshes via Visual Driven Global Optimization with Minimum Intrusion”. In: *ACM Trans. Graph.* 38.6 (Nov. 2019).

[CK10] M. Campen and L. Kobbelt. “Exact and Robust (Self-)Intersections for Polygonal Meshes”. In: *Computer Graphics Forum* 29.2 (2010), pp. 397–406.

[CK16] G. Chirikjian and A. Kyatkin. *Harmonic Analysis for Engineers and Applied Scientists: Updated and Expanded Edition*. Dover Books on Mathematics. Dover Publications, 2016.

[Cox+82] H. S. M. Coxeter, P. Val, H. T. Flather, and J. F. Petrie. *The Fifty-Nine Icosahedra*. 1st ed. Springer New York, NY, 1982, p. 47.

[Cox69] H. S. M. Coxeter. *Introduction to geometry*. Second. John Wiley & Sons, Inc., New York-London-Sydney, 1969, pp. xviii+469.

[DEP19] A. V. Dyskin, Y. Estrin, and E. Pasternak. "Topological Interlocking Materials". In: *Architectured Materials in Nature and Engineering: Archimats*. Ed. by Y. Estrin, Y. Bréchet, J. Dunlop, and P. Fratzl. Cham: Springer International Publishing, 2019, pp. 23–49.

[DG70] R. Duppe and H. Gottschalk. "Automatische Interpolation von Isolinien bei willkürlichen Stützpunkten". In: *Allgemeine Vermessungsnachrichten* 77.10 (1970), pp. 423–426.

[DH87] A. W. M. Dress and D. Huson. "On tilings of the plane". In: *Geometriae Dedicata* 24.3 (1987), pp. 295–310.

[DPH09] L. De Floriani, D. Panozzo, and A. Hui. "Computing and Visualizing a Graph-Based Decomposition for Non-manifold Shapes". In: *Graph-Based Representations in Pattern Recognition*. Ed. by A. Torsello, F. Escolano, and L. Brun. Berlin, Heidelberg: Springer Berlin Heidelberg, 2009, pp. 62–71.

[Dys+01] A. V. Dyskin, Y. Estrin, A. J. Kanel-Belov, and E. Pasternak. "A new concept in design of materials and structures: assemblies of interlocked tetrahedron-shaped elements". In: *Scripta Materialia* 44.12 (2001), pp. 2689–2694.

[Dys+03a] A. V. Dyskin, Y. Estrin, A. J. Kanel-Belov, and E. Pasternak. "Topological interlocking of platonic solids: A way to new materials and structures". In: *Philosophical Magazine Letters* 83.3 (2003), pp. 197–203.

[Dys+03b] A. Dyskin, Y. Estrin, E. Pasternak, H. Khor, and A. Kanel-Belov. "Fracture Resistant Structures Based on Topological Interlocking with Nonplanar Contacts". In: *Advanced Engineering Materials* 5.3 (Mar. 2003). Publisher: John Wiley & Sons, Ltd, pp. 116–119.

[Ebe+24] M. Ebert, E. Akleman, V. Krishnamurthy, R. Kulagin, and Y. Estrin. "VoroNoodles: Topological Interlocking with Helical Layered 2-Honeycombs". In: *Advanced Engineering Materials* 26.4 (2024), p. 2300831.

[EKA21] Y. Estrin, V. R. Krishnamurthy, and E. Akleman. "Design of architectured materials based on topological and geometrical interlocking". In: *Journal of Materials Research and Technology* 15 (2021), pp. 1165–1178.

[Fré38] A. F. Frézier. *La theorie et la pratique de la coupe des pierres et des bois, pour la construction des voutes et autres parties des bâtimens civils & militaires, ou Traité de stereotomie a l'usage de l'architecture*. Vol. 2. Doulsseker, 1738.

[Fru49] R. Frucht. "Graphs of Degree Three with a Given Abstract Group". In: *Canadian Journal of Mathematics* 1.4 (1949), pp. 365–378.

[Fru82] R. W. Frucht. "How I became interested in graphs and groups". In: *J. Graph Theory* 6.2 (1982), pp. 101–104.

[Gal35] J.-G. Gallon. *Machines et inventions approuvées par l'Académie Royale des Sciences depuis son établissement jusqu'à present; avec leur Description*. Académie royale des Sciences, 1735.

[GAP] *GAP – Groups, Algorithms, and Programming, Version 4.13.0*. The GAP Group. 2024.

[GCV21] P. Goetschalckx, K. Coolsaet, and N. Van Cleemput. "Local orientation-preserving symmetry preserving operations on polyhedra". In: *Discrete Math.* 344.1 (2021), Paper No. 112156, 10.

[GF09] A. Golovinskiy and T. Funkhouser. "Consistent Segmentation of 3D Models". In: *Computers and Graphics (Shape Modeling International 09)* 33.3 (June 2009), pp. 262–269.

[Gli84] M. Glickman. "The G-block system of vertically interlocking paving". In: *Second International Conference on Concrete Block Paving*. 1984, pp. 10–12.

[GNP22] T. Goertzen, A. Niemeyer, and W. Plesken. "Topological Interlocking via Symmetry". In: *Proc. of the 6th fib International Congress 2022*. Novus Press, Oslo, Norway, 2022, pp. 1235–1244.

[Goe+23] T. Goertzen, D. Macek, L. Schnelle, M. Weiß, S. Reese, H. Holthusen, and A. C. Niemeyer. "Mechanical Comparison of Arrangement Strategies for Topological Interlocking Assemblies". In: *arXiv e-prints*, arXiv:2312.01958 (Dec. 2023).

[Goe24a] T. Goertzen. "Constructing Interlocking Assemblies with Crystallographic Symmetries". In: *arXiv e-prints*, arXiv:2405.15080 (May 2024).

[Goe24b] T. Goertzen. "Mathematical Foundations of Interlocking Assemblies". In: *arXiv e-prints*, arXiv:2405.17644 (May 2024).

[Gor21] V. Gorin. *Lectures on Random Lozenge Tilings*. Cambridge Studies in Advanced Mathematics. Cambridge University Press, 2021.

[Grü03] B. Grünbaum. *Convex polytopes*. Second. Vol. 221. Graduate Texts in Mathematics. Prepared and with a preface by Volker Kaibel, Victor Klee and Günter M. Ziegler. Springer-Verlag, New York, 2003, pp. xvi+468.

[GS89] B. Grünbaum and G. C. Shephard. *Tilings and patterns*. A Series of Books in the Mathematical Sciences. An introduction. W. H. Freeman and Company, New York, 1989, pp. xii+446.

[HK63] H. Heesch and O. Kienzle. *Flächenschluss. System der Formen lückenlos aneinanderschliessender Flachteile*. Springer-Verlag, Berlin-Göttingen-Heidelberg, 1963, xi + 141 pp. (1 insert).

[HKM14] A. Hujdurović, K. Kutnar, and D. Marušič. "Cubic Cayley Graphs and Snarks". In: *Rigidity and Symmetry*. Ed. by R. Connelly, A. Ivić Weiss, and W. Whiteley. New York, NY: Springer New York, 2014, pp. 27–40.

[HLM91] F. Hoffman, S. Locke, and A. Meyerowitz. "A note on cycle double covers in Cayley graphs." eng. In: *Mathematica Pannonica* 2.1 (1991), pp. 63–66.

[II88] H. IMAI and M. IRI. "Polygonal Approximations of a Curve — Formulations and Algorithms". In: *Computational Morphology*. Ed. by G. T. TOUSSAINT. Vol. 6. Machine Intelligence and Pattern Recognition. North-Holland, 1988, pp. 71–86.

[IUC02] IUCr. *International Tables for Crystallography, Volume A: Space Group Symmetry*. 5. revised edition. International Tables for Crystallography. Dordrecht, Boston, London: Kluwer Academic Publishers, 2002.

[Jae85] F. Jaeger. "A Survey of the Cycle Double Cover Conjecture". In: *Annals of Discrete Mathematics (27): Cycles in Graphs*. Ed. by B. Alspach and C. Godsil. Vol. 115. North-Holland Mathematics Studies. North-Holland, 1985, pp. 1–12.

[JOP+24] E. Jones, T. Oliphant, P. Peterson, et al. *SciPy: Open source scientific tools for Python*. 2024.

[Jor87] C. Jordan. *Cours d'analyse de l'École polytechnique*. Cours d'analyse de l'École polytechnique Bd. 3. Gauthier-Villars et fils, 1887.

[Ken09] R. Kenyon. "Lectures on dimers". In: *Statistical mechanics*. Vol. 16. IAS/Park City Math. Ser. Amer. Math. Soc., Providence, RI, 2009, pp. 191–230.

[KL02] V. Kopsky and D. B. Litvin, eds. *International Tables for Crystallography, Volume E: Subperiodic groups*. 5th. Vol. E. International Tables for Crystallography. Berlin, New York: Springer-Verlag, 2002.

[KN96] S. Kobayashi and K. Nomizu. *Foundations of differential geometry. Vol. I.* Wiley Classics Library. Reprint of the 1963 original, A Wiley-Interscience Publication. John Wiley & Sons, Inc., New York, 1996, pp. xii+329.

[KO05] R. Kenyon and A. Okounkov. "What is ... a dimer?" In: *Notices Amer. Math. Soc.* 52.3 (2005), pp. 342–343.

[KS00] C. S. Kaplan and D. H. Salesin. "Escherization". In: *Proceedings of the 27th Annual Conference on Computer Graphics and Interactive Techniques*. SIGGRAPH '00. USA: ACM Press/Addison-Wesley Publishing Co., 2000, pp. 499–510.

[LB18] Y. Li and J. Barbič. "Immersion of Self-Intersecting Solids and Surfaces". In: *ACM Trans. Graph.* 37.4 (July 2018).

[Li+16] B. Li, H. Johan, Y. Ye, and Y. Lu. "Efficient 3D reflection symmetry detection: A view-based approach". In: *Graphical Models* 83 (2016). SIGGRAPH Asia Workshop on Creative Shape Modeling and Design, pp. 2–14.

[Lov07] L. Lovász. *Combinatorial problems and exercises*. second. AMS Chelsea Publishing, Providence, RI, 2007, p. 642.

[LS16] J. Lauri and R. Scapellato. "Orbital Graphs and Strongly Regular Graphs". In: *Topics in Graph Automorphisms and Reconstruction*. 2nd ed. London Mathematical Society Lecture Note Series. Cambridge University Press, 2016, pp. 64–78.

[Mas72] J. H. Mason. "Can Regular Tetrahedra Be Glued Together Face to Face to Form a Ring?" In: *The Mathematical Gazette* 56.397 (1972), pp. 194–197.

[MG22] C. Mccoid and M. J. Gander. "A Provably Robust Algorithm for Triangle-Triangle Intersections in Floating-Point Arithmetic". In: *ACM Trans. Math. Softw.* 48.2 (May 2022).

[Miu85] K. Miura. "Method of packaging and deployment of large membranes in space". In: *The Institute of Space and Astronautical Science Report* 618 (1985), pp. 1–9.

[Möl97] T. Möller. "A Fast Triangle-Triangle Intersection Test". In: *Journal of Graphics Tools* 2.2 (1997), pp. 25–30.

[MP14] B. D. McKay and A. Piperno. "Practical graph isomorphism, II". In: *Journal of Symbolic Computation* 60 (2014), pp. 94–112.

[MR08] W. Mulzer and G. Rote. "Minimum-weight triangulation is NP-hard". In: *J. ACM* 55.2 (May 2008).

[Mul+22] C. Mullins, M. Ebert, E. Akleman, and V. Krishnamurthy. “Voronoi Spaghetti & VoroNoodles: Topologically Interlocked, Space-Filling, Corrugated & Congruent Tiles”. In: *SIGGRAPH Asia 2022 Technical Communications*. SA ’22. New York, NY, USA: Association for Computing Machinery, 2022.

[Nie+23a] A. Niemeyer, R. Akpanya, T. Görtzen, M. Weiß, and L. Schnelle. *GAPic, Version 0.1-beta*. `https://github.com/GAP-ART-RWTH/GAPic/`. 2023.

[Nie+23b] A. Niemeyer, M. Baumeister, R. Akpanya, T. Görtzen, and M. Weiß. *SimplicicalSurfaces, Version 0.6*. `https://github.com/gap-packages/SimplicialSurfaces`. 2023.

[NPR24] A. C. Niemeyer, W. Plesken, and D. Robertz. “Simplicial Surfaces of Congruent Triangles”. In: *In progress* (2024).

[Pie20] M. Piekarski. “Floor Slabs Made from Topologically Interlocking Prefabs of Small Size”. In: *Buildings* 10.4 (2020).

[Ple96] W. Plesken. “Kristallographische Gruppen”. In: *Group theory, algebra, and number theory (Saarbrücken, 1993)*. de Gruyter, Berlin, 1996, pp. 75–96.

[Pro24] I. Project. *Inkscape: Open Source Scalable Vector Graphics Editor*. Available at `https://inkscape.org`. 2024.

[RC99] J. Rossignac and D. Cardoze. “Matchmaker: Manifold BReps for Non-Manifold r-Sets”. In: *Proceedings of the Fifth ACM Symposium on Solid Modeling and Applications*. SMA ’99. Ann Arbor, Michigan, USA: Association for Computing Machinery, 1999, pp. 31–41.

[Rid21] P. Rideout. *svg3d*. `https://github.com/prideout/svg3d`. 2021.

[SB87] C. S. Smith and P. Boucher. “The Tiling Patterns of Sebastien Truchet and the Topology of Structural Hierarchy”. In: *Leonardo* 20.4 (1987), pp. 373–385.

[SHC] N. Schoeni, W. Hardaker, and G. Chapuis. *Escher Web Sketch*. `https://www.epfl.ch/schools/sb/research/iphys/teaching/crystallography/escher-web-sketch/`. Accessed: 2024-05-23.

[Ska23] V. Skala. “A Brief Survey of Clipping and Intersection Algorithms with a List of References (including Triangle-Triangle Intersections)”. In: *Informatica* 34.1 (2023), pp. 169–198.

[SM03] M. Szilvśi-Nagy and G. Mátyási. “Analysis of STL files”. In: *Mathematical and Computer Modelling* 38.7 (2003). Hungarian Applied Mathematics, pp. 945–960.

[Stü+23] S. Stüttgen, R. Akpanya, B. Beckmann, R. Chudoba, D. Robertz, and A. C. Niemeyer. "Modular Construction of Topological Interlocking Blocks—An Algebraic Approach for Resource-Efficient Carbon-Reinforced Concrete Structures". In: *Buildings* 13.10 (2023).

[Sub+19] S. G. Subramanian, M. Eng, V. Krishnamurthy, and E. Akleman. "Delaunay Lofts: A Biologically Inspired Approach for Modeling Space Filling Modular Structures". In: *Computers & Graphics* 82 (May 2019).

[Sze73] G. Szekeres. "Polyhedral decompositions of cubic graphs". In: *Bulletin of the Australian Mathematical Society* 8.3 (1973), pp. 367–387.

[Tan24] T. Tantau. *The TikZ and PGF Packages*. Available at `https://tikz.dev`. 2024.

[Tru04] S. Truchet. "Mémoire sur les Combinaisons". In: *Mémoires de l'Académie Royale des Sciences* (1704), pp. 363–372.

[Tut63] W. T. Tutte. "How to Draw a Graph". In: *Proceedings of the London Mathematical Society* s3-13.1 (1963), pp. 743–767.

[Vak+22] I. Vakaliuk, T. Goertzen, S. Scheerer, A. C. Niemeyer, and M. Curbach. "Initial numerical development of design procedures for TRC bioinspired shells". In: *Innovation, Sustainability and Legacy – Proceedings of IASS/APCS 2022*. Ed. by S.-d. Xue, J.-z. Wu, and G.-j. Sun. International Association for Shell and Spatial Structures (IASS)/Asia Pacific Conference on Shell & Spatial Structures (APCS). Beijing, China, Oct. 2022, pp. 2597–2608.

[Vin05] J. Vince. *Geometry for Computer Graphics: Formulae, Examples and Proofs*. 1st ed. Published: 05 January 2005. Springer London, 2005, pp. XXII, 342.

[Wan+19] Z. Wang, P. Song, F. Isvoranu, and M. Pauly. "Design and Structural Optimization of Topological Interlocking Assemblies". In: *ACM Trans. Graph.* 38.6 (Nov. 2019). Place: New York, NY, USA Publisher: Association for Computing Machinery.

[Wan21] Z. Wang. "Computational Analysis and Design of Structurally Stable Assemblies with Rigid Parts". eng. PhD thesis. EPFL, 2021.

[Wie+23] S. Wiesenhuetter, T. Goertzen, I. Vakaliuk, M. Curbach, S. Scheerer, A. C. Niemeyer, and J. R. Noennig. "Triply Periodic Minimal Surfaces – A Novel Design Approach for Lightweight CRC Structures". In: *Building for the Future: Durable, Sustainable, Resilient*. Ed. by A. Ilki, D. Çavunt, and Y. S. Çavunt. Cham: Springer Nature Switzerland, 2023, pp. 1449–1458.

[Wil92] R. H. Wilson. "On Geometric Assembly Planning". PhD Thesis. Stanford, CA, USA: Stanford University, 1992.

[WL94] R. H. Wilson and J.-C. Latombe. “Geometric reasoning about mechanical assembly”. In: *Artificial Intelligence* 71.2 (Dec. 1994), pp. 371–396.

[WLG03] M. Wagner, U. Labsik, and G. Greiner. “Repairing non-manifold triangle meshes using simulated annealing”. In: *International Journal of Shape Modeling* 9 (Dec. 2003).

[WSP18] Z. Wang, P. Song, and M. Pauly. “DESIA: A General Framework for Designing Interlocking Assemblies”. In: *ACM Trans. Graph.* 37.6 (Dec. 2018). Place: New York, NY, USA Publisher: Association for Computing Machinery.

[XZZ22] B. Xia, S. Zheng, and S. Zhou. “Cubic graphical regular representations of some classical simple groups”. In: *Journal of Algebra* 612 (2022), pp. 256–280.

[YS09] S. Yamakawa and K. Shimada. “Removing Self Intersections of a Triangular Mesh by Edge Swapping, Edge Hammering, and Face Lifting”. In: *Proceedings of the 18th International Meshing Roundtable*. Ed. by B. W. Clark. Berlin, Heidelberg: Springer Berlin Heidelberg, 2009, pp. 13–29.

[ZHY19] J. Zhu, Y. Hosaka, and H. Yoshioka. “A Robust Algorithm to Remove the Self-intersection of 3D Mesh Data without Changing the Original Shape”. In: *Journal of Physics: Conference Series* 1314.1 (Oct. 2019), p. 012149.